Role of nuclear lamins as integrators of extranuclear signals and regulators of genome organization and function

A thesis

Submitted in partial fulfillment of the requirements

Of the degree of

Doctor of Philosophy

By

Roopali Pradhan

20112002

INDIAN INSTITUTE OF SCIENCE EDUCATION AND RESEARCH PUNE

2018

Acknowledgements

I would like to acknowledge my PhD supervisor Dr. Kundan Sengupta for giving me an opportunity to work in this field and for providing a great environment for scientific research. I sincerely thank him for always allowing a frank dialogue and letting me execute my ideas without any restraint.

I am very grateful to my faculty advisor Dr. Girish Ratnaparkhi for his constant guidance, kindness and help since my first day at IISER. His excellent mentorship has been invaluable throughout my PhD.

I am thankful to my Research Advisory Committee – Dr. Aurnab Ghose and Dr. Richa Rikhy for their critical inputs and suggestions on my work, which helped me execute my project in a timely manner. I also thank Dr. Pramod Pullarkat (RRI, Bangalore) and Dr. Mahendra Sonawane (TIFR, Mumbai) for their inputs and comments.

I acknowledge Genotypic Technology, Bangalore for the RNA Sequencing experiment, and Dr. Krishanpal Karmodiya and Dr. Satyajeet Khare for their help with RNA Seq analyses. I thank my funding agencies – Council of Scientific and Industrial Research (CSIR) and IISER Pune for their fellowships during my PhD tenure, Wellcome Trust-DBT India Alliance for funding the lab and Infosys Foundation, Department of Biotechnology (DBT, India) and European Molecular Biology Organization (EMBO) for travel fellowships. I sincerely thank the equipment and facilities at IISER Pune, IISER Pune Microscopy facility and all members of Biology, IISER Pune for their help with reagents, instruments and technical assistance in experiments.

I am very grateful to Dr. Girish Ratnaparkhi, Dr. Nagaraj Balasubramanian and Dr. Thomas Pucadyil and their lab members for being excellent mentors during my semester projects – particularly Senthil, Mithila, Archana and Srishti.

My work would not have been possible without the unceasing support of my lab members. I will always be grateful to Devika for teaching me everything that I know and for being the most amazing senior any student can ask for. I thank Joyce – my first mentor in IISER, who always encouraged me and familiarized me to the world of research. Ayantika, Maithilee, Shalaka, Sishil and Trupti have been a constant source of inspiration and joy, and I thank them for making my time in this lab and in IISER, memorable and unforgettable. I thank Swetha, Sishil, Sushmitha and Muhunden for working with me and giving me an opportunity to learn from them.

Lastly, I thank my parents and my brother for the love, guidance, optimism and encouragement that they have always given me, without which this thesis would not have been possible.

Table of contents

List of abbreviations

2D	2-dimensional
3D	3-dimensional
µM	micromolar
µl	microliter
µm	micrometer
µg	microgram
mg	milligram
ml	milliliter
mM	millimolar
nM	nanomolar
BAC	Bacterial artificial chromosome
BDM	2,3-Butanedione Monoxime
BSA	Bovine serum albumin
Chr	Chromosome
CSK	Cytoskeleton buffer
CT	Chromosome territory
DAPI	4’,6-Diamidino-2-Phenylindole
DMSO	Dimethyl sulfoxide
DNA	Deoxyribonucleic acid
DPBS	Dulbecco’s phosphate buffered saline
ECM	Extracellular matrix
ESCs	Embryonic stem cells
FA	Formamide
FISH	Fluorescence *in situ* hybridization
FPKM	Fragments per kilobase of transcript per million mapped reads
GAGs	Glycosaminoglycans
GPa	Gigapascal
Hsp	Heat shock protein
INM	Inner nuclear membrane

KASH	Klarsicht, ANC-1, Syne homology
Kd	Knockdown
kDa	Kilodalton
kPa	Kilopascal
LAD	Lamina associated domain
LAP	Lamina associated polypeptide
LEM	LAP2α-Emerin-MAN1
LINC	Linker of nucleoskeleton and cytoskeleton
Mbp	Megabase pair
MSCs	Mesenchymal stem cells
NET	Nuclear envelope transmembrane
NFW	Nuclease free water
NLS	Nuclear localization signal
NM1	Nuclear myosin I
ONM	Outer nuclear membrane
PAA	Polyacrylamide
PBS	Phosphate buffered saline
PDMS	Polydimethylsiloxane
PFA	Paraformaldehyde
Pol	Polymerase
RD	Radial Distance
RNA	Ribonucleic acid
SSC	Saline sodium citrate
SUN	Sad1p, UNC-84
TBS	Tris buffered saline
TF	Transcription factor
Tyr	Tyrosine
UV	Ultraviolet
WT	Wild type

Abstract

The nuclear envelope and its associated proteins integrate different types of intra and extracellular signals perceived by the cell and relay them into the nucleus to elicit signal specific transcriptional responses. The nuclear envelope maintains structure, mechano-responsiveness and plasticity of the nucleus via the Linker of Nucleoskeleton and Cytoskeleton (LINC) complex, nuclear Lamins and mechanosensitive proteins such as Emerin that interacts with Lamin A/C. A structurally and functionally pliable nucleus modulates genome organization and function across cellular processes. Studying the role of nuclear envelope proteins as responders and effectors of extranuclear signals is essential to understand the regulation of mechanical and biochemical signal transduction into the nucleus. Here we examined the impact of two different signaling paradigms – i) perception of altered extracellular substrate stiffness and ii) heat shock response, on nuclear structure-function relationships in diploid DLD-1 cells and their regulation by nuclear envelope proteins like Lamins and Emerin. RNA sequencing and 3-Dimensional fluorescence in situ hybridization (3D-FISH) analyses in DLD-1 cells on softer polyacrylamide matrices revealed mislocalization of transcriptionally deregulated chromosomes – Chr. 1 and 19, as well as Chr. 18 with least transcriptional changes, towards the nuclear interior. Furthermore, nuclear Lamins which modulate chromosome positioning, were also mislocalized into the nuclear interior in these cells. We identified a novel phosphorylation of Emerin at Tyr99 in cells on softer matrices, the inhibition of which in a phospho-deficient mutant (emerinY99F), selectively retained chromosome territories as well as Lamins at their conserved nuclear locations. Taken together, Emerin functions as a key mechanosensor, that selectively modulates the spatial organization of chromosome territories in the interphase nucleus in a Lamin dependent manner. Interestingly, we observed that Lamin A and B1 were upregulated during heat shock response in DLD-1 cells. Additionally, Lamins were specifically required for the heat shock mediated induction of the heat shock gene

HSPA1A, potentially at two different stages of transcriptional regulation. Remarkably, depletion of Lamin A/C, and not the B-type lamins, abrogated movement of Hsp70 gene locus towards the nuclear interior as well as the nuclear translocation of Hsp70 protein upon thermal stress. Thus, our results highlight a novel role for Lamins in regulating the heat shock response. In summary, this study demonstrates the novel aspects of regulation exerted by nuclear Lamins and their interactors in conjunction, to modulate responses of the nucleus to extranuclear signals.

Synopsis

Introduction

Cell–extracellular matrix (ECM) crosstalk regulates cell growth, proliferation, survival, differentiation and homeostasis (DuFort et al., 2011). The cues from the extracellular environment must reach the nucleus, and ultimately the genome, for signal-specific changes in gene expression and transcription. Since cell fate decisions are dependent on signals from the ECM reaching the genome while traversing the cytoplasm, the nuclear envelope acts as an integrator of these signals. This is further reinforced by the presence of various proteins and protein-complexes in the nuclear envelope that regulate signaling into the nucleus (Wilson and Berk, 2010), for instance –

a) Linker of Nucleoskeleton and Cytoskeleton (LINC) complex, which interacts with cytoskeletal elements towards the outer nuclear membrane (ONM) and nuclear proteins at the inner nuclear membrane (INM) (Crisp et al., 2006; Mellad et al., 2011; Tapley and Starr, 2013).

b) Nuclear Pore Complexes (NPCs), that act as gatekeepers of the nucleus modulating nuclear import-export and also maintain a transcriptionally permissive environment at the nuclear periphery (D'Angelo, 2018; Gu, 2018; Hezwani and Fahrenkrog, 2017; Raices and D'Angelo, 2017).

c) LEM domain containing proteins in the INM – Lap2β, Emerin and MAN1, which regulate nuclear mechanotransduction and transcription factor based biochemical signal transduction (Barton et al., 2015; Guilluy et al., 2014; Lammerding et al., 2005).

d) Nuclear lamins, that provide structural support and plasticity to the nucleus, further modulating nuclear architecture and genome organization (Gruenbaum and Medalia, 2015; Osmanagic-Myers et al., 2015; Prokocimer et al., 2009; Shimi et al., 2008).

Nuclear lamins are type V intermediate filament proteins with documented roles in a variety of processes like DNA replication, transcriptional regulation, chromatin silencing, DNA damage response and maintenance of nuclear structure among others (Butin-Israeli et al., 2015; Dechat et al., 2008; Ghosh et al., 2015; Gibbs-Seymour et al., 2015; Ranade et al., 2017; Shumaker et al., 2008; Singh et al., 2013). The nuclear lamina is a 'molecular shock absorber' that maintains nuclear morphology to counter extraneous mechanical tension (Dahl et al., 2004; Dahl et al., 2006; Stephens et al., 2017; Stephens et al., 2018a; Stephens et al., 2018b; Swift and Discher, 2014). Interestingly, extracellular substrate stiffness modulates expression levels and phosphorylation of Lamin A (Buxboim et al., 2014; Swift and Discher, 2014; Swift et al., 2013). Lamin associated nuclear envelope proteins namely, emerin, LAP2α/β and MAN1 (LEM Domain proteins) modulate signal transduction into the nucleus and downstream gene expression changes. This regulation is elicited by the direct interaction of these proteins with transcriptional regulators such as β-catenin (emerin), Lmo7 (emerin), HDAC3 (emerin, LAP2β), Btf (emerin, MAN1), GCL (emerin, MAN1, LAP2β), rSmads (MAN1) and pRb (LAP2α) among others (Barton et al., 2015; Bengtsson, 2007; Berk et al., 2013; Cohen et al., 2007; Haraguchi et al., 2004; Holaska et al., 2003; Holaska et al., 2006; Ishimura et al., 2006; Lin et al., 2005; Markiewicz et al., 2006). The LEM-D proteins participate in tethering chromatin at the nuclear periphery (Brachner and Foisner, 2011). In addition, emerin is a mechanosensor that directly interacts with Lamin A/C and is phosphorylated in response to increased mechanical stress (Guilluy et al., 2014). Taken together, these studies highlight the vital regulation of signal transduction into the nucleus by nuclear envelope proteins.

It is well established that the genome is non-randomly organized in the interphase nucleus, with gene rich chromosome territories toward the nuclear interior, while gene poor chromosome

territories are proximal to the nuclear periphery (Bolzer et al., 2005; Cremer et al., 2001; Cremer et al., 2003). However, this otherwise conserved chromosome organization is altered during differentiation and in serum starved cells or in cells treated with DNA damaging agents, within a duration of minutes to hours (Bridger et al., 2000; Foster et al., 2005; Kuroda et al., 2004; Mehta et al., 2010; Mehta et al., 2013; Nagele et al., 1999; Rozwadowska et al., 2013). Interestingly, Lamins interact with chromatin via Lamina-Associated Domains (LADs), tether heterochromatin to the nuclear periphery and modulate chromosome territory positions in the interphase nucleus (Guelen et al., 2008; Malhas et al., 2007; Meuleman et al., 2013; Mewborn et al., 2010; Taimen et al., 2009). It is important to note that the organization of chromosome territories or gene loci, in response to extranuclear signals is not completely understood. Both biochemical and mechanical properties of the extracellular substrate influence gene expression patterns. For instance, human mesenchymal stem cells (hMSCs) when plated on collagen coated polyacrylamide gels having different elastic moduli that mimic *in vivo* elasticities of the brain (0.1-1 kPa), muscles (8-17 kPa) and bones (25-40 kPa), differentiate into neurogenic, myogenic and osteogenic lineages respectively (Engler et al., 2006). While laminin and laminin-rich Matrigel® substrates enhance differentiation of hESCs into neural progenitors and neurons (Ma et al., 2008). Interestingly, even gene loci show non-random and tissue specific positioning (Zink et al., 2004). Independent subsets of gene loci reposition in breast and prostate cancer cells as compared to their normal counterparts (Meaburn et al., 2009; Meaburn et al., 2016). In many instances, gene loci are known to reposition depending on their transcriptional status – moving away from their chromosome territories and the nuclear periphery if highly expressed and vice versa when repressed. Clusters of functionally related genes like the epidermal differentiation cluster (on Chr. 1) or the major histocompatibility complex (on Chr. 6) ‘loop out’ of their chromosome territories in cell types where they are

overexpressed (Volpi et al., 2000; Williams et al., 2002). Additionally, Hsp70 (heat shock protein 70) gene locus moves directionally towards the nuclear speckles and contacts them for enhanced expression following a heat shock signal (Jolly et al., 1999; Khanna et al., 2014).

Understanding the relay of extranuclear signals into the genome and their underlying regulation by the nuclear envelope proteins in a cell and tissue specific manner is an important question in this field. The focus of this thesis has been to understand how extranuclear signals – both biochemical and mechanical, are relayed to the genome by nuclear lamins and nuclear envelope proteins, and the ensuing effects on genome organization and transcription. We approached this central question in the following sub-aims:

1. Impact of altered extracellular substrate stiffness on genome organization and function
2. Role of nuclear envelope factors - Lamins and Emerin in genome reorganization in response to altered substrate stiffness
3. Role of nuclear lamins in the regulation of heat shock signaling

1. Impact of altered extracellular substrate stiffness on genome organization and function

We examined the effect of lowering extracellular substrate stiffness using softer polyacrylamide matrices as a paradigm to address the impact of altered mechanical forces on nuclear structure-function relationships in human cancer cell lines. We independently exposed DLD-1 (colorectal adenocarcinoma), SW480 (colorectal adenocarcinoma), A549 (lung carcinoma), MCF7 (breast adenocarcinoma) and HT1080 (Fibrosarcoma) cells to polyacrylamide matrices with contrasting stiffness of ~2 kPa or ~55 kPa, at two time points of 90 mins and ~21 hrs. We observed that each cell type adapts differentially to optimize its morphology, commensurate with substrate stiffness,

in a temporal manner. We selected DLD-1 cells for further experiments considering their karyotypic stability across passages which distinguishes them from other aneuploid cell lines. Additionally, the increase in cell and nuclear surface areas of these cells on softer matrices plateaus by ~90 mins.

To understand the functional impact of lowered extracellular substrate stiffness, RNA sequencing was performed on DLD-1 cells exposed to softer matrices (2 kPa and 55 kPa) and collagen coated glass coverslips for 90 mins. Using cells on glass as reference, our analyses revealed 1655 and 1477 genes that were deregulated on the 2 kPa and 55 kPa matrices respectively. Transcriptional deregulation was accompanied by a downregulation of active histone mark H3K4me3 and nucleoplasmic accumulation of inactive histone mark H3K27me3. We further identified the transcription factors and miRNAs that potentially regulate gene expression changes on softer matrices. Interestingly, 3-Dimensional Fluorescence *In Situ* Hybridization (3D-FISH) analyses in cells on softer polyacrylamide matrices revealed mislocalization of transcriptionally deregulated chromosomes – Chr. 1 and 19, as well as Chr. 18 with minimum transcriptional changes, towards the nuclear interior. Furthermore, switching cells from softer matrices to stiff glass coverslips exposed the differential sensitivity of chromosome territories (CTs) to increase in matrix stiffness – CT19 remained mislocalized towards the nuclear interior, CT1 relocalized partially towards the nuclear periphery while CT18 completely regained its conserved nuclear location proximal to the nuclear envelope within ~90 mins. Taken together, these results highlight the remarkably rapid response of cells to lowered matrix stiffness and sensitivity of genome organization and function to altered mechanical forces on the nucleus.

2. Role of nuclear envelope factors - Lamins and Emerin in genome reorganization in response to altered substrate stiffness

We examined molecular mechanisms underlying genome reorganization in response to altered extracellular matrix stiffness. We assessed the effect of lowered matrix stiffness on the expression and localization of nuclear envelope proteins – Lamins, Emerin and SUN proteins. Nuclear lamins were downregulated and mislocalized into the nuclear interior in DLD-1 cells on softer matrices by ~90 mins. Of note, the expression and localization of Lamins was rescued upon switching cells from softer matrices to stiff glass coverslips. While Lamin B2 overexpression retained CT1 and CT18 near the nuclear periphery even upon lowered matrix stiffness, Lamin A overexpression repositioned CT18 further into and CT19 away from the nuclear interior. We also found that inducing nucleoplasmic accumulation of Lamin A on glass, using a phosphomimetic Lamin A S22D mutant, mislocalized CT19 towards the nuclear periphery but had no effect on CT18 positions. Taken together, we demonstrate the important role of nuclear lamins in regulating chromosome territory positions on softer matrices.

Interestingly, cells on softer matrices activated Emerin phosphorylation at a novel Tyr99 residue. Inhibition of emerin phosphorylation either using Src kinase inhibitor or a phospho-deficient mutant (emerinY99F), selectively retained chromosome 18 and 19 as well as Lamins, but not chromosome 1, at their conserved nuclear locations even upon lowered matrix stiffness Furthermore, emerin Y99F showed enhanced interaction with Lamin A, suggesting that phosphorylation of Emerin at Tyr99 (on softer matrices) potentially weakens its interaction with Lamin A, further promoting the nucleoplasmic accumulation of Lamin A and destabilization of the nuclear lamina. In summary, Emerin functions as a key mechanosensor, that selectively

modulates the spatial organization of chromosome territories in the interphase nucleus in a Lamin dependent manner.

3. Role of nuclear lamins in the regulation of heat shock signaling

We examined the regulatory crosstalk between nuclear lamins and the heat shock response pathway in DLD-1 cells. Heat shock stimulus (at 42ºC) upregulated Lamin A and B1 transcripts by ~10 mins and protein expression by ~15 to 60 mins. We examined the role of lamins at the following stages during heat shock – i) expression of *HSPA1A* (one of the genes in the Hsp70 gene locus) and ii) nuclear import of Hsp70 protein. Lamin A/C, B1 and B2 were all specifically required for heat shock induced upregulation of *HSPA1A*. Remarkably, depletion of Lamin A/C, and not the B-type lamins, abrogated the movement of Hsp70 gene locus towards the nuclear interior (required for its transcriptional upregulation) as well as the nuclear translocation of Hsp70 protein upon thermal stress. Lamin A/C was required for the heat shock induced increase in intranuclear Nuclear Myosin I (NM1 – nuclear motor protein) foci, which was further essential for the movement and consequently upregulation of *HSPA1A.* Thus, we speculate that A and B-type lamins modulate two different stages of heat shock signaling – Lamin A/C facilitates the movement of Hsp70 gene locus towards nuclear speckles by regulating NM1 activity, while B-type lamins are potentially key players in the recruitment of other accessory transcription factors required for the upregulation of Hsp70 locus expression after it has contacted the nuclear speckles. Taken together, our results highlight a novel role for lamins in regulating the heat shock response.

Summary

This thesis highlights the novel roles of nuclear Lamins and emerin in regulating signal transduction into the nucleus. Here we summarize major findings of this thesis as follows –

Spatial organization of chromosome territories – We suggest that a close interplay between gene density, transcriptional profiles and nuclear envelope proximity of chromosome territories, modulates their positions in response to altered nuclear mechanotransduction. We show that nuclear lamins are important effectors of chromosome territory repositioning in cells on softer matrices. We demonstrate differential effects of A and B-type lamins on chromosome territory positions. While B-type lamins act as tethers for heterochromatin and gene poor, peripheral chromosome territories, Lamin A has a stronger influence on gene rich chromosomes possibly via its nucleoplasmic fraction. Additionally, nuclear envelope proteins like emerin function as upstream sensors of extranuclear signals potentially by undergoing signal-specific post-translational modifications.

Transcriptional profiles – We demonstrate genome-wide transcriptional perturbations in response to altered nuclear mechanotransduction, which largely correlate with repositioning and altered topologies of chromosome territories. Additionally, we suggest the role of predominantly Lamin A in modulating expression profiles of certain gene subsets potentially via a regulatory network of closely interacting transcription factors and miRNAs.

Positional regulation of gene expression – We show the transcriptional and positional control of Hsp70 gene locus by nuclear lamins, which underscores the impact of lamins on signaling induced gene expression changes and chromatin reorganization. These observations for the first time highlight the importance of (i) the functional divergence between Lamin A and B-type in their

regulation of the dynamics and expression of Hsp70 gene locus (ii) protein-protein interactions of lamins (Lamin A-Emerin-NM1 in the heat shock response pathway and Lamin A-Emerin in the reorganization of chromosome territories) for chromatin reorganization and function in response to extranuclear signals.

Results from this thesis have been published as a part of the following manuscript:

Roopali Pradhan, Devika Ranade, Kundan Sengupta; **Emerin modulates spatial organization of chromosome territories in cells on softer matrices**, Nucleic Acids Research, Volume 46, Issue 11, 20 June 2018, Pages 5561–5586.

References

Barton, L. J., Soshnev, A. A. and Geyer, P. K. (2015). Networking in the nucleus: a spotlight on LEM-domain proteins. *Curr. Opin. Cell Biol.* **34**, 1–8.

Bengtsson, L. (2007). What MAN1 does to the Smads. TGFbeta/BMP signaling and the nuclear envelope. *FEBS J.* **274**, 1374–1382.

Berk, J. M., Tifft, K. E. and Wilson, K. L. (2013). The nuclear envelope LEM-domain protein emerin. *Nucleus* **4**, 298–314.

Bolzer, A., Kreth, G., Solovei, I., Koehler, D., Saracoglu, K., Fauth, C., Müller, S., Eils, R., Cremer, C., Speicher, M. R., et al. (2005). Three-dimensional maps of all chromosomes in human male fibroblast nuclei and prometaphase rosettes. *PLoS Biol.* **3**, e157.

Brachner, A. and Foisner, R. (2011). Evolvement of LEM proteins as chromatin tethers at the nuclear periphery. *Biochem. Soc. Trans.* **39**, 1735–1741.

Bridger, J. M., Boyle, S., Kill, I. R. and Bickmore, W. A. (2000). Re-modelling of nuclear architecture in quiescent and senescent human fibroblasts. *Curr. Biol.* **10**, 149–152.

Butin-Israeli, V., Adam, S. A., Jain, N., Otte, G. L., Neems, D., Wiesmüller, L., Berger, S. L. and Goldman, R. D. (2015). Role of lamin b1 in chromatin instability. *Mol. Cell. Biol.* **35**, 884–898.

Buxboim, A., Swift, J., Irianto, J., Spinler, K. R., Dingal, P. C. D. P., Athirasala, A., Kao, Y.-R. C., Cho, S., Harada, T., Shin, J.-W., et al. (2014). Matrix elasticity regulates lamin-A,C phosphorylation and turnover with feedback to actomyosin. *Curr. Biol.* **24**, 1909–1917.

Cohen, T. V., Kosti, O. and Stewart, C. L. (2007). The nuclear envelope protein MAN1 regulates TGFbeta signaling and vasculogenesis in the embryonic yolk sac. *Development* **134**, 1385–

1395.

Cremer, M., von Hase, J., Volm, T., Brero, A., Kreth, G., Walter, J., Fischer, C., Solovei, I., Cremer, C. and Cremer, T. (2001). Non-random radial higher-order chromatin arrangements in nuclei of diploid human cells. *Chromosome Res.* **9**, 541–567.

Cremer, M., Küpper, K., Wagler, B., Wizelman, L., von Hase, J., Weiland, Y., Kreja, L., Diebold, J., Speicher, M. R. and Cremer, T. (2003). Inheritance of gene density-related higher order chromatin arrangements in normal and tumor cell nuclei. *J. Cell Biol.* **162**, 809–820.

Crisp, M., Liu, Q., Roux, K., Rattner, J. B., Shanahan, C., Burke, B., Stahl, P. D. and Hodzic, D. (2006). Coupling of the nucleus and cytoplasm: role of the LINC complex. *J. Cell Biol.* **172**, 41–53.

Dahl, K. N., Kahn, S. M., Wilson, K. L. and Discher, D. E. (2004). The nuclear envelope lamina network has elasticity and a compressibility limit suggestive of a molecular shock absorber. *J. Cell Sci.* **117**, 4779–4786.

Dahl, K. N., Scaffidi, P., Islam, M. F., Yodh, A. G., Wilson, K. L. and Misteli, T. (2006). Distinct structural and mechanical properties of the nuclear lamina in Hutchinson-Gilford progeria syndrome. *Proc Natl Acad Sci USA* **103**, 10271–10276.

Dechat, T., Pfleghaar, K., Sengupta, K., Shimi, T., Shumaker, D. K., Solimando, L. and Goldman, R. D. (2008). Nuclear lamins: major factors in the structural organization and function of the nucleus and chromatin. *Genes Dev.* **22**, 832–853.

DuFort, C. C., Paszek, M. J. and Weaver, V. M. (2011). Balancing forces: architectural control of mechanotransduction. *Nat. Rev. Mol. Cell Biol.* **12**, 308–319.

D'Angelo, M. A. (2018). Nuclear pore complexes as hubs for gene regulation. *Nucleus* **9**, 142–148.

Engler, A. J., Sen, S., Sweeney, H. L. and Discher, D. E. (2006). Matrix elasticity directs stem cell lineage specification. *Cell* **126**, 677–689.

Foster, H. A., Abeydeera, L. R., Griffin, D. K. and Bridger, J. M. (2005). Non-random chromosome positioning in mammalian sperm nuclei, with migration of the sex chromosomes during late spermatogenesis. *J. Cell Sci.* **118**, 1811–1820.

Ghosh, S., Liu, B., Wang, Y., Hao, Q. and Zhou, Z. (2015). Lamin A Is an Endogenous SIRT6 Activator and Promotes SIRT6-Mediated DNA Repair. *Cell Rep.* **13**, 1396–1406.

Gibbs-Seymour, I., Markiewicz, E., Bekker-Jensen, S., Mailand, N. and Hutchison, C. J. (2015). Lamin A/C-dependent interaction with 53BP1 promotes cellular responses to DNA damage. *Aging Cell* **14**, 162–169.

Gruenbaum, Y. and Medalia, O. (2015). Lamins: the structure and protein complexes. *Curr. Opin. Cell Biol.* **32**, 7–12.

Gu, Y. (2018). The nuclear pore complex: a strategic platform for regulating cell signaling. *New Phytol.* **219**, 25–30.

Guelen, L., Pagie, L., Brasset, E., Meuleman, W., Faza, M. B., Talhout, W., Eussen, B. H., de Klein, A., Wessels, L., de Laat, W., et al. (2008). Domain organization of human

chromosomes revealed by mapping of nuclear lamina interactions. *Nature* **453**, 948–951.

Guilluy, C., Osborne, L. D., Van Landeghem, L., Sharek, L., Superfine, R., Garcia-Mata, R. and Burridge, K. (2014). Isolated nuclei adapt to force and reveal a mechanotransduction pathway in the nucleus. *Nat. Cell Biol.* **16**, 376–381.

Haraguchi, T., Holaska, J. M., Yamane, M., Koujin, T., Hashiguchi, N., Mori, C., Wilson, K. L. and Hiraoka, Y. (2004). Emerin binding to Btf, a death-promoting transcriptional repressor, is disrupted by a missense mutation that causes Emery-Dreifuss muscular dystrophy. *Eur. J. Biochem.* **271**, 1035–1045.

Hezwani, M. and Fahrenkrog, B. (2017). The functional versatility of the nuclear pore complex proteins. *Semin. Cell Dev. Biol.* **68**, 2–9.

Holaska, J. M., Lee, K. K., Kowalski, A. K. and Wilson, K. L. (2003). Transcriptional repressor germ cell-less (GCL) and barrier to autointegration factor (BAF) compete for binding to emerin in vitro. *J. Biol. Chem.* **278**, 6969–6975.

Holaska, J. M., Rais-Bahrami, S. and Wilson, K. L. (2006). Lmo7 is an emerin-binding protein that regulates the transcription of emerin and many other muscle-relevant genes. *Hum. Mol. Genet.* **15**, 3459–3472.

Ishimura, A., Ng, J. K., Taira, M., Young, S. G. and Osada, S.-I. (2006). Man1, an inner nuclear membrane protein, regulates vascular remodeling by modulating transforming growth factor beta signaling. *Development* **133**, 3919–3928.

Jolly, C., Vourc'h, C., Robert-Nicoud, M. and Morimoto, R. I. (1999). Intron-independent association of splicing factors with active genes. *J. Cell Biol.* **145**, 1133–1143.

Khanna, N., Hu, Y. and Belmont, A. S. (2014). HSP70 transgene directed motion to nuclear speckles facilitates heat shock activation. *Curr. Biol.* **24**, 1138–1144.

Kuroda, M., Tanabe, H., Yoshida, K., Oikawa, K., Saito, A., Kiyuna, T., Mizusawa, H. and Mukai, K. (2004). Alteration of chromosome positioning during adipocyte differentiation. *J. Cell Sci.* **117**, 5897–5903.

Lammerding, J., Hsiao, J., Schulze, P. C., Kozlov, S., Stewart, C. L. and Lee, R. T. (2005). Abnormal nuclear shape and impaired mechanotransduction in emerin-deficient cells. *J. Cell Biol.* **170**, 781–791.

Lin, F., Morrison, J. M., Wu, W. and Worman, H. J. (2005). MAN1, an integral protein of the inner nuclear membrane, binds Smad2 and Smad3 and antagonizes transforming growth factor-beta signaling. *Hum. Mol. Genet.* **14**, 437–445.

Ma, W., Tavakoli, T., Derby, E., Serebryakova, Y., Rao, M. S. and Mattson, M. P. (2008). Cell-extracellular matrix interactions regulate neural differentiation of human embryonic stem cells. *BMC Dev. Biol.* **8**, 90.

Malhas, A., Lee, C. F., Sanders, R., Saunders, N. J. and Vaux, D. J. (2007). Defects in lamin B1 expression or processing affect interphase chromosome position and gene expression. *J. Cell Biol.* **176**, 593–603.

Markiewicz, E., Tilgner, K., Barker, N., van de Wetering, M., Clevers, H., Dorobek, M., Hausmanowa-Petrusewicz, I., Ramaekers, F. C. S., Broers, J. L. V., Blankesteijn, W.

M., et al. (2006). The inner nuclear membrane protein emerin regulates beta-catenin activity by restricting its accumulation in the nucleus. *EMBO J.* **25**, 3275–3285.

Meaburn, K. J., Gudla, P. R., Khan, S., Lockett, S. J. and Misteli, T. (2009). Disease-specific gene repositioning in breast cancer. *J. Cell Biol.* **187**, 801–812.

Meaburn, K. J., Agunloye, O., Devine, M., Leshner, M., Roloff, G. W., True, L. D. and Misteli, T. (2016). Tissue-of-origin-specific gene repositioning in breast and prostate cancer. *Histochem. Cell Biol.* **145**, 433–446.

Mehta, I. S., Amira, M., Harvey, A. J. and Bridger, J. M. (2010). Rapid chromosome territory relocation by nuclear motor activity in response to serum removal in primary human fibroblasts. *Genome Biol.* **11**, R5.

Mehta, I. S., Kulashreshtha, M., Chakraborty, S., Kolthur-Seetharam, U. and Rao, B. J. (2013). Chromosome territories reposition during DNA damage-repair response. *Genome Biol.* **14**, R135.

Mellad, J. A., Warren, D. T. and Shanahan, C. M. (2011). Nesprins LINC the nucleus and cytoskeleton. *Curr. Opin. Cell Biol.* **23**, 47–54.

Meuleman, W., Peric-Hupkes, D., Kind, J., Beaudry, J.-B., Pagie, L., Kellis, M., Reinders, M., Wessels, L. and van Steensel, B. (2013). Constitutive nuclear lamina-genome interactions are highly conserved and associated with A/T-rich sequence. *Genome Res.* **23**, 270–280.

Mewborn, S. K., Puckelwartz, M. J., Abuisneineh, F., Fahrenbach, J. P., Zhang, Y., MacLeod, H., Dellefave, L., Pytel, P., Selig, S., Labno, C. M., et al. (2010). Altered chromosomal positioning, compaction, and gene expression with a lamin A/C gene mutation. *PLoS ONE* **5**, e14342.

Nagele, R. G., Freeman, T., McMorrow, L., Thomson, Z., Kitson-Wind, K. and Lee, H. y (1999). Chromosomes exhibit preferential positioning in nuclei of quiescent human cells. *J. Cell Sci.* **112 (Pt 4)**, 525–535.

Osmanagic-Myers, S., Dechat, T. and Foisner, R. (2015). Lamins at the crossroads of mechanosignaling. *Genes Dev.* **29**, 225–237.

Prokocimer, M., Davidovich, M., Nissim-Rafinia, M., Wiesel-Motiuk, N., Bar, D. Z., Barkan, R., Meshorer, E. and Gruenbaum, Y. (2009). Nuclear lamins: key regulators of nuclear structure and activities. *J. Cell. Mol. Med.* **13**, 1059–1085.

Raices, M. and D'Angelo, M. A. (2017). Nuclear pore complexes and regulation of gene expression. *Curr. Opin. Cell Biol.* **46**, 26–32.

Ranade, D., Koul, S., Thompson, J., Prasad, K. B. and Sengupta, K. (2017). Chromosomal aneuploidies induced upon Lamin B2 depletion are mislocalized in the interphase nucleus. *Chromosoma* **126**, 223–244.

Rozwadowska, N., Kolanowski, T., Wiland, E., Siatkowski, M., Pawlak, P., Malcher, A., Mietkiewski, T., Olszewska, M. and Kurpisz, M. (2013). Characterisation of nuclear architectural alterations during in vitro differentiation of human stem cells of myogenic origin. *PLoS ONE* **8**, e73231.

Shimi, T., Pfleghaar, K., Kojima, S., Pack, C.-G., Solovei, I., Goldman, A. E., Adam, S. A., Shumaker, D. K., Kinjo, M., Cremer, T., et al. (2008). The A- and B-type nuclear lamin networks: microdomains involved in chromatin organization and transcription. *Genes Dev.* **22**, 3409–3421.

Shumaker, D. K., Solimando, L., Sengupta, K., Shimi, T., Adam, S. A., Grunwald, A., Strelkov, S. V., Aebi, U., Cardoso, M. C. and Goldman, R. D. (2008). The highly conserved nuclear lamin Ig-fold binds to PCNA: its role in DNA replication. *J. Cell Biol.* **181**, 269–280.

Singh, M., Hunt, C. R., Pandita, R. K., Kumar, R., Yang, C.-R., Horikoshi, N., Bachoo, R., Serag, S., Story, M. D., Shay, J. W., et al. (2013). Lamin A/C depletion enhances DNA damage-induced stalled replication fork arrest. *Mol. Cell. Biol.* **33**, 1210–1222.

Stephens, A. D., Banigan, E. J., Adam, S. A., Goldman, R. D. and Marko, J. F. (2017). Chromatin and lamin A determine two different mechanical response regimes of the cell nucleus. *Mol. Biol. Cell* **28**, 1984–1996.

Stephens, A. D., Banigan, E. J. and Marko, J. F. (2018a). Separate roles for chromatin and lamins in nuclear mechanics. *Nucleus* **9**, 119–124.

Stephens, A. D., Liu, P. Z., Banigan, E. J., Almassalha, L. M., Backman, V., Adam, S. A., Goldman, R. D. and Marko, J. F. (2018b). Chromatin histone modifications and rigidity affect nuclear morphology independent of lamins. *Mol. Biol. Cell* **29**, 220–233.

Swift, J. and Discher, D. E. (2014). The nuclear lamina is mechano-responsive to ECM elasticity in mature tissue. *J. Cell Sci.* **127**, 3005–3015.

Swift, J., Ivanovska, I. L., Buxboim, A., Harada, T., Dingal, P. C. D. P., Pinter, J., Pajerowski, J. D., Spinler, K. R., Shin, J.-W., Tewari, M., et al. (2013). Nuclear lamin-A scales with tissue stiffness and enhances matrix-directed differentiation. *Science* **341**, 1240104.

Taimen, P., Pfleghaar, K., Shimi, T., Möller, D., Ben-Harush, K., Erdos, M. R., Adam, S. A., Herrmann, H., Medalia, O., Collins, F. S., et al. (2009). A progeria mutation reveals functions for lamin A in nuclear assembly, architecture, and chromosome organization. *Proc Natl Acad Sci USA* **106**, 20788–20793.

Tapley, E. C. and Starr, D. A. (2013). Connecting the nucleus to the cytoskeleton by SUN-KASH bridges across the nuclear envelope. *Curr. Opin. Cell Biol.* **25**, 57–62.

Volpi, E. V., Chevret, E., Jones, T., Vatcheva, R., Williamson, J., Beck, S., Campbell, R. D., Goldsworthy, M., Powis, S. H., Ragoussis, J., et al. (2000). Large-scale chromatin organization of the major histocompatibility complex and other regions of human chromosome 6 and its response to interferon in interphase nuclei. *J. Cell Sci.* **113 (Pt 9)**, 1565–1576.

Williams, R. R. E., Broad, S., Sheer, D. and Ragoussis, J. (2002). Subchromosomal positioning of the epidermal differentiation complex (EDC) in keratinocyte and lymphoblast interphase nuclei. *Exp. Cell Res.* **272**, 163–175.

Wilson, K. L. and Berk, J. M. (2010). The nuclear envelope at a glance. *J. Cell Sci.* **123**, 1973–1978.

Zink, D., Amaral, M. D., Englmann, A., Lang, S., Clarke, L. A., Rudolph, C., Alt, F., Luther, K., Braz, C., Sadoni, N., et al. (2004). Transcription-dependent spatial arrangements of CFTR and adjacent genes in human cell nuclei. *J. Cell Biol.* **166**, 815–825.

Chapter 1: Introduction and review of literature

1.1 Introduction to signal transduction into the nucleus

The hierarchy of organization in multicellular organisms is built from a single cell. Growth, proliferation, differentiation, survival and homeostasis of a cell are the basis of life of an organism. However, the cues that initiate these processes are not dependent only on the molecular and biochemical pathways occurring inside the cell. They are also dependent on cell-to-cell crosstalk and interaction of the cell with its environment. The extracellular matrix (ECM) is the non-cellular component of the cellular environment that provides a physical scaffold and a structural support to the cells. It is primarily composed of proteoglycans and fibrous proteins like collagens, fibronectins, elastins and laminins. While the proteoglycans fill the extracellular interstitial space forming a hydrated gel-like structure, the fibrous proteins act as ligands for specific cell surface receptors, so that the cells can adhere. The ECM composition and its biochemical and mechanical properties vary greatly with different tissue types and this is a result of the dynamic and continuous communication between the ECM and the cells (Frantz et al., 2010). Of the cell surface proteins that interact with the ECM, integrins are heterodimeric transmembrane receptors that bind different ECM proteins via their extracellular head domain and they bind cytoskeletal elements, cytoplasmic kinases and growth factor receptors via their cytoplasmic tail domain through various adaptor proteins. Thus, they bridge the ECM and the cell and are transducers of extracellular signals that dictate proliferation, differentiation, survival of the cell (Giancotti and Ruoslahti, 1999; Yamada et al., 2003).

Cues from the extracellular environment have to reach the nucleus, and ultimately the genome, so that signal-specific changes in gene expression and transcription can take place which will elicit specific responses. Thus, cell fate decisions are dependent on the signals from ECM reaching the

genome, while having to traverse the cytoplasm and therefore, the nuclear envelope acts as an integrator of these signals. This is demonstrated by the presence of various proteins and protein-complexes in the nuclear envelope that regulate signaling into the nucleus (Wilson and Berk, 2010), for instance –

a) Linker of Nucleoskeleton and Cytoskeleton (LINC) complex, which interacts with cytoskeletal elements towards the outer nuclear membrane (ONM) and nuclear proteins at the inner nuclear membrane (INM) (Crisp et al., 2006; Mellad et al., 2011; Tapley and Starr, 2013).

b) Nuclear Pore Complexes (NPCs), that act as gatekeepers of the nucleus modulating nuclear import-export and also maintain a transcriptionally permissive environment at the nuclear periphery (D'Angelo, 2018; Gu, 2018; Hezwani and Fahrenkrog, 2017; Raices and D'Angelo, 2017).

c) LEM domain containing proteins in the INM – Lap2β, Emerin and MAN1, which regulate nuclear mechanotransduction and transcription factor based biochemical signal transduction (Barton et al., 2015; Guilluy et al., 2014; Lammerding et al., 2005).

d) Nuclear lamins, that provide structural support and plasticity to the nucleus, further modulating nuclear architecture and genome organization (Gruenbaum and Medalia, 2015; Osmanagic-Myers et al., 2015; Prokocimer et al., 2009; Shimi et al., 2008).

In its lifetime, a cell responds to various cues like biochemical signals as well as internal and external mechanical forces. Biochemical signal transduction cascades typically involve activation of transmembrane or nuclear receptors by primary stimuli, which in turn amplify and relay the signal via secondary messengers, further leading to signal-specific responses generated by the cell (Boudreau and Bissell, 1998). Internal mechanical forces in the cell include those generated by

cytoskeletal movements, osmotic pressure; while external forces vary with the type of tissue and ECM, and include forces due to axial/cyclic stretch in fibroblasts, shear forces in endothelial cells, compression forces in bones and cartilages (Wang and Thampatty, 2006). Perception of mechanical stimuli and their conversion into downstream biochemical signaling is termed as mechanotransduction and this process is required for the maintenance of tissue homeostasis, normal cellular phenotype, growth, development and differentiation (Ingber, 2006; Jaalouk and Lammerding, 2009). Mechanotransduction can lead either to activation of mechanosensitive ion channels (e.g. Na^{+}, K^{+} and Ca^{++}) or to activation of protein kinases and other signaling molecules (e.g. Integrin signaling at focal adhesions or signaling at cell-cell junctions) or direct stress wave propagation to the nucleus from the plasma membrane via the cytoskeleton-LINC complex connections (Mellad et al., 2011; Tapley and Starr, 2013). As the end result of any of these mechanisms is a signal-specific response from the genome, study of signal transduction into the nucleus is essential to understand biochemical and mechanical regulation of structure, function and organization of the genome.

1.2 Early insights into the regulation of cellular processes by extracellular matrix

Role of the extracellular substrate in cellular homeostasis has been appreciated since the 1970s from experiments that highlighted the association between substrate-mediated cell shape changes, cellular growth, DNA replication and apoptosis. Folkman and Moscona showed for the first time that changing cell shape affected the ability of bovine endothelium, WI-38 and Swiss 3T3 cells to undertake DNA synthesis. Cell shape was modulated either by coating tissue culture plastic dishes with varying concentrations of poly-2-hydroxy-ethylmethacrylate (poly-HEMA, wherein greater concentrations inhibited adhesivity and therefore cell spreading) or by increasing the number of

cells plated per unit area (wherein higher confluency of cells limited cell spreading). It was observed that cells that were allowed to spread more, underwent greater proliferation and showed increased DNA synthesis as measured by incorporation of ^{3}H-thymidine (Folkman and Moscona, 1978). These results reiterated the interdependence of cell growth and proliferation, substrate adhesivity and inter-cell contacts. The extracellular substrate also seems to influence the response of cells to different growth factors by modulating cellular shape. For example, bovine corneal epithelial cells when grown *in vitro* on tissue culture plastic adopted a flattened morphology and consequently, responded to fibroblast growth factor (FGF) by undergoing proliferation but not to epidermal growth factor (EGF). Interestingly, growing these cells either in an organ culture or on collagen-coated dishes lead to a columnar morphology and cell proliferation was observed in response to EGF and not FGF (Gospodarowicz et al., 1978). This suggested that extracellular substrate regulates cell shape and thereby modulates the selective response of cells to different mitogens and growth factors. However, the mechanism that connected cell shape, cytoskeletal rearrangement and nuclear response to extracellular signals was not completely understood. Growing human capillary endothelial cells on fibronectin-coated adhesive islands of varying areas (microscale patterns), Chen *et al* showed that projected areas of the cell, and not the cell-ECM contact areas, dictate growth and apoptotic programs in cells. Cells with larger projected areas show comparatively higher percentage of growth and lower percentage of apoptosis (Chen et al., 1997). Interestingly, initiation of S phase during cell cycle also requires a critical nuclear size (Nicolini et al., 1986). Substrate dependent cell shapes and sizes also regulate differentiation programs of mammalian cells. Adhesive islands that allow human epidermal keratinocytes to spread extensively promote DNA synthesis and proliferation, while islands which restrict cells to a round shape promote terminal differentiation and inhibition of DNA synthesis (Watt et al., 1988).

These results indicate that substrate dependent cytoskeletal remodeling coupled with a corresponding remodeling of the nucleus – both at the level of its physical properties and gene expression profiles, is required for determining response of the cell to its environment.

1.3 Biochemical and mechanical properties of the extracellular matrix

In vivo, the mechanical properties of ECM are defined by elasticity, rigidity or stiffness of the substrate as a result of varying structural attributes of the ECM proteins (e.g. formation of long fibrils by collagen); whereas *in vitro*, these properties are a result of varying degrees of polymerization of the artificial substrates being used (e.g. changing acrylamide polymerization by altering ratio of acrylamide and crosslinker bis-acrylamide) (Kanta, 2015; Walters and Stegemann, 2014; Wang et al., 2011). In order to study the effects of altered mechanical properties of ECM on cells, gels of variable stiffness or compliance are created by varying collagen concentration (natural substrate) or by using differentially polymerized materials like polyacrylamide, methacrylamide chitosan, polyurethane or polystyrene (artificial substrates) (Arslan-Yildiz et al., 2016; Joddar and Ito, 2013). Mechanical properties like the elastic modulus, viscous modulus etc. can be quantified for each of these substrates using methods such as atomic force microscopy (AFM) and micro-rheology among others (Evans et al., 2009; Leipzig and Shoichet, 2009). Biochemical properties of the ECM are defined by the composition of the substrate i.e. concentrations of different ECM proteins, proteoglycans and GAGs. These properties can be studied either by extracting ECM from cells or tissues (growing in culture or from the animal) (Evans et al., 2010) or by using commercially available formulations made up of different compositions of ECM components – for instance, Matrigel® (Wilschut et al., 2010) or Cardiogel® (Baharvand et al., 2005).

1.3.1 Effect of mechanical properties of the ECM on cell signaling and gene expression programs

Using either naturally derived or artificially prepared substrates, mechanical properties of the ECM are altered and effects of these changes on cellular differentiation and gene expression are studied with different cell types as models. Human mesenchymal stem cells (hMSCs) when plated on collagen coated polyacrylamide gels having different elastic moduli that mimic *in vivo* elasticities of the brain (0.1-1 kPa), muscles (8-17 kPa) and bones (25-40 kPa), differentiated into neurogenic, myogenic and osteogenic lineages respectively. This lineage specification was seen at the level of cellular morphology as well as expression of lineage specific markers, for e.g. neurogenic hMSCs showed neurite outgrowths and expression of TUBB4, NRG1 while myogenic hMSCs showed a spindle shape and expression of MYOG, PAX7 and osteogenic hMSCs showed a polygonally spread morphology with expression of BGLAP, SMADs, BMPs. Interestingly, blocking the activity of non-muscle myosin II (NMM II) with Blebbistatin abolished the substrate elasticity-dependent differentiation. This points to the role of cytoskeletal contractility and extracellular traction forces in cellular differentiation (Engler et al., 2006).

Independent groups have shown that differentiation of hMSCs using TGFβ (Transforming Growth Factor β) is also dependent on substrate stiffness wherein a stiff matrix (~15.0 kPa) promotes differentiation into the smooth muscle cell lineage, while a soft matrix (~1.0 kPa) promotes differentiation into chondrogenic and adipogenic lineages (Park et al., 2011). The differentiation of embryonic stem cells (ESCs) into neural lineage (along with expression of lineage specific markers) (Leipzig and Shoichet, 2009) and neuronal maturation is promoted better on soft substrates (~1 kPa) (Teixeira et al., 2009). On the contrary, rigid extracellular substrate is required

for osteogenic differentiation of ecto-mesenchymal stem cells from human exfoliated deciduous teeth (Viale-Bouroncle et al., 2012). Since the microenvironment of the developing embryo provides essential cues for survival, proliferation, differentiation among others, the embryonic stem cells are known to rely on signals from extracellular matrix for regulating their cellular processes. It has been demonstrated that expression of pluripotency markers in ESCs is dependent on substrate stiffness, with promotion of cell spreading, proliferation and osteogenic differentiation as stiffness is increased from 0.041 MPa to 2.7 MPa (Evans et al., 2009). Similarly, mouse ESCs self-renew homogeneously on softer substrate (~0.6 kPa) due to the low traction forces that cells experience from the soft matrix, which result in altered transcriptional regulation (Chowdhury et al., 2010). These observations reiterate the importance of cell microenvironment and its associated force equilibrium in establishing and maintaining specific gene expression profiles.

1.3.2 Effect of biochemical properties of the ECM on cell signaling and gene expression programs

Biochemical properties of ECM depend upon composition of the substrate, i.e. concentrations of different ECM proteins, proteoglycans and GAGs. Both mechanical properties of ECM and its biochemical composition varies in accordance to tissue or cell type variations, and this is a direct result of the cell-ECM crosstalk. Laminin and laminin-rich Matrigel® substrates enhance differentiation of hESCs into neural progenitors and neurons (Ma et al., 2008) and also promote myogenic differentiation of porcine stem cells (Wilschut et al., 2010). It is interesting to note that differentiation towards a specific lineage is enhanced and more homogenous when progenitor cells are grown in the presence of ECM derived from differentiated adult cells of the same lineage (Stern et al., 2009). Taken together, these results strongly suggest the need for the cells to be maintained in conditions that are as close as possible to their *in vivo* environment. It is likely that progenitor

cells, when maintained in culture conditions that mimic natural *in vivo* conditions, are better exposed to specific lineage directing signals and hence can differentiate towards a particular cell fate in a more homogenous manner. These signals could either be growth factors or signaling proteins embedded in the ECM or could be specific ECM protein-integrin pairs that specify distinct cell fate pathways.

1.4 Mechanical regulation of the nucleus

Shape of the nucleus varies across different cell types, from spherical nuclei in monocytes to multi-lobulated nuclei in granulocytes (acidophils, basophils and neutrophils). By early 1920s, observations of nuclei of many invertebrate and vertebrate cells by different biologists led to certain common hypotheses being proposed with regards to regulation of nuclear shape. These included i) effect of surface tension – a homogenous surface tension leads to spherical nucleus, while a non-uniform surface tension creates polymorphism, ii) mechanical deformation due to cytoplasmic inclusions (e.g. Fat, Lecithin, Yolk) and cytoskeleton and iii) effect of the movement of the centrosome. The cell and nuclear shapes were shown to be highly correlated and it was speculated that nuclear shape, regulation of cell division and cellular differentiation were interdependent (Champy and Carleton 1921). We now know that molecular connectivity between extracellular environment and the nucleus created via the ECM – integrins – cytoskeleton – LINC complex – INM proteins and nuclear lamins, enables signal transduction into the nucleus further modulating nuclear responses by different mechanisms (Alam et al., 2014; Lombardi and Lammerding, 2011; Maniotis et al., 1997; Razafsky and Hodzic, 2009).

1.4.1 Regulation of nuclear positioning

The LINC complex, which acts as an anchor of the nucleus to the cytoskeleton, was discovered in *C. elegans* through genetic screens to target nuclear migration defects. Mutations in conserved nuclear envelope proteins Unc-84 (SUN domain containing protein) and Unc-83 (KASH domain containing protein) resulted in impaired nuclear migrations of P-cells, during formation of hyp-7 syncytium and during intestinal lumen formation in intestinal primordium (Starr et al., 2001). Microtubules (MT) can position the nucleus either by directly applying forces (pulling/pushing) on it or via the centrosome and MT motors, both of which closely associate with the nuclear envelope (Aronson, 1971; Labbé et al., 2004). Similarly, the actin cytoskeleton can also position the nucleus by generation of actomyosin contraction. The TAN (Transmembrane Actin associated Nuclear) lines, formed by linear arrays of Nesprin2 and SUN2, also couple the actin network to the nucleus and organize actin flow which is vital for movement of the nucleus during cell migration (Luxton et al., 2010). Functional coupling of actin to the nuclear membrane via LINC complex in order to generate movement of the nucleus is analogous to the coupling of integrins on plasma membrane to the cytoskeleton for generating cellular movement, and could provide insights into actin-dependent arrays for force transduction. Lastly, intermediate filament proteins like vimentin, nestin and GFAP, can also be involved in positioning the nucleus (Dupin et al., 2011; Gerashchenko et al., 2009; Maniotis et al., 1997).

Interestingly, along with the cell-ECM signaling, cell-cell (adherens) junction signaling mediated by N-cadherin in conjunction with the ECM regulates the centrosome and nuclear movements in absence of any other polarizing cues (Dupin and Etienne-Manneville, 2011; Dupin et al., 2009). Position of the nucleus also acts as a sensor to determine the type of mechanical forces the cell is

exposed to. For example, endothelial cells sense the direction and strength of blood flow through the hydrodynamic drag applied to their nucleus and resulting changes in its position. This change in nuclear positioning is essential for polarization of these cells against the flow (Tkachenko et al., 2013). During cell migration, change in nuclear position defines the front and rear polarity of the cell. Integrin activation in the lamellipodium leads to downstream activation of FAK, SRC kinases followed by induction of p190RhoGAP signaling. This further leads to activation of Rho, which brings about repositioning of the nucleus by modulating actin dynamics (Maninová et al., 2013).

1.4.2 Regulation of physical attributes of the nucleus (nuclear shape, size and deformability)

The karyoplasmic (nucleus/cytoplasm) ratio is an important modulator of cellular processes like cell cycle progression and is known to be disturbed in diseases such as cancers (Yen and Pardee, 1979; Futcher, 1996; Sato et al., 1994; Schmidt and Schibler, 1995; Zink et al., 2004; Slater et al., 2005; Roca-Cusachs et al., 2008). The robust maintenance of N/C ratio was demonstrated by Harris in 1967, wherein implantation of small nuclei from hen erythrocytes into HeLa cells resulted in expansion of the nuclei to a size appropriate for their new environment (Harris, 1967). Nuclear size is also tightly controlled by monitoring the nucleus/cytoplasm ratio in fission yeast. This ratio needs to be constant for normal cellular processes and the cell actively regulates nuclear size depending on this ratio. If the N/C ratio is high, nuclear growth is arrested and only the cell grows, whereas if this ratio is low, rapid nuclear growth occurs (Neumann and Nurse, 2007). In *Drosophila*, developmental control of nuclear shape and size during the process of cellularization is maintained by the proteins Kugelkern and Kurzkern. Their absence results in defective nuclear elongation, and as onset of zygotic transcription and rearrangement of chromatin architecture is associated with correct nuclear elongation, defects are also observed in these two processes

(Brandt et al., 2006). Since both Kugelkern and Kurzkern localize to the inner nuclear membrane and Kugelkern has a CxxM motif (site for farnesylation, lamins being the other nuclear proteins with this motif), this suggests a putative role for NE proteins in relaying mechanical and biochemical signals to the nucleus.

It is interesting to note that reduction in nuclear size during the progressive stages of frog, chicken and mouse development coincides with changes in Lamin isoform expression (Stick and Hausen, 1985; Lehner et al., 1987; Rober et al., 1989). Additionally, Lamin A/C and Lamin B Receptor are important regulators of the nuclear shape in neutrophils – cells of the immune system which are famous for their multi-lobulated nuclei. Lamin A/C is downregulated in neutrophils during granulopoiesis, which leads to the formation of highly deformable and multi-lobulated nuclei characteristic of these cells, which further facilitates migration through narrow constrictions (Rowat et al., 2013). Mutations in Lamins and Emerin (for e.g. Lamin A G608G in Hutchison-Gilford Progeria Syndrome, Emerin Δ236-241 and Δ95-99 in Emery-Dreifuss Muscular Dystrophy) and alterations in their levels either by RNAi or overexpression have been well studied in changing nuclear shape, deformability as well as nuclear mechanotransduction (Liu et al., 2000; Fairley et al., 2002; Furukawa et al., 2003; Lammerding et al., 2005; Capell and Collins, 2006; Polychronidou and Grosshans, 2011; Booth-Gauthier et al., 2013; Davidson et al., 2014; Mitchell et al., 2015; McGregor et al., 2016; Reis-Sobreiro et al., 2018).

Changing physical properties of the ECM leads to coordinated changes in the nuclear shape and size. Cells grown on polyacrylamide or collagen gels of varying elastic moduli or adhesive areas, on micro-pillared surfaces or on topographically patterned substrates with grooves and ridges show

changes in the nuclear shape, size and deformability depending on the mechanical forces that are generated in response to the substratum (Bray et al., 2010; Dahl et al., 2008; McKee et al., 2011; Pan et al., 2012). The transduction of these forces is dependent on the network of actin filaments. The actin cap is essential for maintenance of nuclear shape on fibronectin coated micropatterns of varying dimensions (Khatau et al., 2009). Actin cap, anchored to the nucleus by LINC complex, exerts a compressive load on the nucleus (Fabrikant et al., 2013) and transduces low physiological mechanical stresses (e.g. shear stress of 0.05 dyne/cm^2) at fast time scales (~30 secs) (Chambliss et al., 2013).

Force transduction into the nucleus depends on the focal adhesion-associated proteins (talin, zyxin) on one hand and the LINC complex, nuclear lamina and nuclear envelope proteins (like emerin) on the other hand (Chambliss et al., 2013). Shear and compression induced changes in the elastic modulus of the nucleus - leading to changes in its deformability, are mediated by the cytoskeleton via the LINC complex (Caille et al., 2002; Deguchi et al., 2005). Thus, it is interesting to note that the perinuclear actin cap formation as embryonic stem cells differentiate (both mouse and human) is dependent on the proper expression and localization of the LINC complex and Lamin A/C [actin cap is absent in stem cells, (Khatau et al., 2012a)]. These results establish that changes in mechanical properties of the ECM or cell are transduced to the nucleus via the integrin-cytoskeleton-LINC complex bridge that brings about corresponding changes in physical properties of the nucleus. These changes also elicit specific gene expression programs that further define the cellular state.

1.4.3 Effect on genome organization and gene expression

It has been demonstrated that the extracellular environment drives a plethora of changes in cellular and nuclear structure, and that these ECM-mediated changes are transduced across the cytoplasm via the ECM-integrin-cytoskeleton-LINC complex bridge to the nucleus. On reaching the nucleus, these signals (either direct mechanical stress waves, or changes in ion concentrations due to opening/closing of mechanosensitive ion channels or direct biochemical signals) have to elicit a functional response at the level of the genome. Thus, chromatin reorganization and gene expression changes are typically considered as the functional consequences of these mechanical or biochemical stimuli.

SUN1, a SUN-domain containing component of the LINC complex, interacts with the shelterin complex present at the telomeres and clusters telomeres towards the nuclear periphery (Crabbe et al., 2012; Ding et al., 2007; Ferreira et al., 2013; Scherthan et al., 2011). KASH5, a KASH-domain containing component of the LINC complex, interacts with microtubule-associated dynein-dynactin complex (Horn et al., 2013; Morimoto et al., 2012; Stewart and Burke, 2014). By virtue of the above interactions, the SUN-KASH complex brings about movement of chromosomes to facilitate their rearrangement and homologous pairing during meiosis (Chikashige et al., 2007). Such LINC complex mediated movements may also be used for transmitting mechanical signals from the cytoskeleton to the genome in interphase nuclei.

Since mechanical signals are also transduced into the nucleus via opening/closing of mechanosensitive ion channels (Wiegert and Bading, 2011), a direct consequence of such a change in ion concentrations is a corresponding change in osmotic conditions. Rapid changes in osmolality

can induce alterations in nuclear shape, size and chromatin condensation. Hyperosmotic conditions induce the nucleus to shrink and the chromatin to condense, while hypoosmotic conditions cause nuclear swelling and chromatin decondensation (Delpire et al., 1985; Finan et al., 2011; Irianto et al., 2013; Oswald et al., 2006). While these changes are uniformly transduced in a 2D monolayer of chondrocytes, the changes in nuclear shape/size and chromatin condensation are non-uniform in a 3D agarose culture. This is attributed to the difference in the number and nature of adhesion contacts being formed in 2D vs 3D and the resultant differential mechanotransduction (Irianto et al., 2013). Modulating cell shape by growing endothelial cells on fibronectin coated adhesive islands of different geometries, leads to alterations in both the cell shape index (CSI) and the nuclear shape index (NSI). Lateral compression of cells is characterized by decrease in CSI and increase in NSI, which further leads to increased chromatin condensation (Versaevel et al., 2012). Similarly, laser micro-dissection of perinuclear actin fibers relieves the constraint on nuclear shape further leading to chromatin decondensation (Nagayama et al., 2011). These results indicate the importance of the cytoskeleton in mechanotransduction induced changes in genome condensation that can have a functional implication in regulation of gene expression.

Chromosome condensation is generally associated with decreased gene expression levels wherein a more condensed region of the genome is inaccessible to transcription factors and hence is transcriptionally less active (Martin and Cardoso, 2010; Sproul et al., 2005; van de Corput et al., 2012; Wang et al., 2014). Embryonic stem cell genome is characterized by a general decondensed state and hyper-dynamic chromatin (Mattout and Meshorer, 2010; Melcer and Meshorer, 2010; Meshorer et al., 2006; Talwar et al., 2013). As these cells undergo differentiation towards a specific lineage, chromatin is condensed to silence genes associated with other lineages, cell and nuclear

stiffness increases, Lamin A/C is upregulated to decrease nuclear deformability and the cytoskeletal network is reorganized (Bártová et al., 2008a; Bošković et al., 2014; Constantinescu et al., 2006; Melcer et al., 2012; Yourek et al., 2007). Interestingly, these changes are triggered even before actual differentiation, at a stage when the stem cells have just initiated repression of pluripotency associated transcription factors like Nanog, Oct4 and Sox2 (Chalut et al., 2012). Taken together, an accurate regulation of nuclear position, shape, size, deformability and osmotic balance is required for correct response to extranuclear signals.

1.5 Nuclear envelope as an integrator and regulator of extranuclear signals

For the nucleus to act as a precise sensor of diverse stimuli, it is essential that all the extranuclear signals are faithfully relayed to it. During this relay, nuclear envelope behaves as an integrator of the signals before transmitting them to the genome. This regulation is mediated by the LINC complex in the perinuclear space, mechanosensitive proteins like emerin in the inner nuclear membrane (INM) and the nuclear lamina between INM and peripheral heterochromatin (Wilson and Berk, 2010).

1.5.1 Non-random and territorial organization of the genome

Each chromosome occupies a distinct sub-volume in the interphase nucleus known as ‘chromosome territory’ (CT) and these chromosome territories are non-randomly organized either depending on their i) gene density (No. of genes/Mbp) – chromosomes with higher gene density are positioned towards the nuclear interior and gene poor chromosomes are proximal to the nuclear periphery, or ii) size – smaller chromosomes are positioned near the nuclear interior and larger chromosomes towards the nuclear periphery (Bolzer et al., 2005; Cremer et al., 2003; Sun et al.,

2000). The non-random organization of at least the most gene rich – Chr. 19 and most gene poor – Chr. 18, has remained conserved across evolution over millions of years and is partially maintained in many tumor cell nuclei (Tanabe et al., 2002). Moreover, even artificially introduced extra copies of human chromosomes 7, 18 or 19 tend to occupy conserved gene density-based positions similar to their diploid counterparts (Sengupta et al., 2007). Interestingly in mouse-human hybrid nuclei, human chromosomes occupy positions in the mouse nucleus which are similar to those of their syntenic mouse counterparts, and not based on gene density (Meaburn et al., 2008; Sengupta et al., 2008). Insights into genome organization in the interphase nucleus largely performed using chromosome painting methodologies like 2-dimensional and 3-dimensional Fluorescence *In Situ* Hybridization (2D and 3D FISH) have also been complemented by high-throughput approaches of chromosome conformation capture (CCC) like 3C, 4C, 5C and Hi-C that map contact frequencies of chromatin (Lieberman-Aiden et al., 2009; van Berkum et al., 2010). Hi-C contact maps show greater cis interaction of chromosomes than trans, further re-iterating territorial confinement of chromosomes (Kalhor et al., 2011). Another aspect of genome organization is the distance between different chromosomes or 'chromosome neighborhoods' (De and Babu, 2010). This is particularly important in i) spatial clustering of co-regulated genes present on different chromosomes (Fraser and Bickmore, 2007; Göndör and Ohlsson, 2009; Schoenfelder et al., 2010) and ii) understanding patterns of chromosomal translocations, since higher frequency of translocations is correlated with spatial closeness of the chromosomes (Parada et al., 2002; Parada et al., 2004; Roix et al., 2003). Though not completely understood, the mechanisms of genome organization include regulation by both chromatin intrinsic as well as extrinsic factors.

Figure 1.1

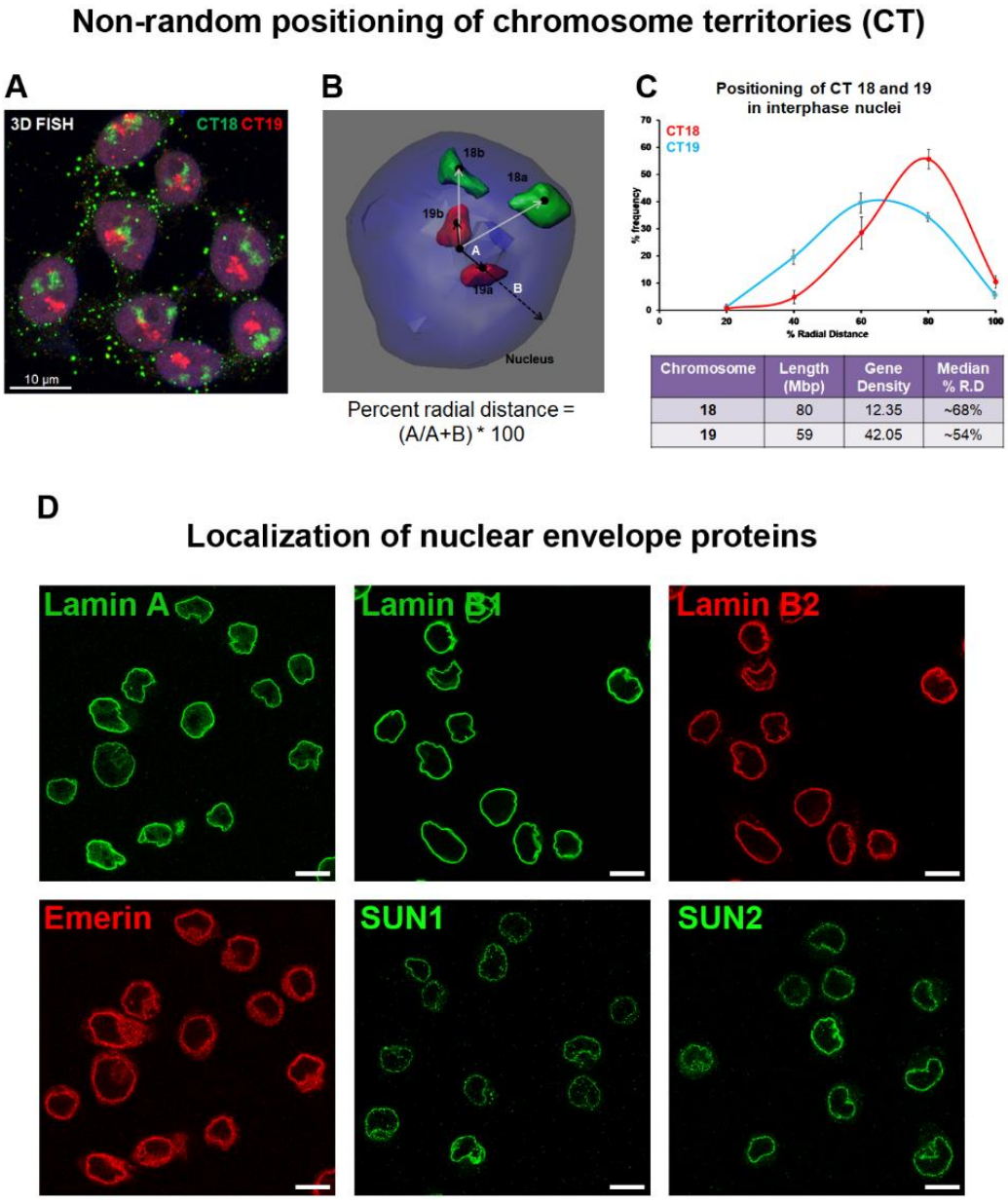

Figure 1.1 Non-random positioning of chromosome territories. A) Representative maximum intensity projection of confocal z-stacks showing 3D-FISH hybridization for CT18 (gene poor, peripheral) and CT19 (gene rich, internal) in diploid DLD-1 adenocarcinoma cells. B) 3D reconstruction of a single representative nucleus depicting radial positioning analysis of chromosome territory positions. C) % Radial distance distribution profile of CT18 and 19 in DLD-1 cells, representing the gene density based positioning of gene poor CT18 towards the nuclear periphery and CT19 towards the nuclear interior. **Localization of nuclear envelope proteins.** D) Localization of nuclear envelope proteins – Lamins, Emerin and SUN proteins, is predominantly observed near the nuclear periphery in DLD-1 cells grown on glass. **Scale bar ~10 µm.**

1.5.2 Nuclear envelope proteins and tissue specific genome organization

It is important to note that despite the large extent of conservation observed in genome organization, tissue and cell type specific differences still exist. Most human chromosomes except 8, 20 and 21 are similarly positioned in lymphoblast and dermal fibroblast nuclei (Boyle et al., 2001; Meaburn et al., 2008). This cell type specific positioning of certain chromosome territories is observed in murine and porcine lymphoblasts and fibroblasts as well (Foster et al., 2012). Although extensive studies for tissue specific CT positions have not been performed *in vivo,* analyses of chromosomes 1, 5, 6, 12, 14 and 15 in primary cells freshly isolated from a variety of mouse tissues by Parada *et al* highlighted important variations in CT positions across tissue types. HSA 5 is located towards the nuclear interior in liver cells, towards the nuclear periphery in small and large lung cells and at an intermediate position in lymphocytes (Parada et al., 2004). Analyses of positions of the aforementioned chromosomes in kidney, liver, large/small lung cells, lymphoblasts and myeloblasts revealed that all chromosomes were positioned differentially in at least 3 cell types. Additionally, distinct patterns of inter-chromosomal distances and chromosome neighborhoods were also observed in each cell type further suggesting that the tissue environment and function can fine-tune genome organization (Parada et al., 2004).

Of note, even smaller genomic entities like gene loci demonstrate non-random and tissue specific positioning (Zink et al., 2004). Independent subsets of gene loci are repositioned in breast and prostate cancer cells as compared to their normal counterparts (Meaburn et al., 2009; Meaburn et al., 2016). In many instances, gene loci are known to reposition depending on their transcriptional status. Clusters of functionally related genes like the epidermal differentiation cluster (on Chr. 1) or the major histocompatibility complex (on Chr. 6) have been shown to ‘loop out’ of their

chromosome territories in cell types where they are overexpressed (Volpi et al., 2000; Williams et al., 2002). Additionally, gene clusters that are induced in response to environmental stress show movement towards transcriptionally permissive sub-compartments of the nucleus for enhanced expression - for instance, the movement of heat shock protein 70 (Hsp70) gene locus towards the nuclear speckles (Khanna et al., 2014). Tissue and cell type specificity in spatial locations of large genomic entities like chromosome territories as well as smaller gene loci hint towards unifying mechanisms that establish a particular 3D genomic configuration depending on cell function and specialization. Proteomic studies have identified many Nuclear Envelope Transmembrane proteins (NETs) that are differentially expressed in tissues and reversibly reposition certain gene loci and chromosome territories upon altered expression (de Las Heras et al., 2017; Korfali et al., 2012; Zuleger et al., 2013). For instance, overexpression of NET29 and NET39 in HT1080 (human fibrosarcoma) cells repositions chromosomes 5 and 13 towards the nuclear periphery, while co-depletion of NET45 and NET47 – that are highly expressed in human liver cells, repositions Chr. 5 towards the nuclear interior in HepG2 (hepatocellular carcinoma) cells (Zuleger et al., 2013). Tissue specific expression of NETs could potentially establish an initial organization of genome which is further reinforced by ubiquitously expressed nuclear envelope proteins.

Nuclear lamins are type V intermediate filament proteins with documented roles in a variety of processes like DNA replication, transcriptional regulation, chromatin silencing, DNA damage response and maintenance of nuclear structure among others (Butin-Israeli et al., 2015; Dechat et al., 2008; Ghosh et al., 2015; Gibbs-Seymour et al., 2015; Ranade et al., 2017; Shumaker et al., 2008; Singh et al., 2013). More importantly, Lamins are regulators of genome organization and chromosome territory positions (Malhas et al., 2007; Mewborn et al., 2010; Osmanagic-Myers et

al., 2015; Prokocimer et al., 2009; Shimi et al., 2008; Taimen et al., 2009). The A-type (Lamin A and C, splice variants encoded by *LMNA*) and B-type (Lamin B1 and B2, encoded by *LMNB1* and *LMNB2* respectively) lamins form independent as well as interdependent and interacting networks below the INM and bind chromatin either directly or indirectly (Shimi et al., 2008; Shimi et al., 2015). Lamins are one of the proteins that bind chromatin at the Lamina Associated Domains (LADs), which are 0.1-10 Mb stretches of chromatin characterized by presence of H3K9me2/3, low density of protein coding genes and more enrichment on gene poor and peripherally positioned chromosomes like Chr. 18 (Guelen et al., 2008; Meuleman et al., 2013). LADs are collectively bound by Lamins and many of the nuclear envelope proteins like emerin, Lap2β (Lamina Associated Polypeptide), LBR (Lamin B Receptor) (Amendola and van Steensel, 2015; Kind and van Steensel, 2014; Peric-Hupkes and van Steensel, 2010). While LADs bound by B-type lamins are predominantly heterochromatic in nature, those bound by Lamin A/C are enriched in both euchromatin and heterochromatin (Gesson et al., 2016; Oldenburg and Collas, 2016; Zheng et al., 2015). Live imaging studies for LADs across cell cycle using m6A-Tracer technology revealed the stochastic nature of LADs where the same LAD profile is not observed in mother and daughter cells (Kind et al., 2013). Additionally, despite the engagement of many nuclear envelope proteins, LADs are not restricted only to the nuclear periphery (Kind et al., 2013). LAD profiles are also altered during differentiation and lineage specifying genes present in LADs are generally activated and positioned away from the nuclear periphery as a result (Peric-Hupkes et al., 2010).

Interestingly, in addition to the variable levels of the Lamins across cell types, Lamin A expression has been shown to scale with tissue stiffness (Swift et al., 2013). Given the i) lower expression of Lamin A/C in embryonic stem cells, ii) presence of B-type lamins in most cell types including

ESCs and iii) induction of increased Lamin A/C expression upon stem cell differentiation (Constantinescu et al., 2006; Eckersley-Maslin et al., 2013); Lamins could act as modulators of genome organization in a tissue or cell type specific manner. Furthermore, emerin (direct interactor of Lamin A/C) and LINC complex proteins regulate nuclear mechanotransduction (Guilluy et al., 2014; Lammerding et al., 2005; Rowat et al., 2006). Thus, the specific interactors of A-type (emerin, LAP2α, BANF1, LINC complex proteins, LEM2, MAN1 among others) and B-type Lamins (LBR, HP1, LAP2β among others) and the differences in stoichiometries of Lamins themselves could possibly supplement and reinforce the tissue specific genome organization, initiated by tissue specific NETs beforehand (Brachner et al., 2005; Clements et al., 2000; Dechat et al., 2000; Lee et al., 2001; Liang et al., 2011; Libotte et al., 2005; Mislow et al., 2002; Sakaki et al., 2001; Wilson and Foisner, 2010; Ye et al., 1997). Lamins directly interact and sequester several transcription factors at the nuclear periphery like c-Fos, Rb, SREBP1, MOK2 and OCT1 (Capanni et al., 2005; Dreuillet et al., 2002; Heessen and Fornerod, 2007; Imai et al., 1997; Ivorra et al., 2006; Johnson et al., 2004). LEM domain containing proteins like emerin, LAP2β and MAN1 also interact with a variety of transcription factors like β-catenin, rSmads, Lmo7, GCL, BTF among others and regulate their target gene expression (Bengtsson, 2007; Cohen et al., 2007; Haraguchi et al., 2004; Holaska et al., 2003; Holaska et al., 2006; Ishimura et al., 2006; Lin et al., 2005; Markiewicz et al., 2006). Thus lamins, along with their interacting proteins, are potential effectors of changes in chromatin architecture and gene expression in response to both mechanical and biochemical signals.

1.5.3 Nuclear envelope proteins and disease

Absence or mutations in either the LINC complex, the nuclear envelope proteins or the nuclear lamins leads to a spectrum of disorders known as "Nuclear Envelopathies". These include Hutchison Gilford Progeria Syndrome (HGPS), Emery-Dreifuss Muscular Dystrophy (EDMD), Duchenne Muscular Dystrophy (DMD), Cerebellar ataxia, Arthrogryposis, Adult onset leukodystrophy, Partial lipodystrophy, atypical Werner syndrome and dilated cardiomyopathies (Bonne and Quijano-Roy, 2013; Burke et al., 2001; Chi et al., 2009; Nagano and Arahata, 2000; Somech et al., 2005; Worman et al., 2010). Many of these disorders show abnormal nuclear morphology and impaired mechanotransduction to the genome. For instance, examination of fibroblasts derived from mouse models of Progeria/EDMD or actual human patients, Lamin A null cells or cells with Lamin A mutations (e.g. L530P) shows a defective nucleo-cytoskeletal coupling and hence, a compromised cellular force balance due to mislocalization of the LINC complex proteins and disruption of the perinuclear actin cap (Hale et al., 2008; Khatau et al., 2009). These cells also show a decrease in the nuclear viscosity and elasticity as compared with their normal counterparts (Celedon et al., 2011). In case of progeroid MAFs (mouse adult fibroblasts), the absence of correct mechanosensation can be attributed to the defective synthesis of the extracellular matrix coupled with reduced Lef-1 dependent transcription due to inhibition of Wnt/β-catenin signaling pathway (Hernandez et al., 2010). Thus, laminopathy disease models reiterate the importance of a functional ECM, ECM-dependent signal transduction to the nucleus and an intact cytoskeletal network in normal cell growth and proliferation.

An imbalance in growth, proliferation, differentiation and apoptosis leads to the induction of a cancerous phenotype in normal cells. The progression of cancer from being a resident tumor to a

metastasizing mass of cells is dependent on its ECM (Lu et al., 2012; Reuter et al., 2009). Early studies have shown that the absence of an intact basal lamina/basement membrane and resulting distribution of ECM proteins leads to neoplastic disorganization of tissue architecture (Ingber et al., 1981). Along similar lines, it is now being appreciated that the biophysical properties of the ECM also regulate cancer progression (Baker et al., 2009; Beck et al., 2013; Nguyen-Ngoc et al., 2012). Cancer cells migrate non-proteolytically on matrices of low stiffness and proteolytically on matrices of higher stiffness (Ehrbar et al., 2011). In order for a cell to migrate and metastasize, a cell should be able to squeeze through even very minute openings and hence, it follows that a highly metastatic population of cancer cells will be more deformable – at the cellular as well as at the nuclear level (Badique et al., 2013). Interestingly, migration of cells in 3D is dependent on the organization of the perinuclear actin cap by the LINC complex and the ensuing deformation of the nucleus (Khatau et al., 2012b). It is possible that nuclear deformability could be an important parameter that dictates nuclear architecture and genome organization/regulation changes during cancer progression.

1.6 Open questions

Although it has been well established in the field that changing ECM properties leads to corresponding changes in the genome via the integrin-cytoskeleton-LINC complex bridge, the molecular mechanisms acting downstream of the LINC complex have not been completely elucidated. Once the extracellular signal reaches the LINC complex, it is possible that (Fig 1.2) – i**)** stretch/stress induced changes in the cytoskeletal network bring about decondensation and further activation of specific regions in the peripheral facultative heterochromatin (by virtue of its being closest to the nuclear envelope) (Fig 1.2A-B),

ii) LINC complex proteins and nuclear lamins sequester certain transcription factors (TFs) or co-activators to the nuclear periphery. Mechanical loading of the LINC complex brings about conformation changes such that the sequestered TFs are released, and the expression of specific target genes is induced (Fig 1.2C),

iii) extra-nuclear signals are passed on from the cytoskeleton to the nucleoskeleton and nuclear lamins, by the LINC complex and INM proteins, which leads to changes in the nucleoskeleton further bringing about rearrangements of large chromosome domains/territories (Fig 1.2D),

iv) extra-nuclear signals bring about changes in the binding of matrix attachment regions (MARs) to the nuclear matrix proteins and re-localize genomic regions from a transcriptionally repressive to a more permissive environment or vice versa (Fig 1.2E),

v) genomic sub-regions could either gain or lose direct or indirect binding to the LINC complex components and nuclear lamins in response to signal transduction into the nucleus (Fig 1.2F).

Figure 1.2

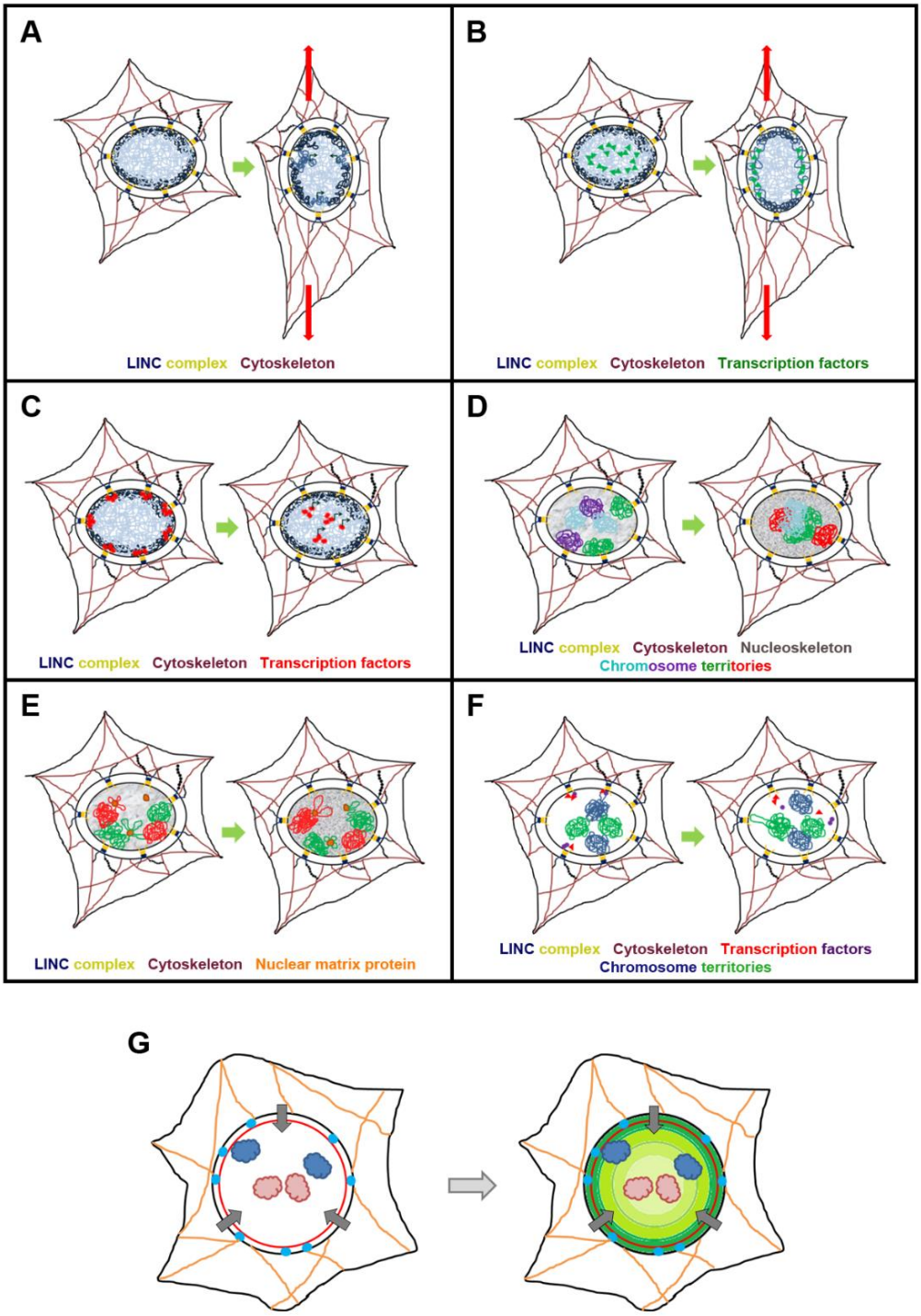

Figure 1.2 Possible downstream genomic responses to extranuclear signals, relayed via nuclear envelope proteins.

Both mechanical and biochemical signaling can induce a reorganization of the genome and changes in nuclear architecture, either independently or in a coordinate manner. However, how the relatively rapid mechanical signals are transmitted and integrated with the slower diffusion based biochemical signals is as yet unknown. Does a subset of genome regulatory events strictly necessitate smaller time scales for signal transduction while for other events, slower transmission of extranuclear cues is permissible? For instance, since the genome present towards the center of the nucleus (predominantly gene rich chromosomes) is farther away from the nuclear envelope, does signal transduction to the euchromatin and gene rich chromosomes need to be faster as compared to the transmission to the regions at the nuclear periphery (predominantly gene poor chromosomes) which are much closer to the nuclear envelope? Is the response to a mechanical or biochemical signal elicited in a graded manner wherein the region of the genome closest to the signal transducer is the first responder? (Fig 1.2G). In such a scenario, one can expect that the genes present on chromosomes proximal to the nuclear periphery are more responsive to external stimuli compared to genes on chromosomes present towards nuclear interior. However, it is important to remember that regulation of gene expression is a multifactorial phenomenon and position of the gene is just one of those factors.

Tissue specific organization of the genome – both at the level of chromosome territories as well as small gene loci, begs the question as to how this organization is dynamically regulated. While NETs, nuclear lamins and inner nuclear membrane protein may be players in this process, the sequence of signaling events that triggers this organization is poorly understood. Bearing in mind the observations that embryonic stem cell genome is highly pliable and dynamic, and that tissue specific genome organization is achieved post-differentiation; it is important to understand how

genomic rearrangements are facilitated to ensure a highly specialized and function-oriented configuration as seen in terminally differentiated cells. Interestingly, as a follow-up to this question, is it possible to alter tissue specific chromosome territory positions and gene expression profiles if terminally differentiated cells from a particular tissue are exposed to matrices mimicking *in vivo* stiffness properties of a completely different tissue? Understanding the relay of extranuclear signals (mechanical and biochemical) into the genome and their underlying regulation by the nuclear envelope proteins in a cell and tissue specific manner is an ongoing exercise in this field. We were therefore interested in understanding how extranuclear signals – both biochemical and mechanical, are relayed to the genome by nuclear lamins and nuclear envelope proteins, and the resulting changes in genome organization and transcriptional profiles. We approached this central question through the following sub-aims –

1. Impact of altered extracellular substrate stiffness on genome organization and function
2. Role of nuclear envelope factors - Lamins and Emerin in genome reorganization in response to altered substrate stiffness
3. Role of nuclear lamins in the regulation of heat shock signaling

Chapter 2: Materials and methods

2.1 Methods commonly used throughout the study

2.1.1 Cell Culture

Cells in culture were maintained either in RPMI (Invitrogen, RPMI 1640, 11875-093) or DMEM media (Invitrogen, DMEM high glucose, 11995-073) supplemented with 10% Fetal Bovine Serum (FBS, Invitrogen, 6140-079 Carlsbad, USA) and antibiotics - Penicillin (100 U/mL) and Streptomycin (100 μg/ml, Invitrogen, 15070-063) at 37°C with 5% CO_2. All cell lines were authenticated by karyotyping. Cells in culture were routinely tested and found to be free of mycoplasma contamination.

Table 2.1 Cell lines used in this study

Name of cell line	Origin	Source	Cell culture media used
DLD-1 (used for most of the assays in this study)	Colorectal adenocarcinoma	Dr. Thomas Ried Lab, NIH, USA	RPMI 1640 + 10% FBS
SW480	Colorectal adenocarcinoma	Dr. Thomas Ried Lab, NIH, USA	DMEM + 10% FBS
A549	Lung carcinoma	Dr. Amit Dutt Lab, ACTREC, India	DMEM + 10% FBS
HT1080	Fibrosarcoma	ATCC	DMEM + 10% FBS
MCF7	Breast adenocarcinoma	Dr. Mayurika Lahiri Lab, IISER Pune, India	DMEM + 10% FBS
HCT116	Colorectal carcinoma	Dr. Mayurika Lahiri Lab, IISER Pune, India	DMEM + 10% FBS
U2OS	Osteosarcoma	Dr. Mayurika Lahiri Lab, IISER Pune, India	DMEM + 10% FBS

2.1.2 Preparation of metaphase spreads

Cells were blocked in metaphase using Colcemid (0.1µg/ml) for 90 mins. Hypotonic treatment (using 0.075 M KCl) was performed for 45 mins followed by fixation in 5-6 drops of fixative (Methanol:Acetic Acid, 3:1). After four washes in the fixative, cells were dropped onto glass slides and metaphases were stained with DAPI.

Table 2.2 Modal chromosome numbers of cell lines used in this study

Name of cell line	Modal chromosome number documented in literature	Modal chromosome number obtained by DAPI karyotyping
DLD-1 (Fig 3.3A)	44-46	45-46
SW480	52-58	57
A549	66	66
HT1080	46 (Range 44-48)	45-46
MCF7	82 (Range 66-87)	73
HCT116	44-46	44
U2OS	Both hyper-triploid and hypo-diploid populations are observed	47 (with ~60% nuclei showing >2 copies of Chr. 19)

Data acknowledgement for karyotyping

SW480: Devika Ranade

A549 and HCT116: Maithilee Khot

MCF7: Ayantika Sen Gupta

2.1.3 Immunofluorescence Assay

Cells plated on coverslips or polyacrylamide gels were washed twice using 1X PBS (5 minutes)

followed by fixation with 4% Paraformaldehyde (PFA, Sigma, 158127) prepared in 1X PBS (pH 7.4) for 12 mins. Cells were permeabilized in 0.5% Triton-X-100 (prepared in 1X PBS) and blocked in 1% BSA (Sigma, A2153) solution. Primary and secondary antibody incubations were carried out for 90 and 60 mins respectively. Washes post primary antibody incubation were carried out using 1X PBST (PBS + 0.1% Triton X-100). Cells were counterstained with 0.05 μg/ml 4',6-Diamidino-2-Phenylindole (DAPI) for 2 minutes at RT, washed in 1X PBS for 3-4 mins, mounted in Slowfade Gold Antifade (Invitrogen, S36937) and stored in 4°C until they were imaged. Quantification of fluorescence intensities from the acquired confocal images was done in ImageJ (Schneider et al., 2012) by selecting the mid-optical section and plotting an intensity profile for the line-scans manually drawn across each nucleus.

Following primary antibodies were used - Rabbit anti-Lamin A (ab26300, 1:500), Rabbit anti-Lamin B1 (ab16048, 1:500), Mouse anti-Lamin B2 (ab8983, 1:400), Mouse anti-Emerin (SC-25284, 1:500), Rabbit anti-SUN1 (ab125770, 1:500), Rabbit anti-SUN2 (ab124916, 1:500), Rabbit anti-H3K27Me3 (07-449, 1:500), Rabbit anti-H3K4Me3 (07-473, 1:500) and Rabbit anti-Hsp70 (ab47455, 1:250). Primary antibody dilutions were prepared in 0.5% BSA solution.

Phalloidin conjugated to Alexa-488 (A12379, 1:100) and secondary antibodies - Goat anti-Rabbit Alexa-488 (A11034, 1:1000), Goat anti-Rabbit Alexa-633 (A21070, 1:750) and Goat anti-Mouse Alexa-568 (A11004, 1:1000) were used. Secondary antibody dilutions were prepared in 1X PBST (1X PBS + 0.1% Triton X-100).

2.1.4 Western blotting

Cell lysates were prepared using Radio Immuno-Precipitation Assay (RIPA) Buffer and quantified using BCA (Bicinchoninic Acid) Kit (Pierce, 23225). Samples were denatured by boiling in 4X

Laemmli's Buffer and resolved on 10% or 15% acrylamide-bisacrylamide gel, followed by transfer to an activated PVDF membrane at constant voltage of 90V for 100 mins. Membrane post-transfer was blocked in 5% non-fat dried milk prepared in 1X TBST (Tris Buffered Saline + 0.1% Tween20). Primary and secondary antibody dilutions were prepared in 0.5% milk in 1X TBST. Blots were developed using chemiluminescent substrate (GE ECL Prime, 89168-782) and images acquired at incremental exposures of 10 seconds under a chemiluminescence system LAS4000 (GE). Band intensity analyses were performed manually using the ImageJ 'Plot Lanes' tool.

Following molecular weight markers were used: Precision Plus Protein Dual Color Standards (250-10 kDa, Biorad, Cat. No. 161-0374) and SeeBlue Prestained ladder (198-3 kDa, Invitrogen, P/N 100006636).

Primary antibodies used were: Rabbit anti-Lamin A (ab26300, 1:1000), Mouse anti-Lamin A/C (ab40567, 1:200), Rabbit anti-Lamin B1 (ab16048, 1:1000), Mouse anti-Lamin B2 (ab8983, 1:400), Rabbit anti-Lamin B2 (AV46356, 1:500), Rabbit anti-Emerin (06-1052, 1:3000), Rabbit anti-Emerin (ab40688, 1:1500), Rabbit anti-SUN1 (ab74758, 1:1000), Rabbit anti-SUN2 (ab124916, 1:1000), Rabbit anti-H3K4me3 (Millipore 07-473, 1:500), Rabbit anti-H3K27me3 (Millipore 07-449, 1:500), Rabbit anti-Histone H3 (ab1791, 1:1000), Mouse anti-Actin (ab3280, 1:400), Rabbit anti-GAPDH (G9545, 1:5000), Rat anti-Tubulin (ab6161, 1:6000) and Mouse anti-Phospho-tyrosine conjugated with HRP (610011, 1:1000).

Secondary antibodies used were Sheep anti-mouse IgG-HRP (NA9310V, 1: 10,000), Donkey anti-rabbit IgG HRP (NA9340V, 1:10000) and Goat anti-rat IgG-HRP (ab97057, 1: 10,000).

2.1.5 3-Dimensional Fluorescence in situ hybridization (3D-FISH)

Fixation

Cells on glass coverslips (18X18 mm or 22X22 mm) and softer polyacrylamide matrices for 90 minutes were washed thrice in 1X PBS (5 mins), incubated on ice for 6-7 mins in CSK buffer (0.1 M NaCl, 0.3 M Sucrose, 3 mM MgCl2, 10 mM PIPES (pH 7.4), 0.5% Triton-X-100) and immediately fixed in 4% Paraformaldehyde (PFA, pH 7.4) for 15 mins. Permeabilization was performed in 0.5% Triton-X-100 for 15 mins and incubation in 20% glycerol for 60 mins followed by 4-5 freeze-thaw cycles in liquid nitrogen. Cells were washed in 1X PBS (thrice/5 mins) and incubated in 0.1 N HCl for 10 mins followed by 1X PBS washes (thrice/5 mins). Cells were stored in 50% formamide (FA)/2X SSC (pH 7.4) overnight at 4°C or until used for hybridization.

Hybridization

Chromosome painting probes were obtained from Applied Spectral Imaging (ASI, Israel) and MetaSystems (Germany). Probes were pre-warmed at 37°C for 5 minutes (with agitation at 750 rpm on a thermomixer) followed by denaturation at 80°C for 5 min (82°C for MetaSystems probes), and quick chilled on ice for 2 minutes followed by pre-annealing at 37°C for 45 minutes. Denatured probe (5 μl) was spotted onto fixed cells and subjected to co-denaturation at 80°C for 10-12 mins (2 kPa matrix and glass coverslips) and 15 mins (55 kPa matrix). Hybridization was carried out for 48 hours in a humidified box at 37°C.

Detection

Post hybridization, coverslips were washed in 50% FA/2X SSC (pH 7.4), thrice/5 mins each at 45°C, followed by 0.1X SSC washes (thrice/5 mins) at 60°C. Coverslips were counterstained with DAPI for 2 mins, washed in 2X SSC (Saline Sodium Citrate), mounted in Slowfade Gold Antifade and stored at 4°C until imaged.

Imaging

Confocal images were acquired on Zeiss LSM 710 confocal microscope (Carl Zeiss, Thornwood, NJ, USA) and Leica TCS SP8 confocal laser scanning microscope. LSM/LAS X image stacks were processed using Image Pro Plus software (v 7.1).

Radial distance measurements of chromosome territories

3D reconstructions and distance measurements were performed using Image-Pro Plus software (v 7.1). Briefly, LSM or LASX files with optical sections (z = 0.34 μm) of hybridized nuclei were subjected to 3D surface rendering. Individual nuclei were cropped for 3D reconstruction. The acquired images were thresholded for each of the red, green and blue channels. The geometric centers of the DAPI stained nucleus (blue channel) and the chromosome territories (red and green channels) were determined using Image-Pro Plus software, and the distance between the center of the nucleus and that of the territory was measured (R). The vector R from the center of nucleus (N) to that of the chromosome territory (C) was extended to a third collinear point on the nuclear periphery (B). The distance (Y) between the center of the nucleus and point B was calculated. The relative distance of a chromosome territory from the center of the nucleus was expressed as a percentage of its total distance from the center of the nucleus to the nuclear periphery, %Radial Distance = (R/Y) X 100 (Tanabe et al., 2002).

2.1.6 Imaging and acquisition parameters

Confocal images were acquired on Zeiss LSM 710 confocal microscope (Carl Zeiss, Thornwood, NJ, USA) with 63X Plan-Apochromat 1.4 NA oil immersion objective using charge-coupled device camera (AxioCam MRm Rev.3, Zeiss), ZEN software and scan zoom of 2.0-2.5. Z-stacked images were acquired at 512 X 512 pixels per frame using 8-bit pixel depth for each channel at a

voxel size of 0.105 μm X 0.105 μm X 0.34 μm and line averaging set to 2 collected sequentially in a three-channel mode. Imaging was also performed using Leica TCS SP8 confocal laser scanning microscope with 63X Plan-Apochromat 1.4 NA oil immersion objective, LAS X software and scan zoom of 1.5-2.0. Z-stacked images were acquired at 512 X 512 pixels per frame using 8-bit pixel depth for each channel at a voxel size of 0.105 μm X 0.105 μm X 0.34 μm and frame averaging set to 4 collected sequentially in a three-channel mode. Slides were mounted in Slowfade Gold Antifade and fluorochromes used were as follows – DAPI, Alexa Fluor-488 and Alexa Fluor-568. LSM/LAS X image stacks were processed using Image Pro Plus software (v 7.1) or ImageJ. High resolution imaging of Emerin GFP-tagged constructs was performed using Leica TCS STED 3X Nanoscope using 100X HC Plan-Apochromat 1.4 NA oil immersion objective. Depletion lasers of 592 nm and 660 nm were used for GFP and Alexa Fluor 568 respectively. Slides were mounted in 80% glycerol (in 1X PBS). Acquisition was carried out using the LASX software, scan zoom between 4–6 and 1352 × 1352 pixels per frame at a voxel size of 0.03 μm × 0.03 μm × 1 μm.

2.1.7 Statistical Analysis

The frequency distribution of % Radial Distance (% R.D) profiles was plotted in bins of 20% R.D. All distribution profiles were tested for normality using Kolmogorov-Smirnov (K-S test) and Shapiro Wilk normality tests. The median % radial distances of chromosome territories were compared between independent categories using the Mann Whitney Wilcoxon sum rank test using Graph Pad Prism 5.0 software. The band intensity (western blotting), fluorescence intensity (IFA) and average fold change (qRT-PCR) values were compared using Student's t-test. Surface area, volume measurements and distances from Lamin staining were also compared using Mann

Whitney test. p-value < 0.05 was considered statistically significant. Graphs were plotted using Graph Pad Prism 5.0 and Microsoft Excel.

2.2 Specific methods for Chapter 3.

2.2.1 *Preparation of polyacrylamide gels*

Polyacrylamide gels were prepared following established protocol (Fischer et al., 2012). Glass coverslips stored in 70% ethanol solution were sonicated in 1M KOH for 15 minutes in probe Sonicator (Sonics *VibraCell* Model No. VCX130; Amplitude – 50%, Cycle – 4 secs ON/5 secs OFF). After washing with MiliQ water, coverslips were coated with 1% silane solution (3-Aminopropyl-triethoxysilane, Sigma, 440140) for 40 minutes. Coverslips were cured at 50-55°C and allowed to dry completely, followed by treatment with 0.5% Glutaraldehyde (Sigma, G7776) for 60 minutes at room temperature. Polyacrylamide gels were prepared by the sandwich method using 5% acrylamide/0.2% bisacrylamide solution for ~2 kPa gel and 12% acrylamide/0.6% bisacrylamide solution for the ~55 kPa gel. Gels were activated using Sulpho-Sanpah (Pierce, 22589), followed by coating with 100 µg/ml rat-tail Collagen (BD Biosciences, 354236) at 4°C.

2.2.2 Cell cycle analysis

Cell cycle analyses was performed for DLD-1 cells plated on 2 kPa, 55 kPa matrices and collagen coated glass coverslips using Fluorescence assisted cell sorting (FACS). Cells (~0.8 million) were seeded on 2 kPa, 55 kPa matrices and glass coverslips for 90 minutes followed by trypsinization and centrifugation at 10°C/1000 rpm for 5 mins. Cell pellets were washed once with DPBS, the subsequent pellets were resuspended in 1 ml 70% ethanol solution under constant agitation and stored at 4°C overnight. Cells fixed in 70% ethanol were centrifuged at 10°C/1050 rpm for 7-10 mins. The pellet was resuspended in 1 ml 1X PBS followed by addition of 5-7 µl RNase A (Stock – 10 mg/ml) and 10-12 µl propidium iodide (Stock – 1mg/ml) and incubated at 37°C for 60 minutes with intermittent tapping. Cell suspensions (2 kPa, 55 kPa and glass – stained, and glass –

unstained control) were passed through cell strainer and collected in FACS tubes. Cell cycle analysis was performed in BD FACSCalibur™ (BD Biosciences) with 30,000 cell counts per sample.

2.2.3 RNA Sequencing and analyses

RNA Sequencing

DLD-1 cells were plated on 2 kPa, 55 kPa polyacrylamide matrices and collagen coated glass coverslips for 90 mins. Cells were harvested in Trizol® reagent. RNA-Sequencing over two independent biological replicates was performed by Genotypic Technology, Bangalore on Illumina NextSeq 500 sequencing platform followed by quality control of paired end raw reads using FastQC v2.2. Reference genome alignment was performed using TopHat v2.0.7 and Cufflinks v2.0.1, and differential expression analysis was performed using Cufflinks v2.0.1 – Cuffdiff (Langmead and Salzberg, 2012; Trapnell et al., 2009; Trapnell et al., 2010). Homology searches were performed against Ensemble cDNA sequences (GRch37/hg19 build) using ncbi-BLAST-2.2.29. Prior to the final analyses of deregulated genes, the RNA sequencing data was run through UCSC Table Browser using the GRch38/hg38 assembly to get complete annotations for all the previously unannotated transcripts (Karolchik et al., 2004).

Spearman and Pearson correlation coefficients between the two independent biological replicates (for the soft matrices) was performed using deepTools2 as a part of the Galaxy platform (Afgan et al., 2016; Ramírez et al., 2016). Pearson correlation coefficient for the two biological replicates was as follows: 2 kPa – 0.94 and 55 kPa – 1.0, while the Spearman coefficient for the two biological replicates was as follows: 2 kPa – 0.90 and 55 kPa – 0.9. The total deregulation (%) on each chromosome was calculated by normalizing total number of deregulated genes on each

chromosome (on both 2 kPa and 55 kPa, reference—glass) to the total number of transcribing genes (FPKM > 1.0) on that chromosome. Enrichment of deregulated genes (up- and downregulated) on each chromosome on 2 kPa and 55 kPa matrices was calculated by normalizing total number of deregulated genes on each chromosome to the total number of genes deregulated on soft (2 or 55 kPa) matrices (reference—glass). Gene Expression Omnibus (GEO) accession number for the RNA Sequencing data is **GSE108907**.

Assigning Gene Ontology (GO) classes to the deregulated genes

GO categories for up- and downregulated genes were assigned using DAVID Bioinformatics Resource 6.7 (NIAID, NIH) (Huang et al., 2009a; Huang et al., 2009b). Briefly, genes up and downregulated [fold change ≥ 2-fold (log2)] on either 2 kPa (reference—glass) or 55 kPa (reference—glass) matrices were analyzed using the Functional Annotation Tool. Categories with $p<0.05$were plotted as the $-\log_{10}$(p-value).

Gene Set Enrichment Analysis (GSEA) for transcription factor and miRNA binding

Promoter sequences of the genes that were deregulated on 2 kPa and 55 kPa matrices (Reference – Glass) were analyzed for motifs and binding sites for transcription factors (TFs) and miRNAs using the GSEA – Molecular Signature Database (MSigDB) (Mootha et al., 2003; Subramanian et al., 2005). Lists of genes up or downregulated on 2 kPa or 55 kPa matrices were used as input files for the database, which compared them with curated gene sets with annotated TF motifs and miRNA binding sites. Top 20 gene datasets were obtained with FDR value fixed at 0.05. For computing overlap between the enriched transcription factors and known Lamin interactors, the Biological General Repository for Interaction Database (BioGRID3.4) was used to collect the curated lists of Lamin A/C, B1 and B2 interacting proteins (Stark et al., 2006).

2.2.4 Micropattern printing on glass coverslips

PDMS stamps (with 20 µm diameter circular patterns) were washed with 100% acetone 2-3 times, followed by 2 washes with 100% ethanol and then sonicated 15 minutes in 100% ethanol using probe Sonicator (Sonics *VibraCell* Model No. VCX130; Amplitude – 70%, Cycle – 15 secs ON/5 secs OFF). The stamps were allowed to dry, followed by activation with UV light for 30 mins (under sterile conditions) and kept for collagen (100 µg/ml) coating at 4ºC overnight. Coverslips (stored in 70% ethanol) were sonicated in 1M KOH using the probe sonicator (Amplitude – 70%, Cycle – 15 secs ON/5 secs OFF), followed by rinsing 3-4 times in MiliQ water. Coverslips were immersed in silane solution (1% APTES, 5% acetic acid in methanol) for 40 mins and then dried at 50-55ºC in dry air oven. Coverslips were then treated with UV light for ensuring sterility and collagen coated PDMS stamps (rinsed twice in DPBS and dried) were inverted on the coverslips, the patterned side facing down. The stamps were pressed gently to ensure even print and kept undisturbed for 30-45 mins. After removing the stamps, pluronic acid solution (2 mg/ml in MiliQ water) was added on the coverslips and kept for 60 mins. Following this the coverslips were washed thrice with DPBS, medium was added and cells were seeded on the coverslips for 90 mins.

2.3 Specific methods for Chapter 4.

2.3.1 *Generation of Lamin A, Lamin B2 and Emerin mutants*

The pEGFP-Lamin A and Lamin B2-GFP constructs were received as kind gifts from Kaushik Sengupta (SINP, Kolkata, India) and Takeshi Tomonaga (NIBIO, Osaka, Japan). Details of Lamin domains were procured from Uniprot. Lamin A Δ425-553 and Lamin B2 Δ570-582 mutants were made from above plasmids using the following primers –

Lamin A Δ425-553 sense 5'-CAAACTGGAGTCCACTGAGGATGAGGATGGAG-3',

Lamin A Δ425-553 antisense 5'-CTCCATCCTCATCCTCAGTGGACTCCAGTTTG-3',

Lamin B2 Δ570-582 sense 5'-GGTTAACGCGGATGGCATGCGTGAGAATGAGA-3' and

Lamin B2 Δ570-582 antisense 5'-TCTCATTCTCACGCATGCCATCCGCGTTAACC-3'.

Lamin A S22D mutant was generated from GFP-Lamin A WT plasmid using the following primers -

Lamin A S22D sense 5'-AGCTCCACTCCGCTGGATCCCACCCGCATCACC-3' and

Lamin A S22D antisense 5'-GGTGATGCGGGTGGGATCCAGCGGAGTGGAGCT-3'

GFP-Emerin and GFP-Emerin Δ95-99 constructs were received as kind gifts from Katherine Wilson (JHMI, Baltimore, USA). Emerin Y74F, Y95F, Y74/95FF and Y99F single point mutants were made from GFP-Emerin plasmid using the following primers –

Emerin Y74F sense 5'-TTCTTGGGAAGATCAAACATATCTGCATCCCCTCTAG-3',

Emerin Y74F antisense 5'-CTAGAGGGGATGCAGATATGTTTGATCTTCCCAAGAA-3',

Emerin Y95F sense 5'-GAAGTAGCTCTCTTCAAAGTAGTCGTCATTGTAGCC-3',

Emerin Y95F antisense 5'-GGCTACAATGACGACTACTTTGAAGAGAGCTACTTC-3',

Emerin Y99F sense 5'-AAGTCCTGGTGGTGAAGAAGCTCTCTTCATAGTAG-3' and

Emerin Y99F antisense 5'-CTACTATGAAGAGAGCTTCTTCACCACCAGGACTT-3'.

WT GFP-Emerin and Emerin Y99F were made shRNA insensitive using the following primers – sense 5'-

TGCACTCCTCTTCAGAAGAAGATAATAGGTCATCGTCGTGCACTTGGTGATGGAAAG CGTCAGCATCTG-3' and

antisense 5'-

CAGATGCTGACGCTTTCCATCACCAAGTGCACGACGATGACCTATTATCTTCTTCTG AAGAGGAGTGCA-3'.

Primers were generated using the QuikChange Primer Design software from Agilent Genomics. PCR was carried out using Accuprime *Pfx* Supermix (Invitrogen, 12344-040). 100 ng plasmid DNA was used as template, primers were used at a concentration of 200 nM and extension time per cycle was 7.5 mins. The product obtained after 35 cycles was treated with DpnI, used for transformation of *E. coli* DH5α cells and colonies obtained were screened using Sanger sequencing to check incorporation of desired mutations.

2.3.2 Generation of emerin knockdown (shEmerin) clones of DLD-1 cells

DLD-1 cells (~0.8 million) were seeded in a 60 mm culture dish, followed by transfection with either shRNA (8 µg) against emerin (pLKO.1/puro TRC1.5 vector backbone, Sigma TRCN0000083012) or pLKO.1 empty vector (as vector control) using Lipofectamine LTX and Plus reagent (Invitrogen, 15338100). Emerin shRNA sequence is as follows -

5'-

CCGGAGGTGCATGATGACGATCTTTCTCGAGAAAGATCGTCATCATGCACCTTTTTT G-3'. After 48 hrs, cells were trypsinized and seeded into 100 mm culture dishes under 2.5 µg/ml Puromycin (Invitrogen, A1113802) selection. The shEmerin colonies were screened using western

blotting and immunofluorescence for knockdown of emerin (empty vector colonies were used as control). Selected vector control and shEmerin clones were maintained under continuous puromycin selection (2.5 µg/ml).

2.3.3 Overexpression of Lamin A, Lamin B2 and Emerin

DLD-1 cells were transfected with overexpression vectors for Lamin A (GFP-Lamin A, GFP-Lamin A Δ425-553, GFP-Lamin A S22D), Lamin B2 (Lamin B2-GFP, Lamin B2-GFP Δ570-582) and Emerin (GFP-Emerin WT, Y74F, Y95F, Y74/95FF, Y99F) using Lipofectamine LTX and Plus reagent (Invitrogen, 15338100) for 48 hrs. Following this, cells were trypsinized and plated on 2 kPa polyacrylamide gel (or glass – Lamin overexpression) for 90 mins and then processed for western blotting (Lamin and Emerin overexpression) and 3D-FISH fixation (Lamin overexpression).

Overexpression of WT GFP-Emerin and GFP-Emerin Y99F (resistant to shRNA) in vector control and shEmerin clones was performed using TransIT-2020 transfection reagent (Mirus Bio LLC) at a concentration of 1.5 µl/µg of plasmid. Overexpression was carried out for 48 hrs, following which cells were trypsinized and plated on 2 kPa polyacrylamide gel for 90 mins and then processed for western blotting, immunofluorescence or 3D-FISH fixation.

2.3.4 Treatment of DLD-1 cells with Src kinase inhibitor (PP2)

Cells growing in tissue culture plastic dishes were trypsinized and seeded on 2 kPa polyacrylamide matrices and collagen coated glass coverslips. Cells were kept in 37ºC/5% CO_2 incubator for 3-4 mins to initiate cell adhesion. Following this 20 µM PP2 was added to the cells and equal volume of DMSO was added as control. Cells were incubated with PP2 for 30 or 90 mins and then

processed for western blotting, immunostaining or 3D-FISH fixation.

2.3.5 Co-immunoprecipitation of GFP-Emerin and Lamin A/C

Cells overexpressing EGFP-N1, GFP-Emerin WT, GFP-Emerin Y99F, GFP-Emerin Y99D or GFP-Emerin Δ95-99 were lysed in co-immunoprecipitation buffer (50 mM Tris-Cl pH ~8.0, 150 mM NaCl and 0.5% NP-40), kept on ice for 15 mins and centrifuged at 14000 rpm for 20 mins at 4ºC. The lysates were subjected to pre-clearing using 5 µl Dynabeads Protein A (Invitrogen, 10001D) for 45 mins at 4ºC on a rotary shaker at 8-9 rpm. Post pre-clearing, the protein concentration was estimated using BCA Kit and 1 µg of either Rabbit anti-GFP (Sigma, G1455) or Normal Rabbit IgG (Invitrogen, 10500C) was added to 250 µg lysate. Antigen-antibody incubation was carried out at 4ºC on a rotary shaker at 8-9 rpm overnight. 20 µl Dynabeads Protein A, previously blocked with 0.5 mg/ml BSA solution for 30 mins at 4ºC, were added to pulldown the antigen-antibody complex for 4 hrs at 4ºC on a rotary shaker at 8-9 rpm. The beads containing the complex were washed 5-6 times with chilled co-immunoprecipitation buffer for 10 mins at 4ºC on a rotary shaker at 12-13 rpm. After the washes, antigen-antibody complex was eluted from the beads by boiling them at 95ºC for 15 mins in 2X Laemmli's buffer and SDS-PAGE followed by western blotting was carried out.

2.4 Specific methods for Chapter 5.

2.4.1 Heat shock induction in DLD-1 cells

Untreated DLD-1 cells, siLacZ treated cells or cells with Lamin A/C, Lamin B1 and Lamin B2 knockdown were first changed from complete RPMI 1640 medium to Leibovitz L-15 medium (Gibco, 21083-027; pre-warmed to RT before use). Culture dishes (either 35 mm x 10 mm dishes with 8 cm^2 area, or 6-well plates with 9.5 cm^2 area per well, Corning®) containing cells were then sealed with parafilm and exposed to either 37ºC (incubation temperature control) or 42ºC (heat shock temperature) in water baths (for required time points) - pre-set at these temperatures for at least 30-45 mins to prevent temperature fluctuations.

2.4.2 siRNA mediated knockdown

For siRNA transfections, ~0.2 X 10^6 cells were seeded overnight. siRNA transfection mix was prepared using Lipofectamine RNAimax in reduced serum medium - Opti MEM (Invitrogen Cat No. 31985-070) containing 100 nM siRNA against *LACZ*, *LMNA/C*, *LMNB1* or *LMNB2* and incubated at RT for 30 mins. The siRNA mix was then (i) added to cells in complete RPMI 1640 medium and knockdown was continued for 48 hrs after which cells were used for further assays (Lamin A/C and B2 knockdown) or (ii) added to cells in Opti MEM for 6 hrs, after which the medium was changed to complete RPMI 1640 and knockdown continued for 48 hrs. Cells were then used for further assays (Lamin B1 knockdown). Following siRNAs were used-

si*LACZ* 5’ CGUACGCGGAAUACUUCGA 3’

si*LMNA/C* 5’ CAGUCUGCUGAGAGGAACA 3’

si*LMNB2* 5’ GAGCAGGAGAUGACGGAGA 3’

si*LMNB1* 5’ AGACAAAGAGAGAGAGAUG 3’

2.4.3 Cadmium Sulphate treatment for HSPA1A induction

Untreated DLD-1 cells, siLacZ treated cells or cells with Lamin A/C, Lamin B1 and Lamin B2 knockdown were first changed to fresh complete RPMI 1640 medium, followed by addition of required volume of Cadmium Sulphate solution (Stock – 1mM, prepared in nuclease free water). Equal volume of nuclease free water was added as control and cells were kept in 37ºC/5% CO_2 incubator for 2 hrs.

2.4.4 Overexpression of siResistant GFP-Lamin A for rescue experiments

siRNA resistant GFP-Lamin A construct was generated by Devika Ranade using SDM protocol mentioned in Section 2.3.1. For siRNA transfections, ~0.2 X 10^6 cells were seeded overnight. siRNA transfection mix was prepared using Lipofectamine RNAimax in reduced serum medium - Opti MEM (Invitrogen Cat No. 31985-070) containing 100 nM siRNA against *LACZ* and *LMNA/C*, and incubated at RT for 30 mins. siRNA mix was then added to cells in complete RPMI 1640 medium and knockdown was continued for 24 hrs. After 24 hrs, cells were transfected with either EGFP-N1 (empty vector) or siResistant GFP-Lamin A using Lipofectamine LTX and Plus reagent (Invitrogen, 15338100) for 48 hrs. After 48 hrs, heat shock induction was carried out as mentioned in Section 2.4.1.

2.4.5 RNA isolation

Cells post-heat shock or other treatments were harvested in Trizol® reagent (Invitrogen, 15596018), collected in 1.5 ml microfuge tubes, vortexed briefly for 10 secs and 100 µl chloroform per 500 µl Trizol was added. The mixture was vortexed for 10 secs and kept at RT for 10 mins.

Centrifugation was then carried out at 4ºC/12000g/15 mins. The aqueous phase post-centrifugation was carefully collected in fresh 1.5 ml microfuge tubes. Equal volume of isopropanol was added, followed by vortexing for 10 secs and incubation at RT for 15 mins. Centrifugation was then carried out at 4ºC/12000g/15 mins. The RNA pellet was washed with 70% ethanol, residual ethanol removed and pellet was allowed to dry at 37ºC for 10-15 mins. After complete drying, RNA pellet was reconstituted in desired volume of Nuclease Free Water (NFW) and incubated at 37ºC for 5 mins, 65ºC for 5 mins (without shaking). RNA was then stored at -80ºC till further use. RNA quantification was performed using Nanodrop.

2.4.6 Preparation of cDNA and quantitative Real Time (RT) PCR

cDNA was prepared using oligo(dT) primers and ImProm-II Reverse Transcription System (Promega, A3800). Quantitative RT-PCR was performed from cDNA templates using Kapa SyBr Fast qPCR Master Mix (2X) Universal (KK4602) and real-time PCR system (Biorad, CFX96). Transcript levels were determined after (first) normalization to the internal control GAPDH and further (second normalization) to the specific experimental control. Following primers were used-

LMNA/C F- 5’ CCGCAAGACCCTTGACTCA 3’,

LMNA/C R- 5’ TGGTATTGCGCGCTTTCAG 3’

LMNB2 F- 5’ AGTTCACGCCCAAGTACATC 3’,

LMNB2 R- 5’ CTTCACAGTCCTCATGGCC 3’

LMNB1 F- 5’ CGACCAGCTGCTCCTCAACT 3’,

LMNB1 R- 5’ CTTGATCTGGGCGCCATTA 3’

HSPA1A F- 5’ AGAAGGACGAGTTTGAGCACA 3’,

HSPA1A R- 5’ TGGTACAGTCCGCTGATGATG 3’

GAPDH F- 5’ CGAGATCCCTCCAAAATCAAG 3’,

GAPDH R- 5’ GCAGAGATGATGACCCTTTTG 3’

2.4.7 Immuno-3DFISH

Fixation

DLD-1 cells treated with either siLacZ, siLamin A/C, siLamin B1 or siLamin B2, growing on coverslips and subjected to heat shock were treated with CSK buffer for 6-7 mins, followed by fixation using 4% PFA for 12 mins at RT. After 2 washes in 1X PBS, permeabilization was carried out using 0.5% Triton X-100 (in 1X PBS) for 15 mins and nuclei were incubated in 20% glycerol (in 1X PBS) for 45 mins. 5-6 freeze-thaw cycles were carried out in liquid nitrogen, followed by 3 washes in 1X PBS, 10 mins in 0.1 N HCl, and 2 washes in 50% FA-2X SSC (pH 7.4). Nuclei were stored at 4ºC overnight (or till further use).

Immunofluorescence

Immunofluorescence protocol was followed as mentioned previously. Briefly, fixed nuclei stored at 4ºC were washed twice in 1X PBS, incubated with primary antibody (prepared in 0.5% BSA) for 90 mins, washed thrice in 1X PBST and incubated with secondary antibody (prepared in 1X PBST) for 60 mins. After the final 3 washes of 1X PBST, coverslips were stored in 1X PBST for 30 mins. Post-fixation was carried out in 4% PFA for 7 mins and post-permeabilization in 0.5% Triton X-100 for 7 mins, followed by 2 washes in 1X PBS and 2 washes in 50% FA-2X SSC.

Preparation of BAC DNA probe for FISH

BAC clone RP11-92G8 (purchased from CHORI BACPAC Resources) for *HSPA1A* was purified using BAC isolation protocol by Villalobos et al, optimized for 100 ml cultures (Villalobos et al., 2004). BAC DNA was labelled with Orange 552 dUTP (Enzo, ENZ-42842) or Red 580 dUTP

(Enzo, ENZ-42844) using Nick Translation Kit (Roche 11745808910, following kit protocol). The labelling reaction was carried out at 15ºC for 2 hrs, terminated using 0.5 M EDTA and DNA was precipitated using 3 M sodium acetate and ethanol. Labelled DNA pellet was resuspended in deionized formamide at 37ºC, followed by addition of Master Mix containing dextran sulphate and 2X SSC. Probe was stored at -20ºC till further use.

BAC Clone	Genes covered
RP11-92G8	MSH5-SAPCD1, VWA7, VARS, LSM2, HSPA1A, HSPA1L, HSPA1B, C6orf48, NEU1, SLC44A4, EHMT2, ZBTB12

Hybridization

HSPA1A probe was kept at 37ºC for 7 mins/750 rpm, followed by denaturation at 80ºC for 5 mins and quick chill on ice for 2 mins. Pre-annealing was carried out at 37ºC for 45 mins. Co-denaturation of *HSPA1A* probe and immunostained nuclei was carried out at 80ºC for 7 mins. Hybridization was carried out in moist sealed chamber at 37ºC for 48 hrs.

Detection

Post hybridization, coverslips were washed in 50% FA/2X SSC (pH 7.4), thrice/5 mins each at 45°C, followed by 0.1X SSC washes (thrice/5 mins) at 60°C. Coverslips were counterstained with DAPI for 2 mins, washed in 2X SSC, mounted in Slowfade Gold Antifade and stored in 4°C until imaged.

Imaging

Confocal images were acquired on Zeiss LSM 710 confocal microscope (Carl Zeiss, Thornwood, NJ, USA). LSM image stacks were processed using Huygens Professional.

Measurement of shortest distance of HSPA1A loci from Lamin staining

3D reconstruction of confocal LSM stacks was performed using Huygens Professional software for DAPI (blue channel), *HSPA1A* (red channel) and Lamin A or B1 (far red channel). Lamin staining was set as envelope anchor. The center of mass (CM) for the thresholded *HSPA1A* locus signal was determined and shortest distance in µm between the anchor (Lamin staining) and CM was computed.

2.4.8 NM1 inhibition using BDM

siLacZ or siLamin A/C treated cells were changed from complete RPMI 1640 medium to Leibovitz L-15 medium (pre-warmed to RT before use). 1 mM BDM (Stock – 50 mM in nuclease free water) was added to the cells (equal volume of NFW was used as control) and cells were kept in 37ºC/5% CO_2 incubator for 30 mins. Following this, cells (in the presence of BDM) were exposed to either 37ºC (incubation temperature control) or 42ºC (heat shock temperature) in water baths for 60 mins and further assays were carried out.

Chapter 3: Impact of altered extracellular substrate stiffness on genome organization and function

Results from this chapter have been published as a part of the following manuscript:

Roopali Pradhan, Devika Ranade, Kundan Sengupta; **Emerin modulates spatial organization of chromosome territories in cells on softer matrices**, Nucleic Acids Research, Volume 46, Issue 11, 20 June 2018, Pages 5561–5586.

3.1 Introduction

Cell–extracellular matrix (ECM) crosstalk regulates cell growth, proliferation, survival, differentiation and homeostasis (DuFort et al., 2011). ECM composition and its biochemical and mechanical properties vary greatly with different tissue types and this is a result of the dynamic and continuous communication between the ECM and the cells – wherein the ECM provides extracellular signals that can dictate cell fate. Cells in turn remodel ECM according to their requirements (Frantz et al., 2010). It is well established that mechanical properties of the extracellular substrate independently regulate cell fate decisions in stem cells. For instance, human mesenchymal stem cells (hMSCs) when plated on collagen coated polyacrylamide gels having different elastic moduli that mimic *in vivo* elasticities of the brain (0.1-1 kPa), muscles (8-17 kPa) and bones (25-40 kPa), differentiate into neurogenic, myogenic and osteogenic lineages respectively. This lineage specification is observed at the level of cellular morphology as well as expression levels of lineage specific markers like TUBB4, NRG1 for neurogenic, MYOG, PAX7 for myogenic and BGLAP, BMPs for osteogenic lineages (Engler et al., 2006). Interestingly, mouse stem cells cultured on softer polyacrylamide matrices maintain self-renewal capacity and homogenous undifferentiated colonies; while mouse embryonic fibroblasts and human dermal fibroblasts show enhanced stem cell-like properties on softer matrices of ~0.1-0.5 kPa stiffness (Chowdhury et al., 2010; Higuchi et al., 2014). Taken together, perception of mechanical properties of the extracellular substrate namely elasticity, rigidity, geometry among others leads to coordinate changes in morphology and transcriptional profiles of the cells.

Cues from the extracellular environment must reach the nucleus, and ultimately the genome, for signal-specific changes in gene expression and transcription. Since cell fate decisions are

dependent on signals from the ECM reaching the genome while traversing the cytoplasm, the nuclear envelope functions as an integrator of these signals (Aureille et al., 2017; Crisp and Burke, 2008; Enyedi and Niethammer, 2016; Shimi et al., 2012). The nuclear envelope is composed of myriad proteins and protein complexes that facilitate mechanotransduction into the nucleus (Tapley and Starr, 2013; Wilson and Berk, 2010; Wilson and Foisner, 2010). The Linker of Nucleoskeleton and Cytoskeleton – LINC complex, nuclear lamins and inner nuclear membrane protein - emerin, relay extranuclear signals to the genome by either direct contact with chromatin (Lamina Associated Domains or LADs - regions of chromatin bound by lamins) or indirectly through their interaction partners (emerin interacts with BAF which is a DNA-binding protein) (Alam et al., 2016; Barton et al., 2015; Berk et al., 2013; Guelen et al., 2008; Lombardi and Lammerding, 2011; Zastrow et al., 2004). These protein-protein interactions maintain the nuclear structure, function and genome organization in coordination (Kaminski et al., 2014).

The genome is non-randomly organized in the interphase nucleus and every chromosome occupies a distinct sub-volume known as the ‘chromosome territory’ (CT) (Bolzer et al., 2005; Cremer et al., 2001). Chromosome territories adopt either a gene density-based organization in largely spherical nuclei (such as lymphocytes), wherein gene rich chromosomes are present to towards the nuclear interior and gene poor chromosomes towards the nuclear periphery (Cremer et al., 2003). In flat ellipsoidal nuclei (such as fibroblasts), chromosomes assume a size-based organization wherein smaller chromosomes are present towards the nuclear interior and larger chromosomes are proximal to the periphery (Bolzer et al., 2005; Sun et al., 2000). Gene-density based chromosomal locations are conserved across evolution and also partially maintained in tumor cell nuclei (Cremer et al., 2003; Tanabe et al., 2002). However, chromosome organization is altered in

dynamic processes such as adipocyte and myogenic differentiation, spermatogenesis (Foster et al., 2005; Kuroda et al., 2004; Rozwadowska et al., 2013), in serum starved or quiescent cells (Bridger et al., 2000; Mehta et al., 2010; Nagele et al., 1999) and in cells treated with DNA damaging agents (Mehta et al., 2013). For instance, the relative distance between chromosome territories 12 and 16 decreases when human preadipocytes differentiate into adipocytes (Kuroda et al., 2004), while centromeres of chromosomes 1, 3, 12, 17 and X are repositioned during differentiation of human myoblasts into myotubes (Rozwadowska et al., 2013). While these changes in genome organization occur over days in differentiation paradigms, serum starvation induces movement of gene poor CT13 and 18 towards the nuclear interior within 15 mins. Furthermore, DNA damage induction using cisplatin repositions gene rich CT17, 19 and 20 towards the nuclear periphery by ~4 hrs (Mehta et al., 2010; Mehta et al., 2013). This indicates that dynamic changes in the nuclear organization of chromosome territories occur given the presence of appropriate and context-specific extrinsic or intrinsic signals.

Interestingly, the impact of external mechanical forces on non-random chromosome positions and transcription is not completely understood. Hi-C studies, coupled with RNA sequencing analyses, reveal that chromatin organization and gene expression profiles differ significantly in human fibroblasts grown on 2D versus 3D microenvironments (Chen et al., 2015; Chen et al., 2017). Cells on micropatterned surfaces increase histone acetylation (AcH3) and methylation (H3K4me2/me3) levels, suggesting that altered substrate architecture is potentially perceived by the genome and fine-tuned by the epigenome (Downing et al., 2013; Jain et al., 2013; Li et al., 2011). Micro-patterned surfaces alter Lamin B1 organization and mislocalize human chromosome 1 territories closer to the nuclear periphery (McNamara et al., 2012). In addition, heterochromatinization and

transcriptional repression is induced in cells on relatively softer matrices (<50 kPa), potentially relayed to the genome via the LINC complex (Alam et al., 2014; Alam et al., 2016; Kocgozlu et al., 2010; Rabineau et al., 2015). Interestingly, 3D chromosome positions, degree of intermingling between chromosome territories and transcriptional activity are significantly altered between NIH 3T3 fibroblasts grown on isotropic (circular) and anisotropic (rectangular) micropatterns (Wang et al., 2017). These studies reveal that changes in mechanical forces perceived by cells can impact chromosome organization and function. Chromosome positioning studies have been performed on cells cultured on tissue culture plastic or glass surfaces, whose stiffness is orders of magnitude higher (~10 GPa) than that experienced by cells under physiological conditions (~0.1-200 kPa), or in fixed non-adherent lymphocytes (Cremer et al., 2001; Croft et al., 1999; Georges and Janmey, 2005; Miller and Janmey, 2015; Tanabe et al., 2002). Studies in murine and porcine tissues have examined *in vivo* genome organization that highlight tissue specific differences in the positioning of chromosome territories, gene loci and expression of nuclear envelope transmembrane proteins (NETs) (de Las Heras et al., 2017; Foster et al., 2012; Meaburn et al., 2016; Parada et al., 2004). These experiments suggest that the *in vivo* tissue architecture and extracellular matrix stiffness can enforce cell type specific genome organization and gene expression programs.

Here, we addressed the effect of altered extracellular substrate stiffness on the non-random organization of chromosome territories in the interphase nucleus and the functional response elicited in terms of transcription profiles. From a group of cancer cell lines, we selected and studied morphological changes in the diploid DLD-1 colorectal adenocarcinoma cells upon exposure to polyacrylamide matrices of two different stiffness properties. We further performed RNA sequencing of these cells to identify i) chromosomes that exhibit transcriptional changes and

enrichment of deregulated genes upon lowered substrate stiffness and ii) genes and pathways that are responsive to alterations in extracellular matrix stiffness. DLD-1 cells exposed to softer matrices for ~90 mins showed the (i) downregulation of the active histone mark H3K4me3 (ii) nucleoplasmic accumulation of the inactive histone mark H3K27me3 and (iii) altered chromosome wide transcriptional profiles. Furthermore, we observed that transcriptionally deregulated chromosomes such as Chr. 1 and 19, as well as Chr. 18 with lower gene expression changes, all reposition towards the nuclear interior in cells on softer matrices in relatively short duration of ~90 mins. Interestingly, differential extent of repositioning was observed for each of the chromosomes upon switching cells from softer to stiffer matrices. Taken together, we demonstrate that the altered transcriptional profiles in cells on softer matrices largely correlate with repositioning of chromosome territories and that the non-random organization of the genome is remarkably sensitive to changes in extracellular matrix stiffness.

3.2 Results

3.2.1 Nuclear and cell surface areas and volumes are sensitive to matrix stiffness

Cells experience a wide range of stiffness conditions and extracellular forces based on their tissue microenvironment. For instance, brain tissue is softer (~0.2 kPa), while bones are considerably stiffer (~50-200 kPa) (Engler et al., 2006; Georges et al., 2006; Hengsberger et al., 2002; Winer et al., 2009). Additionally, cells can sense the rigidity of their substrates and respond to it by modulating cell spreading, shape and stiffness; cytoskeletal organization and proliferation among others (McBeath et al., 2004; Vishavkarma et al., 2014). For examining the response of cell lines of different origins to changes in extracellular substrate stiffness, we exposed DLD-1 (colorectal adenocarcinoma), SW480 (colorectal adenocarcinoma), A549 (lung carcinoma), MCF7 (breast adenocarcinoma) and HT1080 (Fibrosarcoma) cells to polyacrylamide matrices of either ~2 kPa or ~55 kPa for two time points of 90 mins and ~21 hrs (Fig 3.1A). This was followed by Phalloidin and DAPI staining to quantify cell and nuclear surface areas and volumes respectively (Fig 3.1A). We observed a significant difference in nuclear surface areas (calculated at the mid-optical section of individual cells) for DLD-1, MCF7, A459 and HT1080 cells between the early (90 mins) and late (~21 hrs) time points on the 2 kPa matrices, while SW480 cells were unaltered (Fig 3.1B, Table 3.1). On the other hand, nuclear surface areas of SW480, MCF7 and A549 cells showed a significant difference between the two time points on 55 kPa matrices, while DLD-1 and HT1080 cells were unaltered (Fig 3.1D, Table 3.2). Additionally, the nuclear volume was altered for DLD-1, MCF7 and HT1080 cells on 2 kPa matrices and for DLD-1, SW480 and A549 cells on the 55 kPa matrices at ~21 hrs as compared to 90 mins (Fig 3.1C and E, Table 3.3 and 3.4).

Figure 3.1

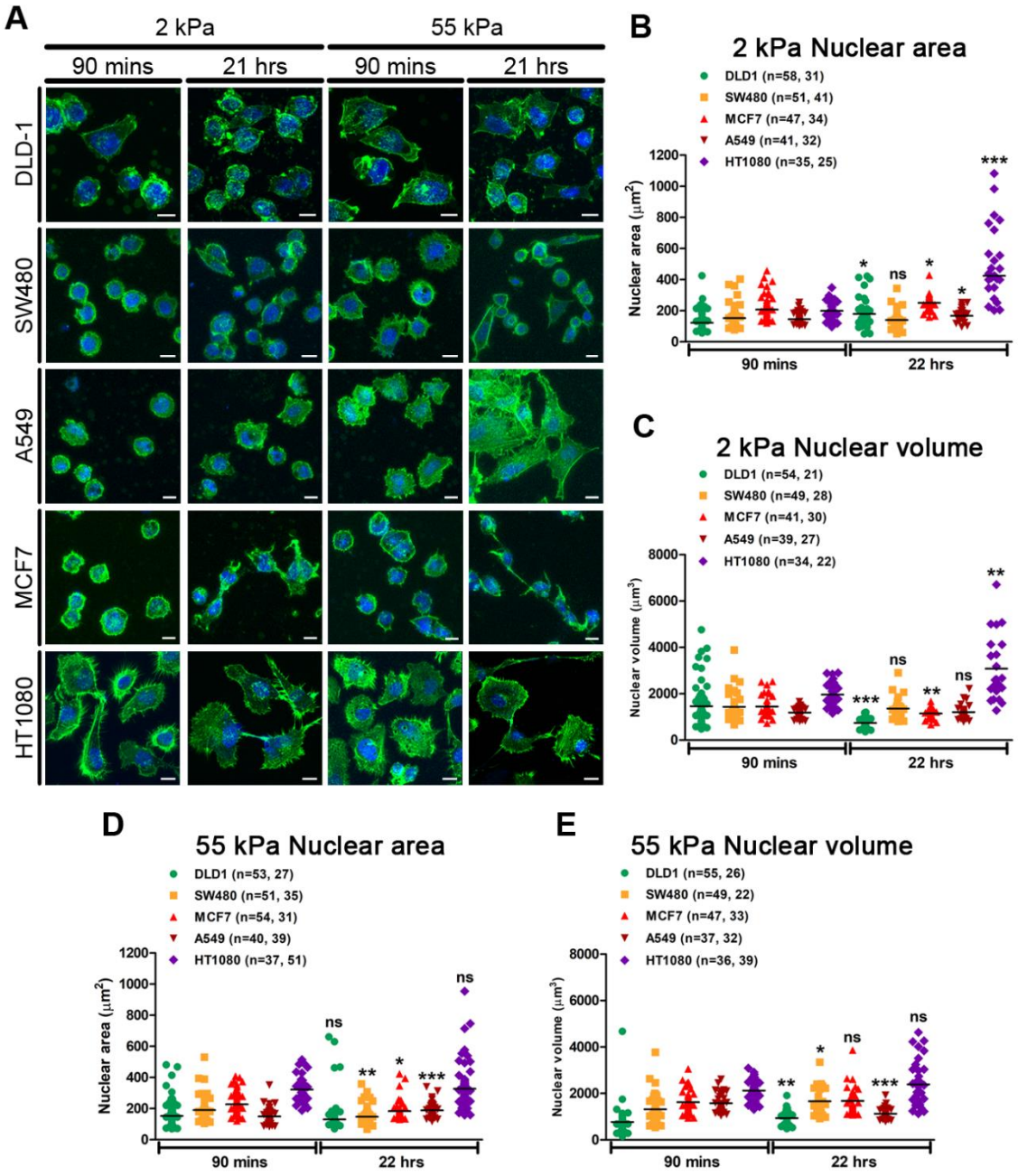

Figure 3.1 Nuclear surface areas and volumes are sensitive to matrix stiffness. A) DLD-1, SW480, A549, MCF7 and HT1080 cells stained with phalloidin and DAPI. Cells were plated on softer matrices (~2 kPa and ~55 kPa) for two time points ~90 min and ~21 hrs. B-E) Dot scatter plot for DLD-1, SW480, MCF7, A549 and HT1080 cells showing (B) nuclear area on 2 kPa for 90 mins and 21 hrs, (C) nuclear volume on 2 kPa for 90 mins and 21 hrs, (D) nuclear area on 55 kPa for 90 mins and 21 hrs, (E) nuclear volume on 55 kPa for 90 mins and 21 hrs *(Data from a single experiment, n: No. of cells, Black horizontal bar: Median, Statistical comparisons were performed using Student's t-test for each cell line between 90 mins and 21 hrs).* **Scale bar ~10 µm.**

Figure 3.2

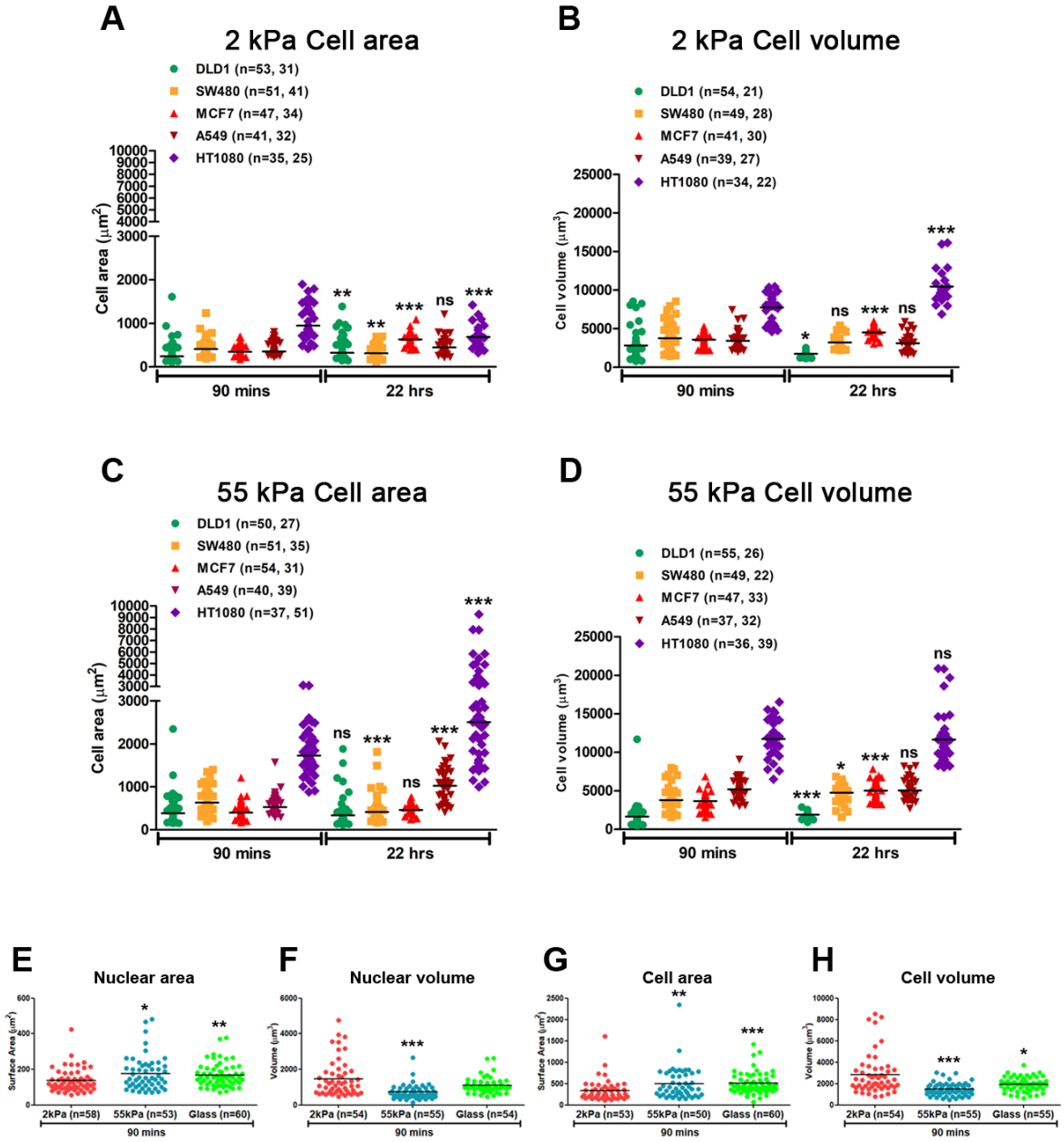

Figure 3.2 Cell surface areas and volumes are sensitive to matrix stiffness. A-D) Dot scatter plot for DLD-1, SW480, MCF7, A549 and HT1080 cells showing (A) cell area on 2 kPa for 90 mins and 21 hrs, (B) cell volume on 2 kPa for 90 mins and 21 hrs, (C) cell area on 55 kPa for 90 mins and 21 hrs, (D) cell volume on 55 kPa for 90 mins and 21 hrs *(Data from a single experiment, n: No. of cells, Black horizontal bar: Median, Statistical comparisons were performed using Student's t-test for each cell line between 90 mins and 21 hrs).* (E-H) Dot scatter plot for DLD-1 cells on 2 kPa, 55 kPa matrices and glass for 90 mins to compare (E) nuclear area, (F) nuclear volume, (G) cell area and (H) cell volume *(Data from a single experiment, n: No. of cells, Black horizontal bar: Median, Statistical comparisons were performed using Student's t-test with respect to 2 kPa).*

Interestingly, the cell surface areas of DLD-1, SW480, MCF7 and HT1080, and cell volumes of DLD-1, MCF7 and HT1080 were significantly altered on 2 kPa matrices between the early and late time points (Fig 3.2A-B, Table 3.1 and 3.3). While the cell surface areas of SW480, A549 and HT1080, and cell volumes of DLD-1, SW480, MCF7 and HT1080 showed a difference on 55 kPa matrices between the two time points (Fig 3.2C-D, Table 3.2 and 3.4). These observations suggest that although cells from diverse origins are capable of perceiving changes in substrate stiffness (here ~2 and 55 kPa), each cell type may adapt differentially in order to optimize its morphology, commensurate with substrate stiffness, which may vary in a cell-type specific and temporal manner (Table 3.5).

Table 3.1 Nuclear and cell surface areas of different cell lines on 2 kPa polyacrylamide matrices

Cell line	Median nuclear area (μm^2) 90 mins	Median nuclear area (μm^2) 21 hrs	Median cell area (μm^2) 90 mins	Median cell area (μm^2) 21 hrs
DLD-1	122.6	149.9	242.4	324.0
SW480	152.8	140.5	409.5	315.0
A549	148.8	167.3	352.6	445.3
MCF7	207.4	250.9	347.4	629.4
HT1080	199.5	424.6	947.7	689.6

Table 3.2 Nuclear and cell surface areas of different cell lines on 55 kPa polyacrylamide matrices

Cell line	Median nuclear area (μm^2) 90 mins	Median nuclear area (μm^2) 21 hrs	Median cell area (μm^2) 90 mins	Median cell area (μm^2) 21 hrs
DLD-1	152.0	170.5	384.9	335.5
SW480	190.1	177.4	632.0	414.4
A549	135.6	188.8	527.2	1025.0
MCF7	228.0	183.8	400.6	460.3
HT1080	322.4	327.4	1728.0	2507.0

Table 3.3 Nuclear and cell volumes of different cell lines on 2 kPa polyacrylamide matrices

Cell line	Median nuclear volume (μm^3) 90 mins	Median nuclear volume (μm^3) 21 hrs	Median cell volume (μm^3) 90 mins	Median cell volume (μm^3) 21 hrs
DLD-1	988	712	2157	1635
SW480	1279	1283	3280	2902
A549	1234	1129	3103	2801
MCF7	1336	1121	3456	4487
HT1080	1913	2611	8069	9750

Table 3.4 Nuclear and cell volumes of different cell lines on 55 kPa polyacrylamide matrices

Cell line	Median nuclear volume (μm^3) 90 mins	Median nuclear volume (μm^3) 21 hrs	Median cell volume (μm^3) 90 mins	Median cell volume (μm^3) 21 hrs
DLD-1	584	862	1351	1972
SW480	1248	1500	3613	5161
A549	1450	1059	5174	4501
MCF7	1489	1541	3759	4815
HT1080	2097	2303	11650	10867

Table 3.5 Comparison of nuclear and cell surface areas and volumes of various cell lines across time and substrate stiffness

Time point	**90 mins**		**21 hrs**	
Cell line	Significantly different between 2 and 55 kPa?		Significantly different between 2 and 55 kPa?	
	Nuclear area	**Cell area**	**Nuclear area**	**Cell area**
DLD-1	Yes	Yes	Yes	Yes
SW480	Yes	Yes	Yes	Yes
A549	Yes	Yes	Yes	Yes
MCF7	No	No	Yes	Yes
HT1080	Yes	Yes	Yes	Yes
Time point	**90 mins**		**21 hrs**	
Cell line	Significantly different between 2 and 55 kPa?		Significantly different between 2 and 55 kPa?	
	Nuclear volume	**Cell volume**	**Nuclear volume**	**Cell volume**
DLD-1	Yes	Yes	Yes	No

SW480	No	No	No	Yes
A549	Yes	Yes	No	Yes
MCF7	No	No	Yes	No
HT1080	No	Yes	No	No

3.2.2 Increase in cell and nuclear surface area of DLD-1 cells on softer matrices plateaus by ~90 minutes

To further characterize the response of cells to altered extracellular matrix stiffness, we selected DLD-1 cells because (i) these cells perceive and respond to matrix stiffness between ~2 kPa and ~55kPa polyacrylamide gels and showed a significant difference in their nuclear and cell surface areas between the two matrices (Fig 3.1B and D, 3.2A and C, Table 3.1, 3.2 and 3.5), (ii) DLD-1 cells are stably diploid with a modal chromosome number of 44-46, maintain their ploidy across passages and are devoid of polyploid sub-populations (Fig 3.3A). We measured cell and nuclear surface areas of diploid DLD-1 cells exposed to softer polyacrylamide matrices (2 kPa and 55 kPa), for increasing durations – 15 mins to ~21 hrs (Fig 3.3B). Cell and nuclear surface area increased with time but plateaued at ~90 minutes on both the matrices (Fig 3.3C-F, Table 3.6). Furthermore, DLD-1 cells showed an increase in nuclear and cell surface areas on the comparatively stiffer 55 kPa matrices (Fig 3.3E-F, Table 3.6). We therefore selected a duration of ~90 minutes for all our assays. Comparison of cell and nuclear surface areas and volumes of DLD-1 cells between the 2 kPa, 55 kPa matrices and collagen coated glass coverslips at the end of 90 mins showed that (i) both cell and nuclear surface areas are significantly larger on 55 kPa and glass (Cell SA in μm^2 – 2 kPa M: 242.4, 55 kPa M: 384.9 and Glass M: 455.2; Nuclear SA in μm^2 – 2 kPa M: 122.6, 55 kPa M: 152.0 and Glass M: 155.0) and (ii) both cell and nuclear volumes are

significantly lowered on 55 kPa matrices (Cell volume in μm^3 – 2 kPa M: 2157, 55 kPa M: 1351 and Glass M: 1974; Nuclear volume in μm^3 – 2 kPa M: 1088, 55 kPa M: 684 and Glass M: 1015) (Fig 3.2E-H). Of note, we did not detect any significant sub-populations of arrested or senescent cells at the end of ~90 mins, as assessed by Fluorescence assisted cell scanning (FACS) analyses (Fig 3.4A-C).

Table 3.6 Nuclear and cell surface areas for DLD1 cells on softer matrices (2 kPa and 55 kPa) across time (*$p<0.05$)

Time (min)	**Nuclear area (μm^2)**		**Cell area (μm^2)**	
	2 kPa	**55 kPa**	**2 kPa**	**55 kPa**
15	97.28	115.1	183.9	241.2
30	**112.4***	**137.9***	**241.8***	**318.6***
45	112.2	134.6	280.6	**367.2***
60	**133.0***	**161.2***	283.5	381.1
90	137.0	162.1	336.1	**413.9***
145	138.5	164.5	327.2	469.4
420	131.8	162.1	354.1	482.8
1260	130.5	152.7	335.4	479.0

Figure 3.3

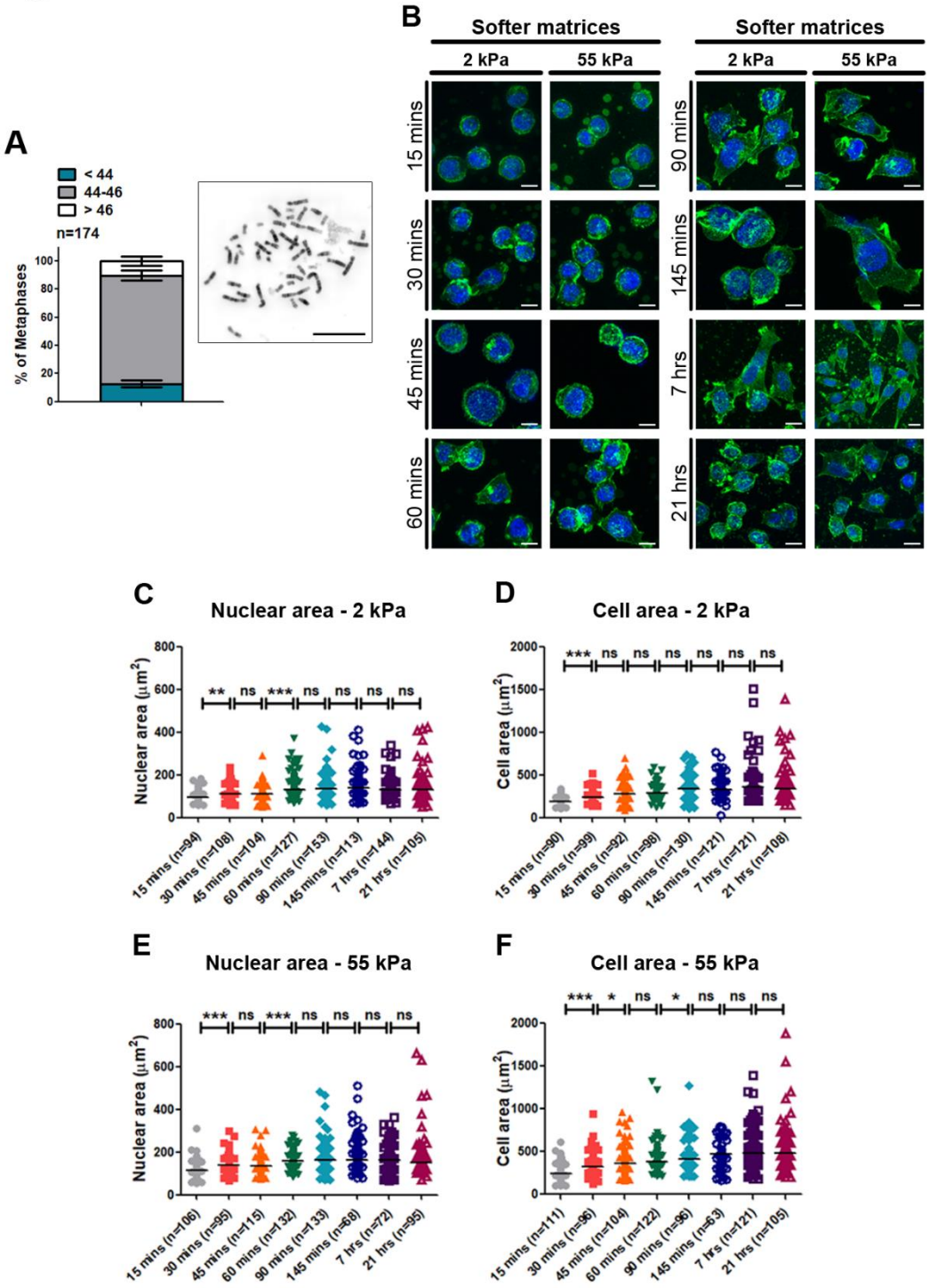

Figure 3.3 Increase in cell and nuclear surface area of DLD-1 cells on softer matrices plateau by ~90 minutes. A) Validation of DLD-1 cell line by karyotyping metaphase chromosomes. DLD-1 cells are near diploid with modal chromosome number of 44-46. *(Inset)* Representative metaphase spread of DLD-1 cells (inverted DAPI, n=153 independent metaphases compiled from 3 independent biological replicates). B) DLD-1 cells stained with phalloidin and DAPI. Cells were plated on softer matrices from ~15 min up to ~21 hrs. C-F) Dot scatter plots with median nuclear and cell areas respectively for DLD-1 cells on 2 kPa (C, D) and on 55 kPa matrices (E, F) across time. Area comparisons were performed between successive time points. *(Pooled data from N=3 independent biological replicates, n: number of cells).* *** p<0.001, ** p<0.01, * p<0.05 (Mann Whitney test). **Scale bar ~10 µm.**

Figure 3.4

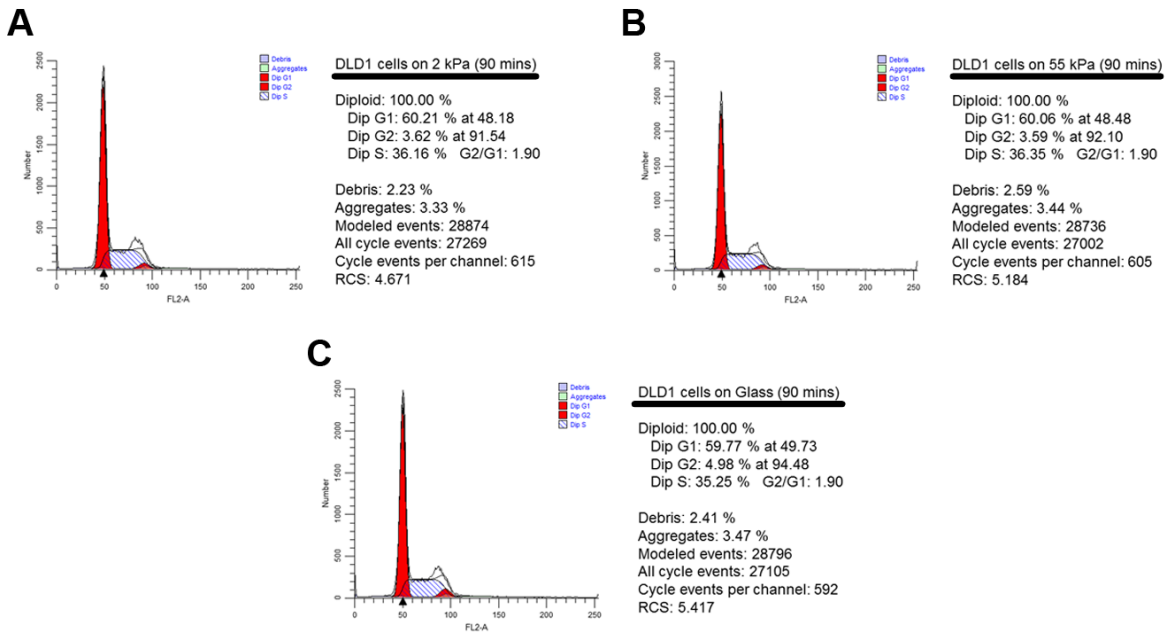

Figure 3.4 Cell cycle profile of DLD-1 cells is unaltered on softer matrices at the end of ~90 minutes. A-C) FACS analyses reiterating a predominant diploid (2n) status of DLD-1 cells on softer matrices 2 kPa (A), 55 kPa (B) and glass (C) at ~90 mins.

3.2.3 Inactive histone marks are mislocalized into the nuclear interior in cells on softer matrices

The levels and distribution of histone marks modulate gene expression (Jaenisch and Bird, 2003). Histone marks such as H3/H4 lysine acetylation, H3K4me3, H3K79me3 and H3K36me3 are generally associated with transcriptional activation (Zhang et al., 2015)**.** While inactive histone marks such as H3K9me2/3 and H3K27me3 are predominantly associated with transcriptional repression and are typically enriched as foci associated with heterochromatin predominantly at the nuclear periphery (Hattori et al., 2013; Zhang et al., 2015; Zinner et al., 2006). We examined nuclear localization and expression levels of active and inactive histone marks by immunofluorescence staining followed by confocal imaging, and independently by western

Figure 3.5

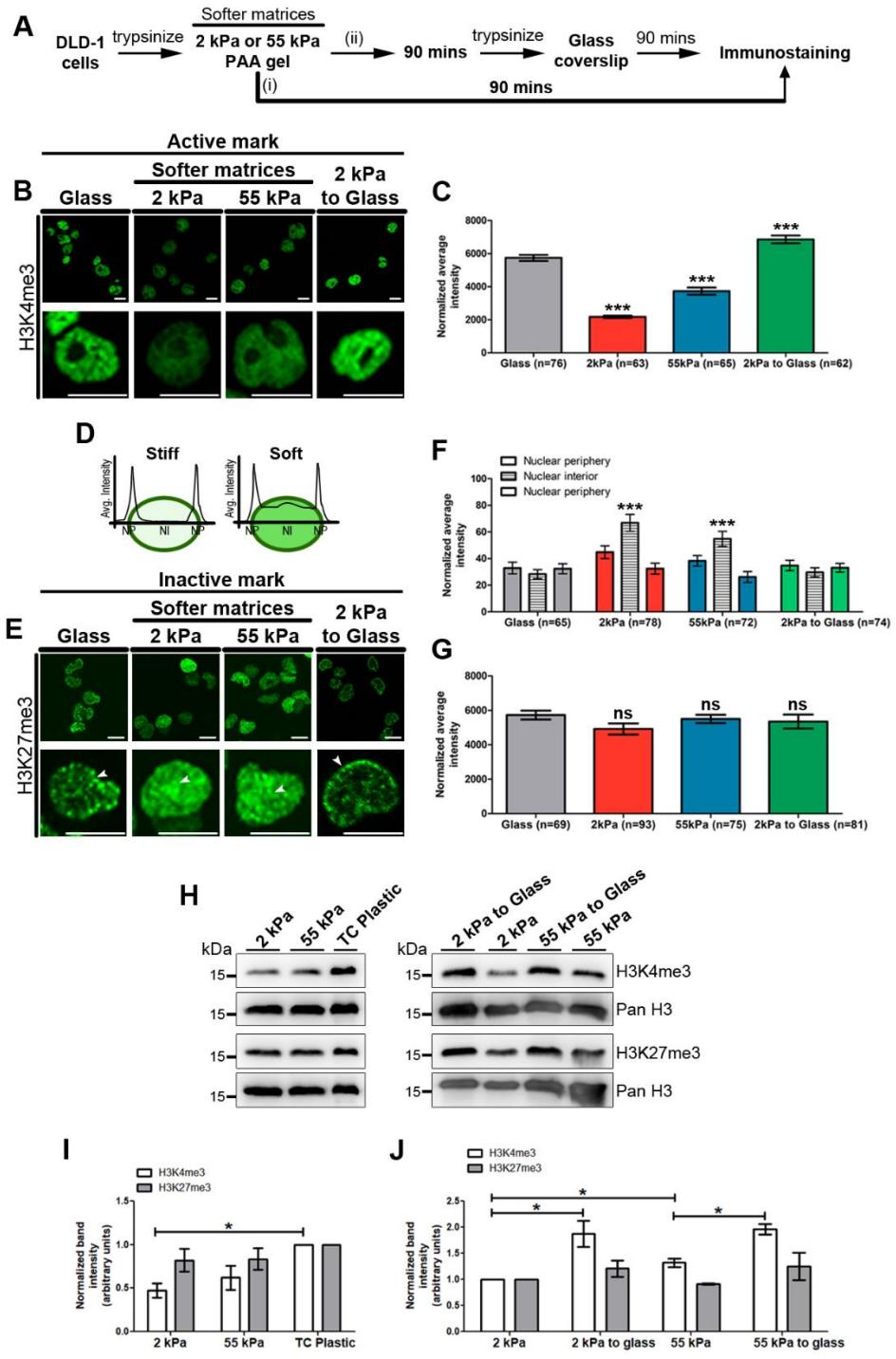

Figure 3.5 Inactive histone marks are mislocalized into the nuclear interior in cells on softer matrices. A) Experimental scheme. B-C) Representative mid-optical sections *(N=2)* from confocal z-stack of DLD-1 cells immunostained for H3K4me3 on softer matrices (2 kPa and 55 kPa), glass coverslips and cells switched from 2 kPa to glass. Lower panel: zoom of single nucleus. (C) Normalized average total fluorescence intensity of H3K4me3 under the above conditions (normalized to total nuclear surface area). D) Representation of fluorescence intensity quantification for each nucleus using line-scan analysis. E-G) Representative mid-optical sections *(N=2)* from confocal z-stack of DLD-1 cells immunostained for H3K27me3 on softer matrices (2 kPa and 55 kPa), glass coverslips and cells switched from 2 kPa to glass. Lower panel: zoom of single nucleus (F) Normalized average fluorescence intensity from line-scans across nuclei of H3K27me3 under the above conditions. (G) Normalized average total fluorescence intensity of H3K27me3 under the above conditions. *(C, F and G: n: No. of nuclei, Pooled data from N=2 independent biological replicates, Error bar: SEM, Mann Whitney test).* *** $p<0.0001$. **Scale bar ~10 µm.**

Figure 3.5 *continued.* H) *(Left)* Representative western blots *(N=3)* for H3K4me3 and H3K27me3 expression levels in DLD-1 cells on soft matrices (2 kPa and 55 kPa) and tissue culture (TC) plastic after 90 mins. *(Right)* Representative western blots *(N=3)* for H3K4me3 and H3K27me3 expression levels in DLD-1 cells on softer matrices (2 kPa and 55 kPa) and upon switching cells from softer matrices to glass (90 mins). Pan Histone H3 was used as loading control. I) Densitometric quantification of H3K4me3 and H3K27me3 levels on softer matrices (2 kPa and 55 kPa) and TC plastic after 90 mins. *(Pooled data from N=3 independent biological replicates).* * $p<0.05$ (Student's t-test). I) Densitometric quantification of H3K4me3 and H3K27 me3 levels on softer matrices (2 kPa and 55 kPa) and upon switching cells from softer matrices to glass (90 mins). *(Pooled data from N=3 independent biological replicates).* * $p<0.05$ (Student's t-test).

blotting in cells exposed to the 2 and 55 kPa matrices for 90 mins (Fig 3.5Ai). Interestingly, quantification of the fluorescence intensities of the active mark (H3K4me3) from immunofluorescence staining or overall levels from western blots showed a significant reduction (~3 fold on 2 kPa and ~1.5 fold on 55 kPa) in cells on softer matrices after ~90 minutes (Fig 3.5B-C, H-I). In contrast, the inactive mark (H3K27me3), otherwise enriched toward the nuclear periphery as distinct foci, mislocalized to the nuclear interior in cells on softer matrices (Fig 3.5D-F). However, there was no change in the overall levels of the inactive mark (Fig 3.5G-I).

We next transferred DLD-1 cells from softer 2 kPa matrices (after 90 mins) to stiffer collagen coated glass coverslips (for 90 mins), to examine if expression levels and localization of histone marks were restored (Fig 3.5Aii). Immunostaining and western blotting showed that the active H3K4me3 marks increased to basal levels in cells transferred from the softer to the stiffer glass substrates (Fig 3.5B-C, H-J). Furthermore, the inactive mark (H3K27me3 foci) was restored to the nuclear periphery in cells transferred from the softer to stiffer matrices (glass) in ~90 minutes (Fig 3.5E-F, H-J). Despite the unambiguous redistribution of H3K27me3 towards the nuclear interior in cells on softer matrices, we observed differences in the immunostaining wherein some cells showed greater H3K27me3 staining while others showed weaker staining for the inactive histone mark. H3K27me3 propagates through cell cycle via continuous modification of both new and old

histones, and has been shown to decrease during S phase (Lanzuolo et al., 2011; Alabert et al., 2015; Ma et al., 2015). Since we used an unsynchronized population of cells for the experiment, the possible reason for heterogeneity in H3K27me3 immunostaining could be the inherent heterogeneity in cell cycle stages of the DLD-1 population. In summary, cells on softer matrices show (i) a decrease in the overall levels of active marks and (ii) mislocalization of inactive histone marks into the nuclear interior, indicating a possible destabilization of the cellular transcriptome and suggestive of a potential reorganization of the genome.

3.2.4 Transcriptional deregulation is induced in cells on softer matrices

It is well established that the extracellular matrix modulates gene expression programs (Alam et al., 2016; Assoian and Klein, 2008; Mammoto et al., 2009; Roskelley et al., 1994). Since we detected altered expression and localization of histone marks in cells on softer matrices (Fig 3.5C and F), we sought to determine the effect of lowered matrix stiffness on the cellular transcriptome by performing RNA-Seq analyses of diploid DLD-1 cells exposed to 2 kPa and 55 kPa matrices for 90 minutes (Fig 3.6A). Cells on collagen coated glass coverslips for the same duration served as reference (Fig 3.6A). RNA-Seq analyses revealed 783 genes that were upregulated, while 872 genes were downregulated in cells on the 2 kPa matrices (log fold≥2) (Fig 3.6B-C). In contrast, 649 genes were upregulated, and 828 genes were downregulated in cells on the 55 kPa matrices (log fold≥2) (Fig 3.6B-C). We next performed Gene Ontology (GO) analyses using DAVID to identify categories of the significantly deregulated genes in cells exposed to the softer matrices. This analysis revealed distinct subsets of genes associated with (i) mRNA processing, splicing and export (RNA binding category) (ii) cell cycle and (iii) DNA damage and repair that were strikingly up and downregulated on 2 kPa matrices (Fig 3.6D-E).

Figure 3.6

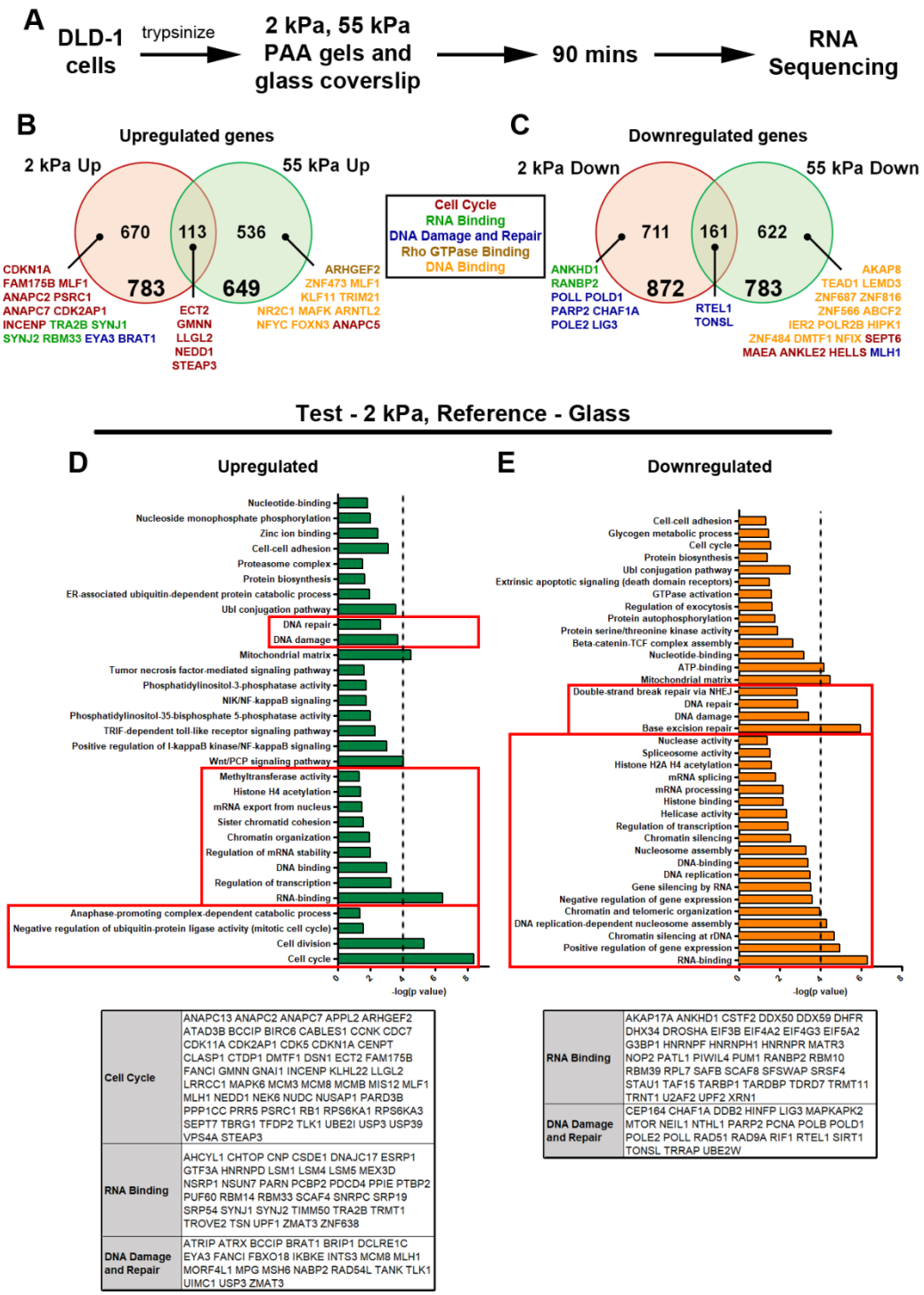

Figure 3.6 Transcriptional deregulation is induced in cells on softer matrices. A) Experimental scheme for RNA sequencing *(N=2 independent biological replicates).* B) Total number of genes upregulated (≥ log 2-fold) on the softer matrices – 2 kPa (783 genes) and 55 kPa (649 genes), 670 and 536 genes were uniquely upregulated on 2 kPa and 55 kPa matrices respectively, while 113 genes were commonly upregulated on both the matrices. Selected genes from the maximally deregulated GO categories that are upregulated uniquely (>log2 - 10 fold) and commonly (>log2 -2 fold) on both the soft matrices are displayed. C) Total number of genes downregulated (≥ log 2-fold) on the softer matrices – 2 kPa (872 genes) and 55 kPa (828 genes), 711 and 667 genes were uniquely downregulated on 2 kPa and 55 kPa matrices respectively, while 161 genes were commonly downregulated on both the matrices. Selected genes from the maximally deregulated GO categories that are downregulated uniquely (>log2 - 10 fold) and commonly (>log2 -2 fold) on both the soft matrices are displayed.

Figure 3.6 *continued.* Classification of ≥ log 2-fold up and downregulated genes on 2 kPa matrices into Gene Ontology (GO) categories. D) GO category classification of genes upregulated (≥ log 2-fold) in cells on 2 kPa matrices. Red boxes indicate the GO categories that are closely related to i) Cell cycle ii) Chromatin associated processes and iii) DNA damage and repair. Genes mapping to the GO categories of Cell cycle, RNA binding and DNA damage and repair are listed below. E) GO category classification of genes downregulated (≥ log 2-fold) in cells on 2 kPa matrices. Red boxes indicate the GO categories that are closely related to i) Chromatin associated processes and ii) DNA damage and repair. Genes mapping to the GO categories of RNA binding and DNA damage and repair are listed below.

Figure 3.7

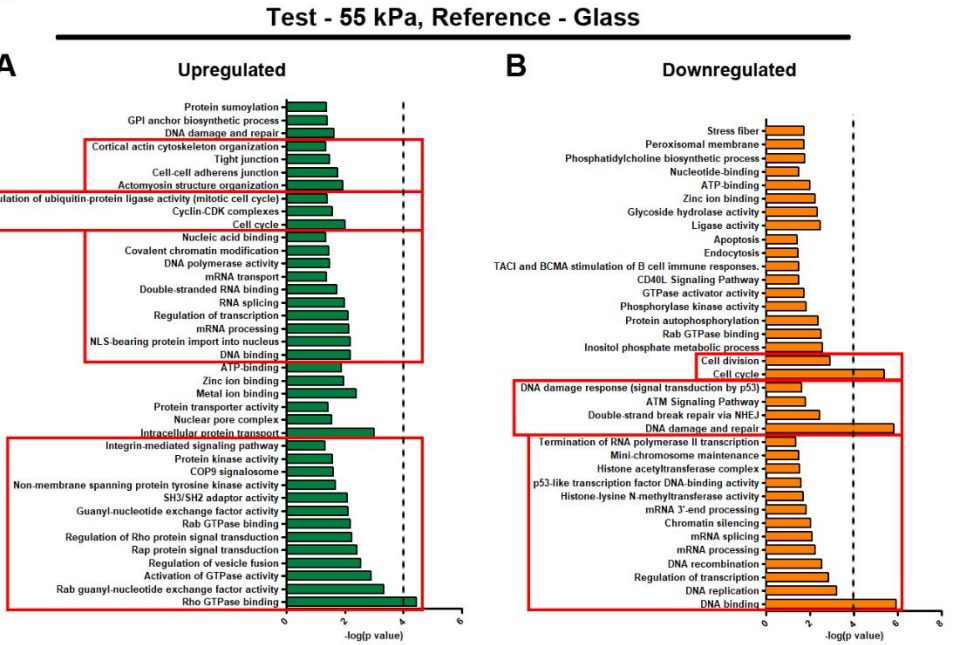

Rho GTPase Binding	AKAP13 ARHGEF16 ARHGEF2 DOCK11 ECT2 IQGAP2 MYO9B FMNL3
DNA Binding	APTX ARID4B ARNTL2 ASH2L BBX CHRAC1 CLSPN CSRNP2 DEDD2 EGR2 EGR3 ETV3 EXO1 FOXJ3 FOXN3 FOXP4 FUS HNF4A HOXB9 HSF2 KIN KLF11 LBR LCOR MAFK MBD4 MITF MLF1 MND1 NFYC NR2C1 NR4A3 ORC1 PAPD7 PHC1 POLK PSMC3IP RAD51D RAD54L2 STAT6 TAF4B TCF12 TCF7L2 THRA TNFAIP3 TOP3B TRIM21 TRIM33 UBN1 USF2 XRCC3 ZBTB10 ZMYND11 ZNF131 ZNF195 ZNF285 ZNF322 ZNF33B ZNF414 ZNF441 ZNF473 ZNF556 ZNF611 ZNF664 ZNF678 ZNF70 ZNF778 ZNF793 ZNF808
Cell Cycle	ANAPC5 ANAPC7 ARHGEF2 CCNG1 CCNT2 CDC27 CDK2 CDK6 CEP250 CLSPN CSNK2A1 ECT2 FOXN3 GMNN LLGL2 MLF1 NEDD1 NEK3 PAPD7 PRNP SKA3 STEAP3 STK11 TP53BP2 TRIM21 UBE2I
Actomyosin Structure and Organization	EPB41 EPB41L1 FRMD6 MYH10 EPB41L2

DNA Binding	ABCF2 ADAR AKAP8 APLP2 ARNT ARNTL ASXL1 ATM BANP BRCA1 CHD4 CHD8 CHTF8 DMTF1 E2F6 ERCC4 EZH2 FAM200B HIPK1 HIST1H2AD HIST1H2AH HIST1H2AJ HIST1H2BN HIST1H4A HIST2H2AB HMCES IER2 IMPDH1 IRF2 KMT2D LEMD3 LIG3 LIG4 MBD5 MCM4 MCM8 MCM9 MIER1 MLXIP MUS81 NCOR1 NCOR2 NFATC3 NFIX NFYB NME2 ORC4 ORC6 POGZ POLD2 POLE2 POLQ POLR2B PPARG PQBP1 PUF60 RFX7 RNF6 RUNX2 SCMH1 SCML2 SETDB1 SON STAT3 TAF12 TAF6 TBX3 TEAD2 TFDP1 TGIF2-C20ORF24 TP53 TRIM26 ZBED1 ZFX ZKSCAN5 ZNF207 ZNF251 ZNF26 ZNF283 ZNF343 ZNF384 ZNF408 ZNF426 ZNF433 ZNF484 ZNF566 ZNF589 ZNF627 ZNF655 ZNF687 ZNF700 ZNF749 ZNF816 ZNF91
DNA Damage and Repair	APLF BRCA1 CEP164 CHAF1A CHEK2 DCLRE1C ERCC4 FANCB FANCC HELB INIP INO80C LIG3 LIG4 MCM8 MCM9 MLH1 MORF4L2 MUM1 MUS81 NSMCE4A PAXIP1 POLQ RAD23B RRM2B RTEL1 SFPQ TONSL UBR5 MORF4L1
Cell Cycle	ANAPC15 ANKLE2 ATM BANP BECN1 BOD1 BRCA1 CDK2AP1 CENPE CEP164 CHAF1A CHEK2 CHTF8 CNTRL DMTF1 E2F6 GNAI2 HELLS LIG3 LIG4 MAEA MCM4 MCM8 MCMBP MLH1 MPLKIP NDE1 NEK2 NPAT OIP5 PARD6A PDCD6IP POGZ PRC1 PRPF40A SEPT6 SON SPIN2B SUV39H2 TBRG1 TFDP1 TP53 ZNF207

Figure 3.7 Classification of ≥ log 2-fold up and downregulated genes on 55 kPa matrices into Gene Ontology (GO) categories. A) GO category classification of genes upregulated (≥ log 2-fold) in cells on 55 kPa matrices. Red boxes indicate the GO categories that are closely related to i) GTPase signaling ii) Chromatin associated processes iii) Cell cycle and iv) Cytoskeleton and cell junctions. Genes mapping to the GO categories of Rho GTPase binding, DNA binding, Cell cycle and Actomyosin structure and organization are listed below. B) GO category classification of genes downregulated (≥ log 2-fold) in cells on 55 kPa matrices. Red boxes indicate the GO categories that are closely related to i) Chromatin associated processes ii) DNA damage and repair and iii) Cell cycle. Genes mapping to the GO categories of DNA binding, DNA damage and repair and Cell cycle are listed below.

Genes associated with the Rho-GTPase signaling pathway were significantly upregulated and those associated with (i) transcription regulation, chromatin and chromosome organization (DNA binding category) (ii) cell cycle and (iii) DNA damage and repair were downregulated in cells on the 55 kPa matrices (Fig 3.7A-B). Of note, although common pathways were enriched in either of the matrices, non-overlapping and unique subsets of genes were deregulated in each of these categories.

3.2.5 Motif enrichment analysis reveals overlapping and unique transcription factors that may regulate gene expression in cells on softer matrices

Since we were interested in identifying the factors involved in modulating transcription as a response to altered extracellular matrix stiffness, we performed *in silico* analysis of promoters of genes deregulated in cells exposed to softer matrices (2 kPa and 55 kPa independently) for enrichment of consensus motifs belonging to transcription factors or miRNAs using GSEA (Gene Set Enrichment Analysis). Lists of genes up and downregulated on either the 2 kPa or 55 kPa matrices were independently compared with curated data sets in GSEA Molecular Signature Database (MSigDB) to determine consensus motifs and miRNA binding sites within the gene lists of interest. Motif enrichment analysis revealed both unique and common transcription factors and miRNAs that could potentially regulate gene expression changes elicited by exposure to lowered matrix stiffness (Fig 3.8A, Table 3.7-3.10). The unique transcription factors and miRNAs for the different categories were as follows: Genes upregulated on 2 kPa – MIR429, MIR200B, MIR200C, AP1, ERR1; Genes downregulated on 2 kPa – MIR506, ARNT; Genes upregulated on 55 kPa – MIR524, MIR9, MIR330, MIR518A2, MYOD, FREAC2, ETS; Genes downregulated on 55 kPa – MIR26A, MIR26B, E2F1, CETS1P54 (Fig 3.6A, Table 3.9). Besides these, motifs for the

transcription factors SP1, LEF1, E12, NFY, FOXO4, MAZ, NRF1 and NFAT were found commonly in genes either up or downregulated on both the softer matrices (Table 3.11). It is important to note that the presence of consensus motifs for transcription factors and miRNAs binding sites suggests both transcriptional and post-transcriptional regulation of gene expression upon altered matrix stiffness.

Table 3.7 Motif/miRNAs enrichment observed for upregulated genes in DLD-1 cells on 2 kPa matrices

Sr. No.	Transcription factor	Motif/miRNA	p value
1	SP1	GGGCGGR	2.41E-41
2	ELK1	SCGGAAGY	3.21E-32
3	GABP	MGGAAGTG	2.48E-31
4	NFY	GATTGGY	2.51E-23
5	LEF1	CTTTGT	4.05E-23
6	E12	CAGGTG	1.19E-21
7	Unknown	AACTTT	1.63E-20
8	E4F1	GTGACGY	2.21E-19
9	AP4	CAGCTG	2.44E-17
10	NFAT	TGGAAA	8.55E-17
11	NRF1	RCGCANGCGY	9.90E-17
12		MicroRNA GCACTTT, MIR175P, MIR20A, MIR20B, MIR106A, MIR106B, MIR519D	1.10E-16
13	ETS2	RYTTCCTG	4.99E-16
14	Unknown	GGGYGTGNY	1.13E-15
15	Unknown	TGACATY	5.64E-15
16	MAZ	GGGAGGRR	1.16E-14
17	FOXO4	TTGTTT	2.54E-14
18	AP1	TGANTCA	9.91E-14
19		MicroRNA CAGTATT, MIR200B, MIR200C, MIR429	1.67E-13
20	ERR1	TGACCTY	2.16E-13

Figure 3.8

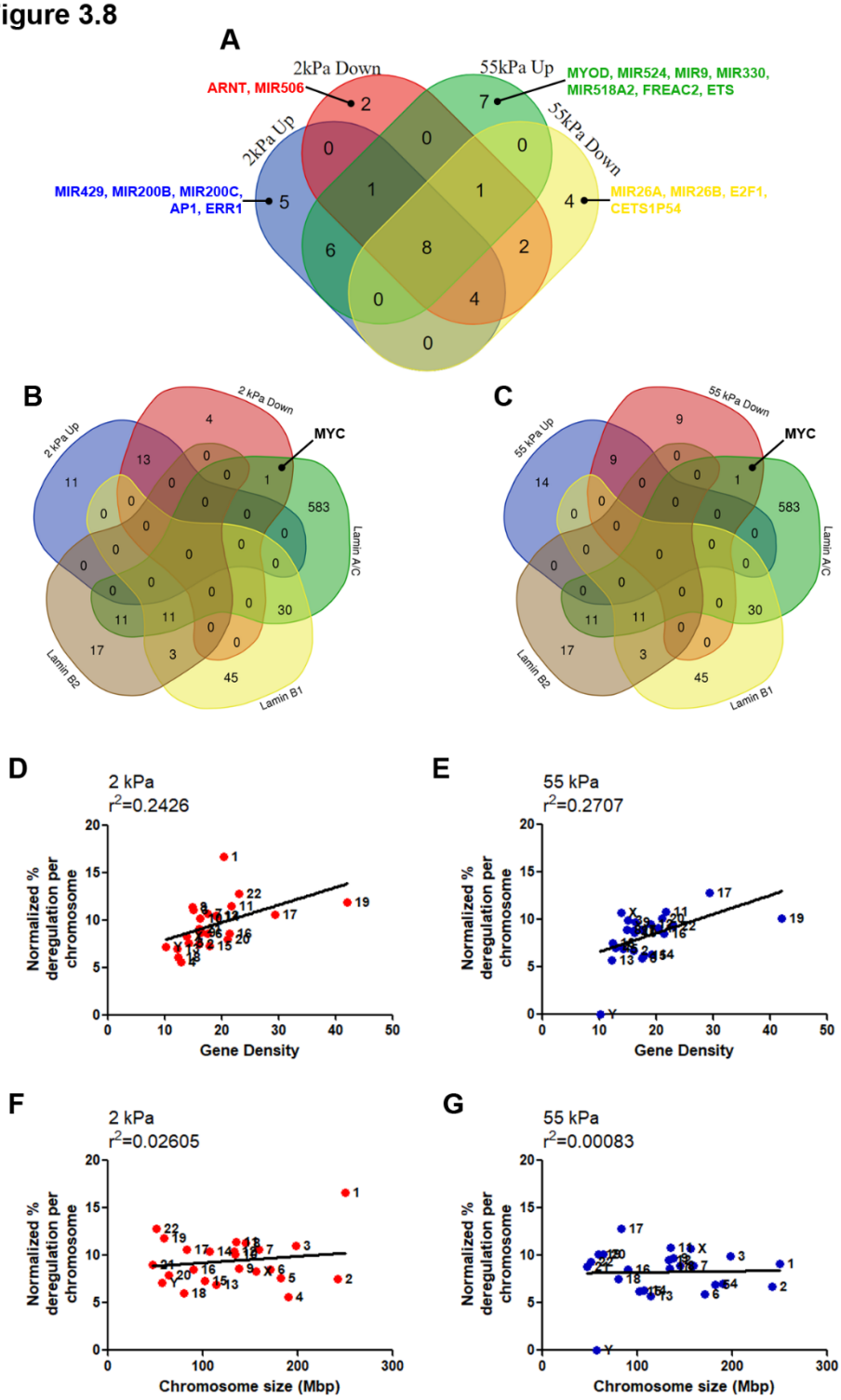

Figure 3.8 Motif enrichment analysis reveals overlapping and unique transcription factors that may regulate gene expression in cells on soft matrices. A) Venn diagram depicting the number of common and unique transcription factors and miRNAs with motifs/binding sites enriched in genes up and downregulated in cells on 2 kPa and 55 kPa matrices. Transcription factors and miRNAs with unique enrichment in genes upregulated or downregulated on 2 kPa or 55 kPa have been displayed. B) Venn diagram depicting the overlap between transcription factors with motifs enriched in up and downregulated genes in cells on 2 kPa matrices, and protein interactors of Lamin A/C, B1 and B2 (compiled from BioGRID). C) Venn diagram depicting the overlap between transcription factors with motifs enriched in up and downregulated genes in cells on 55 kPa matrices, and protein interactors of Lamin A/C, B1 and B2 (compiled from BioGRID).

Figure 3.8 *continued.* Correlation between transcriptional deregulation and chromosome size and gene density. D) Plot of correlation between % chromosomal deregulation on 2 kPa matrices and gene density (No. of genes/Mbp). E) Plot of correlation between % chromosomal deregulation on 55 kPa matrices and gene density (No. of genes/Mbp). F) Plot of correlation between % chromosomal deregulation on 2 kPa matrices and chromosome size (Mbp). G) Plot of correlation between % chromosomal deregulation on 55 kPa matrices and chromosome size (Mbp).

Table 3.8 Motif/miRNAs enrichment observed for downregulated genes in DLD-1 cells on 2 kPa matrices

Sr. No.	Transcription factor	Motif/miRNA	p value
1	SP1	GGGCGGR	3.01E-40
2	ELK1	SCGGAAGY	9.32E-26
3	NRF1	RCGCANGCGY	9.45E-20
4	NFY	GATTGGY	1.32E-19
5	MAZ	GGGAGGRR	4.68E-19
6	FOXO4	TTGTTT	4.63E-17
7	E12	CAGGTG	6.51E-17
8	LEF1	CTTTGT	2.55E-16
9	GABP	MGGAAGTG	2.74E-16
10	AP4	CAGCTG	1.26E-14
11	Unknown	AACTTT	1.15E-13
12	MYC	CACGTG	2.54E-13
13	ETS2	RYTTCCTG	5.35E-13
14	E4F1	GTGACGY	9.15E-13
15	Unknown	TGCGCANK	9.69E-13
16	PAX4	GGGTGGRR	5.86E-12
17	NFAT	TGGAAA	4.73E-11
18		MicroRNA GTGCCTT, MIR506	2.77E-10
19	YY1	GCCATNTTG	2.77E-10
20	ARNT		2.84E-10

Table 3.9 Motif/miRNAs enrichment observed for upregulated genes in DLD-1 cells on 55 kPa matrices

Sr. No.	Transcription factor	Motif/miRNA	p value
1	SP1	GGGCGGR	4.04E-42
2	MAZ	GGGAGGRR	2.42E-30
3	E12	CAGGTG	3.56E-27
4	LEF1	CTTTGT	3.63E-22
5	FOXO4	TTGTTT	2.78E-19
6	ETS2	RYTTCCTG	1.77E-18
7	NFAT	TGGAAA	3.97E-18
8	PAX4	GGGTGGRR	2.84E-16
9	Unknown	AACTTT	4.45E-16
10	NRF1	RCGCANGCGY	2.25E-14
11		MicroRNA ACCAAAG, MIR9	6.62E-14
12		MicroRNA CTTTGTA, MIR524	2.81E-13
13	FREAC2	RTAAACA	1.58E-12
14	MYOD	GCANCTGNY	1.89E-12
15	ETS		3.22E-12
16	LEF1	CTTTGT	4.36E-12
17		MicroRNA TGCTTTG, MIR330	5.48E-12
18	NFY	GATTGGY	6.10E-12
19		MicroRNA GCACTTT, MIR175P, MIR20A, MIR20B, MIR106A, MIR106B, MIR519D	8.06E-12
20		MicroRNA TTTGCAG, MIR518A2	9.18E-12

Table 3.10 Motif/miRNAs enrichment observed for downregulated genes in DLD-1 cells on 55 kPa matrices

Sr. No.	Transcription factor	Motif/miRNA	p value
1	SP1	GGGCGGR	4.66E-47
2	ELK1	SCGGAAGY	4.26E-34
3	NFY	GATTGGY	5.92E-20
4	GABP	MGGAAGTG	9.43E-20
5	E12	CAGGTG	1.43E-19
6	AP4	CAGCTG	3.57E-18
7	NRF1	RCGCANGCGY	5.27E-18
8	LEF1	CTTTGT	6.62E-18
9	PAX4	GGGTGGRR	7.97E-16
10	MYC	CACGTG	1.33E-14
11	Unknown	AACTTT	1.06E-13
12	LEF1	CTTTGA	1.40E-13
13	FOXO4	TTGTTT	1.52E-13
14	MAZ	GGGAGGRR	2.05E-13
15	YY1	GCCATNTTG	2.42E-13
16	NFAT	TGGAAA	2.61E-12
17	E4F1	GTGACGY	4.34E-12
18		MicroRNA TACTTGA, MIR26A, MIR26B	4.69E-12
19	E2F1		5.16E-12
20	CETS1P54		6.97E-12

Table 3.11 Unique and common miRNAs or transcription factors with enriched motifs in genes deregulated on soft matrices

Category	No. of TFs/miRNAs	Names
Only 2 kPa Up	5	MicroRNA CAGTATT, MIR429, MIR200B, MIR200C, AP1, ERR1
Only 2 kPa Down	2	MicroRNA GTGCCTT, MIR506, ARNT
Only 55 kPa Up	7	MircoRNA ACCAAAG, MicroRNA CTTTGTA, MicroRNA TGCTTTG, MicroRNA TTTGCAG, MIR524, MIR9, MIR330, MIR518A2, MYOD, FREAC2, ETS
Only 55 kPa Down	4	MicroRNA TACTTGA, MIR26A, MIR26B, E2F1, CETS1P54
2 kPa Up and 55 kPa Up	15	MicroRNA GCACTTT, MIR519D, MIR20A, MIR20B, MIR106A, MIR106B, MIR175P, SP1, LEF1, E12, NFY, FOXO4, MAZ, NRF1, NFAT, ETS2
2 kPa Down and 55 kPa Down	15	YY1, MYC, SP1, LEF1, E12, NFY, FOXO4, MAZ, NRF1, NFAT, PAX4, ELK1, GABP, E4F1, AP4
2 kPa Up and Down	13	SP1, LEF1, E12, NFY, FOXO4, MAZ, NRF1, NFAT, ETS2, ELK1, GABP, E4F1, AP4
55 kPa Up and Down	9	SP1, LEF1, E12, NFY, FOXO4, MAZ, NRF1, NFAT, PAX4
2 kPa and 55 kPa Up and Down	8	SP1, LEF1, E12, NFY, FOXO4, MAZ, NRF1, NFAT

Nuclear lamins, particularly Lamin A/C, regulate nuclear structure and its mechano-responsiveness (Buxboim et al., 2014; Dechat et al., 2008; Lammerding et al., 2005; Smith et al., 2017; Swift et al., 2013; Zwerger et al., 2015). Lamins also modulate RNA Polymerase II mediated transcription and sequester various transcription factors at the nuclear periphery – a location for gene repression (Heessen and Fornerod, 2007; Spann et al., 2002). To examine if the transcriptional deregulation observed in cells on softer matrices was directly under Lamin regulation, we sought to identify transcription factors (from the motif enrichment analysis) that were interactors of Lamin A/C, B1 or B2. Only Myc – whose consensus motif is enriched in genes downregulated on both 2 kPa and 55 kPa matrices, directly interacts with Lamin A/C (Fig 3.8B-C). In summary, gene expression changes in response to lowered substrate stiffness could be modulated both transcriptionally (by specific transcription factors) as well as post-transcriptionally (by miRNAs), and may potentially have a partial regulation via Lamin A/C and Myc.

3.2.6 Chromosome-wise transcriptional deregulation in cells on softer matrices

While RNA-Seq analysis elucidated expression changes at the level of individual genes, we were also interested in understanding the transcriptional regulation of whole chromosome territories in response to changes in extracellular matrix stiffness. To determine if transcriptional changes were selective towards specific chromosomes, we examined the correlation between transcriptional deregulation and (i) chromosome size (ii) gene density. Transcriptional deregulation per chromosome was plotted by normalizing the total number of up and downregulated genes on the chromosome to the total number of transcribing genes (FPKM>1.0 from RNA-Seq data) on that chromosome. The plot of % normalized deregulation per chromosome vs gene density showed a weak correlation with r^2=0.2426 and r^2=0.2707 for cells on 2 kPa and 55 kPa matrices respectively

(Fig 3.8D-E). On the other hand, the plot of % normalized deregulation per chromosome vs chromosome size did not show any correlation (r^2=0.026 and r^2=0.0008 for cells on 2 kPa and 55 kPa matrices respectively) (Fig 3.8F-G). In summary, gene density based selection does not completely explain the chromosome wide transcriptional changes in cells on softer matrices.

We next classified the up and downregulated genes into bins of increasing fold change to identify chromosomes that were enriched for transcriptionally deregulated genes (Fig 3.9A-B). Most chromosomes showed an equivalent enrichment of up and downregulated genes on both the matrices (Fig 3.9A-B). However, the maximum number of transcriptionally deregulated genes mapped to human Chr. 1 (~33%) - the largest chromosome in the human genome (Gene Density ~20.31 genes/Mbp, DNA content ~250 Mbp) in cells on the 2 kPa matrices, while all other chromosomes showed an enrichment of up to ~15% (Fig 3.9A and C, black arrow, Table 3.12). We examined human Chr. 18 and 19, that represent chromosomes of divergent gene densities but comparable DNA content. Gene rich Chr. 19 (Gene Density ~42.05 genes/Mbp, DNA content ~59 Mbp) showed a significantly greater enrichment of transcriptionally deregulated genes than gene poor Chr. 18 (Gene Density ~12.35 genes/Mbp, DNA content ~80 Mbp) in cells on either of the matrices (2 or 55 kPa) (Fig 3.9A-D, black/red box, Table 3.12). Interestingly, human Chr. 1 again harbored the maximum number of transcriptionally deregulated genes (~19%) in cells on 55 kPa matrices, albeit to a lower extent than cells on the 2 kPa matrices (Fig 3.9B and D, Table 3.12).

Figure 3.9

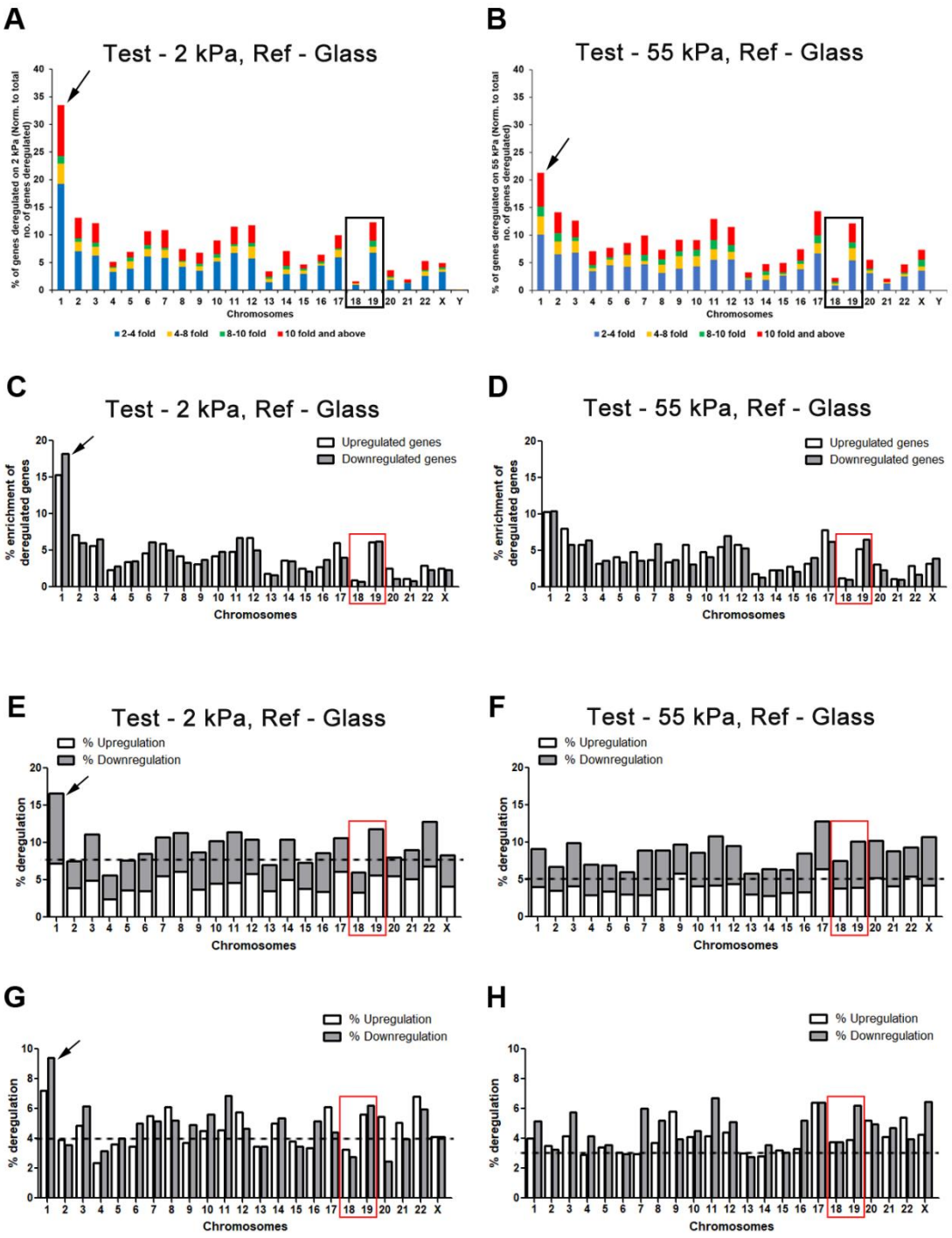

Figure 3.9 Chromosome wide transcriptional deregulation in cells on soft matrices. A) Bar graph depicting % enrichment of deregulated genes (up and down together) in cells on 2 kPa matrices, on all the chromosomes. ≥ log 2-fold deregulated genes (up and down together – 1655 genes) were classified into bins of fold change (2-4 fold, 4-8 fold, 8-10 fold and >10 fold) and mapped onto chromosomes. *(Arrow)* Chromosome 1 shows the maximum enrichment of deregulated genes on 2 kPa (~33.5%). *(Black box)* Chromosome 18 is amongst the chromosomes showing least enrichment of transcriptionally deregulated genes, while chromosome 19 is amongst the chromosomes showing high enrichment. B) Bar graph depicting % enrichment of deregulated genes (up and down together) in cells on 55 kPa matrices, on all the chromosomes. ≥ log 2-fold deregulated genes (up and down together – 1432 genes) were classified into bins of fold change (2-4 fold, 4-8 fold, 8-10 fold and >10 fold) and mapped onto chromosomes. *(Arrow)* Chromosome 1 shows enrichment of deregulated genes on 55 kPa (~19.2%) to a much lesser extent than on 2 kPa (~33.5%). *(Black box)* Chromosome 18 is amongst the chromosomes showing least enrichment of transcriptionally deregulated genes, while chromosome 19 is amongst the chromosomes showing high enrichment.

Figure 3.9 ***continued.*** C) Bar graph depicting % enrichment of up and downregulated genes (≥ log 2-fold up – 783 genes, down – 872 genes) in cells on 2 kPa matrices, on all the chromosomes. D) Bar graph depicting % enrichment of up and downregulated genes (≥ log 2-fold up – 649 genes, down – 783 genes) in cells on 55 kPa matrices, on all the chromosomes. E) Stacked bar graph depicting % deregulation (up and down) in cells on 2 kPa matrices, on all the chromosomes. ≥ log 2-fold deregulated genes (up and down separately) on each chromosome were normalized to the total number of transcribing genes (FPKM>1) on that chromosome. *(Arrow)* Chromosome 1 shows the maximum deregulation on 2 kPa (~13.15%). *(Red box)* Chromosome 18 is amongst the chromosomes showing least transcriptional changes, while chromosome 19 is amongst the chromosomes showing high transcriptional deregulation. F) Stacked bar graph depicting % deregulation (up and down) in cells on 55 kPa matrices, on all the chromosomes. ≥ log 2-fold deregulated genes (up and down separately) on each chromosome were normalized to the total number of transcribing genes (FPKM>1) on that chromosome. *(Red box)* Chromosome 18 shows less transcriptional deregulation as compared to chromosome 19. G) Bar graph depicting % up and downregulation in cells on 2 kPa matrices, on all the chromosomes. ≥ log 2-fold deregulated genes (up and down separately) on each chromosome were normalized to the total number of transcribing genes (FPKM>1) on that chromosome. H) Bar graph depicting % up and downregulation in cells on 55 kPa matrices, on all the chromosomes. ≥ log 2-fold deregulated genes (up and down separately) on each chromosome were normalized to the total number of transcribing genes (FPKM>1) on that chromosome.

To ensure that the total number of genes on each chromosome did not bias our conclusions, we normalized the total number of up and downregulated genes on every chromosome to the total number of transcribing genes (FPKM>1 from the RNA-Seq data) on that chromosome as done previously. Plots of % deregulation of each chromosome reiterated that Chr. 1 is maximally deregulated on the 2 kPa matrices (~16%), while all other chromosomes show ~9% deregulation (Fig 3.9E and G, Table 3.13). Additionally, the gene rich Chr. 19 is deregulated to a greater extent than the gene poor Chr. 18 in cells on both 2 kPa and 55 kPa matrices (Fig 3.9E-H, red box, Table 3.13). Some of the other chromosomes that show lesser transcriptional changes on 2 kPa matrices are 2, 4, 5, 13, 15, 20 and those that show greater transcriptional deregulation are 3, 7, 8, 10, 11, 12, 14, 17, 22 (Fig 3.9E and G). On the other hand, chromosomes 6, 13, 14, 15 are deregulated to a lesser extent on 55 kPa matrices, while all the other chromosomes show more or less comparable expression changes (Fig 3.9F and H).

Table 3.12 Enrichment of deregulated genes in cells on softer matrices (2 kPa and 55 kPa) on all chromosomes

	2 kPa		55 kPa	
Chr.	**%Upregulated (out of 786 genes)**	**%Downregulated (out of 856 genes)**	**%Upregulated (out of 651 genes)**	**%Downregulated (out of 828 genes)**
1	15.27	18.22	8.52	10.63
2	7.12	5.96	6.62	5.84
3	5.60	6.54	4.83	6.89
4	2.29	2.80	2.67	3.74
5	3.44	3.50	3.44	3.27
6	4.58	6.07	3.94	3.74
7	5.85	5.02	3.05	5.84
8	4.20	3.27	2.80	3.74
9	3.05	3.74	4.83	3.15
10	4.20	4.79	3.94	4.44
11	4.83	6.66	4.58	6.89
12	6.74	5.02	4.83	5.14
13	1.78	1.64	1.53	1.40
14	3.56	3.50	1.91	2.34
15	2.54	2.10	2.29	2.10
16	2.67	3.74	2.67	4.32
17	5.98	3.97	6.49	6.31
18	0.89	0.70	1.02	0.93
19	6.11	6.19	4.33	6.66
20	2.54	1.05	2.54	2.34
21	1.15	0.82	0.89	0.93
22	2.93	2.34	2.42	2.10
X	2.54	2.34	2.67	3.97
Y	0.13	0.00	0.00	0.00

Table 3.13 % deregulation of all chromosomes in cells on softer matrices (2 kPa and 55 kPa)

	2 kPa		55 kPa	
Chr.	**%Upregulation**	**%Downregulation**	**%Upregulation**	**%Downregulation**
1	7.23	9.40	4.00	5.13
2	3.93	3.58	3.50	3.23
3	4.87	6.19	4.13	5.77
4	2.40	3.20	2.90	4.14
5	3.60	4.01	3.40	3.53
6	3.49	5.04	3.04	2.94
7	5.52	5.16	2.94	6.00
8	6.13	5.20	3.70	5.21
9	3.71	4.95	5.78	3.96
10	4.54	5.64	4.10	4.49
11	4.58	6.87	4.15	6.69
12	5.77	4.68	4.41	5.10
13	3.49	3.49	3.02	2.76
14	5.03	5.39	2.80	3.55
15	3.85	3.46	3.21	3.04
16	3.40	5.18	3.32	5.21
17	6.14	4.44	6.42	6.42
18	3.26	2.79	3.77	3.77
19	5.62	6.21	3.90	6.19
20	5.49	2.47	5.21	4.95
21	5.08	3.95	4.12	4.71
22	6.85	5.95	5.38	3.97
X	4.15	4.15	4.24	6.46
Y	7.14	0.00	0.00	0.00

3.2.7 Chromosome territories are mislocalized into the nuclear interior in cells on softer matrices

The gene density based organization of chromosome territories is generally conserved, wherein gene rich chromosomes are present towards the nuclear interior and gene poor chromosomes towards the nuclear periphery (Cremer et al., 2003; Tanabe et al., 2002). However, the repositioning of chromosome territories can occur in dynamic processes, in response to external or internal cues and upon changes in physical attributes of the nucleus among others (Bridger et al., 2000; McNamara et al., 2012; Meaburn et al., 2007; Mehta et al., 2010; Mehta et al., 2013). We therefore examined spatial organization of chromosome territories in cells exposed to softer matrices. We visualized Chr. 1, 18 and 19 territories in the interphase nucleus of DLD-1 cells exposed to 2 kPa matrices since (i) Chr. 1 harbored the maximum subset of transcriptionally deregulated genes in cells on the 2 kPa matrices (Fig 3.9A and E) (ii) gene poor Chr. 18 and gene rich Chr. 19 represent chromosomes of strikingly divergent gene densities but of comparable DNA content and also show very different transcriptional deregulation on both 2 kPa and 55 kPa matrices (Fig 3.9A-B and E-F). Cells exposed to collagen coated glass coverslips for ~90 minutes served as control (100 µg/ml Collagen, referred to as glass hereafter) (Fig 3.10A-B). Remarkably, 3-Dimensional fluorescence in situ hybridization (3D-FISH) followed by confocal imaging, 3D reconstruction and radial distance measurements of chromosome territories, showed that CT1 was strikingly mislocalized toward the nuclear interior (R.D ~50.57%) in cells on softer matrices (2 kPa), from its otherwise conserved location closer to the nuclear periphery in cells on glass (R.D ~66.81%) (Fig 3.10B-C, Table 3.14). It is well established that the spatial positions of human Chr. 18 (gene poor, peripheral) and 19 (gene rich, internal) territories in the nucleus are non-random and are largely conserved across cell types (Cremer et al., 2003; Tanabe et al., 2002).

Figure 3.10

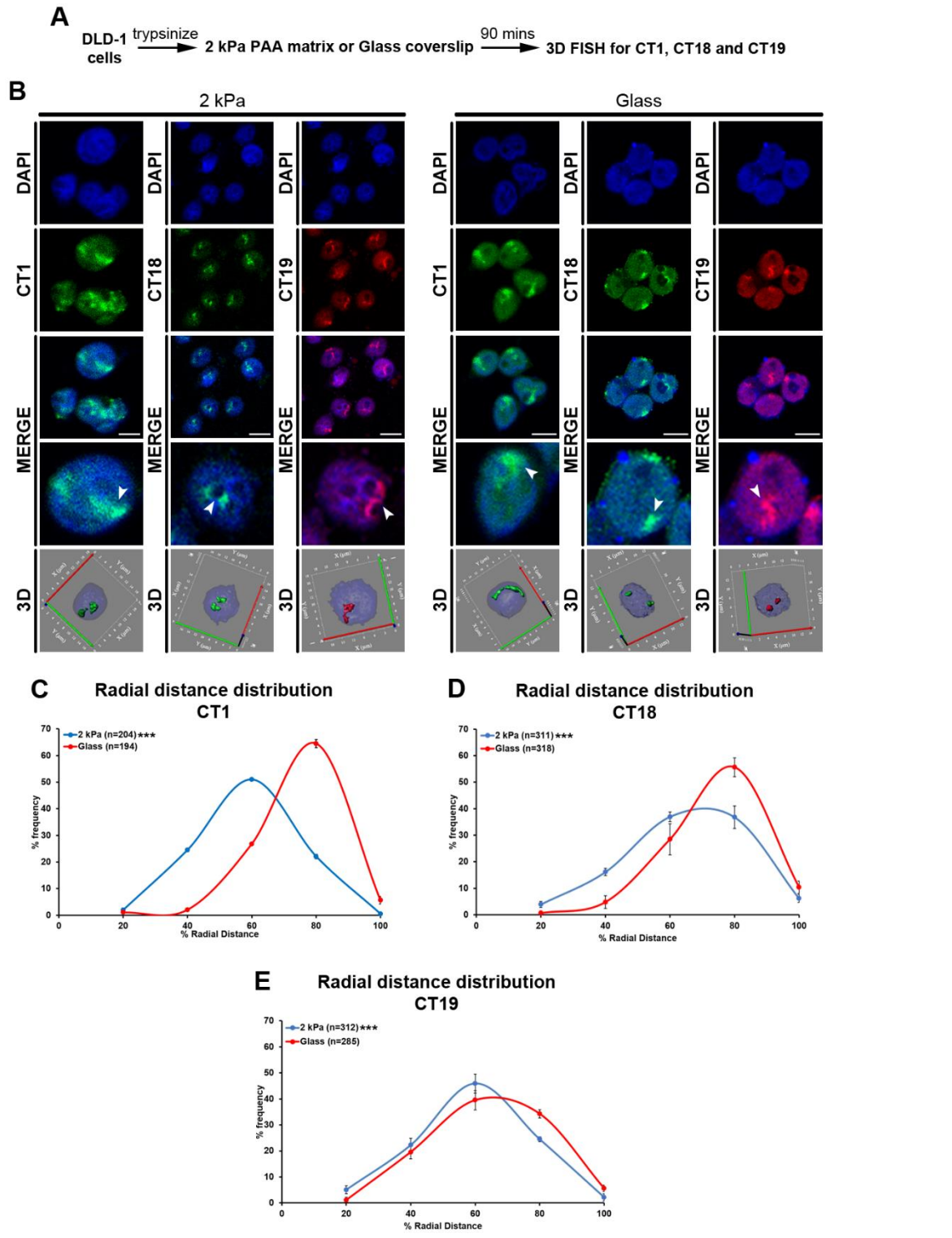

Figure 3.10 Chromosome territories are mislocalized into the nuclear interior in cells on softer matrices. A) Experimental scheme. B) Representative mid-optical sections from 3D-FISH hybridization for CT1, CT18 and CT19 in DLD-1 cells on softer matrices (2 kPa) and glass for 90 mins. Arrowheads show specific hybridization for CT1 (green), CT18 (green) and CT19 (red), resolved in 3D: reconstruction of single representative nucleus. C) Radial distance distribution profiles for CT1 on 2 kPa (*N=2*, M=50.57%) and glass (*N=2*, M=66.81%) for 90 mins. D) Radial distance distribution profiles for CT18 on 2 kPa (*N=3*, M=56.56%) and glass (*N=3*, M=66.38%) for 90 mins. E) Radial distance distribution profiles for CT19 on 2 kPa (*N=3*, M=49.40%) and glass (*N=3*, M=54.73%) for 90 mins *(C-E: Pooled data from N independent biological replicates, n: number of CTs, X-axis: 0% - Nuclear center and 100% - Nuclear periphery, Error bar: SEM, Mann Whitney test).* *** p<0.0001. **Scale bar ~10 µm.**

3D-FISH, confocal imaging, 3D reconstruction and radial distance measurements (R.D) of CT18 and CT19 in cells on glass consistently recapitulated their relatively peripheral and interior nuclear locations respectively (CT18: R.D ~66.38%, CT19: R.D ~54.73%; Fig 3.10B and D-E). Remarkably, the gene poor CT18 significantly mislocalized toward the nuclear interior in cells on softer matrices (2 kPa: R.D ~56.56%, 55 kPa: R.D ~59.72%) from its otherwise peripheral nuclear localization in cells on glass (R.D ~66.38%) (Fig 3.10B and D-E, Fig 3.13C-D, Table 3.15). Furthermore, CT19 also shifted more into the nuclear interior in cells on softer matrices (2 kPa: R.D ~49.40%, 55 kPa: R.D ~50.01%, Glass: R.D ~54.73%) (Fig 3.10B and D-E, Fig 3.13C-D, Table 3.15). % Radial distance analysis involves reconstruction of the 3D image stacks, determining geometric centers of the nucleus and each chromosome territory (CT) after thresholding, and further calculating the relative distance of the CT from nuclear center (Section 2.1.5). We additionally calculated the shortest distance of chromosome 1, 18 and 19 territories (center of mass) from the nuclear periphery (demarcated by DAPI staining) to further validate the relocalization of the chromosome territories (Fig 3.11). We observed a decrease in sphericity of nuclei on 55 kPa matrices after 90 mins, however the nuclear roundness was unaltered (Fig 3.11 A-B). Both CT 18 and 19 showed a significant movement away from the nuclear periphery in cells on the softer matrices (CT18: Glass M = 1.75 µm, 2 kPa M = 2.25 µm and 55 kPa M = 2.21 µm; CT19: Glass M = 2.43 µm, 2 kPa M = 3.10 µm and 55 kPa M = 3.13 µm) (Fig 3.11C-D). CT1 was also relocalized away from the nuclear periphery in cells on the 2 kPa matrices (Glass M = 1.86 µm and 2 kPa M = 2.13 µm) (Fig 3.11E). Taken together this suggests that the spatial positions of chromosome territories are sensitive to reduced matrix stiffness and mislocalized toward the nuclear interior.

Figure 3.11

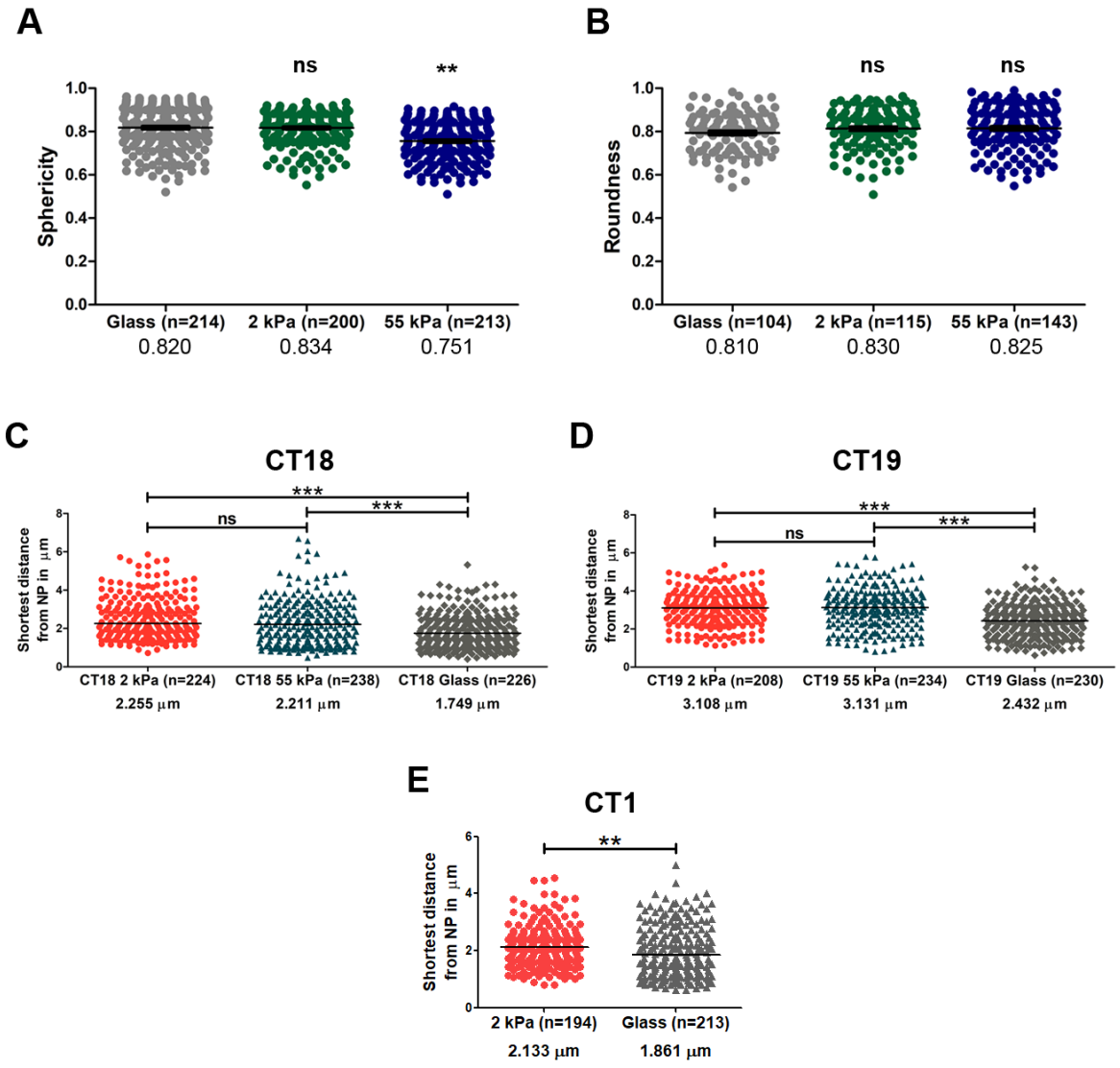

Figure 3.11 Chromosome 1, 18 and 19 territories reposition away from the nuclear periphery on softer matrices. A-B) Scatter plots depicting (A) sphericity and (B) roundness for DLD-1 cell nuclei on softer matrices (2 kPa and 55 kPa) and glass (90 mins) *(A: Pooled data from N=4, B: Pooled data from N=3, n: number of nuclei).* ** p<0.01. C-E) Scatter plots showing shortest distance from DAPI edge (NP: nuclear periphery) for (C) CT18, (D) CT19 and (E) CT1 in DLD-1 cells on softer matrices (2 kPa or 55 kPa) and glass (90 mins) *(C-E: Pooled data from N=2, n: number of each CT, Software used: Huygens Professional, FIJI, analysis performed using 2D maximum intensity projections)* ** p<0.01, *** p<0.0001, N: independent biological replicates.

Table 3.14 Radial distance measurements for CT1 under conditions of altered matrix stiffness

Substrate/ Conditions	Median % Radial Distance (% R.D)	
	CT1	Δ
CT positions on softer matrices after 90 minutes (Reference for comparison: Glass)		
2 kPa (90 min)	**50.57 (p<0.0001)**	0
Glass (90 min)	66.81	+ 16.24
2 kPa (90 mins, control for switch experiment)	**54.45 (p<0.0001)**	+ 3.88
2 kPa to glass	**62.82 (p<0.0001)**	+ 12.25

Median radial distances of CT1. Δ: shift in CT position, calculated with 2 kPa as reference, '+': movement towards the nuclear periphery, '-': movement towards the nuclear center. Values in bold are significant (p value in brackets).

Table 3.15 Radial distance measurements of CT18 and CT19 under conditions of altered matrix stiffness

Substrate/ Conditions	Median % Radial Distance (% R.D)				
	CT18	Δ	CT 19	Δ	Δ (CT18 - CT19)
(I) CT positions on softer matrices after 90 minutes (Reference for comparison: Glass)					
2 kPa (90 min)	**56.56 (p<0.0001)**	0	**49.40 (p=0.0007)**	0	7.16
55 kPa (90 min)	**59.72 (p<0.0001)**	+ 3.16	**50.01 (p=0.0126)**	+ 0.61	9.71
Glass (90 min)	66.38	+ 9.82	54.73	+ 5.33	11.65
2 kPa (7 hrs)	**55.91 (p<0.0001)**	- 0.65	**45.30 (p<0.0001)**	- 4.10	10.61
Glass (7 hrs)	66.73	+ 10.17	54.30	+ 4.90	12.43

2 kPa (21 hrs)	**56.04 (p<0.0001)**	- 0.52	**45.42 (p<0.0001)**	- 3.98	10.62
Glass (21 hrs)	66.93	+ 10.37	53.81	+ 4.41	13.12
2 kPa to glass	67.11	+10.55	**47.04 (p<0.0001)**	- 2.00	20.07
55 kPa to glass	68.75	+ 12.19	52.86	+ 3.46	15.89
2 kPa (90 mins, matrix switching assay)	**54.36 (p<0.0001)**	- 2.2	**49.97 (p=0.0005)**	+ 0.57	4.39
55 kPa (90 mins, matrix switching assay)	**60.41 (p<0.0001)**	+ 3.85	53.27	+ 3.87	7.14
2 kPa to 55 kPa	**58.59 (p<0.0001)**	+ 2.03	**47.05 (p<0.0001)**	- 2.35	11.54
55 kPa to 2 kPa	**51.52 (p<0.0001)**	- 5.04	**50.25 (p=0.0108)**	+ 0.85	1.27
Glass without micropattern	66.53	+ 0.15	50.27	- 4.46	16.26
Glass with micropattern	66.17	- 0.21	53.98	- 0.75	12.19

Median radial distances of CT18 and CT19. Δ: shift in CT position, calculated with 2 kPa as reference, '+': movement towards the nuclear periphery, '-': movement towards the nuclear center. Δ (CT18-CT19): shift in CT position between CT18 and CT19. Values in bold are significant (p value in brackets).

3.2.8 Chromosome 18 and 19 territories remain mislocalized towards the nuclear interior even at longer time points in cells exposed to softer matrices

Since we observed a repositioning of CT18 and 19 towards the nuclear interior, away from their conserved nuclear locations in cells on soft 2 kPa matrices at ~90 mins, we examined if these chromosome territories remain mislocalized even at longer durations. We exposed DLD-1 cells to the softer 2 kPa matrices independently for ~ 7 hrs and ~21 hrs and examined CT18 and 19 positions using 3D-FISH (Fig 3.12A and D). Interestingly, CT18 and C19 retained their state of

mislocalization even upon prolonged exposure to the softer matrices for ~7 and ~21 hrs respectively (7 hrs: CT18 R.D ~55.91%, CT19 R.D ~45.30%; 21 hrs: CT18 R.D ~56.04%, CT19 R.D ~45.42%) (Fig 3.12A-F, Table 3.15), while cells on collagen coated glass coverslips for similar time points exhibited conserved CT18 and 19 radial positions (7 hrs: CT18 R.D ~66.73%, CT19 R.D ~54.30%; 21 hrs: CT18 R.D ~66.93%, CT19 R.D ~53.81%) (Fig 3.12A-F, Table 3.15).

3.2.9 Chromosome 18 territories regain their conserved positions in cells transferred from softer to stiffer matrices

As chromosome territory positions are remarkably sensitive in cells on a softer milieu (Fig 3.10C-E), we asked if chromosome 18 and 19 territories with comparable DNA content but of contrasting gene densities, also respond in cells transferred back to stiffer substrates. To test this, we exposed DLD-1 cells to either 2 kPa or 55 kPa matrices for 90 mins, following which the cells were trypsinized and plated on the opposite substrate i.e. 2 kPa to 55 kPa and vice versa (Fig 3.12G). Interestingly, CT18 repositioned toward the nuclear periphery in cells transferred from 2 kPa to 55 kPa, while positions of gene rich CT19 remained relatively unaltered (CT18: 2 kPa to 55 kPa – R.D ~58.59%, 55 kPa to 2 kPa – R.D ~51.52%; CT19: 2 kPa to 55 kPa – R.D ~47.05%, 55 kPa to 2 kPa – R.D ~50.25%) (Fig 3.12H-J, Table 3.15).

Figure 3.12

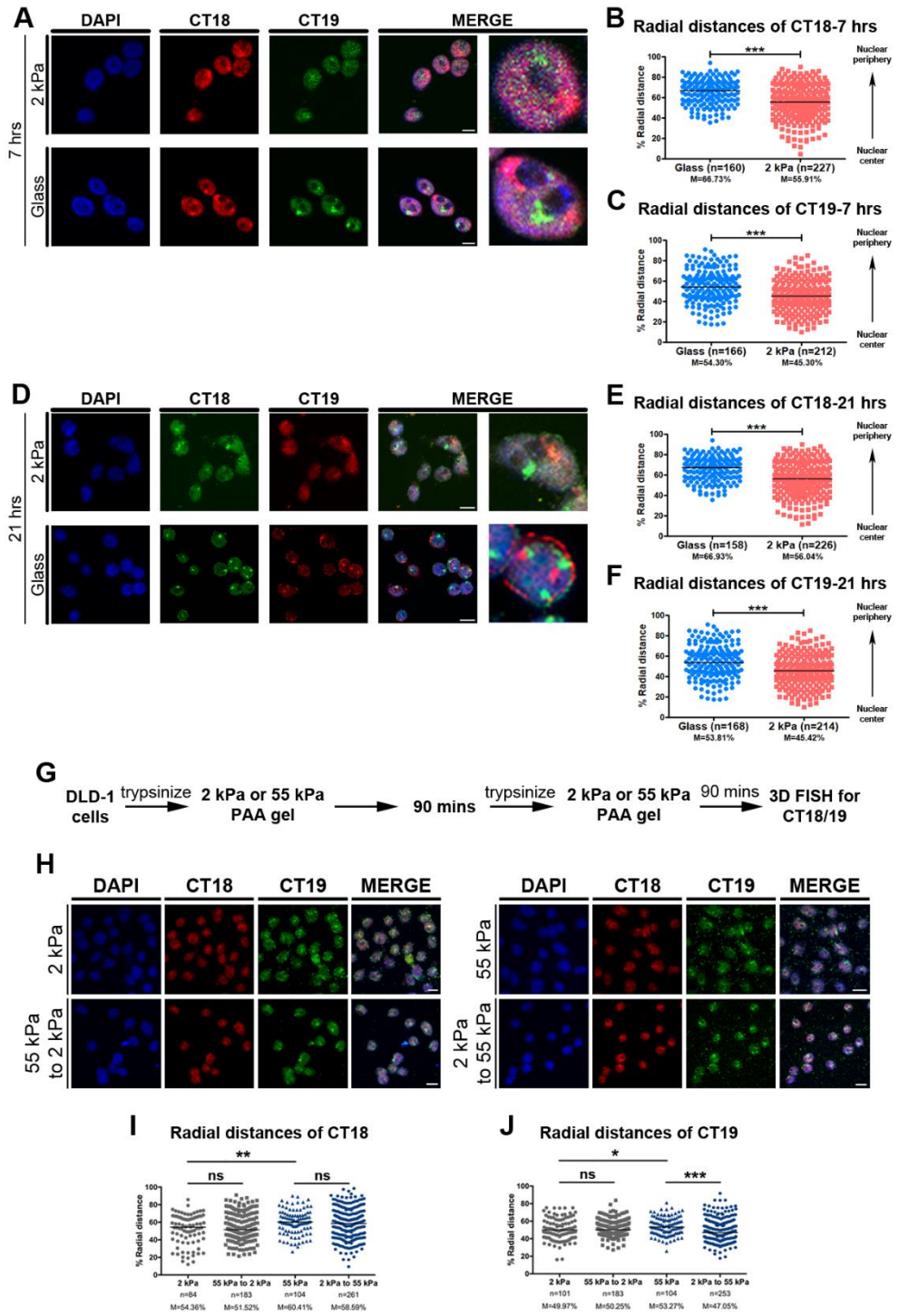

Figure 3.12 Chromosome 18 and 19 territories remain mislocalized towards the nuclear interior even at longer time points. A) Representative mid-optical section *(N=2)* from 3D-FISH hybridization of CT18 and CT19 in DLD-1 cells exposed to 2 kPa matrix and glass for ~7 hours. B) Dot scatter plot with median (M) % R.D values for CT18 on 2 kPa matrix (M=55.91%) and glass (M=66.73%) after ~7 hours *(N=2 independent biological replicates)*. *** p<0.0001 (Mann Whitney test). C) Dot scatter plot with median (M) % R.D values for CT19 on 2 kPa matrix (M=45.30%) and glass (M=54.30%) after 7 hours *(N=2 independent biological replicates)*. *** p<0.0001 (Mann Whitney test). D) Representative mid-optical section *(N=2)* from 3D-FISH hybridization for CT18 and CT19 in DLD-1 cells exposed to 2 kPa matrix and glass for ~21 hours. E) Dot scatter plot with median (M) % R.D values for CT18 on 2 kPa matrix (M=56.04%) and glass (M=66.93%) after 21 hours *(N=2 independent biological replicates)*. *** p<0.0001 (Mann Whitney test). F) Dot scatter plot with median (M) % R.D values for CT19 on 2 kPa matrix (M=45.42%) and glass (M=53.81%) after 21 hours *(N=2 independent biological replicates)*. *** p<0.0001 (Mann Whitney test). **Scale bar ~10 µm.**

Figure 3.12 ***continued.*** **Chromosome territories are repositioned in cells transferred between 2 kPa and 55 kPa matrices.** G) *(For H-J)* Experimental scheme for matrix switching experiment between softer matrices. H) Representative mid-optical sections *(N=2)* from 3D-FISH hybridization for CT18 and CT19 in DLD-1 cells switched between the softer matrices. I) Representative dot scatter plot with median (M) % R.D values for CT18 on 2 kPa (M=54.36%), 55 kPa (M=60.41%) and in cells switched between softer matrices (55 kPa to 2 kPa, M=51.52% and 2 kPa to 55 kPa, M=58.59%) *(N=2 independent biological replicates).* ** $p<0.001$ (Mann Whitney test). J) Representative dot scatter plot with median (M) % R.D values for CT19 on 2 kPa (M=49.97%), 55 kPa (M=53.27%) and in cells switched between softer matrices (55 kPa to 2 kPa, M=50.25% and 2 kPa to 55 kPa, M=47.05%) *(N=2 independent biological replicates).* *** $p<0.0001$, * $p<0.05$ (Mann Whitney test). **Scale bar ~10 µm.**

To confirm the selective repositioning of CT18 upon switching cells to a stiffer substrate, we performed matrix switching assay and plated cells initially exposed to 2 kPa and 55 kPa matrices (for 90 mins), on collagen coated glass coverslips (Fig 3.13A). Remarkably, the gene poor CT18 relocalized to its conserved position closer to the nuclear periphery within ~90 minutes in cells transferred from either of the softer matrices to glass (2 kPa to glass: R.D ~67.11%, 55 kPa to glass: R.D ~68.75%) (Fig 3.13B-C, Table 3.15). In contrast, the gene rich CT19 remained relatively unperturbed near the nuclear interior in cells transferred from the softer matrices (2 kPa) to the significantly stiffer glass substrates but shifted marginally away from the nuclear interior in cells switched from the 55 kPa matrices to glass (2 kPa to glass: R.D ~47.04%, 55 kPa to glass: R.D ~52.86%) (Fig 3.13B and D, Table 3.15). In summary, gene poor CT18 repositions and responds strongly to a switch to stiffer matrices, while the gene rich CT19 near the nuclear interior is relatively less sensitive to an increase in matrix stiffness. Taken together, chromosome territory positions respond differentially in cells exposed to extracellular matrices of altered stiffness properties.

Figure 3.13

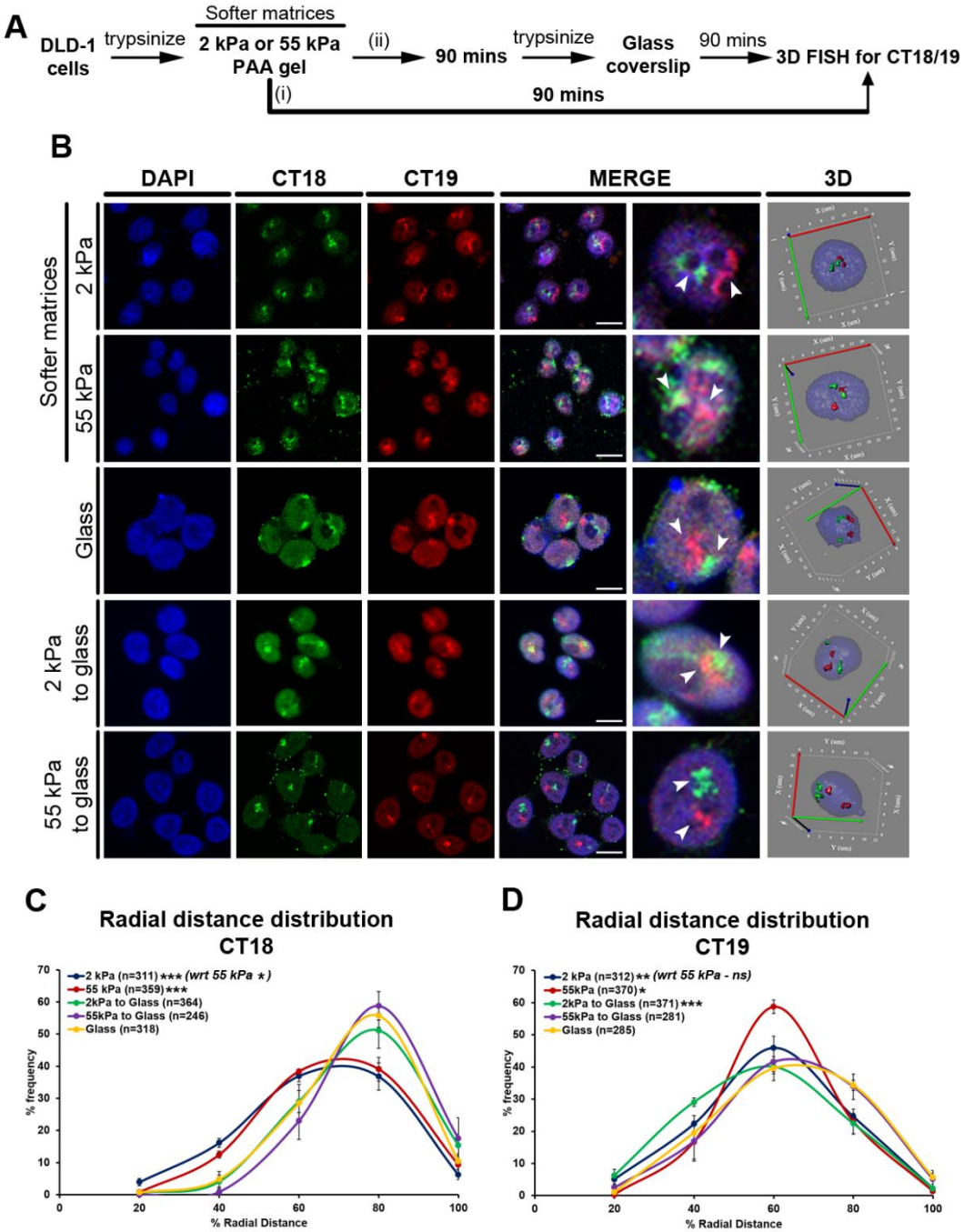

Figure 3.13 Chromosome 18 territories regain their conserved positions in cells transferred from softer to stiffer matrices. A) Experimental scheme. B) Representative mid-optical sections from 3D-FISH hybridization for CT18 and CT19 in DLD-1 cells on softer matrices (2 kPa – from Fig 3.8B and D-E, and 55 kPa) and glass (from Fig 3.8B and D-E) for 90 mins, and in cells switched from softer matrices to glass. Arrowheads show specific hybridization for CT18 (green) and CT19 (red), resolved in 3D: reconstruction of single representative nucleus. C) Radial distance distribution profiles for CT18 on 2 kPa (*N=3*, M=56.56%), 55 kPa (*N=3*, M=59.72%) matrices and glass (*N=3*, M=66.38%) for 90 mins, and in cells switched back to glass (*N=3*, 2 kPa to glass: M=67.11%, 55 kPa to glass: M=68.75%). D) Radial distance distribution profiles for CT19 on 2 kPa (*N=3*, M=49.40%), 55 kPa (*N=3*, M=50.01%) matrices and glass (*N=3*, M=54.73%) for 90 mins, and in cells switched back to glass (*N=3*, 2 kPa to glass: M=47.04%, 55 kPa to glass: M=52.86%) *(C-D: Pooled data from N independent biological replicates, n: number of CTs, X-axis: 0% - Nuclear center and 100% - Nuclear periphery, Error bar: SEM, Mann Whitney test).* *** p<0.0001, ** p<0.001, * p<0.05. **Scale bar ~10 µm.**

3.2.10 Chromosome 1 territories reposition partially towards the nuclear periphery in cells transferred from softer to stiffer matrices

We observed a selective repositioning of the gene poor CT18 upon switching DLD-1 cells from softer to stiffer matrices within 90 mins (Fig 3.13B-C). Chromosome 1 is the largest chromosome in the human genome (~250 Mbp) and also shows maximum transcriptional deregulation in cells on soft matrices (Fig 3.9E-F). Therefore, we determined if CT1, which is mislocalized towards the nuclear interior in cells on 2 kPa matrices, was able to reposition towards the nuclear periphery when cells were switched from softer to stiffer matrices. We exposed DLD-1 cells to 2 kPa matrices for 90 mins, following which the cells were trypsinized and plated on collagen coated glass coverslips (for 90 mins) and 3D-FISH was performed for CT1 and CT18 (Fig 3.14A). CT18 was used as a positive control in this experiment since it shows repositioning towards the nuclear periphery upon switch to glass (Fig 3.13B-C). As observed previously, CT18 repositioned from its location near the nuclear interior on 2 kPa (R.D ~52.56%) towards the nuclear periphery when switched to glass coverslips (R.D ~68.40%) (Fig 3.14B-C). Interestingly CT1, which was positioned towards the nuclear interior in cells on 2 kPa matrices (R.D ~54.45%), also shifted towards the nuclear periphery (R.D ~62.82%) upon transfer to glass coverslips (Fig 3.14B and D, Table 3.14). Taken together, chromosome 1 territories reposition towards the nuclear periphery upon switching cells from soft matrices to glass but are unable to completely regain their conserved nuclear locations.

Figure 3.14

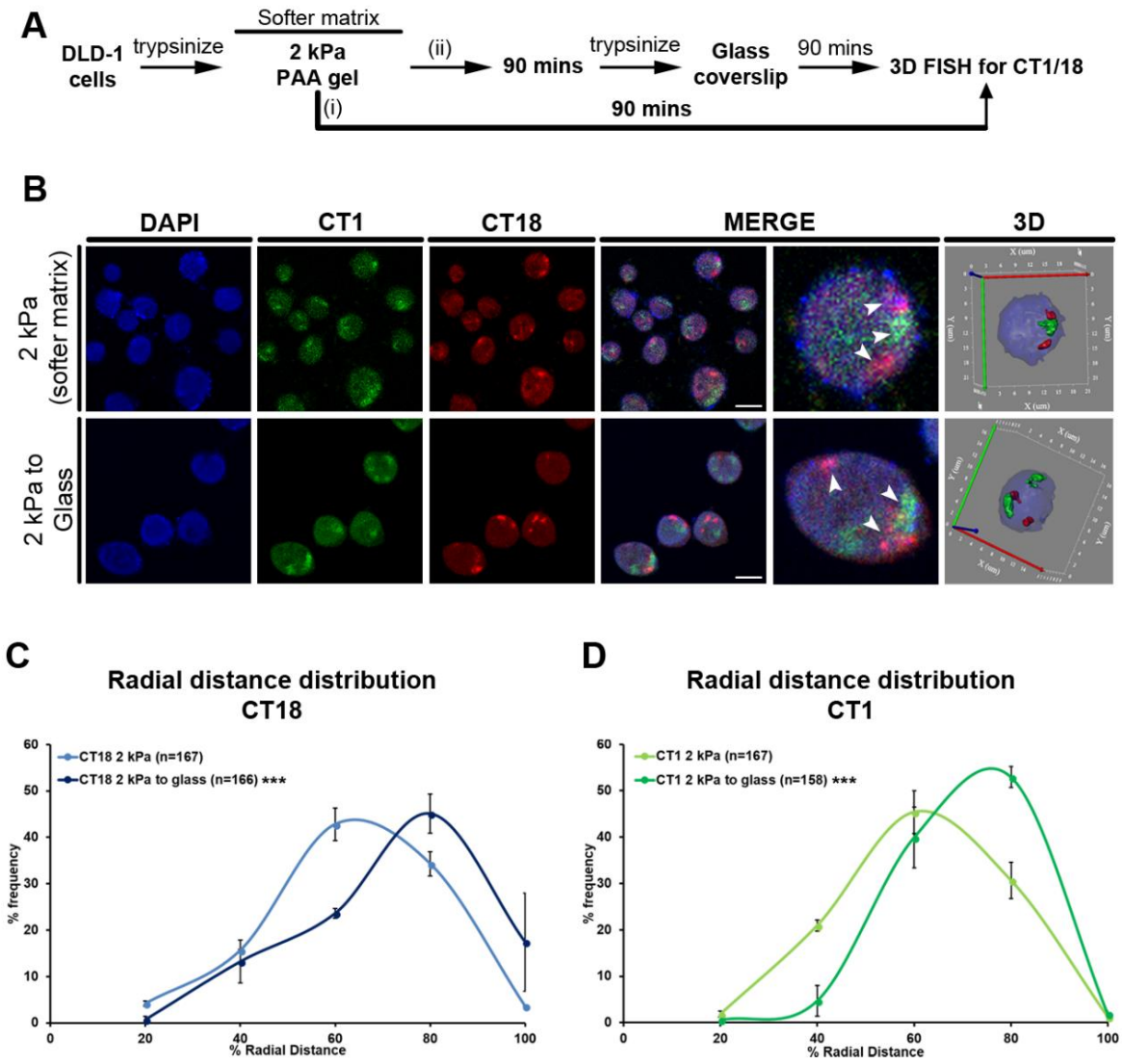

Figure 3.14 Chromosome 1 territories reposition partially towards the nuclear periphery in cells transferred from softer to stiffer matrices. A) Experimental scheme. B) Representative mid-optical sections from 3D-FISH hybridization for CT1 and CT18 in DLD-1 cells on 2 kPa matrices for 90 mins, and in cells switched from 2 kPa matrices to glass. Arrowheads show specific hybridization for CT1 (green) and CT18 (red), resolved in 3D: reconstruction of single representative nucleus. C) Radial distance distribution profiles for CT18 on 2 kPa (*N=2*, M=52.56%) for 90 mins, and in cells switched back to glass (*N=2*, 2 kPa to glass: M=68.40%). D) Radial distance distribution profiles for CT1 on 2 kPa (*N=2*, M=54.45%) for 90 mins, and in cells switched back to glass (*N=2*, 2 kPa to glass: M=62.82%). *(C-D: Pooled data from N independent biological replicates, n: number of CTs, X-axis: 0% - Nuclear center and 100% - Nuclear periphery, Error bar: SEM, Mann Whitney test).* *** p<0.0001. **Scale bar ~10 µm.**

3.2.11 Surface area and volume of chromosome territories is altered in cells on softer matrices

Transcriptional changes are generally associated with chromatin accessibility, wherein chromatin de-condenses for activation, while it is condensed and consequently undergoes repression (Martin and Cardoso, 2010; Sproul et al., 2005; van de Corput et al., 2012; Wang et al., 2014). Since both transcriptional alterations and repositioning of chromosome territories was elicited in cells exposed to soft matrices, we examined the surface area and volume of chromosome 18, 19 and 1 territories to examine their topologies (Fig 3.15). The nucleus itself showed an increase in surface area on both the soft matrices (1.14 and 1.4 fold on 2 kPa and 55 kPa respectively), while the nuclear volume increased marginally on 2 kPa (1.11 fold) and significantly on 55 kPa matrices (1.3 fold) (Fig 3.15A-B). CT18 surface area and volume were significantly increased on both the soft matrices (Area: 1.5 and 1.25 fold, Volume: 1.7 and 1.9 fold on 2 kPa and 55 kPa respectively) (Fig 3.15C-D). Interestingly, the surface area and volume were not restored upon switching cells from softer matrices to glass (Fig 3.15C-D). On the other hand, CT19 surface area (1.1 fold) and volume (1.4 fold) were greater on 55 kPa matrices and remained so even upon switch to glass (Fig 3.15E-F). Chromosome 1 territories exhibited a marginal increase in their areas but a significantly larger volume (1.15 fold) on 2 kPa matrices, and both the area and volume decreased substantially upon transferring the cells from 2 kPa to glass (Fig 3.15G-H). These results suggest that chromatin condensation is altered in response to changes in substrate stiffness, however these changes and their magnitude is likely to vary between chromosome territories.

Figure 3.15

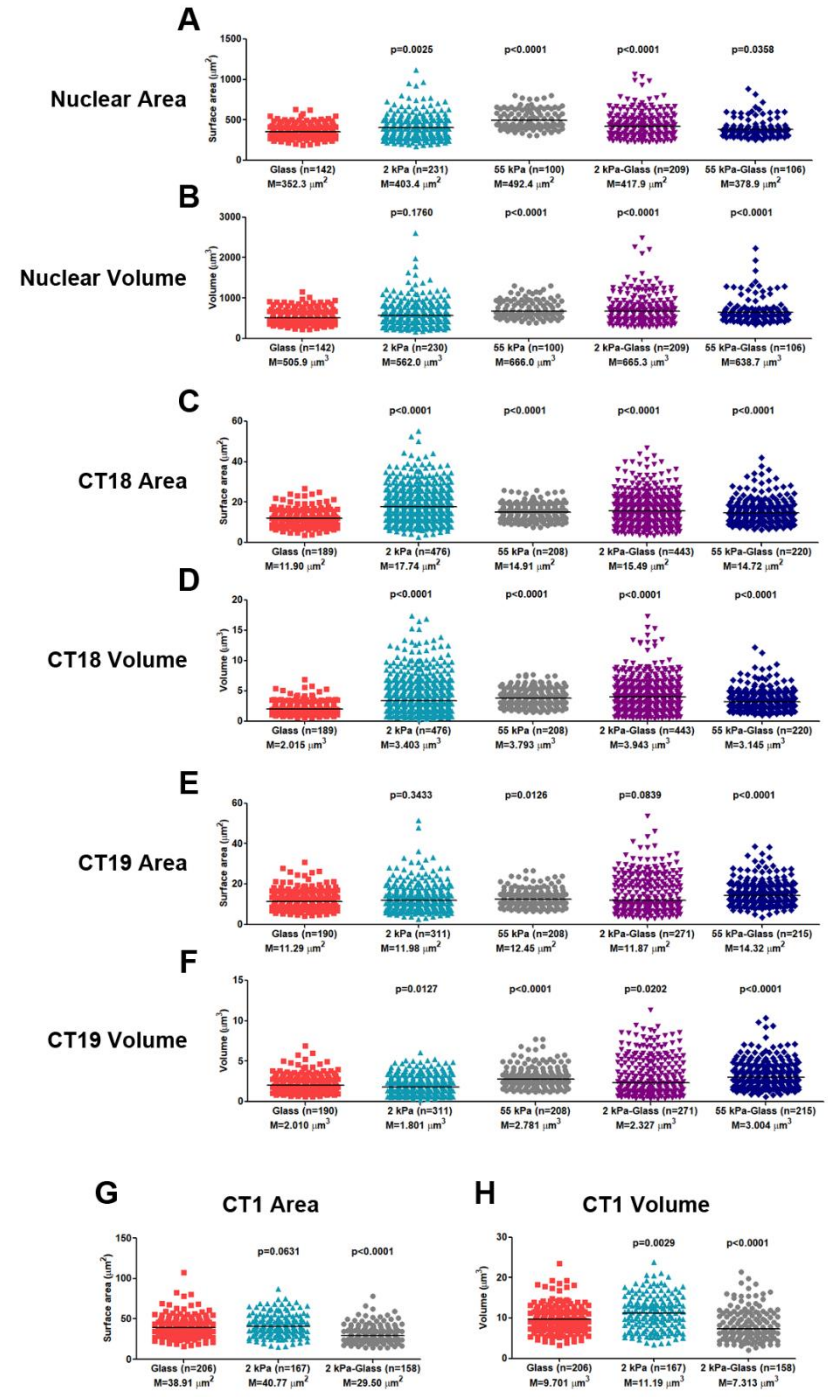

Figure 3.15 Surface area and volume of chromosome territories is altered in cells on softer matrices. A-B) Dot scatter plots with median values (M, horizontal black line) for (A) surface area and (B) volume of nucleus on softer matrices (2 kPa and 55 kPa) and glass after 90 mins, and upon the matrix switching assay (2 kPa or 55 kPa to Glass) *(n: number of nuclei, Pooled data from N=2 independent biological replicates for 55 kPa and N=3 independent biological replicates for rest of the categories).* C-F) Dot scatter plots with median values (M, horizontal black line) for surface area and volume respectively of CT18 (C, D) and CT19 (E, F) on softer matrices (2 kPa and 55 kPa) and glass after 90 mins, and upon the matrix switching assay (2 kPa or 55 kPa to Glass) *(n: number of nuclei, Pooled data from N=2 independent biological replicates for 55 kPa and N=3 independent biological replicates for rest of the categories).* G-H) Dot scatter plots with median values (M, horizontal black line) for (G) surface area and (H) volume of CT1 on softer matrices (2 kPa) and glass after 90 mins, and upon the matrix switching assay (2 kPa to Glass) *(n: number of nuclei, Pooled data from N=2 independent biological replicates).*

Figure 3.16

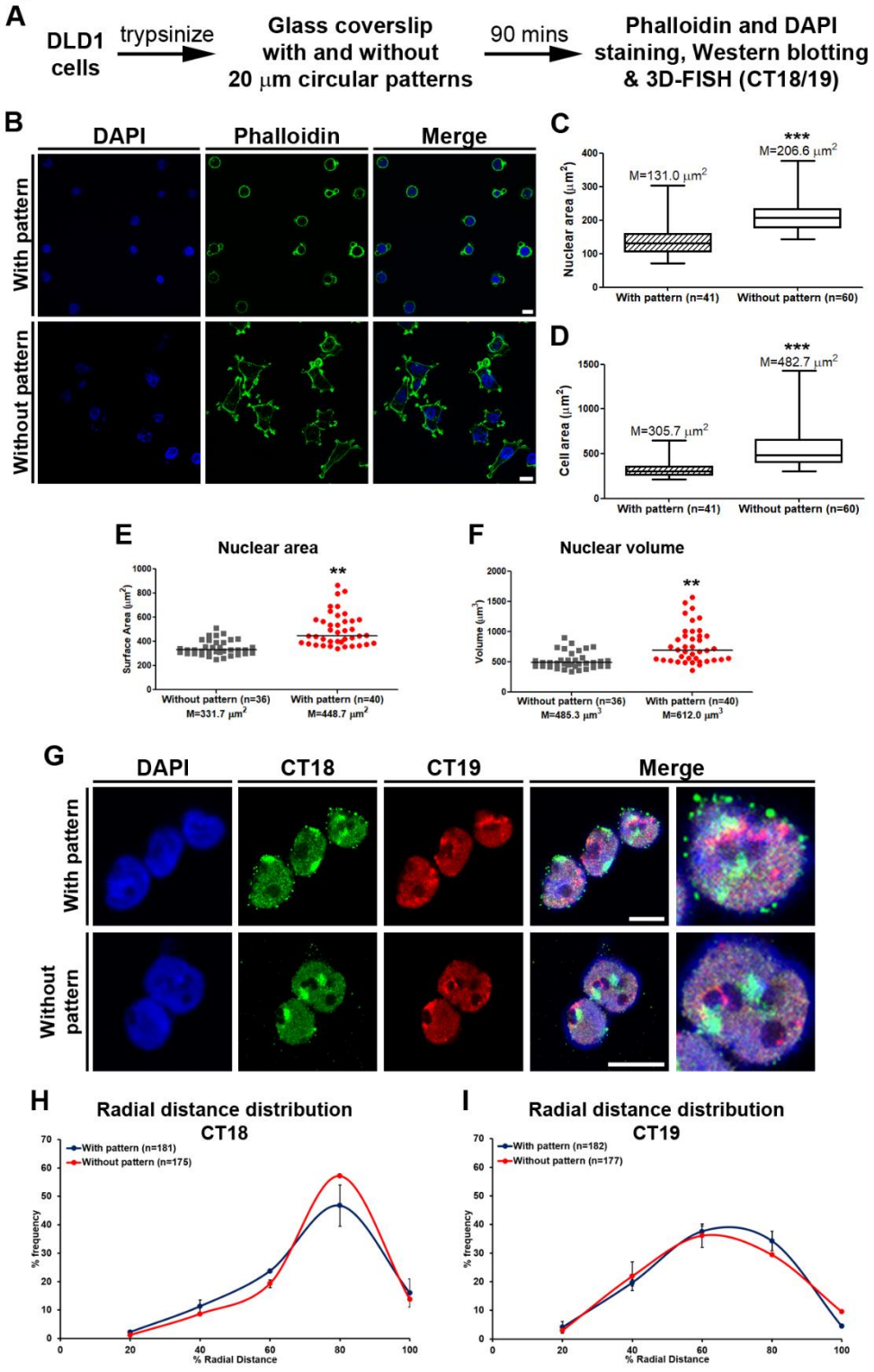

Figure 3.16 Chromosome 18 and 19 repositioning on soft matrices is independent of changes in nuclear area. A) Experimental scheme. B) Representative DAPI and Phalloidin staining of DLD-1 cells on 20 μm circular micropatterns for ~90 mins (control – cells on collagen coated glass coverslips without micropatterns for ~90 mins). C-D) Box-whisker plot showing median (M) nuclear (C) and cell (D) surface areas of DLD-1 cells on glass coverslips with and without circular micropatterns. *(n: number of nuclei in C and number of cells in D, N=2 independent biological replicates).* *** p<0.0001, Mann-Whitney test. E-F) Dot scatter plot showing median (M) nuclear area (E) and volume (F) in DLD-1 cells on glass coverslips with and without circular micropatterns after the 3D-FISH experiment (Fig 3.13G). *(n: number of nuclei, N=2 independent biological replicates).* ** p<0.001, Mann-Whitney test.

Figure 3.16 *continued.* G) Representative 3D-FISH mid-optical sections *(N=2)* from confocal z-stacks for CT18 (green) and CT19 (red) in cells on coverslips with and without circular micropatterns. H) Radial distance distribution profiles for CT18 in cells on coverslips with (*N=2,* 66.17%) and without (*N=2,* 66.53%) circular micropatterns for 90 mins. *(Error bar: SEM, Mann-Whitney test).* I) Radial distance distribution profiles for CT19 in cells on coverslips with (*N=2,* 53.99%) and without (*N=2,* 50.27%) circular micropatterns for 90 mins. *(Error bar: SEM, Mann-Whitney test).* **Scale bar ~10 µm.**

3.2.12 Chromosome 18 and 19 repositioning on softer matrices is independent of changes in nuclear area

Cell spreading and perception of substrate stiffness are closely interconnected (Yeung et al., 2005). Increased cell spreading results in increased nuclear spreading and nuclear flattening due to force application by apical actin stress fibers (Khatau et al., 2009; Vishavkarma et al., 2014). Since we observed changes in nuclear area and volume in cells on soft matrices, we determined if altered chromosome territory positions are a consequence of these nuclear topology changes. To test this, we used PDMS stamps with circular micropatterns of ~20 µm diameter and produced these patterns on collagen coated glass coverslips (Fig 3.16A). By using these circular micropatterns, we were able to restrict DLD-1 cells and their nuclei to the area that they otherwise occupied on 2 kPa matrices, despite being on glass coverslips (as shown below). We confirmed this by plating DLD-1 cells on glass coverslips with and without circular patterns for 90 mins and performing Phalloidin and DAPI staining to quantify cell and nuclear area (Fig 3.16B-F).

Experimental condition	Nuclear area (µm^2)	Cell area (µm^2)
2 kPa (90 mins, Fig)	137.0	336.0
Glass with circular patterns	131.0	305.7
Glass without circular patterns	206.6	482.7

We next studied the radial positions of CT18 and 19 using 3D-FISH in DLD-1 cells plated on glass coverslips with and without circular patterns for 90 mins (Fig 3.16G). Both CT18 and CT19 were present at their conserved nuclear locations in cells on the circular micropatterns (CT18: Without pattern R.D ~66.53%, With pattern R.D ~66.17%; CT19: Without pattern R.D ~50.27%, With pattern R.D ~53.98%) (Fig 3.16H-I). In summary, repositioning of chromosome territories in cells on soft matrices is not just a consequence of changes in the nuclear surface area and volume, and hence the topology of the nucleus.

3.3 Discussion

Chromosome positions are conserved in the interphase nucleus in a gene density dependent manner (Cremer et al., 2003). However, chromosome territory positions are altered in instances like (i) adipocyte and myogenic differentiation (Kuroda et al., 2004; Rozwadowska et al., 2013) (ii) spermatogenesis (Foster et al., 2005) (iii) quiescence or senescence (Bridger et al., 2000), and (iv) DNA damage response, mediated by the nuclear motor - nuclear myosin I (Kulashreshtha et al., 2016; Mehta et al., 2013). Chromosome territories are repositioned within minutes in serum starved cells, or in a few hours upon DNA damage induction and after days during cell differentiation. This suggests that a dynamic but cell type and context specific response, when relayed to the nucleus, repositions chromosome territories. Here we show that downregulation of active histone mark H3K4me3, nucleoplasmic accumulation of inactive histone mark H3K27me3, transcriptional deregulation and chromosome territory repositioning is induced within a relatively short duration of ~90 minutes, in DLD-1 cells exposed to softer extracellular matrices.

3.3.1 Transcriptional deregulation largely correlates with chromosome repositioning in response to reduced matrix stiffness

Substrate stiffness is a well-known modulator of gene expression (Alam et al., 2016; Assoian and Klein, 2008; Mammoto et al., 2009; Roskelley et al., 1994). For instance, PtK2 epithelial cells show increased levels of Heterochromatin Protein 1β (HP1β), heterochromatinization and transcriptional repression on softer extracellular matrices (<50 kPa) (Kocgozlu et al., 2010; Rabineau et al., 2015). Interestingly, RNA-Seq analyses of cells on softer matrices revealed a nearly comparable extent of up and down regulated genes on the softer matrices (Fig 3.6B-C). Remarkably, Chr. 1 was the maximally deregulated chromosome (~13.15% on 2 kPa and ~9% on

55 kPa) and showed a striking enrichment of ~33.5% of deregulated genes out of the total number of genes deregulated on the softer matrices (2 kPa) (Fig 3.9A and E, Table 3.12 and 3.13). Interestingly, although Chr. 18 showed the lowest representation of deregulated genes (~1.6%) and a total deregulation of ~4.69%, CT18 shifted significantly toward the nuclear interior by a radial distance of ~10% (1.013 ± 0.13 μm); while Chr. 1 and 19 with ~33.5% and ~12.3% enrichment of deregulated genes (and total deregulation of ~13.15% and ~9.63%), mislocalized toward the nuclear interior by a radial distance of ~16% (1.74 ± 0.1 μm) and ~5% (0.42 ± 0.13 μm) respectively in cells on softer matrices (2 kPa) (Fig 3.9A and E, Table 3.12-3.15, Fig 3.10C-E). In summary, this analysis suggests that the extent of chromosome territory mislocalization does not necessarily correlate with the extent of its transcriptional deregulation in cells subjected to reduced mechanical stress. It is important to note that the mislocalization of chromosomes 1, 18 and 19 territories into the nuclear interior also decreases their relative spatial separation, further suggesting a relaxation of conserved CT positions as a function of altered mechanical forces (Table 3.14 and 3.15).

3.3.2 Altered transcriptional profile of chromosome 1

Chromosome 1 is significantly enriched in terms of transcriptional deregulation in DLD-1 cells on the softer 2 kPa matrices (Fig 3.9A and E). Human Chr. 1 is transcriptionally deregulated and shows altered nuclear positions in BJ-1 fibroblasts subjected to longitudinal micropatterns (McNamara et al., 2012). Furthermore, CT1 (harboring epidermal differentiation cluster) showed a significant internal nuclear localization in epidermal progenitor cells subjected to biaxial cyclic mechanical strain (Le et al., 2016). These studies coupled with our observations, highlight CT1 as a unique responder to the altered mechanical equilibrium of cells, consistent with its striking

transcriptional imbalance as well as its mislocalization in cells exposed to softer matrices (Fig 3.10C). It is interesting to note the dichotomy between chromosome 1 and 18 – both are present proximal to the nuclear periphery in cells on glass, but respond differently to altered matrix stiffness. While Chr. 18 is transcriptionally deregulated to a lesser extent on softer matrices and repositions towards the nuclear periphery within 90 mins upon switching cells to glass (Fig 3.9A and E, 3.13C), Chr. 1 shows highly altered transcriptional profiles and only repositions partially upon matrix switching (Fig 3.9 A and E, Fig 3.14D). One of the striking differences between these two chromosomes is their DNA content – while Chr. 1 is the largest chromosome in the human genome and ~250 Mbp, Chr. 18 is ~80 Mbp in size. Thus, an important consideration while studying the impact of mechanical changes on CT1 positions could be the steric effects due to its large 3-dimensional topology, further aggravated by the decondensation triggered upon lowering matrix stiffness (Fig 3.15G-H). However, it is important to note that Chr. 18 also undergoes an increase in surface area and volume to a greater extent (fold change) than Chr. 1. It is therefore possible that in cells on softer matrices, changes in spatial positions and decondensation of chromosome territories are coupled together in such a way that while some chromatin domains may retain contact with the nuclear periphery, bulk of the territory undergoes relocalization towards the nuclear interior. We speculate that (i) DNA content (ii) a unique 3D topology of chromosome 1 territory in the interphase nucleus (iii) its extensive association with Lamins and their interactors like Lap2α, BAF among others and (iv) transcriptional status, could collectively contribute to the nuclear dynamics of CT1.

3.3.3 Common pathways but unique subsets of genes are deregulated in cells on softer matrices

Classification of up and downregulated genes on softer matrices into GO categories showed that common pathways modulating DNA damage and repair, cell cycle and chromatin associated processes were deregulated in these cells (Fig 3.6D-E, 3.7A-B). However, unique subsets of genes were enriched in each of the common GO category, suggesting that in the context of altered matrix stiffness, the same pathway may be regulated via a different network of genes depending on the specific signal encountered and the final response to be elicited. Chromatin is relatively "floppier" in cells under reduced nuclear strain. Furthermore, the altered regulation of these cellular processes that closely crosstalk with chromatin, suggests that chromatin organization is potentially modulated in accordance with the stiffness of the extracellular substrate (Li et al., 2014; Makhija et al., 2016).

Interestingly, analyses of protein-protein interaction networks derived from genes either upregulated or downregulated on 2 kPa or 55 kPa matrices, enriched specific pathways as follows:
1) Genes upregulated on 2 kPa – associated with RNA metabolism (SMG6, SMG7, UPF1, RPL26, PSMA3, PSMA4, PSMA5, RPS7, RPS15, HNRNPD, FAU, PSMD13) (Fig 3.17A).
2) Genes downregulated on 55 kPa – associated with MAPK and AKT signaling (MAP3K11, PIK3CB, PTK2, KIT, CSK, RAC1, VAV1, GIT1) (Fig 3.17B).
3) Genes upregulated on 55 kPa – associated with Cell cycle checkpoints (ANAPC5, ANAPC7, CDK6, CDK2, YWHAB, ORC1, CDC27) (Fig 3.17C).
4) Genes downregulated on 55 kPa – associated with DNA damage response (TP53, BRCA1, ATM, CHEK2, MCM4, MCM8, ERCC4, LIG4, RAD23B) and Chromatin remodeling (KAT2A,

KAT5, TAF12, NCOR1, ELP4, DMAP1, SGF29, EZH2, MORF4L1, MORF4L2, CHD4, CHD8, SUDS3, TDRD3, JARID2) (Fig 3.17D).

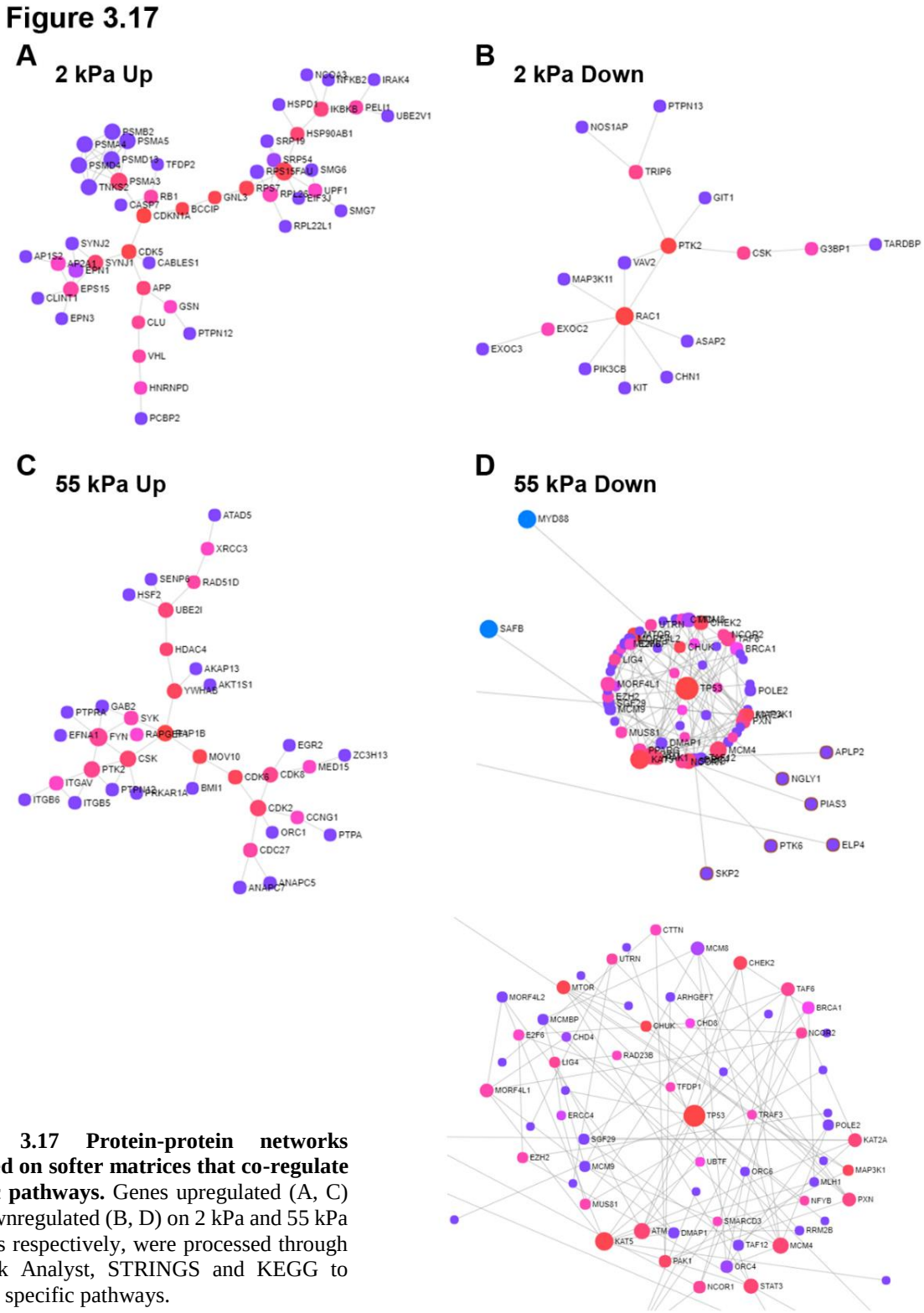

Figure 3.17 Protein-protein networks enriched on softer matrices that co-regulate specific pathways. Genes upregulated (A, C) and downregulated (B, D) on 2 kPa and 55 kPa matrices respectively, were processed through Network Analyst, STRINGS and KEGG to identify specific pathways.

It is noteworthy that the upregulation of genes associated with the Rho-GTPase pathway i.e FMNL3, ARHGEF2, ARHGEF16, AKAP13, IQGAP2, MYO9B, ECT2 and DOCK11 on the 55 kPa matrices is consistent with their role in modulating cytoskeletal organization through Rho proteins, Rac1 and Cdc42 among others (Abiko et al., 2015; Cook et al., 2011; Gadea and Blangy, 2014; Gauvin et al., 2015; Hanley et al., 2010; Makowska et al., 2015; Rao and Zaidel-Bar, 2016; Sandí et al., 2017). This suggests their involvement in substrate stiffness-dependent mechanotransduction, generation of traction and induction of migration in these cells (Fig 3.7A).

Interestingly, analyses of consensus motifs and miRNA binding sites within the transcriptionally deregulated genes in cells on softer matrices revealed both transcriptional (via transcription factors) and post-transcriptional (via miRNAs) regulation of gene expression (Fig 3.8A, Table 3.11). Out of the transcription factors whose consensus motifs were enriched in genes deregulated on softer matrices - MYC, YY1 (2 and 55 kPa), AP1 (2 kPa), AP4 and ELK1 (55 kPa) modulate their activity networks and respond to changes in substrate stiffness (Peñalver Bernabé et al., 2016). Myc directly interacts with Lamin A/C, acts both as a transcriptional activator and repressor and promotes RNA amplification (Myant et al., 2015; Sabò et al., 2014; Wanzel et al., 2003). Additionally, Myc negatively regulates miR-26a and miR-26b whose binding is enriched within genes downregulated on 55 kPa matrices (Chang et al., 2008), suggesting that a potential regulatory axis of Lamin A/C, Myc and miR-26a/b may be involved in transcriptional downregulation of a subset of genes in cells on softer matrices.

3.3.4 Understanding the response of different cell types to altered matrix stiffness

On examining the response of different cancer cell lines (DLD-1, SW480, MCF7, A549 and HT1080) in terms of their nuclear and cell surface areas and volumes to lowered matrix stiffness, we observed that each cell type tries to attain a steady-state morphology in a temporal and stiffness dependent manner. The nuclear/cytoplasmic volume ratio observed on softer matrices was as follows:

	2 kPa		**55 kPa**	
Cell line	**90 mins**	**21 hrs**	**90 mins**	**21 hrs**
DLD-1	0.84	0.77	0.74	0.77
SW480	0.64	0.79	0.53	0.41
MCF7	0.63	0.33	0.65	0.47
A549	0.66	0.67	0.39	0.31
HT1080	0.31	0.36	0.23	0.27

Cancer cells are known to generally have disrupted C/N ratios and reduced mechanosensitivity (Zink et al., 2004; Chin et al., 2016). Here we saw that with the exception of SW480 and MCF7 cells, other cancer cell lines did not show significant deviations of N/C ratios between the soft matrices across time. However, comparisons over multiple time points and with cells on collagen coated glass coverslips are essential to appreciate the true repertoire of cell and tissue type driven responses to altered mechanosensation. Additionally, inherent differences in the expression of cell surface receptors, their cleavage during trypsinization and time taken for their re-expression will vary with cell type and can add to variation in the results obtained. Normal and transformed cells respond differentially to changes in substrate stiffness. Growing normal or H-Ras transformed NIH 3T3 cells on Collagen-I coated polyacrylamide substrates has shown that non-transformed 3T3 cells decrease their rate of DNA synthesis and proliferation, but increase the rate of apoptosis on

the soft matrices (as compared to the stiff matrices). However, the 3T3 H-Ras cells maintained their growth and apoptosis characteristics irrespective of the extracellular substrate stiffness (Wang et al., 2000; Lin et al., 2015). Interestingly, cancer cells from breast (MCF7, MDA-MB-468), bladder (TSGH8301, J82), cervix (SiHa, HeLa), pancreas (ASPC-1, Mia-PaCa-2) are softer than their normal counterparts (Lin et al., 2015). Thus, in this study, it is essential to understand the effect of lowered matrix stiffness on the morphology and genome organization of normal or non-transformed cells as well. To successfully comprehend the role of tissue origin and architecture in regulating mechanotransduction, conventional 2D culture systems have to be complemented with 3D culture models. Although the use of compliant substrates like polyacrylamide, collagen, PDMS and hydrogels can partially mimic *in vivo* tissue stiffness, they lack the 3D microenvironment of an intact tissue. 3D culture systems are important as they provide (i) a defined geometry and cell shape as observed in the nascent environment, (ii) *in vivo* heterogeneity by culturing cells of different phenotypes together and (iii) cell-stroma interactions (Kim, 2005; Pampaloni et al., 2007). Therefore, complementing the 2D culture system of compliant matrices with 3D culture models would impart further insights into the impact of altered extracellular matrix stiffness on genome organization and function.

Chapter 4: Role of nuclear envelope factors - Lamins and Emerin in genome reorganization in response to altered substrate stiffness

Data acknowledgement:

Replicate for Fig 4.3B-H (Glass) and Fig 4.5C-E – Devika Ranade

Results from this chapter have been published as a part of the following manuscript:

Roopali Pradhan, Devika Ranade, Kundan Sengupta; **Emerin modulates spatial organization of chromosome territories in cells on softer matrices**, Nucleic Acids Research, Volume 46, Issue 11, 20 June 2018, Pages 5561–5586.

4.1 Introduction

The cytoskeleton perceives and relays altered extracellular signals and forces from the extracellular matrix into the cell, in order to regulate growth, development and differentiation (DuFort et al., 2011). As the name suggests, the LINC (Linker of Nucleoskeleton and Cytoskeleton) complex acts as a bridge between the cytoskeleton and the nucleus by establishing a continuous molecular connectivity from the cell membrane all the way up to the nucleus (Maniotis et al., 1997; Tapley and Starr, 2013). The LINC complex communicates extracellular forces into the nucleus via cytoskeletal proteins on the cytoplasmic side and lamins at the inner nuclear membrane. LINC complex is composed of SUN-domain (SUN1/2/3) and KASH-domain (Nesprin1/2/3/4) bearing proteins that interact within the nuclear envelope in the perinuclear space. While the SUN-domain proteins interact with the nuclear lamins and other nucleoplasmic proteins, the KASH-domain bearing proteins interact with various cytoskeletal components like actin, microtubules and intermediate filaments (Chen et al., 2014; Lombardi et al., 2011; Mislow et al., 2002; Yang et al., 2013). These interactions form a bridge for signal transduction that originates from the extracellular matrix and traverses the cytoplasm, finally reaching the genome in the nucleus (Lombardi and Lammerding, 2011; Mellad et al., 2011).

Lamins transduce external mechanical signals into the genome to elicit appropriate mechanosensitive gene expression signatures and transcriptional responses (Dahl et al., 2008; Ho et al., 2013; Jaalouk and Lammerding, 2009; Lammerding et al., 2005; Osmanagic-Myers et al., 2015). Mouse embryonic fibroblasts (MEFs) devoid of Lamin A/C or its interacting partner – emerin, show impaired response to mechanical signals and force-mediated expression of mechanosensitive genes (Ho et al., 2013; Lammerding et al., 2005; Rowat et al., 2006).

Additionally, MKL1-SRF signaling is deregulated in Lamin A/C null and mutant (N195K) MEFs, due to altered actin polymerization and dynamics since emerin is mislocalized in these cells (Ho et al., 2013). The nuclear lamina is a 'molecular shock absorber' that maintains nuclear morphology to counter extraneous mechanical tension (Dahl et al., 2004). The lamina is composed of isotropic lamin filaments that respond to forces reversibly by aligning in the direction of the force and redistributing the applied forces evenly within the lamin meshwork (Dahl et al., 2006). Interestingly, while Lamin A/C contributes to mechanical rigidity and viscosity of nuclei, B-type lamins provide elasticity and deformability to the nucleus (Stephens et al., 2017; Stephens et al., 2018a; Stephens et al., 2018b; Swift and Discher, 2014). Recent experiments have demonstrated that Lamin A expression increases with *in vivo* tissue stiffness (Swift et al., 2013), and extracellular substrate stiffness modulates expression levels, localization and phosphorylation of Lamin A (Buxboim et al., 2014).

Lamin associated nuclear envelope proteins namely, emerin, LAP2α/β and MAN1 (LEM Domain proteins) modulate signal transduction into the nucleus and downstream gene expression changes via direct interaction with transcriptional regulators such as β-catenin (emerin), Lmo7 (emerin), HDAC3 (emerin, LAP2β), Btf (emerin, MAN1), GCL (emerin, MAN1, LAP2β), rSmads (MAN1) and pRb (LAP2α) among others (Barton et al., 2015; Bengtsson, 2007; Berk et al., 2013; Cohen et al., 2007; Haraguchi et al., 2004; Holaska et al., 2003; Holaska et al., 2006; Ishimura et al., 2006; Lin et al., 2005; Markiewicz et al., 2006). These LEM-D proteins participate in tethering chromatin at the nuclear periphery (Brachner and Foisner, 2011). Emerin is a mechanosensor, phosphorylated in response to increased mechanical stress in isolated nuclei deformed using magnetic tweezers (Guilluy et al., 2014). This force-dependent phosphorylation of emerin is required for

strengthening Lamin A/C-Nesprin-1 interaction, nuclear stiffening and regulating mechanosensitive gene expression (Guilluy et al., 2014). Furthermore, a mechanosensitive sub-complex of emerin, non-muscle myosin IIA and actin also tethers heterochromatin with the nuclear lamina (Le et al., 2016). Taken together, these studies highlight the vital regulation of nuclear mechanotransduction by lamins and in particular, the importance of Lamin A/C and Emerin as crucial players in this process.

It is well established that the genome is non-randomly organized in the interphase nucleus, with gene rich chromosome territories (CTs) toward the nuclear interior, while gene poor chromosome territories are proximal to the nuclear periphery (Cremer et al., 2001; Cremer et al., 2003; Tanabe et al., 2002). While this gene-density based organization of chromosome territories is generally observed in cells with largely spherical nuclei, a size-based distribution of CTs is observed in flat-ellipsoidal nuclei (Bolzer et al., 2005; Sun et al., 2000). Factors that regulate chromosome territory positions are not completely understood. Lamins are one of the proteins that interact with chromatin via Lamina-Associated Domains (LADs), tether heterochromatin to the nuclear periphery and modulate chromosome territory positions in the interphase nucleus (Guelen et al., 2008; Meuleman et al., 2013). For instance, mouse chromosome 18 is shifted away from the nuclear periphery in Lamin B1 knockout murine cells (Malhas et al., 2007). Loss of function or mutations in the LINC complex, the nuclear envelope proteins (like emerin) or the nuclear lamins leads to “Nuclear Envelopathies” with aberrant nuclear morphologies and impaired mechanotransduction (Chambliss et al., 2013; Chi et al., 2009; Khatau et al., 2009; Lammerding et al., 2005; Lombardi et al., 2011; Somech et al., 2005). Lamin A mutations in cardiomyopathies (E161K) and progeria (G608G) show aberrant chromosome positioning, gene expression profiles

and epigenetic modifications (McCord et al., 2013; Mewborn et al., 2010; Taimen et al., 2009). Furthermore, dermal fibroblast cell lines derived from laminopathy patients (with LMNA mutations - R298L, E358K, R482L among others) and X-EDMD patient derived dermal fibroblasts (with EMD mutations like ED5364) show mislocalization of gene poor chromosomes 13 and 18 away from the nuclear periphery (Meaburn et al., 2007). This underscores the importance of a structurally and functionally resilient nucleus in maintaining chromatin organization and function.

We previously observed that DLD-1 cells in contact with softer polyacrylamide matrices (~2 kPa and ~55 kPa) for 90 mins showed a downregulation of the active histone mark H3K4me3, nucleoplasmic accumulation of the inactive histone mark H3K27me3 and chromosome wide transcriptional deregulation (Chapter 3 – Fig 3.3, 3.7). Interestingly, Chr. 1 and 19 which showed greater transcriptional deregulation and Chr. 18 – one of the chromosomes with least transcriptional changes, were all significantly repositioned and mislocalized towards the nuclear interior in cells on softer matrices (Chapter 3 – Fig 3.7, 3.8). We therefore sought to examine the molecular mechanisms that modulate chromosome territory positions upon altered extracellular matrix stiffness in a fast-responsive and reversible manner. As important regulators of genome organization, gene expression and nuclear mechanotransduction, i) Lamins ii) Emerin and iii) LINC complex proteins were obvious candidates to be tested for their potential role in relaying substrate stiffness changes to the genome. Here we show that the levels and localization of lamins differentially influence chromosome territory positions upon lowered matrix stiffness. Cells on softer matrices also activate emerin phosphorylation at a novel Tyr99 residue, the inhibition of which in a phospho-deficient mutant (emerinY99F) selectively retains chromosome 18 and 19 but

not chromosome 1 territories at their conserved nuclear locations. Taken together, we propose that emerin phosphorylation is a key upstream mechanosensor of lowered matrix stiffness which, along with nuclear lamins, selectively modulates chromosome territory positions in cells on softer matrices.

4.2 Results

4.2.1 Lamin downregulation and emerin phosphorylation is induced in cells on softer matrices

To elucidate the mechanisms that modulate chromosome positioning in cells exposed to reduced matrix stiffness, we examined the levels of proteins that maintain and regulate nuclear architecture – Lamins, Emerin and SUN proteins among others (Dechat et al., 2008; Prokocimer et al., 2009; Taimen et al., 2009; Wilson and Berk, 2010). We performed immunoblotting of whole cell extracts from DLD-1 cells (previously growing on tissue culture plastic) plated on collagen coated tissue culture plastic and the polyacrylamide matrices (2 kPa and 55 kPa) for 90 mins (Fig 4.1A). Lamin B1 showed a marginal decrease in cells on both the soft matrices (compared to tissue culture plastic – TCP), while Lamin B2 expression was significantly downregulated on the soft matrices (Fig 4.1B-C). SUN1 showed a decrease on 2 kPa matrices, while SUN2 expression was unaltered (Fig 4.1B-C). Remarkably, emerin was post-translationally modified in cells on the 2 kPa and 55 kPa matrices, which was reduced or nearly absent in cells on tissue culture plastic (Fig 4.1B, arrow). We further examined the differences in expression levels of lamins, emerin and SUN proteins between the polyacrylamide matrices i.e. between 2 kPa and 55 kPa, by trypsinizing cells growing on TCP and plating on the soft matrices for 90 mins (Fig 4.1D-E). Immunoblotting showed a marginal decrease in the levels of Lamin A, Lamin B1, SUN1 and SUN2, and a significant decrease in Lamin B2 levels in cells on 2 kPa matrices within ~90 mins (Fig 4.1E-F). In sharp contrast, emerin levels increased, with a prominent post-translational modification of emerin on both the matrices (Fig 4.1E-F, arrow).

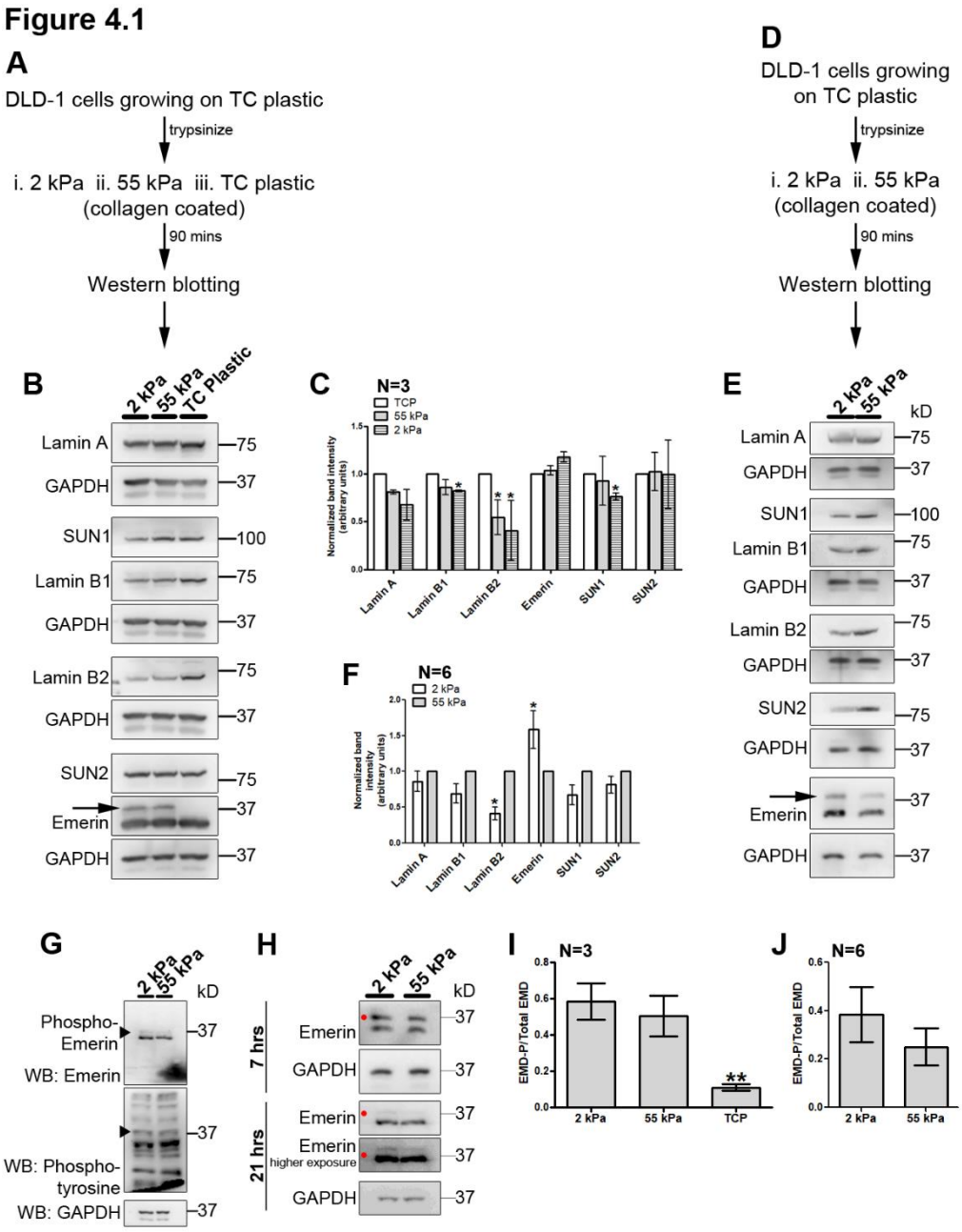

Figure 4.1. Lamin downregulation and emerin phosphorylation is induced in cells on softer matrices. A) Experimental scheme. B) Representative western blots *(N=3)* for Lamin A, SUN1, Lamin B1, Lamin B2, SUN2 and emerin expression levels in DLD-1 cells on softer matrices (2 kPa and 55 kPa) and tissue culture plastic (TCP) after 90 mins. Loading control: GAPDH. Arrow indicates post-translational modification of emerin. C) Densitometric quantification of expression levels of Lamins, emerin and SUN proteins on softer matrices and TCP. Expression was normalized to GAPDH and re-normalized to TCP *(Error bars: SEM, Pooled data from N=3, Student's t-test).* * p<0.05. D) Experimental scheme. E) Representative western blots *(N=6)* for Lamin A, SUN1, Lamin B1, Lamin B2, SUN2 and emerin expression levels in DLD-1 cells on softer matrices (2 kPa and 55 kPa) after 90 mins. Loading control: GAPDH. Arrow indicates post-translational modification of emerin. F) Densitometric quantification of expression levels of Lamins, emerin and SUN proteins on softer matrices. Expression was normalized to GAPDH and re-normalized to 55 kPa *(Error bars: SEM, Pooled data from N=6, Student's t-test * p<0.05).* G) Representative western blot *(N=2)* for emerin expression levels on softer matrices at 90 mins. Blots were probed with anti-emerin and anti Phospho-tyrosine antibodies. Arrowhead indicates tyrosine-phosphorylated form of emerin. GAPDH was used as loading control. H) Representative western blots *(N=2)* showing emerin phosphorylation levels in DLD-1 cells on softer matrices after ~7 and ~21 hrs. GAPDH was used as loading control. Red dot indicates phosphorylated emerin. I-J) Graph depicting phospho-emerin/emerin ratio for DLD-1 cells on (G) softer matrices (2 kPa and 55 kPa) and TCP after 90 mins *(N=3)*, (H) 2 kPa and 55 kPa matrices after 90 mins *(N=6)*; calculated from densitometric quantification of blots from Figure 4.1A and C respectively *(Error bar: SEM, Student's t-test ** p<0.01).* **N: independent biological replicates.**

Emerin has 18 tyrosine residues out of which nearly 13 are phosphorylated *in vivo* (Tifft et al., 2009). Additionally, mechanosensitive phosphorylation of emerin at Tyr74 and 95 has been reported in isolated nuclei upon increased nuclear strain (Guilluy et al., 2014). We determined if the post-translational modification of emerin observed on soft matrices was a phosphorylated form by performing immunoblotting using a phospho-tyrosine antibody (Fig 4.1G). Western blot analysis showed that emerin was phosphorylated by 90 mins on softer matrices, which was sustained till ~7 hrs on the 2 kPa and 55 kPa matrices (Fig 4.1G-H). Emerin phosphorylation decreased by ~21 hrs (Fig 4.1H). The overall levels of phosphorylated emerin (Emerin-P/Total emerin) were comparable on both the softer matrices (2 kPa and 55 kPa) as revealed by immunoblotting (Fig 4.1I-J), while emerin phosphorylation was hardly detectable in cells plated on the stiffer plastic substrates for 90 mins (Fig 4.1B, compare lanes: 2 kPa, 55 kPa with TC plastic). In summary, cells that experience lowered substrate stiffness show a distinctive reduction in the levels of nuclear envelope factors, but a striking activation and increase in emerin and emerin phosphorylation levels.

4.2.2 Lamin expression is restored upon switching cells from softer to stiffer matrices

Since the expression of nuclear envelope proteins was downregulated in cells on softer matrices, we examined if their levels could be restored in cells transferred from softer to stiffer matrices. We exposed DLD-1 cells to the 2 kPa and 55 kPa matrices for 90 mins, following which the cells were trypsinized and plated on collagen coated glass coverslips (Fig 4.2A). Notably, Lamin A, SUN1 and Lamin B2 levels increased and were restored in cells transferred from the softer matrices to the stiffer glass substrates (Fig 4.2B-E). However, emerin phosphorylation was retained even after cells were transferred to the stiffer glass substrates (Fig 4.2C-F). Taken together, the levels of

nuclear envelope proteins - Lamins, Emerin and SUN1/2 are sensitive to extracellular substrate stiffness possibly to varying extents. This suggests the involvement of these proteins as responders and effectors of the signaling cascade that perceives and relays stiffness properties of the extracellular matrix into the nucleus.

Figure 4.2

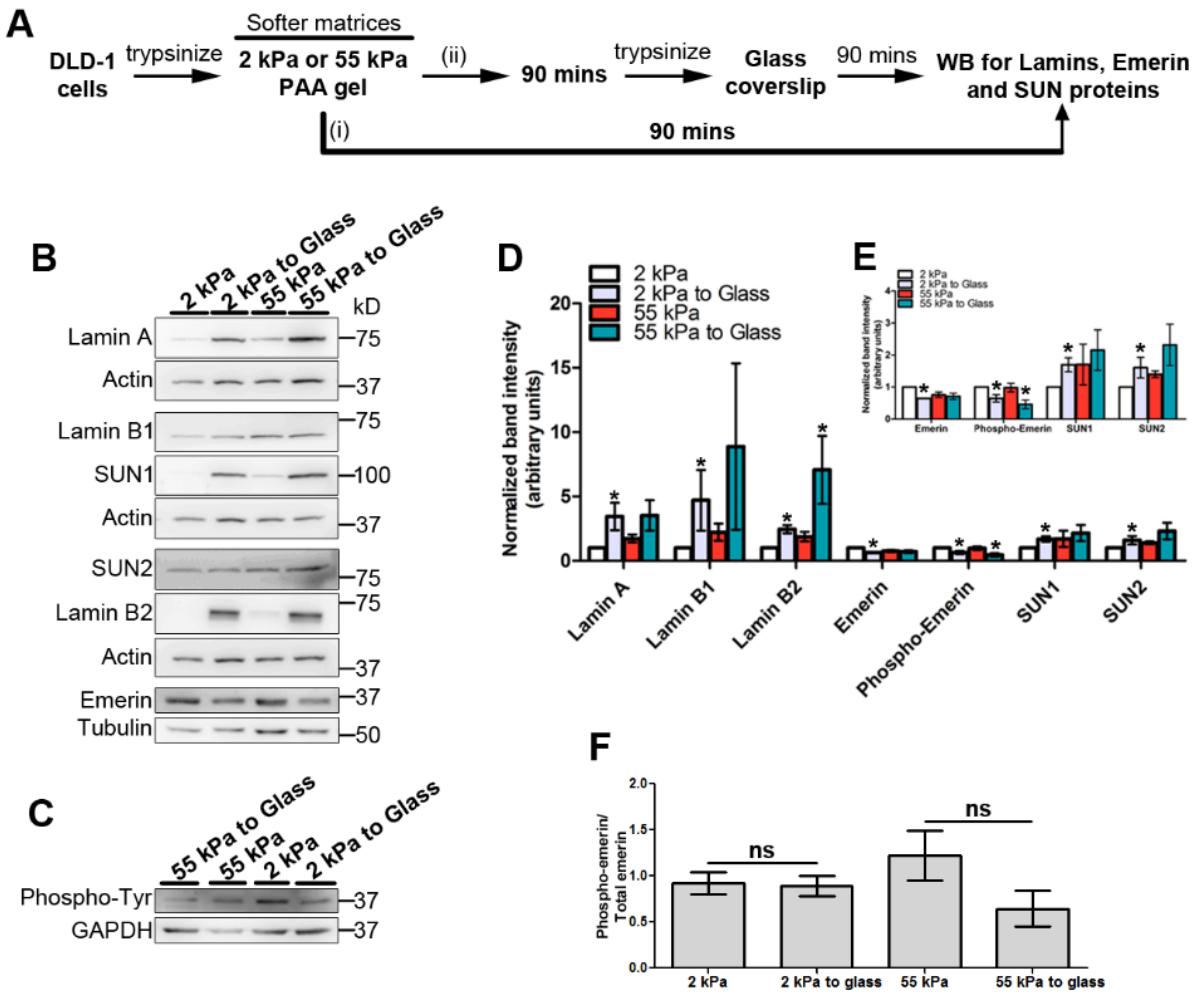

Figure 4.2 Lamin expression is restored upon switching cells from softer to stiffer matrices. A) Experimental scheme. B) Representative western blots *(N=3)* for Lamin A, Lamin B1, SUN1, SUN2, Lamin B2 and emerin expression upon switching cells from softer matrices (2 kPa and 55 kPa) to glass. Loading controls: Actin and Tubulin. C) Representative western blot *(N=3)* for phospho-tyrosine expression upon switching cells from softer matrices (2 kPa and 55 kPa) to glass. Loading control: GAPDH. D-E) Densitometric quantification of expression levels of Lamins, Emerin and SUN proteins from western blots in 4.2B-C). Expression levels were normalized to loading control and re-normalized to 2 kPa *(N=3, Error bars: SEM, Student's t-test * $p<0.05$)*. F) Graph depicting phospho-emerin/emerin ratio for DLD-1 cells on softer matrices (2 kPa and 55 kPa) and switched from softer matrices to glass, calculated from densitometric quantification of blots from Figure 4.2B-C *(N=3, Error bar: SEM, Student's t-test).* **N: independent biological replicates.**

Figure 4.3

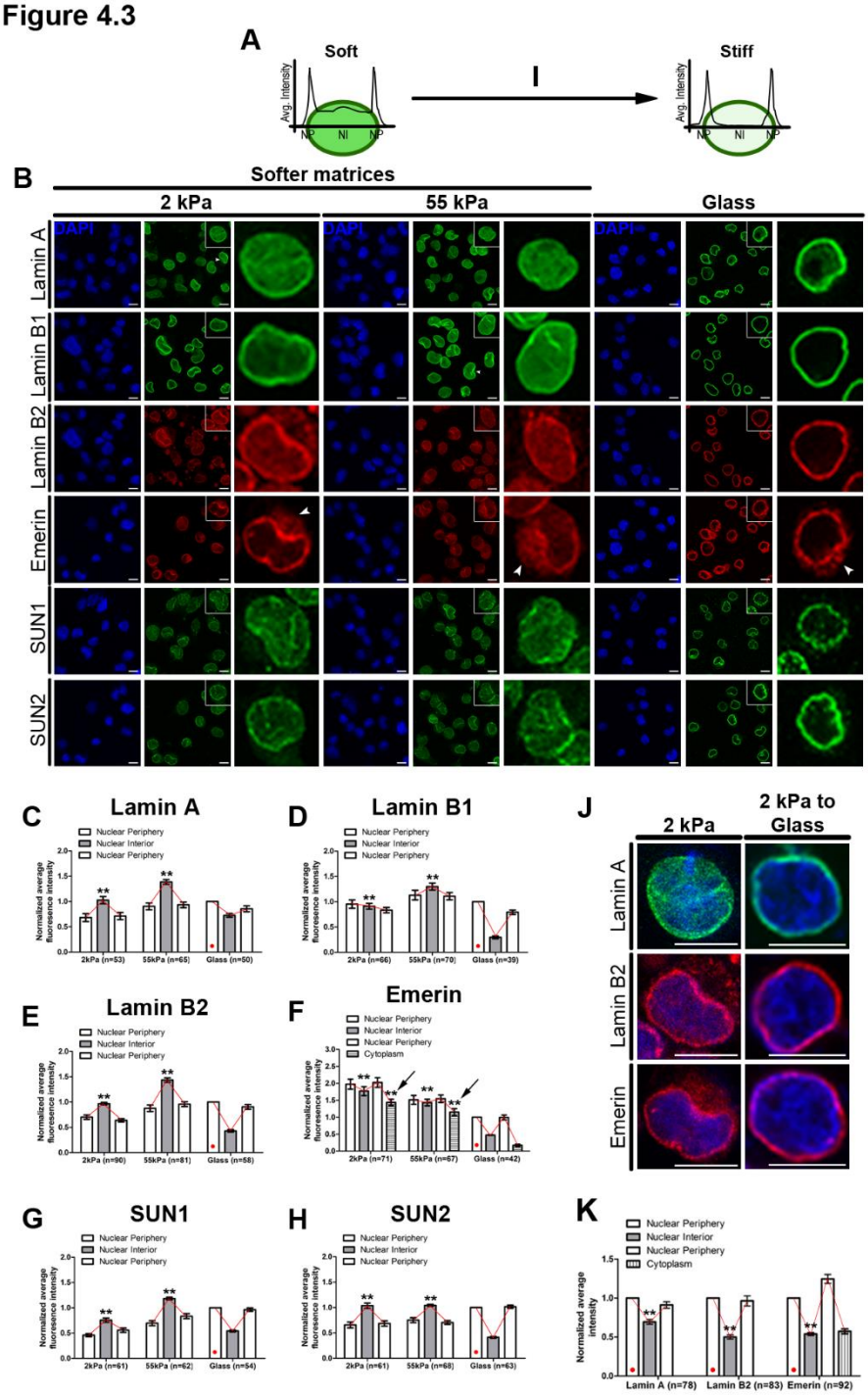

Figure 4.3 Lamin/LINC factors are mislocalized into the nuclear interior in cells on softer matrices. A, I) Scheme represents fluorescence intensity quantification for each nucleus using line-scan analysis. B) Representative mid-optical sections *(N=2 independent biological replicates)* of DLD-1 cells immunostained for Lamins, emerin and SUN proteins on softer matrices and glass coverslips for 90 mins. Zoom of single nucleus (inset) showing nucleoplasmic staining of these proteins on softer matrices. Arrowheads in panels Lamin A, Lamin B1 show altered nuclear morphologies, arrowheads in panel Emerin show extranuclear accumulation of emerin. C-H) Normalized average fluorescence intensity from line-scans across nuclei performed for Lamin A (C), B1 (D), B2 (E), emerin (F), SUN1 (G) and SUN2 (H) in DLD-1 cells on softer matrices and glass after 90 mins. Average intensities for each protein were normalized to their fluorescence intensities at the nuclear periphery in cells on glass (indicated by red dot). *(Pooled data from N=2 independent biological replicates, n: number of nuclei, Error bar: SEM).* ** $p<0.0001$ (Student's t-test).

Figure 4.3 ***continued.*** J) Immunostaining for Lamin A, B2 and emerin in cells switched from 2 kPa matrix to glass (representative 2 kPa images from 4.3B). K) Normalized average fluorescence intensity from line-scans across nuclei performed for Lamin A, B2 and emerin in DLD-1 cells switched from 2 kPa matrix to glass. Average intensities for each protein were normalized to their fluorescence intensities at the nuclear periphery (indicated by red dot) *(Pooled data from N=2 independent biological replicates, n: number of nuclei, Error bar: SEM)*. ** $p<0.05$ (Student's t-test). **Scale bar ~10 µm.**

4.2.3 Lamin/LINC factors are mislocalized into the nuclear interior in cells on softer matrices

We next assessed the sub-nuclear localization of lamin/LINC proteins in single cells by confocal imaging (Fig 4.3). Lamin/LINC proteins are typically localized at the nuclear periphery across cell types (Gerace and Burke, 1988; Wilson and Berk, 2010). Interestingly, cells exposed to softer matrices for ~90 minutes, showed a distinctive mislocalization of Lamin A, B1, B2, emerin, SUN1 and SUN2 into the nuclear interior as opposed to their predominant peripheral nuclear localization in cells on glass (compare alternate panels in Fig 4.3B-H). Furthermore, cells on softer matrices showed distorted nuclear shapes - characteristic of nuclei with lowered lamin levels (Arrowheads in Lamin A and B1 panels, Fig 4.3B) (Dechat et al., 2008; Dechat et al., 2010; Swift et al., 2013; Taimen et al., 2009). Interestingly, emerin showed an extranuclear accumulation in ~90% of cells, consistent with the mislocalization of emerin in cells with reduced lamin A/C levels (Arrows in emerin panel, Fig 4.3B and F) (Vaughan et al., 2001). Remarkably, Lamin A, Lamin B2 and emerin relocalized to the nuclear periphery in cells transferred from the softer matrices (2 kPa) to glass, along with a decrease in the extranuclear accumulation of emerin (Fig 4.3I-K). Thus, the localization of nuclear envelope factors is remarkably sensitive to the stiffness of the extracellular matrix.

4.2.4 Lamin B2 overexpression retains gene poor CT18 proximal to the nuclear periphery

As Lamin expression was decreased and Lamins were mislocalized into the nuclear interior in cells on softer matrices (Fig 4.2B-E, 4.3B-E), we asked if Lamin overexpression modulates chromosome positioning in the interphase nucleus (Fig 4.4). We overexpressed GFP-Lamin A and Lamin B2-GFP for 48 hrs in DLD-1 cells, followed by trypsinizing and plating the cells on either (collagen coated) glass coverslips or 2 kPa polyacrylamide matrices for 90 mins (Fig 4.4A-B). Overexpression of EGFP-N1 empty vector was used as control. Line scan analysis of overexpressed Lamin A and B2 showed that the GFP-tagged proteins were enriched at the nuclear periphery even in cells on 2 kPa matrices, in contrast to the enhanced accumulation of endogenous Lamins observed on soft matrices (Fig 4.4C-D, 4.3B-E). Full length Lamin overexpression also showed a marginal (but not significant) increase in the levels of Lamin A, B1, B2, phospho-emerin, SUN1 and SUN2 on the softer 2 kPa matrices (Fig 4.4E-F). Additionally, overexpression of GFP-Lamin AΔ425-553 and Lamin B2-GFPΔ570-582 showed a marginal (but not significant) decrease in the levels of Lamin B1, SUN1 and SUN2 (Fig 4.4G-H).

We performed 3D-FISH analyses to determine chromosome 18 and 19 territory positions in cells on 2 kPa matrices overexpressing either Lamin B2 or Lamin B2 Δaa570-582 - as this region is predicted to be involved in chromatin association (Fig 4.5A-B) (Taniura et al., 1995). Remarkably, cells on softer matrices (2 kPa) overexpressing the full length Lamin B2, retained CT18 closer toward the nuclear periphery (R.D ~67.41%, Empty vector: R.D ~56.79%) (Fig 4.5C-D, Table 4.1). Of note, CT18 mislocalization toward the nuclear interior was unaffected in cells overexpressing Lamin B2Δ570-582 and exposed to softer matrices (2 kPa) (R.D ~54.07%)

Figure 4.4

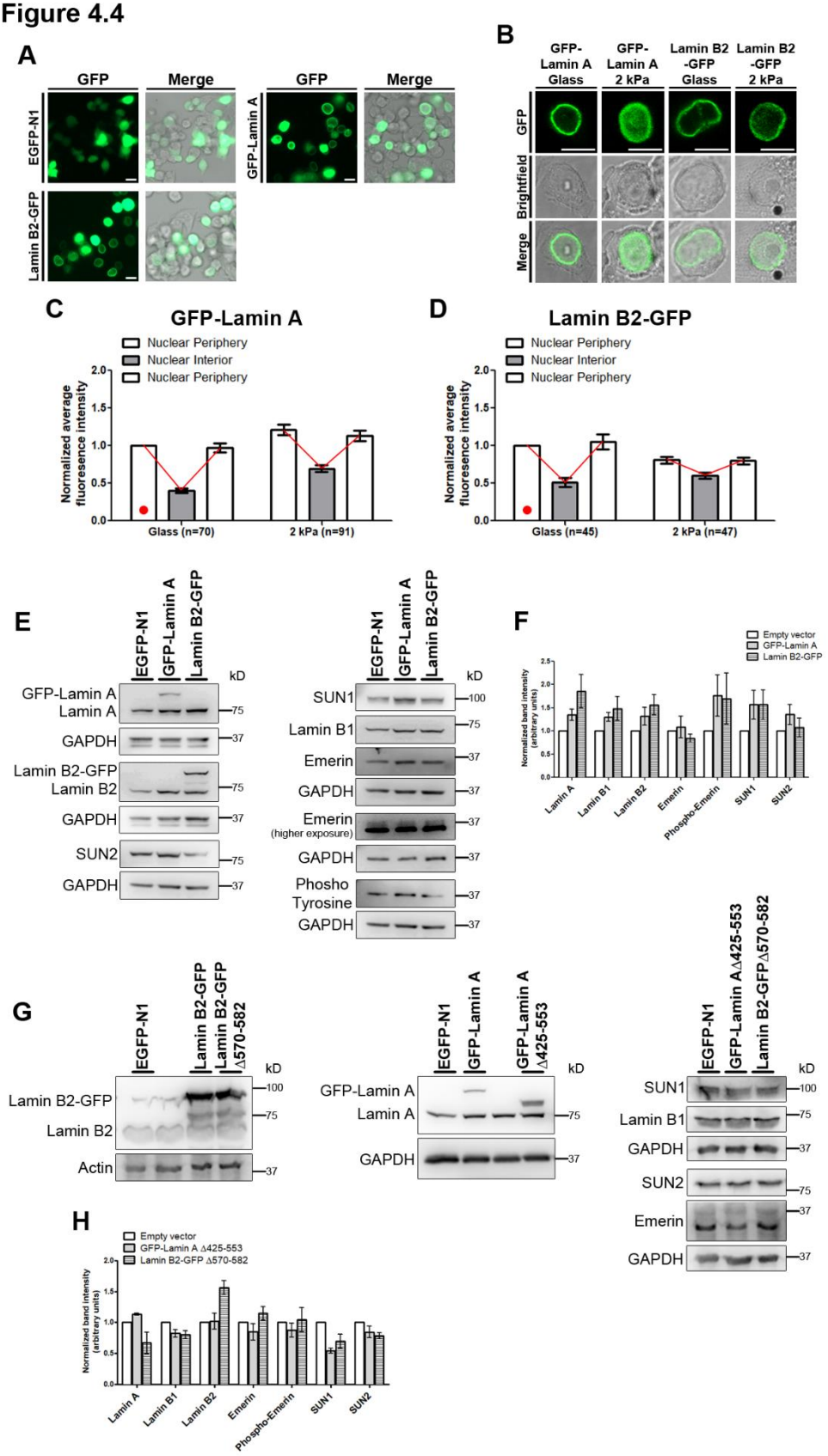

Figure 4.4 Overexpressed GFP-Lamin A and Lamin B2-GFP localize predominantly at the nuclear periphery in cells on 2 kPa matrices. A) Bright-field and fluorescence images of DLD-1 cells (acquired at 20X objective, Invitrogen EVOS FL Auto cell imaging system) transfected with either Empty vector (EGFP-N1), GFP-Lamin A or Lamin B2-GFP. Across replicates, the efficiency of transfection is ~60-65%. B) Representative mid-optical sections from confocal z-stacks of DLD-1 cells transfected with either GFP-Lamin A or Lamin B2-GFP and exposed to softer (2 kPa) matrices and glass for 90 mins. The Lamin constructs localize predominantly towards the nuclear periphery.

Figure 4.4 *continued.* C-D) Normalized average fluorescence intensity from line-scans across nuclei for overexpressed GFP-Lamin A (C) and Lamin B2-GFP (D) in DLD-1 cells, followed by exposing them to either 2 kPa matrix or glass coverslips for 90 min. Average fluorescence intensities normalized to their respective fluorescence intensities at the nuclear periphery in cells on glass (indicated by red dot) *(Pooled data from N=2 independent biological replicates, n: number of nuclei)*. E) Representative western blots *(N=4)* for Lamin A, B1, B2, emerin, SUN1, SUN2 and phospho-tyrosine in DLD-1 cells with over-expression of EGFP-N1, GFP-Lamin A, Lamin B2-GFP and exposed to 2 kPa matrix for 90 mins. GAPDH was used as loading control. F) Densitometric quantification of expression levels of Lamins, emerin and SUN proteins upon Lamin A or B2 overexpression. Expression levels were normalized to GAPDH and re-normalized to EGFP-N1 *(Error bars: SEM, N=4).* G) Representative western blots *(N=2)* for Lamin A, B1, B2, emerin, SUN1 and SUN2 in DLD-1 cells with over-expression of EGFP-N1, GFP-Lamin AΔ425-553, Lamin B2-GFPΔ570-582 and exposed to 2 kPa matrix for 90 mins. GAPDH and Actin were used as loading controls. H) Densitometric quantification of expression levels of Lamins, emerin and SUN proteins upon Lamin A or B2 mutant overexpression. Expression levels were normalized to GAPDH and re-normalized to EGFP-N1 *(Error bars: SEM, N=4).* **N: independent biological replicates, Scale bar ~10 µm.**

(Fig 4.5C-D, Table 4.1). In summary, optimum levels of Lamin B2, its enrichment at the nuclear periphery and ability to interact with chromatin are potentially required for positioning CT18 closer to the nuclear periphery in cells on softer matrices. This further underscores the role of Lamins and their interaction with Lamina Associated Domains (LADs) in positioning CT18 toward the periphery of the interphase nucleus (Guelen et al., 2008; Peric-Hupkes and van Steensel, 2010). In contrast, the internal nuclear localization of gene rich CT19, was largely unaffected in cells on the softer matrices (2 kPa) overexpressing either Lamin B2 (R.D ~53.67%) or Lamin B2Δ570-582 (R.D ~48.93%, Empty vector: R.D ~50.98%) (Fig 4.5C and E, Table 4.1).

We next assessed the impact of Lamin A and Lamin AΔ425-553 (with reduced chromatin association, Taniura et al., 1995) overexpression on the radial positioning of CT18 and 19 on 2 kPa matrices (Fig 4.5A-C). Lamin A overexpressing cells on 2 kPa matrices mislocalized CT18 further into (R.D ~46.41%, Empty vector: R.D ~56.79%) and CT19 away from the nuclear interior (R.D ~58.46%, Empty vector: R.D ~50.98%) (Fig 4.5C-E). However, Lamin AΔ425-553 overexpression did not perturb the mislocalization of either CT18 (R.D ~57.08%) or CT19 (R.D

~48.73%) (Fig 4.5C-E). While creating Lamin AΔ425-553, we retained the NLS sequence (aa 417-422) of Lamin A that interacts with histones, as its absence sequesters Lamin A/C into the endoplasmic reticulum (Wu et al., 2014). In summary, chromosome territory positions are differentially responsive to Lamin A or B2 overexpression in cells on softer matrices.

Interestingly, overexpression of GFP-Lamin A, GFP-Lamin AΔ425-553, Lamin B2-GFP or Lamin B2-GFPΔ570-582 did not affect the relative localization of either CT18 or CT19 in cells on glass (Fig 4.6A-E, Table 4.1). Phosphorylation of Lamin A at Ser22 enhances its nucleoplasmic localization in interphase nuclei and the phosphomimetic Lamin A S22D mutant mimics this localization (Kochin et al., 2014). To determine if the nucleoplasmic accumulation of Lamin A on its own can reposition chromosome territories, we generated the Lamin A S22D phosphomimetic mutant and overexpressed it in DLD-1 cells on glass (Fig 4.6F). We observed that GFP-Lamin A S22D shows greater nucleoplasmic enrichment as compared to the WT Lamin A which is present predominantly only at the nuclear periphery (Fig 4.6F *left*). 3D-FISH for CT18 and 19, followed by confocal imaging and analysis of radial chromosome territory positions showed that overexpression of GFP-Lamin A S22D lead to repositioning of CT19 away from the nuclear interior (R.D ~57.07%; Empty vector: R.D ~48.51%) (Fig 4.6F-G, Table 4.1). CT18 positions remained unaffected (R.D ~67.35%; Empty vector: R.D ~64.79%) (Fig 4.6F-G, Table 4.1). These results suggest that nucleoplasmic Lamin A specifically modulates the nuclear positions of gene rich CT19.

Figure 4.5

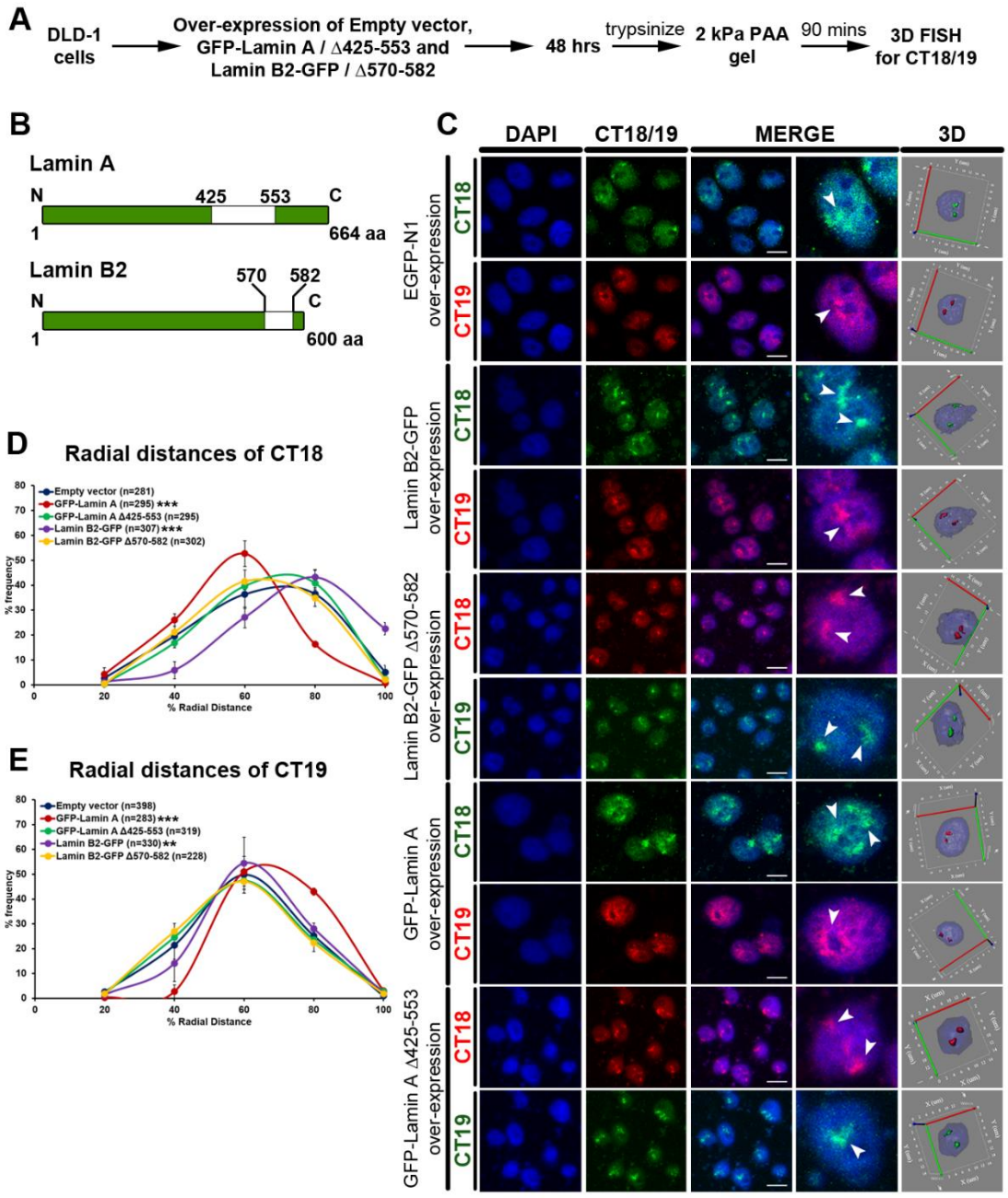

Figure 4.5 Lamin B2 overexpression retains gene poor CT18 proximal to the nuclear periphery. A) Experimental scheme. B) Graphical representation of mutants generated for Lamin A and B2. C) Representative mid-optical sections from 3D-FISH hybridizations for CT18 and 19 in DLD-1 cells on 2 kPa matrix upon overexpression of Empty vector (EGFP-N1), Lamin A (GFP-Lamin A and GFP-Lamin A Δ425-553) and Lamin B2 (Lamin B2-GFP and Lamin B2-GFP Δ570-582). Arrowheads show specific hybridization for CT18 and CT19 resolved in 3D: reconstruction of single representative nucleus, *(N=3 independent biological replicates).* D) Radial distance distribution profiles for CT18 on 2 kPa matrix upon over-expression of Empty vector (M=56.79%), GFP-Lamin A (M=46.41%), GFP-Lamin A Δ425-553 (M=57.08%), Lamin B2-GFP (M=67.41%) and Lamin B2-GFP Δ570-582 (M=54.07%). E) Radial distance distribution profiles for CT19 on 2 kPa matrix upon over-expression of Empty vector (M=50.98%), GFP-Lamin A (M=58.46%), GFP-Lamin A Δ425-553 (M=48.73%), Lamin B2-GFP (M=53.67%) and Lamin B2-GFP Δ570-582 (M=48.93%) *(D-E: Pooled data from N=3 independent biological replicates, n: number of CTs, X-axis: 0% - Nuclear center and 100% - Nuclear periphery, Error bar: SEM, Mann Whitney test)*. *** p<0.0001, ** p<0.01 (compared with Empty vector control). **Scale bar ~10 µm.**

Figure 4.6

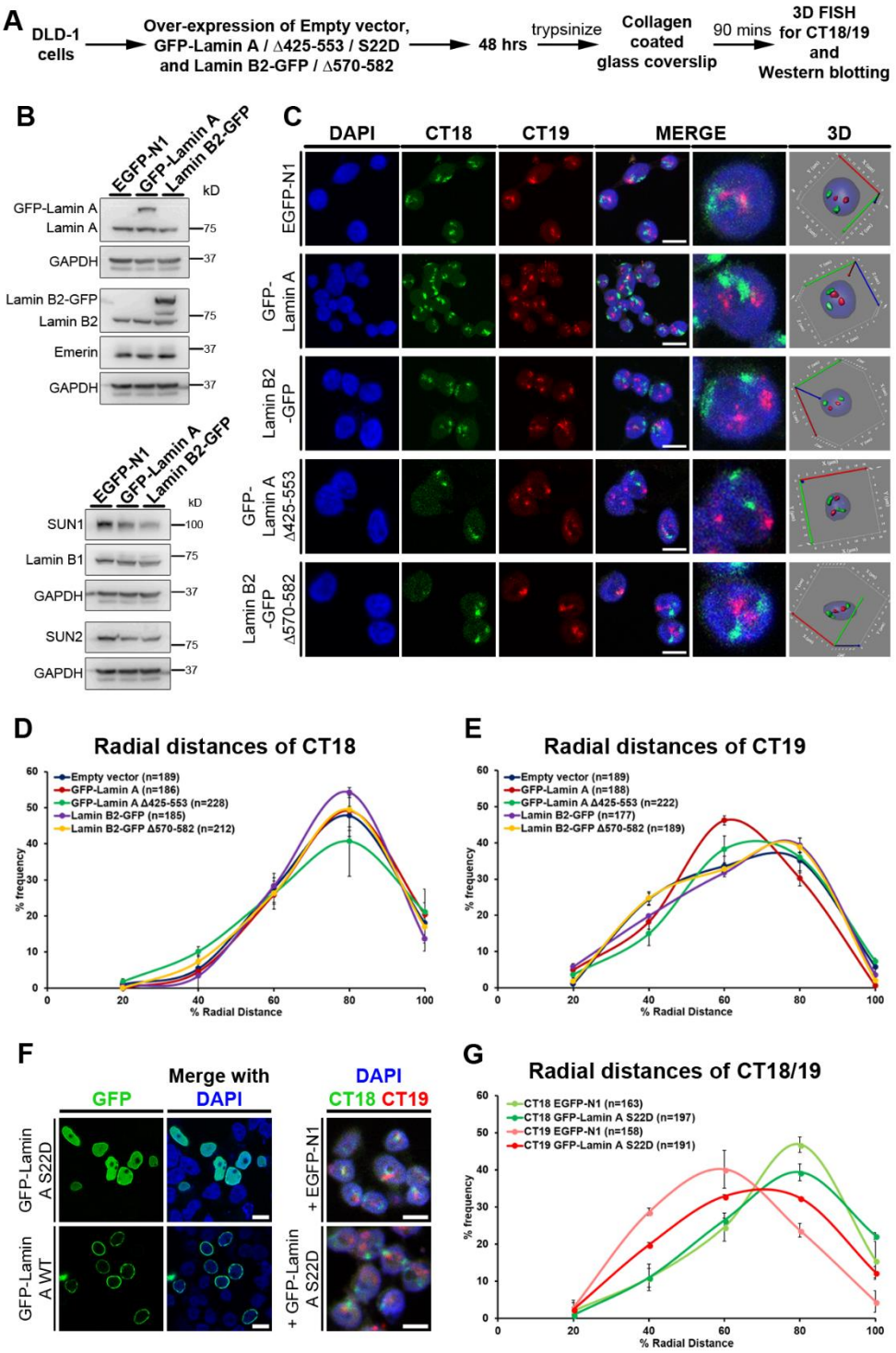

Figure 4.6 Radial positions of CT18 and CT19 are unaltered in cells overexpressing GFP-Lamin A or Lamin B2-GFP and exposed to glass for 90 minutes. A) Experimental scheme. B) Representative western blots *(N=2)* for Lamin A, B1, B2, Emerin, SUN1 and SUN2 levels in DLD-1 cells upon over-expression of EGFP-N1, GFP-Lamin A, Lamin B2-GFP and exposed to glass coverslips for 90 mins. GAPDH was used as loading control. C) Representative mid-optical sections from 3D-FISH hybridization for CT18 and 19 in DLD-1 cells on glass after overexpression of EGFP-N1, GFP-Lamin A, Lamin B2-GFP, GFP-Lamin A Δ425-553 and Lamin B2-GFP Δ570-582. 3D: reconstruction of a single representative nucleus.

Figure 4.6 ***continued.*** D) Radial distance distribution profiles for CT18 on glass after over-expression of EGFP-N1 (M=66.45%), GFP-Lamin A (M=67.39%), Lamin B2-GFP (M=66.84%), GFP-Lamin A Δ425-553 (M=65.44%) and Lamin B2-GFP Δ570-582 (M=66.26%). E) Radial distance distribution profiles for CT19 on glass after over-expression of EGFP-N1 (M=55.32%), GFP-Lamin A (M=54.50%), Lamin B2-GFP (M=54.80%), GFP-Lamin A Δ425-553 (M=56.44%) and Lamin B2-GFP Δ570-582 (M=53.94%). F) *(Left)* Representative mid-optical sections from confocal z-stacks of DLD-1 cells overexpressing either GFP-Lamin A WT or GFP-Lamin A S22D. *(Right)* Representative mid-optical sections from 3D-FISH hybridization for CT18 and 19 in DLD-1 cells on glass after overexpression of EGFP-N1 and GFP-Lamin A S22D. G) Radial distance distribution profiles for CT18 and 19 on glass after over-expression of EGFP-N1 (CT18: M=64.79%, CT19: M=48.51%) and GFP-Lamin A S22D (CT18: M=67.35%, CT19: M=57.07%) *(D, E and G: Pooled data from N=2 independent biological replicates, n: number of CTs, X-axis: 0% - Nuclear center and 100% - Nuclear periphery, Error bar: SEM, Mann Whitney test)*. **Scale bar ~10 µm.**

4.2.5 Lamin overexpression retains chromosome 1 territories close to the nuclear periphery

Chromosome 1 shows maximum transcriptional deregulation and mislocalization towards the nuclear interior in cells on soft matrices (Fig 3.7A and E, 3.8B-C). We also observed that chromosome 1 territories were able to partially regain their positions closer to the nuclear periphery upon switching cells from softer to stiffer matrices (Fig 3.11B and D). Since Lamin B2 overexpression tethered CT18 at the nuclear periphery even on soft matrices, we examined the effect of Lamin overexpression on CT1 radial positioning on soft matrices (Fig 4.5D, 4.7A). Overexpression of full length Lamin B2 retained CT1 closer to the nuclear periphery in DLD-1 cells on 2 kPa matrices (R.D ~65.04%, Empty vector: R.D ~56.53%) (Fig 4.7B-C). Lamin B2Δ570-582 was also able to retain CT1 near the nuclear periphery albeit to a lesser extent than the full length Lamin B2 (R.D ~62.98%) (Fig 4.7B-C, Table 4.2). Overexpression of both Lamin A (R.D ~62.92%) and Lamin A Δ425-553 (R.D ~60.75%) partially prevented the movement of CT1 towards the nuclear interior (Fig 4.7B-C). Taken together, these results show that Lamin B2 retains CT1 closer to the nuclear periphery, compared to Lamin A. Additionally, Lamins may regulate the positions of CT1 via mechanisms other than by direct chromatin interaction.

Table 4.1 Radial distance measurements of CT18 and CT19 under conditions of altered matrix stiffness

Substrate/ Conditions	Median % Radial Distance (% R.D)				
	CT18	**Δ**	**CT 19**	**Δ**	**Δ (CT18 - CT19)**
(I) CT positions upon Lamin overexpression on softer matrices (2 kPa) (Reference for comparison: EGFP-N1)					
EGFP-N1 on 2 kPa	56.79	+ 0.23	50.98	+ 1.58	5.81
GFP-Lamin A on 2 kPa	**46.41 (p<0.0001)**	- 10.15	**58.46 (p<0.0001)**	+ 9.06	12.05
Lamin B2-GFP on 2 kPa	**67.41 (p<0.0001)**	+ 10.85	**53.67 (p=0.0054)**	+ 4.27	13.74
GFP-Lamin A Δ425-553 on 2 kPa	57.08	+ 0.52	48.73	- 0.67	8.35
Lamin B2-GFP Δ570-582 on 2 kPa	54.07	- 2.49	48.93	- 0.47	5.14
(II) CT positions upon Lamin overexpression on Glass (Reference for comparison: EGFP-N1)					
EGFP-N1 on Glass	66.45	+ 9.89	55.32	+ 5.92	11.13
GFP-Lamin A on Glass	67.38	+ 10.82	54.50	+ 5.10	12.88
Lamin B2-GFP on Glass	66.84	+ 10.28	54.80	+ 5.40	12.04
GFP-Lamin A Δ425-553 on Glass	65.44	+ 8.88	56.44	+ 7.04	9.00
Lamin B2-GFP Δ570-582 on Glass	66.26	+ 9.70	53.94	+ 4.54	12.32
EGFP-N1 on Glass (for S22D overexpression)	64.79	+ 8.23	48.51	- 0.89	16.28
GFP-Lamin A S22D on Glass	67.35	+ 10.79	57.07	+ 7.67	10.28
(III) CT positions upon PP2 treatment on softer matrices (2 kPa) (Reference for comparison: respective DMSO control)					

Glass + DMSO	66.31	+ 9.75	53.15	+ 3.75	13.16
Glass + 20 µM PP2	67.93	+ 11.37	54.56	+ 5.16	13.37
2 kPa + DMSO	54.28	- 2.28	48.93	- 0.47	5.35
2 kPa + 20 µM PP2	**66.83 (p<0.0001)**	+ 10.27	**53.83 (p<0.0001)**	+ 4.43	13.00
(IV) CT positions upon Emerin Y99F overexpression on softer matrices (2 kPa) (Reference for comparison: Vector control+EGFP-N1)					
Vector control + EGFP-N1 on 2 kPa	51.43	- 5.13	42.74	- 6.66	8.69
Vector control + WT-EMD on 2 kPa	54.59	- 1.97	43.69	- 5.71	10.9
Vector control + EMD Y99F on 2 kPa	56.22	- 0.34	47.49	- 1.91	8.73
shEmerin + EGFP-N1 on 2 kPa	**61.80 (p<0.0001)**	+ 5.24	**51.13 (p<0.0001)**	+ 1.73	10.67
shEmerin + WT-EMD on 2 kPa	55.72	- 0.84	47.50	- 1.9	8.22
shEmerin + EMD Y99F on 2 kPa	**65.25 (p<0.0001)**	+ 8.69	**53.24 (p<0.0001)**	+ 3.84	12.01

Median radial distances of CT18 and CT19. Δ: shift in CT position, calculated with 2 kPa as reference, '+': movement towards the nuclear periphery, '-': movement towards the nuclear center. Δ (CT18-CT19): shift in CT position between CT18 and CT19. Values in bold are significant (p value in brackets).

Figure 4.7

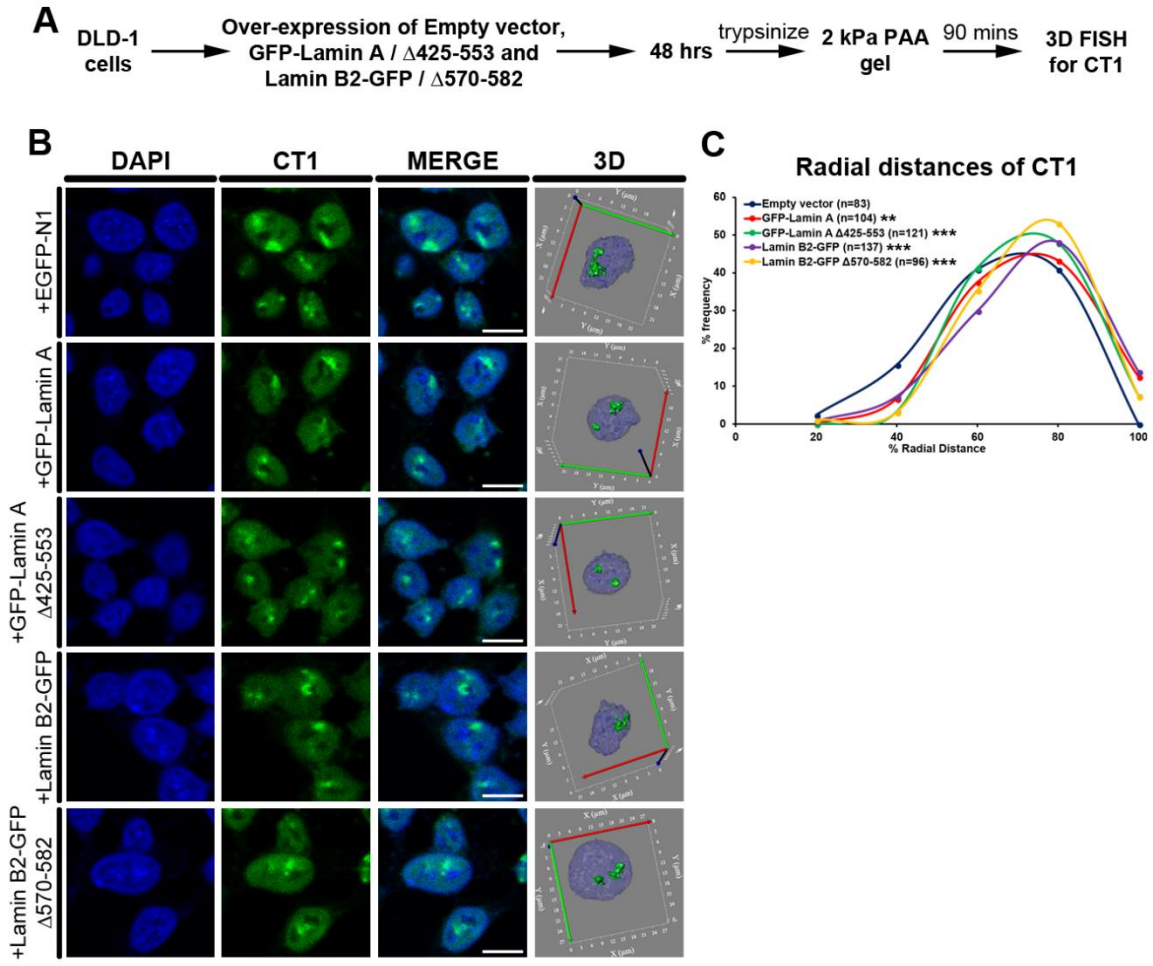

Figure 4.7 Lamin overexpression retains chromosome 1 territories close to the nuclear periphery. A) Experimental scheme. B) Representative mid-optical sections from 3D-FISH hybridization for CT1 in DLD-1 cells on 2 kPa matrix after overexpression of EGFP-N1, GFP-Lamin A, Lamin B2-GFP, GFP-Lamin A Δ425-553 and Lamin B2-GFP Δ570-582. 3D: reconstruction of a single representative nucleus. C) Radial distance distribution profiles for CT1 on 2 kPa matrix after over-expression of EGFP-N1 (M=56.53%), GFP-Lamin A (M=62.92%), Lamin B2-GFP (M=65.04%), GFP-Lamin A Δ425-553 (M=60.75%) and Lamin B2-GFP Δ570-582 (M=62.98%). *(C: Data from single experiment, n: number of CTs, X-axis: 0% - Nuclear center and 100% - Nuclear periphery, Mann Whitney test)*. *** p<0.0001, ** p<0.01 (compared with Empty vector control). **Scale bar ~10 µm.**

Table 4.2 Radial distance measurements for CT1 under conditions of altered matrix stiffness

Substrate/ Conditions	Median % Radial Distance (% R.D)	
	CT1	**Δ**
(I) CT positions upon Lamin overexpression on softer matrices (2 kPa) (Reference for comparison: EGFP-N1)		
EGFP-N1 on 2 kPa	56.53	+ 5.96
GFP-Lamin A on 2 kPa	**62.92 (p=0.0013)**	+ 12.35
Lamin B2-GFP on 2 kPa	**65.04 (p<0.0001)**	+ 14.47
GFP-Lamin A Δ425-553 on 2 kPa	**60.75 (p=0.0004)**	+ 10.18
Lamin B2-GFP Δ570-582 on 2 kPa	**62.98 (p=0.0005)**	+ 12.41
(II) CT positions upon PP2 treatment on softer matrices (2 kPa) (Reference for comparison: respective DMSO control)		
Glass + DMSO	61.00	+ 10.43
Glass + 20 µM PP2	59.75	+ 9.18
2 kPa + DMSO	50.94	+ 0.37
2 kPa + 20 µM PP2	49.7	- 0.87
(III) CT positions upon Emerin Y99F overexpression on softer matrices (2 kPa) (Reference for comparison: shEmerin+EGFP-N1)		
Vector control + EGFP-N1 on 2 kPa	**45.61 (p<0.0001)**	- 4.96
shEmerin + EGFP-N1 on 2 kPa	38.49	- 12.08
shEmerin + WT-EMD on 2 kPa	**45.86 (p=0.0005)**	- 4.71
shEmerin + EMD Y99F on 2 kPa	**43.80 (p=0.0015)**	- 6.77

Median radial distances of CT1. Δ: shift in CT position, calculated with 2 kPa as reference, '+': movement towards the nuclear periphery, '-': movement towards the nuclear center. Values in bold are significant (p value in brackets).

4.2.6 Src kinase inhibition abrogates emerin phosphorylation and Lamin mislocalization in cells on softer matrices

Emerin was phosphorylated specifically in response to cells experiencing lowered matrix stiffness (Fig 4.1A and E). We investigated the importance of emerin phosphorylation in cells on softer matrices and further, its role in the relay of mechanosensitive signals to the genome. Emerin is phosphorylated by Src kinase at Tyr74 and Tyr95 in isolated nuclei deformed by magnetic tweezers (Guilluy et al., 2014). Thus, we examined the impact of inhibiting Src kinase using PP2 [an inhibitor of the Src tyrosine kinase family, (Shin et al., 2009)] on emerin phosphorylation triggered in cells on softer matrices. Cells were treated with 20 μM PP2 or equivalent volume of DMSO ~3-4 mins after they were plated on the softer 2 kPa matrices and incubated with the inhibitor for either 30 or 90 mins (Fig 4.8A). Immunoblotting showed that treatment with PP2 abrogated emerin phosphorylation over time, without affecting the total emerin levels (Fig 4.8B-D). We next used the combination of 20 μM PP2 for 90 mins to study the effect of inhibiting Src kinase activity (and therefore emerin phosphorylation) on the localization of Lamin A and B2 in cells on 2 kPa matrices (Fig 4.8E). Interestingly, inhibition of emerin phosphorylation significantly increased and retained Lamin A and Lamin B2 at the nuclear periphery in cells on 2 kPa matrices (Fig 4.8E-H). Lamin B2 was prominently enriched at the nuclear periphery as compared to the nuclear interior (accumulation in nuclear interior is seen in DMSO control cells on 2 kPa) in PP2 treated cells on 2 kPa matrices, while Lamin A levels at both the nuclear periphery as well as in the nucleoplasm increased (Fig 4.8F-G). Thus, emerin phosphorylation on softer matrices is potentially required for the nucleoplasmic accumulation of nuclear lamins.

Figure 4.8

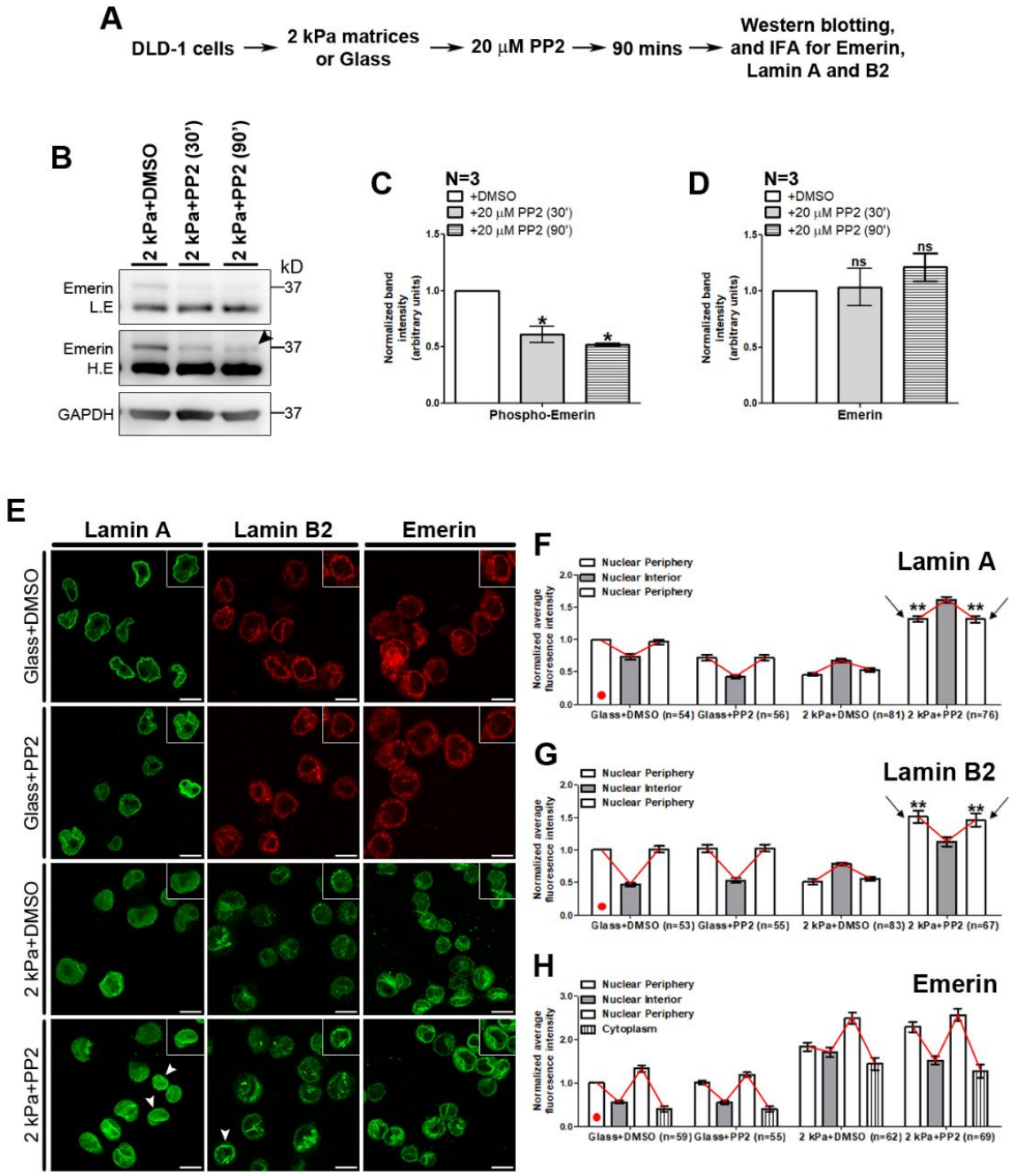

Figure 4.8 Src kinase inhibition abrogates emerin phosphorylation and Lamin mislocalization in cells on softer matrices. A) Experimental scheme. B) Western blot analysis to assess effect of PP2 treatment on emerin phosphorylation. Blot probed with anti-emerin antibody (Upper panel – lower exposure L.E, Lower panel – higher exposure H.E) and GAPDH was used as loading control *(N=3).* Arrowhead indicates significant reduction of phospho-emerin band upon 20 μM PP2 treatment for ~90 mins. C) Densitometric quantification of expression levels of phospho-emerin upon 20 μM PP2 treatment for 30 and 90 mins (from 4.8B). Expression levels were normalized to GAPDH and re-normalized to DMSO control *(N=3, Error bars: SEM, Student's t-test * p<0.05).* D) Densitometric quantification of expression levels of emerin upon 20 μM PP2 treatment for 30 and 90 mins (from 4.8B). Expression levels were normalized to GAPDH and re-normalized to DMSO control *(N=3, Error bars: SEM, Student's t-test).*

Figure 4.8 ***continued.*** E) Representative mid-optical sections of DLD-1 cells immunostained for Lamin A, B2 and emerin on 2 kPa matrix and glass for 90 mins, with and without (DMSO control) 20 µM PP2. Inset: zoom of single nucleus. Arrowheads indicate increased Lamin A and B2 staining at the periphery on 2 kPa matrices with PP2 treatment. F-H) Normalized average fluorescence intensity from line-scans across nuclei performed for Lamin A (F), Lamin B2 (G) and emerin (H) in DLD-1 cells on 2 kPa matrix and glass (with and without PP2) after 90 mins. Average intensities for each protein was normalized to their fluorescence intensities at the nuclear periphery in cells on glass (indicated by red dot). *(Pooled data from N=2 independent biological replicates, n: number of nuclei, Error bar: SEM).* ** $p<0.0001$ (Student's t-test). **Scale bar ~10 µm.**

4.2.7 Inhibition of emerin phosphorylation selectively abrogates mislocalization of chromosome territories

We assessed the impact of inhibiting emerin phosphorylation on the radial positions of CT1, 18 and 19 in cells on softer matrices. Cells were treated with 20 µM PP2 or equivalent volume of DMSO ~3-4 mins after they were plated on the softer 2 kPa matrices (or collagen coated glass coverslips) and incubated with the inhibitor for 90 mins, followed by 3D-FISH (Fig 4.9A-B). Remarkably, neither CT18 nor CT19 mislocalized into the nuclear interior in cells on softer matrices (2 kPa), upon the inhibition of emerin phosphorylation (CT18: 2 kPa+PP2 R.D ~66.83%; CT19: 2 kPa+PP2 R.D ~53.83%) (Fig 4.9C-D, Table 4.1). This suggests a unique role for emerin phosphorylation in modulating the spatial positions of chromosome 18 and 19 territories in cells on softer matrices.

Surprisingly, the inhibition of emerin phosphorylation did not affect the position of CT1 that was mislocalized toward the nuclear interior in cells on softer matrices (2 kPa+DMSO: R.D ~50.94%, 2 kPa+PP2: R.D ~49.70%) (Fig 4.9E-F, Table 4.2). This was in marked contrast to CT18 and CT19 positions, which were retained at their conserved nuclear locations upon inhibition of emerin phosphorylation (Fig 4.9C-D). We determined the positions of CT18 along with CT1 by co-labelling these chromosome territories upon inhibition of emerin phosphorylation in cells on softer

matrices (2 kPa) (Fig 4.9E). As observed previously, CT18 was retained toward the nuclear periphery upon inhibition of emerin phosphorylation (CT18: 2 kPa+DMSO: R.D ~55.47%, 2 kPa+PP2: R.D ~65.73%), while position of CT1 remained unaffected (Fig 4.9E-F). Taken together, these results suggest that the positions of chromosome territories are selectively responsive to emerin phosphorylation.

Figure 4.9

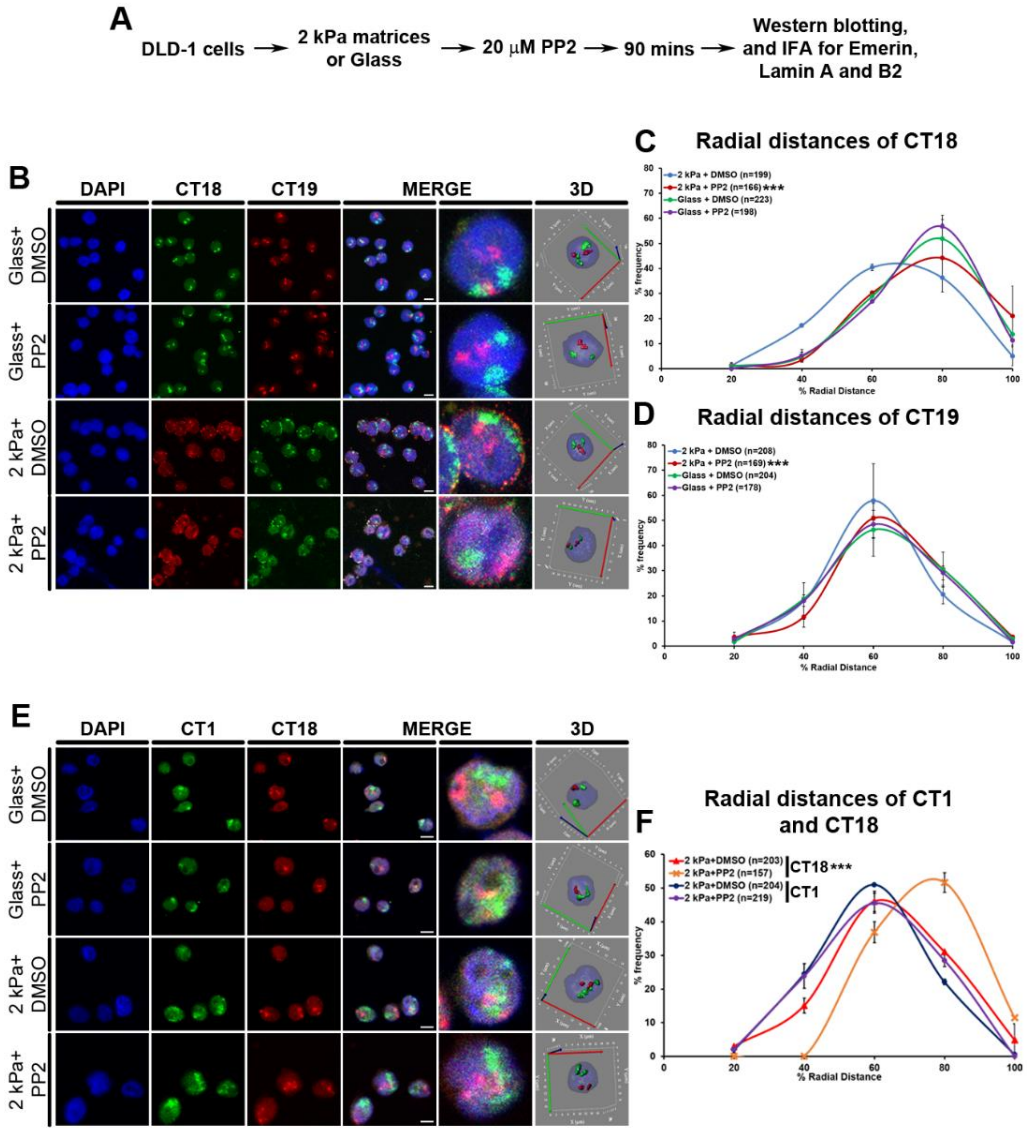

Figure 4.9 Inhibition of emerin phosphorylation selectively abrogates mislocalization of chromosome territories. A) Experimental scheme. B) Representative mid-optical sections from 3D-FISH hybridizations for CT18 and 19 on 2 kPa matrix and glass, with and without (DMSO control) 20 μM PP2 treatment. 3D: reconstruction of single representative nucleus. C) Radial distance distribution profiles for CT18 *(N=2)* on 2 kPa matrix (+PP2: M=66.83% and -PP2: M=54.28%) and glass (+PP2: M=67.93% and -PP2: M=66.31%). D) Radial distance distribution profiles for CT19 *(N=2)* on 2 kPa (+PP2: M=53.83% and -PP2: M=48.93%) and glass (+PP2: 54.56% and -PP2: M=53.15%). *(C-D: Data pooled from N=2 independent biological replicates, n: number of CTs, X-axis: 0% - Nuclear center and 100% - Nuclear periphery, Error bar: SEM, Mann Whitney test).* *** p<0.0001 (compared with 2 kPa+DMSO). **Scale bar ~10 μm.**

Figure 4.9 ***continued.*** E) Representative mid-optical sections from 3D-FISH hybridizations for CT1 and 18 on 2 kPa matrix and glass, with and without (DMSO control) 20 µM PP2 treatment. 3D: reconstruction of single representative nucleus. F) Radial distance distribution profiles of CT1 on 2 kPa (+PP2: M=49.70% and -PP2: M=50.94%) and CT18 on 2 kPa (+PP2: 65.73% and -PP2: M=55.47%) *(Data pooled from N=2 independent biological replicates, n: number of CTs, X-axis: 0% - Nuclear center and 100% - Nuclear periphery, Error bar: SEM, Mann Whitney test).* *** p<0.0001 (compared with 2 kPa+DMSO). **Scale bar ~10 µm.**

4.2.8 Emerin is phosphorylated at the Tyr99 residue in cells subjected to reduced matrix stiffness

We sought to identify the tyrosine residue, phosphorylated in emerin in response to lowered matrix stiffness. Src kinase phosphorylates emerin at tyrosine residues (Y) 59, 74 and 95 (Tifft et al., 2009). Of these, Y74 and Y95 are phosphorylated by Src in a force-dependent manner (Guilluy et al., 2014). We examined if cells expressing the phospho-deficient mutants of emerin i.e, Y74F, Y95F and Y74/95FF were phosphorylated in cells on softer matrices (2 kPa) (Fig 4.10A-B). Interestingly, even these phospho-deficient emerin mutants were phosphorylated, comparable to overexpressed wild type emerin (Arrowhead, Fig 4.10C). This suggested that another tyrosine residue was phosphorylated in emerin. We next exposed cells over-expressing emerin (Δ95-99) - a mutant with reduced affinity to Lamin A/C (Lee et al., 2001), to the softer matrices (2 kPa) (Fig 4.10D). Western blotting showed a distinct reduction of emerin (Δ95-99) phosphorylation (Arrowhead, Fig 4.10E). Since emerin has another tyrosine residue at Tyr99, we tested the phosphorylation status of Y99 (Fig 4.10F). Interestingly, overexpressed emerin Y99F showed a distinctive decrease in phosphorylation levels in cells exposed to softer matrices (2 kPa) (Arrowhead, Fig 4.10G). It is noteworthy that the overexpressed phospho-deficient mutants of emerin (Y74F, Y95F, Y74/95FF and Y99F) were localized at the inner nuclear membrane and a sub-fraction outside the nucleus, comparable to overexpressed wild type (WT) emerin in cells on both soft (2 kPa) matrices and glass (Fig 4.11A-C). Taken together, emerin phosphorylation at

Tyr99 residue is activated in cells and functions as a key mechanosensitive signal in response to lowered matrix stiffness.

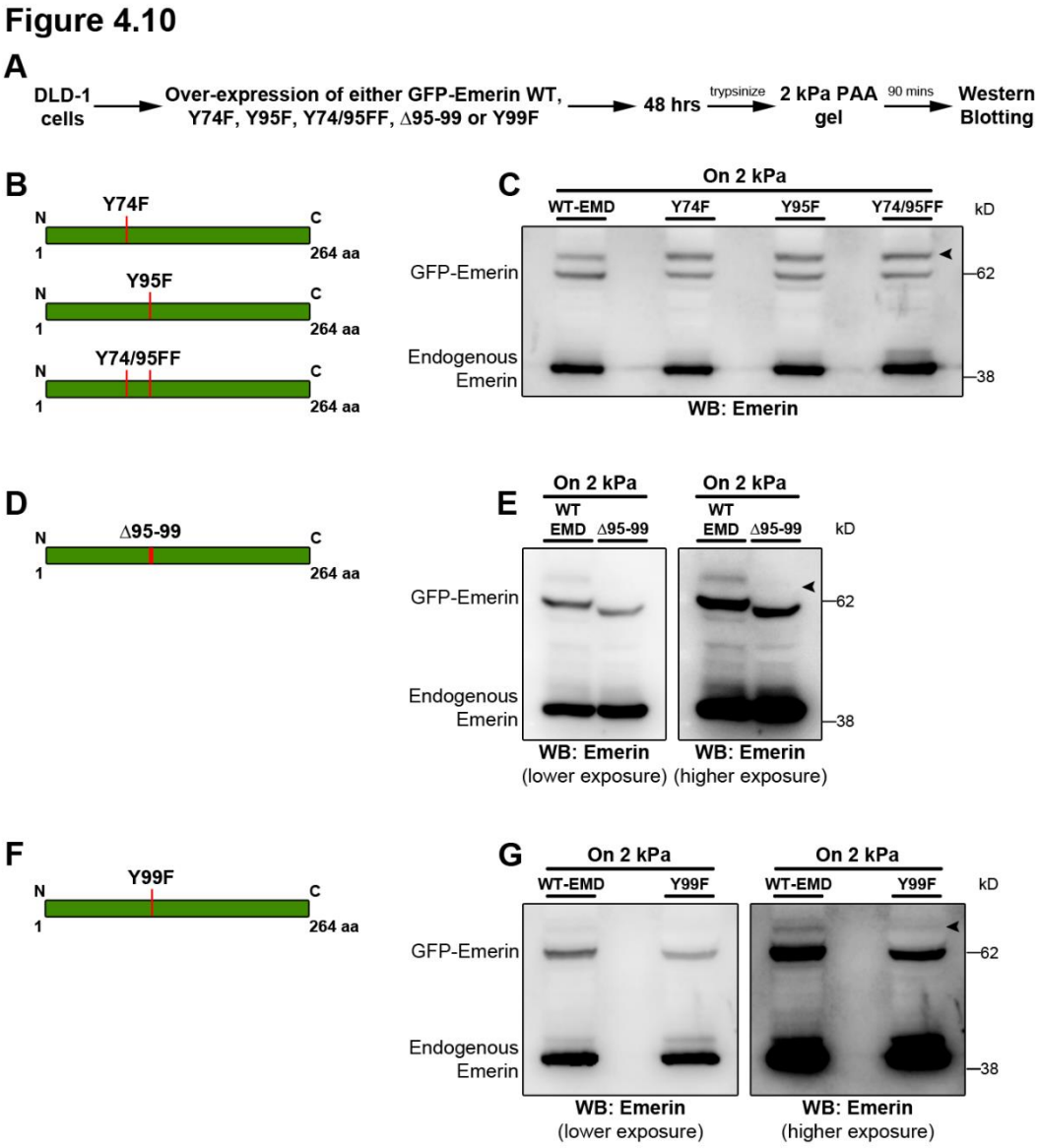

Figure 4.10 Emerin is phosphorylated at the Tyr99 residue in cells subjected to reduced matrix stiffness. A) Experimental scheme. B) Graphical representation of site directed mutations in emerin (Y74F, Y95F, Y74/95FF). C) Representative immunoblot to assess phosphorylation status of Wild Type (WT), Y74F, Y95F and Y74/95FF emerin upon over-expression for 48 hrs, followed by 90 minutes on 2 kPa matrix *(N=2)*. Arrowhead indicates phosphorylation of emerin Y74F, Y95F and Y74/95FF. D) Graphical representation for emerin (Δ95-99). E) Representative immunoblot to assess phosphorylation of WT and emerin (Δ95-99) upon over-expression for 48 hrs, followed by 90 minutes on 2 kPa matrix *(N=2)*. Arrowhead indicates reduced phosphorylation of overexpressed emerin (Δ95-99). F) Graphical representation of site directed mutation (Y99F) in emerin. G) Representative immunoblot to assess phosphorylation of WT and Y99F emerin upon over-expression for 48 hrs, followed by 90 minutes on 2 kPa matrix *(N=2)*. Arrowhead indicates reduced phosphorylation of overexpressed emerin Y99F *(For C, E and G: EMD: emerin)*. **N: independent biological replicates.**

Figure 4.11

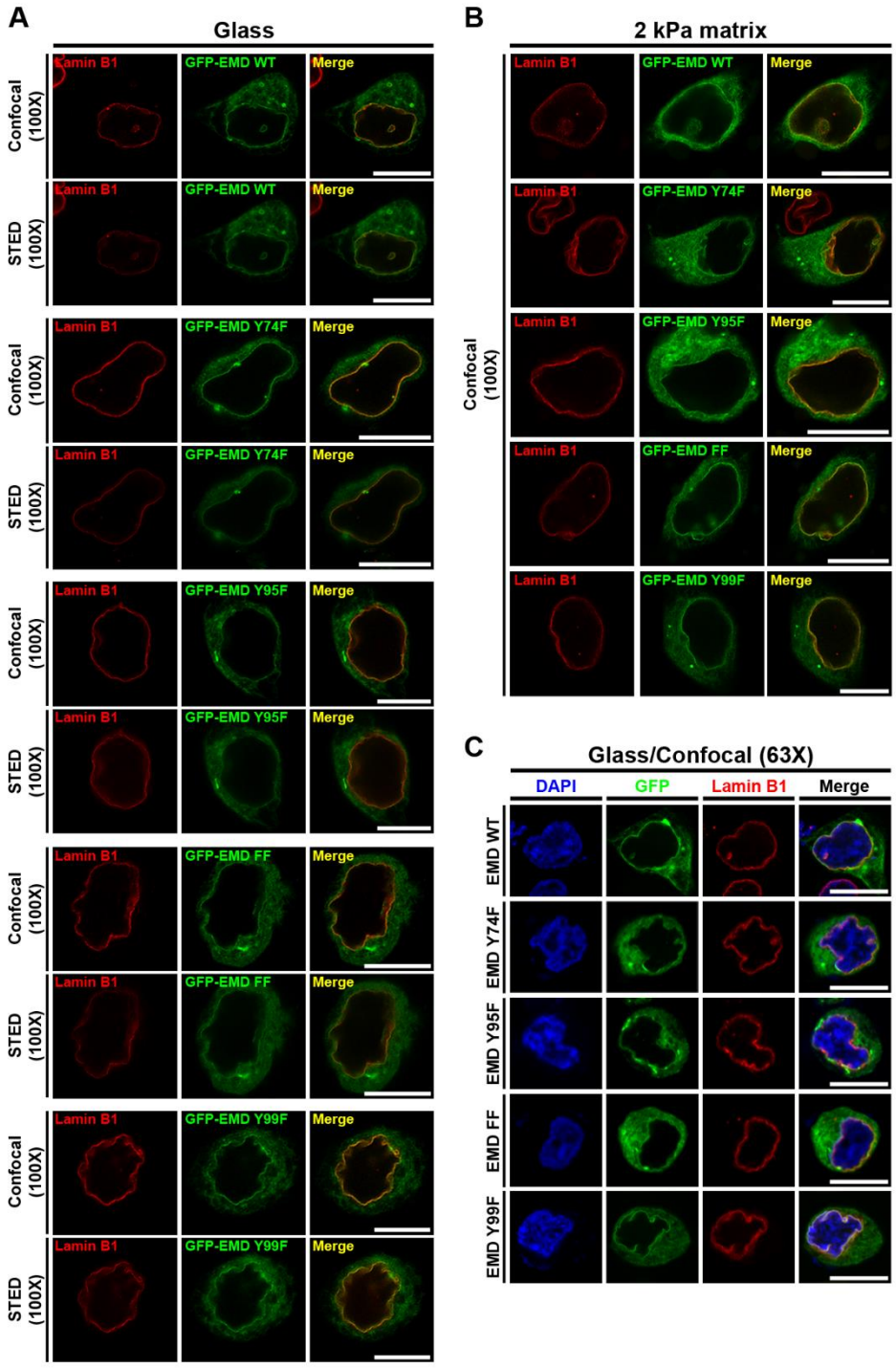

Figure 4.11 Phospho-deficient mutants of emerin show sub-cellular localization similar to wild type emerin. A) Representative confocal (100X) and STED images showing sub-cellular localization of GFP-tagged over-expressed phospho-deficient emerin mutants (Y74F, Y95F, Y74/95FF and Y99F) and GFP-tagged over-expressed wild type (WT) emerin in DLD-1 cells on glass, counterstained for Lamin B1. B) Representative confocal (100X) images showing sub-cellular localization of GFP-tagged over-expressed phospho-deficient emerin mutants (Y74F, Y95F, Y74/95FF and Y99F) and GFP-tagged over-expressed wild type (WT) emerin in DLD-1 cells on 2 kPa matrices, counterstained for Lamin B1. C) Representative confocal (63X) images showing sub-cellular localization of GFP-tagged over-expressed phospho-deficient emerin mutants (Y74F, Y95F, Y74/95FF and Y99F) and GFP-tagged over-expressed wild type (WT) emerin in DLD-1 cells on glass, counterstained for Lamin B1 and DAPI. **Scale bar ~10 µm.**

4.2.9 Overexpression of emerin Y99F in shEmerin DLD-1 cells retains Lamins at the nuclear envelope

To study the role of emerin phosphorylation at Tyr99 in cells on softer matrices, we depleted DLD-1 cells of endogenous emerin using emerin shRNA to generate clonal subpopulation of cells with lowered emerin levels (Fig 4.12A). We next overexpressed either wild type GFP-Emerin or GFP-Emerin Y99F (both made insensitive to the shRNA) in either the shEmerin or vector control cells (shRNA Empty vector) for 48 hrs, followed by trypsinizing the cells and plating them on 2 kPa matrices for 90 mins (Fig 4.12B). Immunoblotting showed significantly lowered levels of GFP-Emerin Y99F phosphorylation as compared to the wild type GFP-Emerin in both vector control and shEmerin cells on 2 kPa (Fig 4.12C-D). To examine the effect of emerin Y99F on lamin localization and expression, immunostaining for Lamin A and B2 was performed in shEmerin cells overexpressing either EGFP-N1, GFP-Emerin WT or GFP-Emerin Y99F and exposed to 2 kPa matrices for 90 mins (Fig 4.12E). Emerin depleted cells overexpressing emerin Y99F (on 2 kPa), showed a significantly greater retention of Lamin A and B2 at the nuclear envelope (Fig 4.12F-G). On the other hand, Lamin A and B2 were predominantly enriched in the nucleoplasm, rather than the nuclear envelope, upon overexpression of WT emerin (Fig 4.12F-G). These results reiterate the possible requirement of emerin phosphorylation in the nucleoplasmic accumulation of nuclear lamins.

Figure 4.12

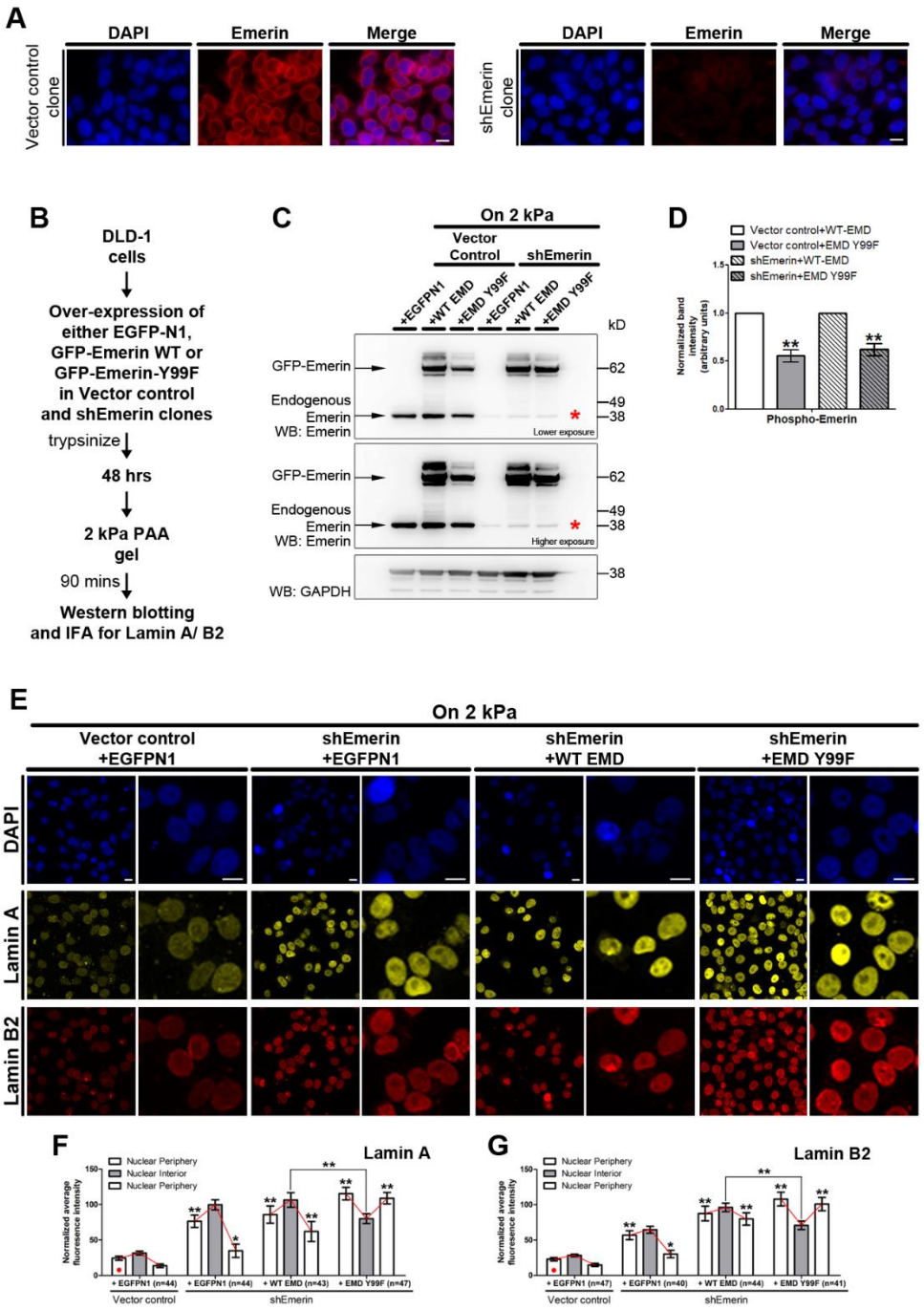

Figure 4.12 Overexpression of emerin Y99F in shEmerin DLD-1 cells retains Lamins at the nuclear envelope. A) Representative mid-optical sections of (DLD-1) empty vector and shEmerin clones immunostained for emerin. shEmerin clone shows pronounced downregulation of emerin as compared to the empty vector clone. B) Experimental scheme for overexpression of WT and Y99F Emerin in shEmerin background. C) Representative immunoblot *(N=3 independent biological replicates)* showing overexpression of GFP-Emerin WT and GFP-Emerin Y99F in vector control and shEmerin clones. Asterisk: Distinct downregulation of endogenous emerin in shEmerin clone. GAPDH was used as loading control. D) Densitometric quantification of GFP-Emerin WT and Y99F phosphorylation in vector control and shEmerin clones. Overexpressed phosphorylated and non-phosphorylated emerin expression was normalized to GAPDH. The phosphorylated emerin levels were then re-normalized to total overexpressed emerin levels. *(Pooled data from N=3 independent biological replicates, Error bars: SEM).* ** $p<0.01$ (Student's t-test).

Figure 4.12 *continued.* E) Representative mid-optical sections *(N=2 independent biological replicates)* from confocal z-stacks of Lamin A and B2 immunostaining in vector control and shEmerin clones on 2 kPa matrices overexpressing EGFPN1, GFP-Emerin WT or GFP-Emerin Y99F. F-G) Normalized average fluorescence intensity from line-scans across nuclei performed for Lamin A and B2 *(images from 4.12E)* in vector control and shEmerin clones on 2 kPa matrices overexpressing EGFPN1, GFP-Emerin WT or GFP-Emerin Y99F *(E-G, EMD: emerin, Pooled data from N=2 independent biological replicates, n: number of nuclei, Error bar: SEM, Student's t-test).* ** $p<0.01$, * $p<0.05$ (compared with Vector control clone+EGFPN1). **Scale bar ~10 µm.**

4.2.10 Overexpression of emerin Y99F selectively abrogates mislocalization of chromosome territories

Since emerin Y99F showed a distinctive reduction in its phosphorylation in cells on softer matrices and its overexpression retained lamins more at the nuclear envelope (Fig 4.10G, 4.12F-G), we asked if emerin Tyr99 that functions as a mechanosensor of reduced matrix stiffness, also modulates chromosome territory positions? We used 3D-FISH to determine radial positions of CT18 and 19 in vector control and shEmerin cells overexpressing either EGFP-N1, GFP-Emerin WT or GFP-Emerin Y99F and exposed to 2 kPa matrices for 90 mins (Fig 4.13A and 4.14A). Vector control DLD-1 cells (endogenous emerin is present) overexpressing either EGFP-N1, GFP-Emerin WT or GFP-Emerin Y99F did not show any change in the mislocalization of CT18 and 19 otherwise observed on 2 kPa matrices (CT18: +EGFP-N1 R.D ~51.43%, +WT-EMD R.D ~54.59%, +EMD-Y99F R.D ~56.22%; CT19: +EGFP-N1 R.D ~42.74%, +WT-EMD R.D ~43.69%, +EMD-Y99F R.D ~47.49%) (Fig 4.13B-D, Table 4.1).

Interestingly, cells depleted of endogenous emerin (shEmerin+EGFP-N1) showed a relatively conserved positioning of CT18 toward the periphery (R.D ~61.80%) and CT19 near the nuclear interior (R.D ~51.13%) on softer matrices (Fig 4.14B-D). This suggests a requirement of emerin phosphorylation in mislocalizing chromosome 18 and 19 territories in cells exposed to softer

matrices. Consistent with these results, X-EDMD patient fibroblasts expressing mutant emerin, mislocalize chromosome 13 and 18 territories toward the nuclear interior (Meaburn et al., 2007), while in contrast lymphocytes with a nonsense mutation in emerin, and therefore emerin loss, nevertheless retained conserved radial positioning of chromosome territories (Boyle et al., 2001). Remarkably, CT18 and CT19 were also retained at their conserved nuclear locations in cells overexpressing emerin Y99F (but depleted of endogenous emerin, CT18: R.D ~65.25%; CT19: R.D ~53.24%) (Fig 4.14C-D). In contrast, the overexpression of WT emerin (in emerin depleted cells) mislocalized CT18 and CT19 on softer matrices (CT18: R.D ~55.72%; CT19: R.D ~47.50%) (Fig 4.14C-D). This further underscores the requirement of emerin phosphorylation in modulating chromosome 18 and 19 territory positions in cells on softer matrices.

Since CT1 was mislocalized toward the nuclear interior despite the inhibition of emerin phosphorylation (Fig 4.9E-F), we determined the effect of overexpressing emerin Y99F on CT1 localization (Fig 4.14E). Interestingly, cells depleted of endogenous emerin (shEmerin) mislocalized CT1 even further into the nuclear interior (Vector control clone+EGFP-N1: R.D ~45.61%, shEmerin+EGFP-N1: R.D ~38.49%) (Fig 4.14F, Table 4.2). Remarkably, overexpression of either WT emerin or emerin Y99F (in shEmerin background) rescued CT1 positions comparable to that of control cells but not back to the proximity of the nuclear periphery (Vector control clone+EGFP-N1: R.D ~45.61%, shEmerin+EGFP-N1: R.D ~38.49%, +WT-EMD: R.D ~45.86%, +EMD Y99F: R.D ~43.80%) (Fig 4.14F). In summary, CT1 mislocalization toward the nuclear interior does not respond to emerin phosphorylation in cells on softer matrices but is modulated by the presence of emerin. Taken together, chromosome territory positions are selectively responsive to the phosphorylation status of emerin.

Figure 4.13

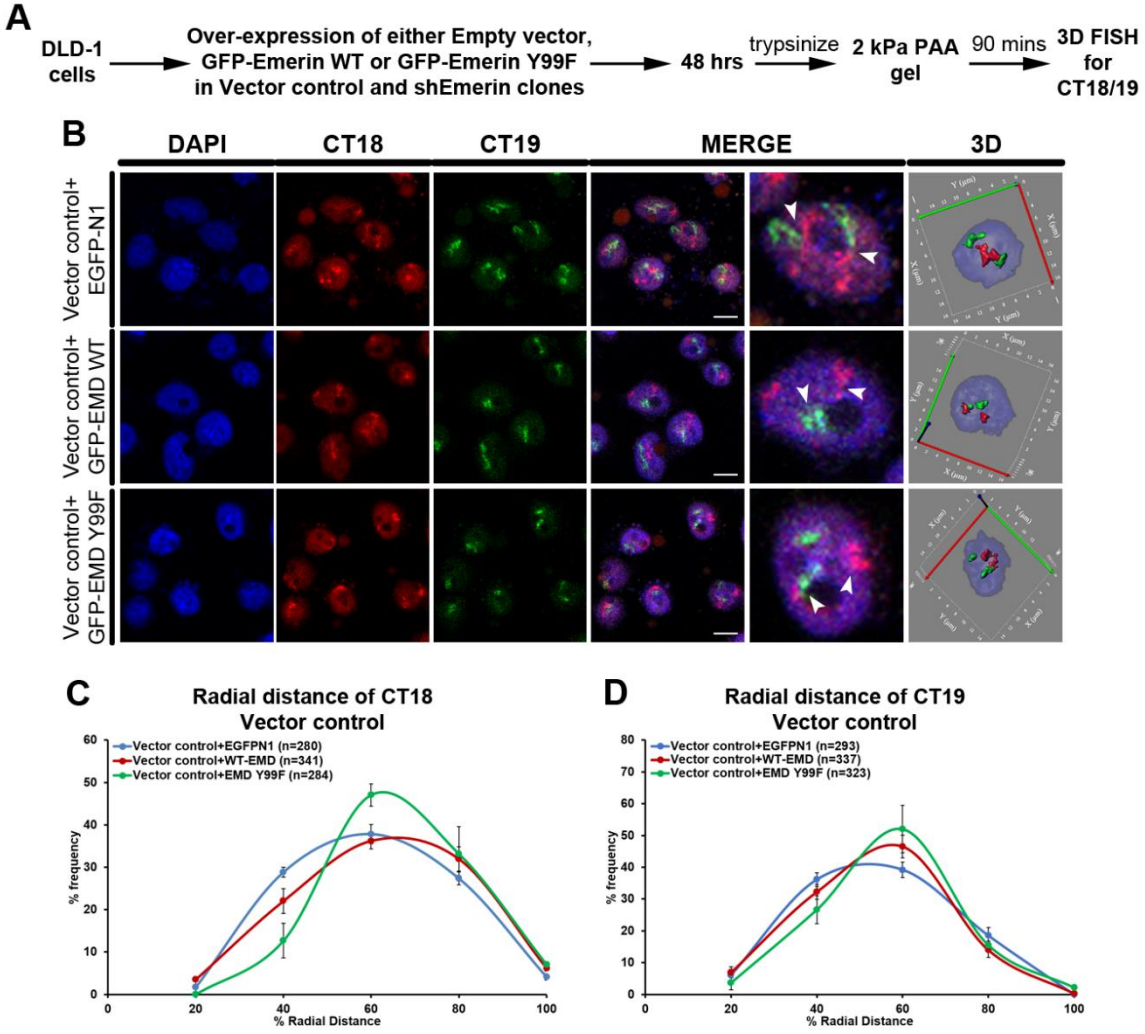

Figure 4.13 Overexpression of emerin Y99F in vector control clone does not affect CT18 and 19 positions. A) Experimental scheme. B) Representative mid-optical sections from 3D-FISH hybridizations for CT18 and 19 in vector control clones on 2 kPa matrix after overexpression of Empty vector (EGFP-N1), WT Emerin (GFP-EMD WT) and Emerin Y99F (GFP-EMD Y99F). Arrowheads show specific hybridization for CT18 and CT19, resolved in 3D: reconstruction of single representative nucleus. C) Radial distance distribution profiles for CT18 in vector control clone (on 2 kPa) after over-expression of Empty vector (*N=3*, M=51.43%), GFP-EMD WT (*N=3*, M=54.59%) and GFP-EMD Y99F (*N=3*, M=56.22%). D) Radial distance distribution profiles for CT19 in vector control clone (on 2 kPa) after over-expression of Empty vector (*N=3*, M=42.74%), GFP-EMD WT (*N=3*, M=43.69%) and GFP-EMD Y99F (*N=3*, M=47.49%) *(B-D, EMD: emerin, Pooled data from N=3 independent biological replicates, n: number of CTs, X-axis: 0% - Nuclear center and 100% - Nuclear periphery, Error bar: SEM)*. **Scale bar ~10 µm.**

Figure 4.14

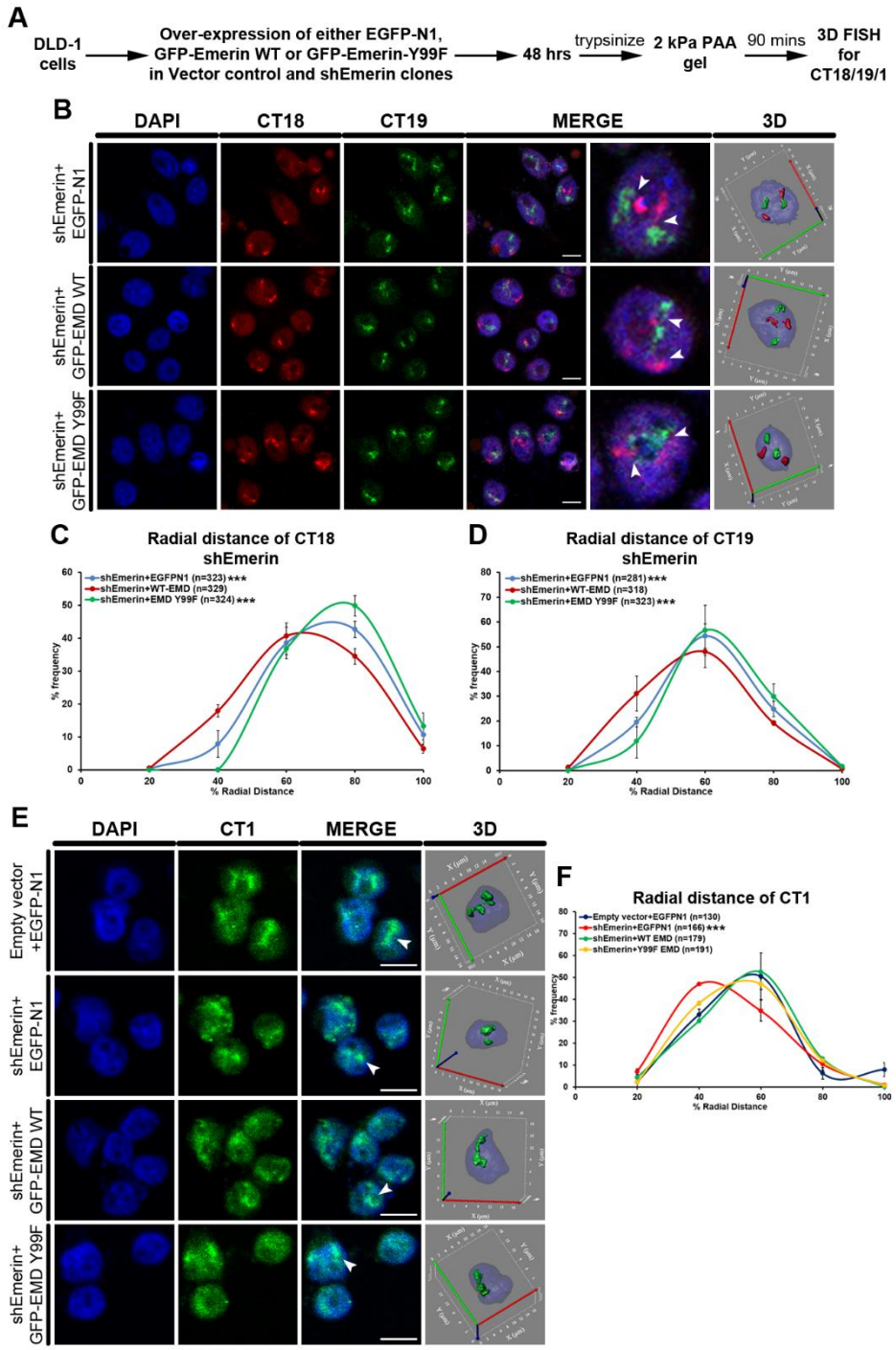

Figure 4.14 Overexpression of emerin Y99F in shEmerin clone selectively abrogates mislocalization of chromosome territories. A) Experimental scheme. B) Representative mid-optical sections from 3D-FISH hybridizations for CT18 and 19 in shEmerin clones on 2 kPa matrix after overexpression of Empty vector (EGFP-N1), WT Emerin (GFP-EMD WT) and Emerin Y99F (GFP-EMD Y99F). Arrowheads show specific hybridization for CT18 and CT19, resolved in 3D: reconstruction of single representative nucleus. C) Radial distance distribution profiles for CT18 in shEmerin clone (on 2 kPa) after over-expression of Empty vector (*N=3*, M=61.80%), GFP-EMD WT (*N=3*, M=55.72%) and GFP-EMD Y99F (*N=3*, M=65.25%). D) Radial distance distribution profiles for CT19 in shEmerin clone (on 2 kPa) after over-expression of Empty vector (*N=3*, M=51.13%), GFP-EMD WT (*N=3*, M=47.50%) and GFP-EMD Y99F (*N=3*, M=53.24%) *(B-D, EMD: emerin, Pooled data from N=3 independent biological replicates, n: number of CTs, X-axis: 0% - Nuclear center and 100% - Nuclear periphery, Error bar: SEM, Mann Whitney test)*. *** p<0.0001 (compared with Vector control+EGFP-N1, Fig 4.13C and D). **Scale bar ~10 µm.**

Figure 4.14 ***continued.*** E) Representative mid-optical sections from 3D-FISH hybridizations for CT1 in vector control clone on 2 kPa matrix after overexpression of Empty vector (EGFP-N1), and shEmerin clones on 2 kPa matrix after overexpression of Empty vector (EGFP-N1), WT Emerin (GFP-EMD WT) and Emerin Y99F (GFP-EMD Y99F). Arrowheads show specific hybridization for CT1, resolved in 3D: reconstruction of single representative nucleus. F) Radial distance distribution profiles for CT1 in vector control clone (on 2 kPa) after overexpression of Empty vector (*N=2*, M=45.61%), and shEmerin clone (on 2 kPa) after over-expression of Empty vector (*N=2*, M=38.49%), GFP-EMD WT (*N=2*, M=45.86%) and GFP-EMD Y99F (*N=2*, M=43.80%) *(E-F, EMD: emerin, Pooled data from N=2 independent biological replicates, n: number of CTs, X-axis: 0% - Nuclear center and 100% - Nuclear periphery, Error bar: SEM, Mann Whitney test)*. *** p<0.0001 (compared with Vector control+EGFP-N1). **Scale bar ~10 µm.**

4.2.11 Emerin Y99F shows greater interaction with Lamin A, than wild type Emerin

Our results suggested that emerin is phosphorylated at Tyr99 in cells on softer matrices and this phosphorylation triggers the nucleoplasmic accumulation of Lamins and a selective repositioning of chromosome territories. Since Tyr99 falls within the interaction domain of Emerin with Lamin A/C, we were curious to examine if phosphorylation of Tyr99 could result in altered Emerin-Lamin A/C interaction (Fig 4.15A-B). Because of the changes in the total levels of Lamin A and Emerin in cells on softer matrices, it was experimentally challenging to perform a co-immunoprecipitation assay for the two proteins under these conditions. We therefore independently overexpressed EGFP-N1, GFP-Emerin WT, GFP-Emerin Y99F, GFP-Emerin Y99D and GFP-Emerin Δ95-99 in DLD-1 cells growing on tissue culture plastic for 48 hrs, followed by a pulldown with Anti-GFP antibody to study the interaction between each of the emerin variants and Lamin A/C (Fig 4.15A). GFP-Emerin Δ95-99 was used as positive control as this deletion mutant is known to exhibit reduced interaction with Lamin A/C (Lee et al., 2001). Indeed, we observed that GFP-Emerin Δ95-99 showed hardly any interaction with Lamin A/C compared to GFP-Emerin WT (Fig 4.15C). Interestingly, GFP-Emerin Y99F showed a greater interaction while GFP-Emerin Y99D showed very reduced interaction with Lamin A/C (Fig 4.15C, red asterisk). These results suggest that phosphorylation of Tyr99 in emerin could potentially trigger the nucleoplasmic accumulation of

Lamin A due to reduced interaction between the two proteins, and this could further lead to a destabilization of the nuclear lamina and mislocalization of chromosome territories (Fig 4.16).

Figure 4.15

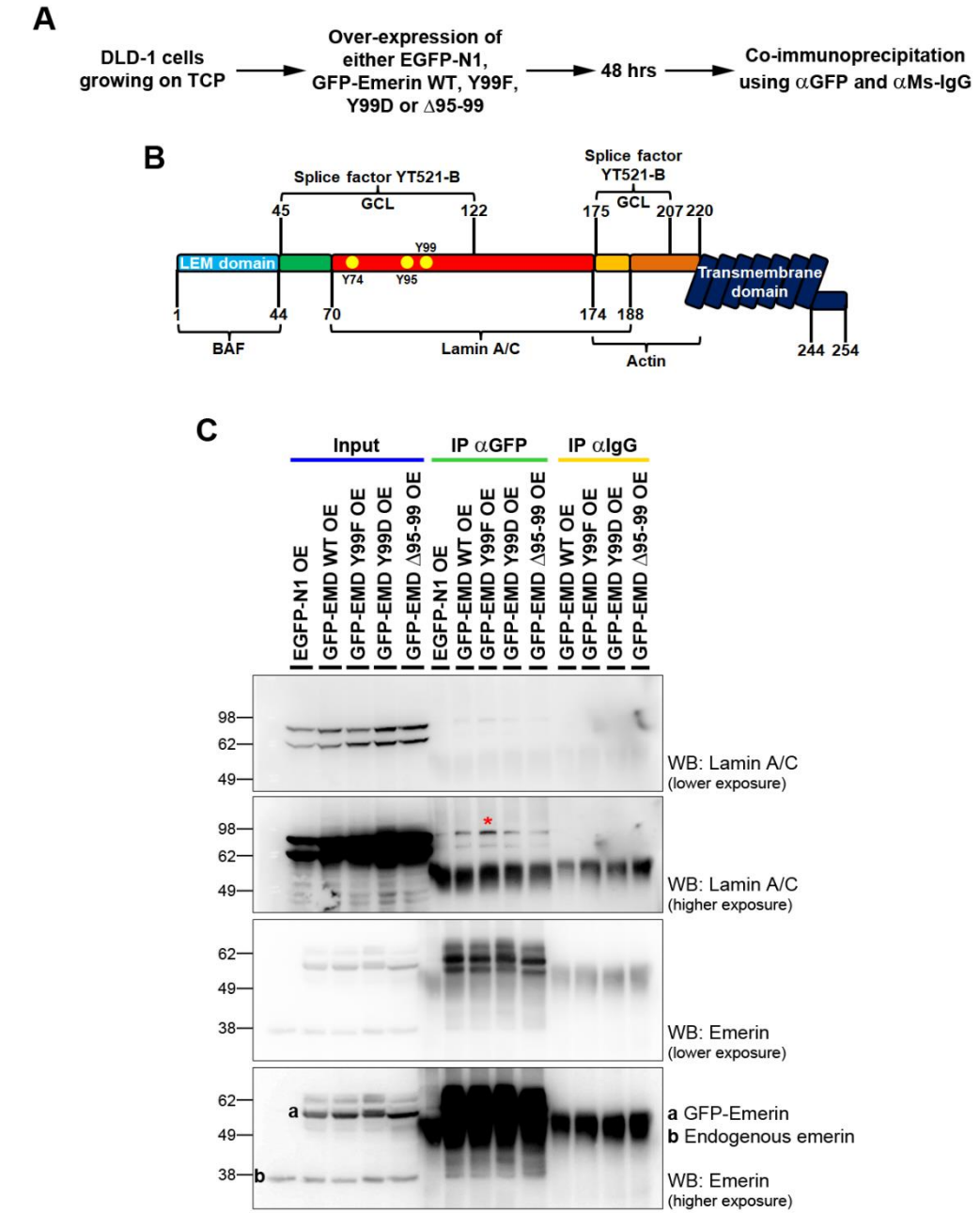

Figure 4.15 Emerin Y99F shows greater interaction with Lamin A, than wild type Emerin. A) Experimental scheme. B) Graphical representation of domain organization and protein interactions of Emerin. C) Representative western blot showing co-immunoprecipitation of Lamin A/C with overexpressed GFP-Emerin WT, GFP-Emerin Y99F, GFP-Emerin Y99D and GFP-Emerin Δ95-99. Overexpression of Empty vector (EGFP-N1) was used as control. Pulldown was performed with Rabbit anti-GFP and Normal Rabbit IgG was used as control. Lamin A/C – lower exposure blot shows 5% Input; higher exposure blot shows interaction between Lamin A/C and different overexpressed emerin variants. Emerin blot shows a) GFP tagged emerin and b) endogenous emerin.

Figure 4.16

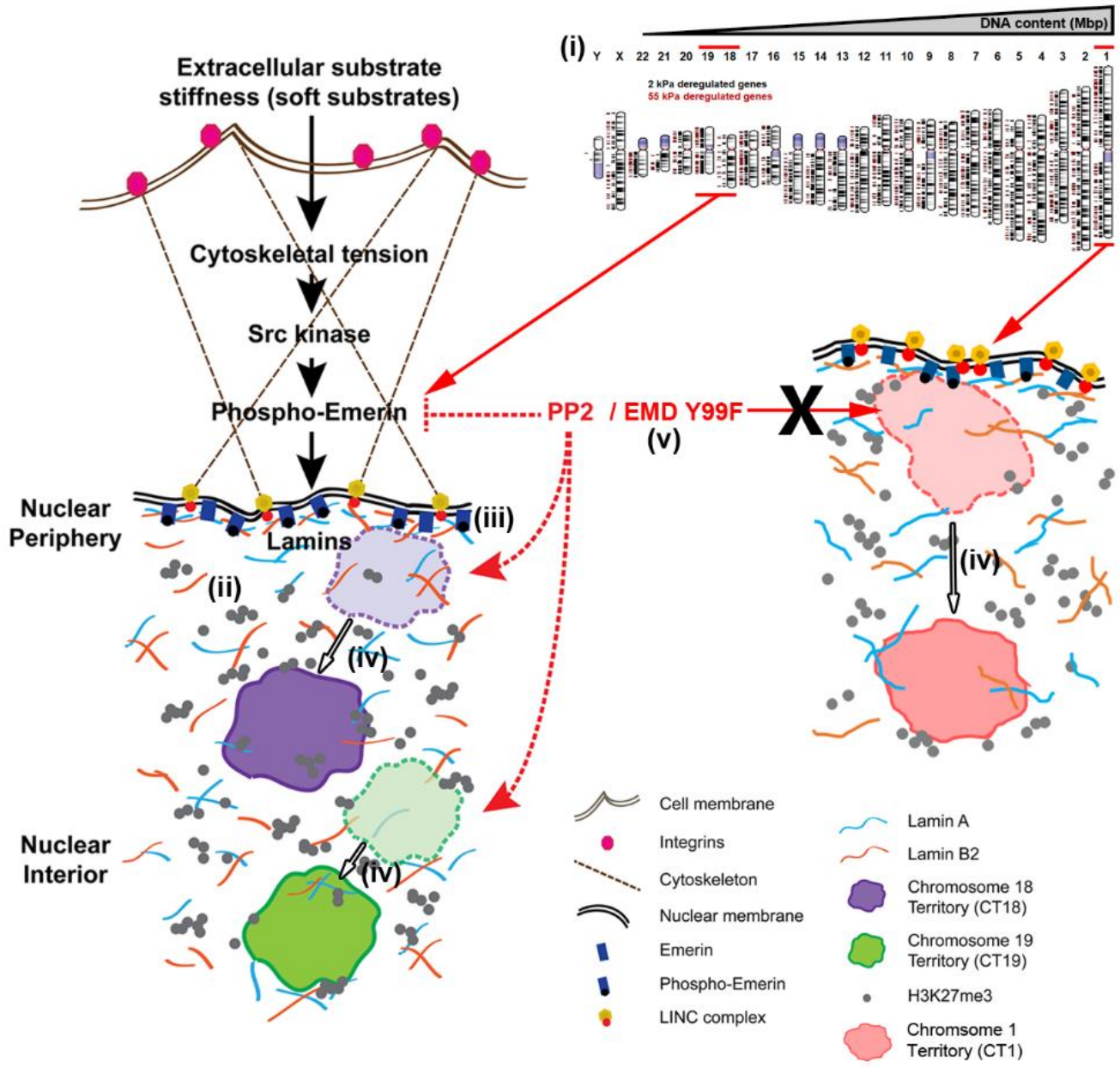

Figure 4.16 Emerin phosphorylation signals the mislocalization of chromosome territories in cells exposed to softer matrices, in a Lamin-dependent manner. Cells in contact with softer matrices show (i) altered transcriptional profiles (ii) nucleoplasmic accumulation of Lamin/LINC complex proteins and inactive histone marks (H3K27me3) (iii) activation of emerin phosphorylation at Tyr99 (iv) Chromosomes territories CT1, CT18 and 19 are collectively mislocalized toward the nuclear interior upon lowered matrix stiffness (v) Inhibition of emerin phosphorylation by Src kinase inhibitor (PP2) or overexpression of phospho-deficient emerin Y99F in cells on softer matrices retains Lamins at the nuclear envelope, CT18 and 19 at their conserved nuclear locations, but not CT1. Emerin phosphorylation is a key upstream mechanosensor of lowered matrix stiffness that selectively modulates chromosome territory positions in cells on softer matrices in a Lamin-dependent manner.

4.3 Discussion

Transcriptional deregulation in cells on softer matrices was accompanied by a repositioning of chromosome 1, 18 and 19 territories towards the nuclear interior (Chapter 3 – Fig 3.9 and 3.10). Here we observed that nuclear Lamins that regulate chromosome positioning, were mislocalized into the nuclear interior in response to lowered matrix stiffness (Fig 4.3). Notably, only full length Lamin B2 overexpression retained CT18 near the nuclear periphery in cells on softer matrices (Fig 4.5). Furthermore, the mislocalization of chromosome territories was dependent on the inner nuclear membrane protein emerin but was differentially sensitive to emerin phosphorylation at Tyr99 (Fig 4.14). This is consistent with an established role of emerin as a mechanosensor, as its Tyr74 and 95 residues are phosphorylated in response to increased nuclear strain (Guilluy et al., 2014). We identified an additional residue on emerin (Tyr99), phosphorylated in response to reduced cellular strain, which also alters lamin localization accompanied by the selective mislocalization of chromosome 18 and 19 but not chromosome 1 territories in the interphase nucleus.

4.3.1 Lamins as effectors of chromosome territory positions

We observed that the spatial position of chromosome 18 territory, closer to the nuclear periphery, was considerably more sensitive to altered matrix stiffness as compared to the gene rich CT19 toward the nuclear interior (Chapter 3 – Fig 3.13). Additionally, repositioning of gene poor CT18 (peripheral) and toward the nuclear interior is accompanied by the mislocalization of Lamins/LINC factors and the inactive histone mark H3K27me3 to the nuclear interior, otherwise associated with heterochromatin at the nuclear periphery (Chapter 3 – Fig 3.5; Fig 4.3). This suggests that lamin mediated heterochromatin association maintains CT18 and potentially

positions of other gene poor chromosome territories toward the nuclear periphery. We speculate that the untethering of gene poor CTs such as CT1 and CT18 from the nuclear periphery is an early event in response to altered force perception preferentially at the nuclear envelope, by virtue of their relative proximity to the nuclear envelope and enrichment of LADs (Bolzer et al., 2005; Guelen et al., 2008). A distinct compartment of repressed chromatin – perinucleolar heterochromatin associated with the nucleolus, is localized relatively closer to the nuclear interior and certain gene loci and LADs stochastically associate with the nucleolus post mitosis (Kind et al., 2013; Politz et al., 2013; Thomson et al., 2004). With recent studies demonstrating a lamin (both A- and B-type) sub-population at the nucleolus, it is conceivable that the gene poor chromosomes enriched in heterochromatin may employ the nucleolus as a landmark upon their mislocalization into the nuclear interior in cells on softer matrices (Kind and van Steensel, 2014; Pochukalina et al., 2016; Sen Gupta and Sengupta, 2017).

Despite the comparable extent of emerin phosphorylation on both the softer matrices (Fig 4.1G-H), CT18 positions were significantly different between the two softer matrices (Chapter 3 – Fig 3.13). It is likely that the differences in the levels of nuclear envelope proteins owing to altered substrate stiffness, in turn function as effectors of mechanosensitive responses in the nucleus. Lamin A/C, B1 and B2 are interdependent for their assembly into higher order structures at the nuclear lamina (Guo et al., 2014; Shimi et al., 2015). In addition, localization and organization of LINC complex proteins (SUN1, SUN2, Nesprin-1α, Nesprin-2) is also dependent on Lamin A, suggesting a cross talk between lamins and nuclear envelope factors that determine the functional organization of the nuclear envelope (Liang et al., 2011; Libotte et al., 2005; Mislow et al., 2002; Taranum et al., 2012; Yang et al., 2013). We surmise that the decrease in the levels of Lamin/LINC

proteins destabilizes the nuclear envelope, further contributing to their mislocalization into the nuclear interior (Fig 4.2 and 4.3). Lamin A phosphorylation at Ser22 is an important determinant of its nucleoplasmic localization and also accumulates under conditions of low nuclear stress and reduced extracellular matrix stiffness (Kochin et al., 2014; Buxboim et al., 2014; Swift et al., 2013). Since the accumulating phosphorylations in Lamin A could loosen the entire polymer, causing its disassembly and therefore giving rise to a nucleoplasmic fraction that is easily accessible by antibodies (for immunostaining); it is important to characterize the nucleoplasmic mislocalization of nuclear envelope proteins (Lamins, Emerin and SUN proteins) using biochemical fractionation and proteomic analyses. Additionally, validation of nucleoplasmic accumulation of NE proteins on soft matrices using multiple antibodies that detect different epitopes and co-staining with a nuclear membrane marker is required to further support this hypothesis. Of note, B-type Lamins retain their farnesyl anchor after maturation (while Lamin A loses it) (Corrigan et al., 2005, Jung et al., 2013, Adam et al., 2013) and therefore the nucleoplasmic mislocalization of Lamin B1 and B2 could be coupled with a loss of farnesylation which can be tested experimentally.

Chromosome positioning on softer matrices is dependent on the levels of Lamin A and Lamin B2 (Fig 4.5). Although, Lamin A or B2 overexpression did not affect emerin phosphorylation (Fig 4.4E-F), chromosome 18 nevertheless remained proximal to the nuclear periphery upon overexpression of Lamin B2 in cells on softer matrices (Fig 4.5D). The chromatin binding domains of Lamin A and B2 are also likely to modulate protein-protein interactions with Lap2α, Histones, Emerin, Actin among others (Wilson and Foisner, 2010; Zastrow et al., 2004). This implies that lamin stoichiometry and interactions too may impinge on chromosome territory positions (Guo et

al., 2014). B-type Lamins interact with LADs in heterochromatin via LBR and HP1α, consistent with a key regulatory role of Lamin B1/B-type Lamins in the positioning of gene poor chromosome territories (Bank and Gruenbaum, 2011; Malhas et al., 2007; Ye et al., 1997). Lamin A/C, on the other hand, interacts with LADs at the nuclear periphery, and in the nuclear interior via its interaction with LAP2α (Gesson et al., 2016; Lund et al., 2015; Naetar and Foisner, 2009). The impact of GFP-Lamin A S22D specifically on CT19 indicates the preferential effect of nucleoplasmic fraction of Lamin A on gene rich chromatin (Fig 4.6F-G). CT18 is unaffected by the enhanced nucleoplasmic Lamin A potentially due to the presence of a strong tethering of gene poor chromatin maintained by B-type Lamins at the nuclear periphery. Thus, overexpression of Lamin A alters the spatial coordinates of chromosome territories, while Lamin B2 overexpression provides positional cues and positions the gene poor CT18 closer to the nuclear periphery (Fig 4.5D-E).

4.3.2 Regulation of CT1 positions on softer matrices

Chr. 1 was the most transcriptionally deregulated chromosome and showed an enrichment of maximum number of deregulated genes in cells on softer matrices (Chapter 3 – Fig 3.7). Interestingly, CT1 was also mislocalized towards the nuclear interior on the 2 kPa matrices (Chapter 3 – Fig 3.10). The overexpression of both Lamin A and Lamin B2 – either full length or lacking the chromatin binding region, was able to rescue CT1 towards the nuclear periphery to a comparable extent statistically (Fig 4.7). However, there were subtle differences observed that suggested a marginally more dominant role of full length Lamin B2 in retaining CT1 proximal to the nuclear envelope. It is important to note that although chromosomes 1 and 18 are present in similar nuclear locations (near the nuclear periphery), the modulation of their radial positioning

may be substantially different due to the divergent transcriptional profiles that the two chromosomes exhibit on softer matrices (Chapter 3 – Fig 3.9). Thus, it is possible that Chr. 1 is positioned in cells on softer matrices via the following hierarchical regulation wherein transcriptional profile > lamin levels and localization > chromatin binding ability of lamins. Furthermore, the observation that emerin phosphorylation at Tyr99 is required for the selective mislocalization of CT18 and 19 toward the nuclear interior, but not CT1 (Fig 4.14), underscores the differential sensitivity of chromosome territories to specific mechanical stimuli.

4.3.3 Emerin as an upstream signal that modulates chromosome territory positions

Lamin A is phosphorylated at Ser22 and shows increased nucleoplasmic localization in response to reduced extracellular matrix stiffness (Buxboim et al., 2014; Kochin et al., 2014; Swift et al., 2013). Our data suggests that in addition to Lamin A, levels of Lamin B1, B2, SUN1 and SUN2 were reduced and mislocalized into the nuclear interior in cells on softer matrices, underscoring that the nuclear envelope is highly perceptive and sensitive to external force transitions (Fig 4.2 and 4.3). We speculate that emerin phosphorylation functions as an upstream regulator of lamin localization (Fig 4.12E-G). Furthermore, the Tyr99 residue of emerin phosphorylated on softer matrices reported here, maps to the interaction domain between emerin and Lamin A/C (Berk et al., 2013; Clements et al., 2000; Sakaki et al., 2001). Through the co-immunoprecipitation experiments we observed that emerin which cannot be phosphorylated at Tyr99 i.e. emerin Y99F, shows higher interaction with Lamin A (Fig 4.15C). It is therefore possible, that substrate stiffness dependent phosphorylation of emerin at Tyr99 by Src kinase lowers the emerin-Lamin A/C interaction, potentially resulting in the mislocalization of Lamin A into the nucleoplasm and a sub-population of emerin outside the nucleus (Fairley et al., 2002) (Fig 4.16). However, considering

the experimental limitations encountered while solubilizing Lamins and their interactors like Emerin, it is important to validate interaction studies under different biochemical sub-fractionation methodologies (Berk and Wilson, 2016). Additionally, the spatiotemporal regulation of emerin phosphorylation, lamin/LINC localization and their role in modulating chromosome organization and transcription remains largely unclear. Furthermore, the effect of Lamin/LINC conformation, polymerization, membrane association and posttranslational modifications in transducing mechanical signals into the nucleus and chromatin that elicit context specific gene expression signatures, will prove to be pivotal to unravel the mechanisms that regulate mechanosignalling and transcription (Buxboim et al., 2014; Osmanagic-Myers et al., 2015; Swift et al., 2013).

Chapter 5: Role of nuclear lamins in regulating heat shock signaling

Data Acknowledgement:

Contribution to Fig 5.1C, 5.2B-E, 5.3B-D, 5.4D-E, 5.7D, 5.8B-E, 5.9B-F –

Muhunden Jayakrishnan

Results from this chapter are part of the following manuscript:

Roopali Pradhan, Muhunden Jayakrishnan, Kundan Sengupta; **Lamin A/C regulates heat shock induced expression of Hsp70 gene locus by assisting its movement away from the nuclear periphery** (Under preparation)

5.1 Introduction

It is essential for cells to maintain genome integrity in order to counter external stress. Cells have diverse mechanisms for their survival even under conditions of temperature fluctuations (Pauli et al., 1992; Tanguay, 1983). The Heat Shock Response pathway is one such mechanism, where heat shock proteins (Hsp70, Hsp90, small heat shock proteins) are synthesized in response to elevated temperature (~5°C above ambient temperature) (Richter et al., 2010; Velichko et al., 2013). These function as molecular chaperones that bind to DNA and proteins in the cell to protect them from single stranded breaks and misfolding respectively (Morimoto, 1998; Richter et al., 2010). Heat shock response in mammalian cells follows a stepwise cascade. Upon heat shock, the transcription factor - Heat Shock Factor 1 (HSF1) is unbound from interactors such as Hsp90, Hsp70 (expressed at low basal levels), undergoes autophosphorylation, translocates into the nucleus and binds to the 5' promoter regions of heat shock genes (Baler et al., 1993; Demirovic et al., 2014; Jolly et al., 1997; Sarge et al., 1993).

Five major families of heat shock proteins are known to be induced under stress conditions and these include HSPA (Hsp70), HSPB (small HSP family), HSPC (Hsp90), HSPD (Hsp60) and HSPH (large HSP family) (Daugaard et al., 2007; Stetler et al., 2010). While mechanisms of HSP activation are under investigation, the transcriptional regulation of Hsp70 gene locus is relatively well-studied. The binding of HSF1 to the promoters of Hsp70 gene locus induces an actin mediated directional movement of the locus towards the nuclear speckles which are rich in transcription factors (Jolly et al., 1999; Khanna et al., 2014). Upon contact with nuclear speckles, transcription of Hsp70 gene locus is enhanced and Hsp70 family proteins formed as a result further function as a molecular chaperones (Daugaard et al., 2007; Hu et al., 2010; Khanna et al., 2014). Post

attenuation of heat shock, HSF1-Hsp70 dimers are reformed, inactivating HSF1 and thereby completing the negative feedback loop (Demirovic et al., 2014; Morimoto, 1998; Sarge et al., 1993). In parallel during the heat shock response, active translocation of Hsp70 into the nucleus is mediated by Hikeshi, a nuclear import carrier (Imamoto and Kose, 2012). The specific function of Hsp70 in the nucleus is unclear, however it is implicated in regulating ribosomal DNA transcription during heat shock and in maintaining cell viability during post-heat shock recovery stage, apart from its activity as a molecular chaperone (Kose and Imamoto, 2014; Kose et al., 2012; Yanoma et al., 2017).

The response of the nucleus to heat shock is not completely understood. Nuclear lamins (Lamin A/C, B1 and B2) maintain structural and functional integrity of the nucleus in partnership with their various interactors (Dechat et al., 2010; Prokocimer et al., 2009; Shimi et al., 2008; Wilson and Foisner, 2010; Zastrow et al., 2004). The role of lamins in heat shock response has been of long standing interest in the field. In Drosophila Schneider 2 cells, heat stress promotes conversion of lamin Dm2 into lamin Dm1 by dephosphorylation (Smith and Fisher, 1984; Smith et al., 1987). Additionally, exposure of Ehrlich Ascites tumour cells to heat shock dephosphorylates Lamin A and C, further affecting the structural stability of the nucleoskeletal network (Krachmarov and Traub, 1993). Studies in mammalian cell lines have reported that Lamin B is a heat shock responsive protein and its expression is upregulated at 45.5ºC in U-1 melanoma and HeLa cells (Dynlacht et al., 1999; Falloon and Dynlacht, 2002; Zhu et al., 1999). Interestingly, small heat shock proteins (sHsps) like αB-crystallin and Hsp25 co-localize with Lamin A/C in the nucleoplasm upon heat shock in C2C12 myoblast cells (Willsie and Clegg, 2002). iTRAQ analyses of mouse pituitary gland tissue shows that heat stress induces increased expression of intermediate

filament proteins – Prelamin A/C, Lamin B1, Vimentin and Keratin (Memon et al., 2016). Taken together, these results suggest a regulatory crosstalk between the heat shock response and nuclear lamins.

Nuclear proteins such as BAF, LAP2α (interactors of lamins) and nucleolar protein - NPM1 undergo changes in localization and dynamics during heat stress in different types of cells (Bar et al., 2014; Snyers and Schöfer, 2008; Vanderwaal et al., 2009; Willsie and Clegg, 2002). However, the underlying mechanisms through which the heat shock response is regulated and fine-tuned by proteins that maintain nuclear structure and architecture remain elusive. Such a crosstalk could potentially exist at multiple levels. Changes in expression and localization of proteins that maintain nuclear architecture could modulate the perception of heat shock by the nucleus depending on the time-temperature regime. An interesting example is the hypersensitivity to heat stress observed in fibroblasts derived from HGPS patient with the G608G mutation in Lamin A/C (Paradisi et al., 2005). Furthermore, the downstream signaling into the nucleus that elicits transcriptional responses during the course of heat shock could also be under the direct or indirect regulation of nuclear proteins. Given the regulation of epigenetic controllers such as the Polycomb repressive complex by Lamin A/C both at the nuclear interior and periphery, and the global transcriptional changes that are elicited during heat stress, lamins could potentially mediate transcriptional fine-tuning of the genome during heat shock (Cesarini et al., 2015; Kantidze et al., 2015; Marullo et al., 2016).

Here we studied lamin mediated regulation of the heat shock response. We show that exposing cells to heat shock (42ºC) upregulates Lamin B1 at the nuclear periphery and Lamin A at both the

nuclear interior and periphery. Furthermore, Lamin A/C, B1 and B2 are required for heat shock mediated induction of the heat shock gene *HSPA1A*, potentially at two different stages of transcriptional regulation. Remarkably, depletion of Lamin A/C, but not the B-type lamins, abrogates the movement of Hsp70 gene locus towards the nuclear interior as well as the nuclear translocation of Hsp70 protein from the cytoplasm, upon thermal stress. Taken together, our results highlight a novel role of lamins in regulating the heat shock response.

5.2 Results

5.2.1 Induction of the heat shock response in DLD-1 cells

To study heat shock signaling in DLD-1 cells, we examined two aspects of the heat shock response – i) induction of the heat shock gene *HSPA1A* and ii) nuclear translocation of the heat shock protein Hsp70. We exposed DLD-1 cells to heat shock at 42ºC for increasing durations - 5, 10, 30 and 60 mins (similar time regimen at 37ºC served as controls), following which we estimated the transcript levels of *HSPA1A* using qRT-PCR (Fig 5.1A). The *HSPA1A* gene is upregulated within ~5-10 mins of heat shock at 42ºC and is maximally expressed by ~60 mins of heat shock (Fig 5.1A). We next performed immunostaining of Hsp70 in cells subjected to heat shock at 42ºC for increasing durations (identical durations at 37ºC served as controls), followed by recovery at 37ºC for 1 hr, 2 hrs and 4 hrs (after 60 mins heat shock) (Fig 5.1B-C). Quantification of nuclei showing Hsp70 translocation revealed that Hsp70 is imported into ~80% of the nuclei within ~15 mins of heat shock (Fig 5.1D). This distribution largely remains a constant until ~60 mins of heat shock, while ~35-40% nuclei continued to retain Hsp70 in the nucleus after 2 hrs of recovery at 37ºC (Fig 5.1D). Control cells at 37ºC did not show any nuclear/nucleolar translocation of Hsp70.

5.2.2 Lamin A and B1 expression is upregulated during heat shock response

Both A and B-type lamins regulate nuclear structure, function and plasticity (Dechat et al., 2010; Prokocimer et al., 2009; Shimi et al., 2008; Wilson and Foisner, 2010; Zastrow et al., 2004). Notwithstanding the role of Lamin B as a heat shock responsive protein (Dynlacht et al., 1999), relatively little is known about the role and response of nuclear lamins in heat shock response. Small heat shock proteins (sHsps) such as αB-crystallin and Hsp25 co-localize with Lamin A/C

Figure 5.1

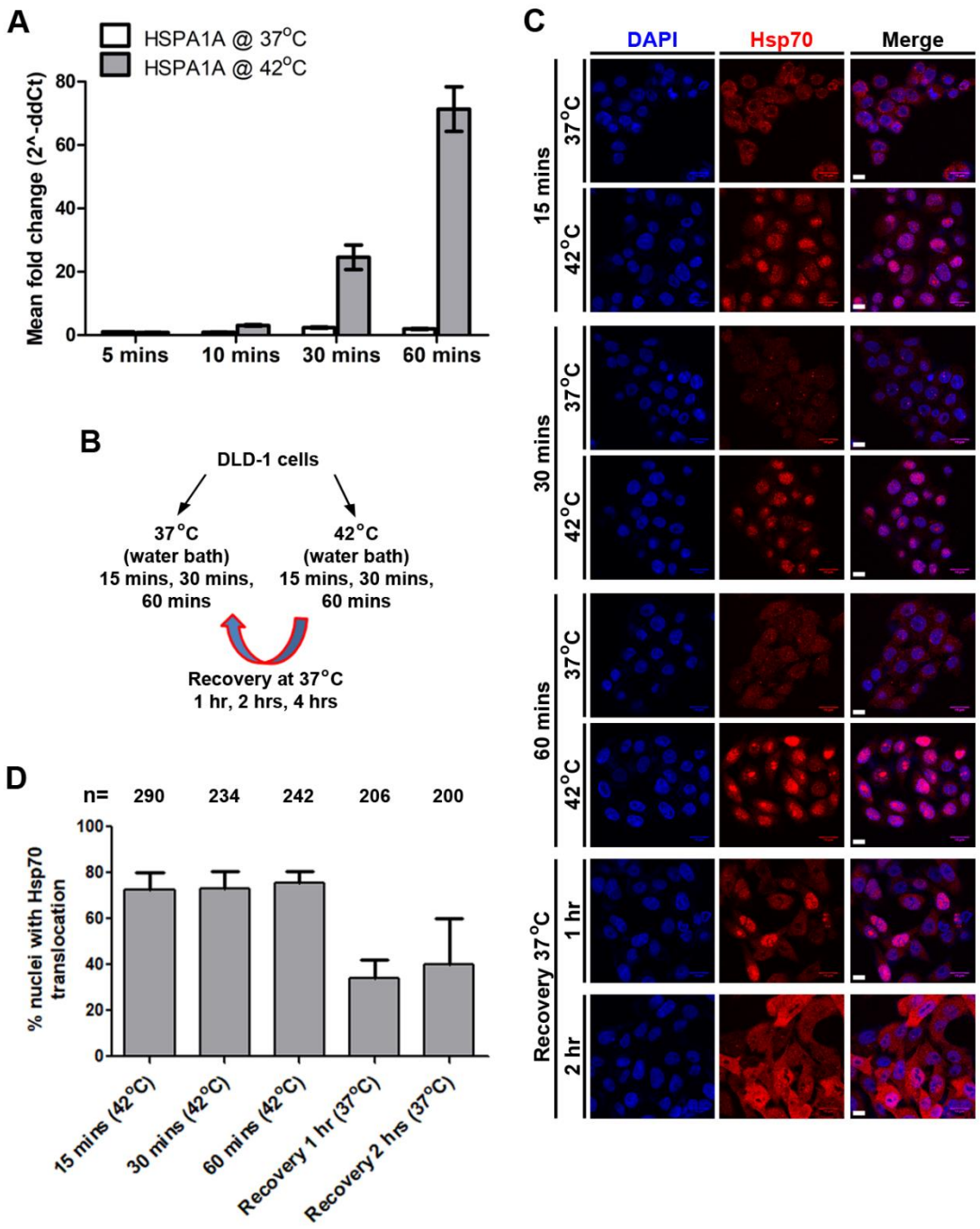

Figure 5.1 Induction of heat shock response in DLD-1 cells. A) Measurement of *HSPA1A* expression using qRT-PCR in DLD-1 cells upon heat shock at 42ºC for 5, 10, 30 and 60 mins. Expression was normalized to internal control – GAPDH and then to 37ºC/5 mins. *(Combined data from N=3 independent biological replicates, Error bar: SEM)*. B) Scheme for heat shock and recovery experiment. C) Representative mid-optical section images *(N=2)* from confocal z-stacks showing immunostaining of Hsp70 in DLD-1 cells exposed to heat shock at 42ºC for 15, 30, 60 mins (same time points at 37ºC were used as controls) and cells under recovery for 1, 2 hrs at 37ºC post 60 mins heat shock. D) Quantification of % nuclei showing Hsp70 nuclear or nucleolar translocation after heat shock in cells exposed to heat shock at 42ºC for 15, 30, 60 mins and cells under recovery for 1, 2 hrs at 37ºC post 60 mins heat shock. Controls at 37ºC show no nuclear translocation of Hsp70. *(Combined data from N=2 independent biological replicates. Error bar: SEM. n: number of nuclei)*. **Scale bar ~10 µm.**

Figure 5.2

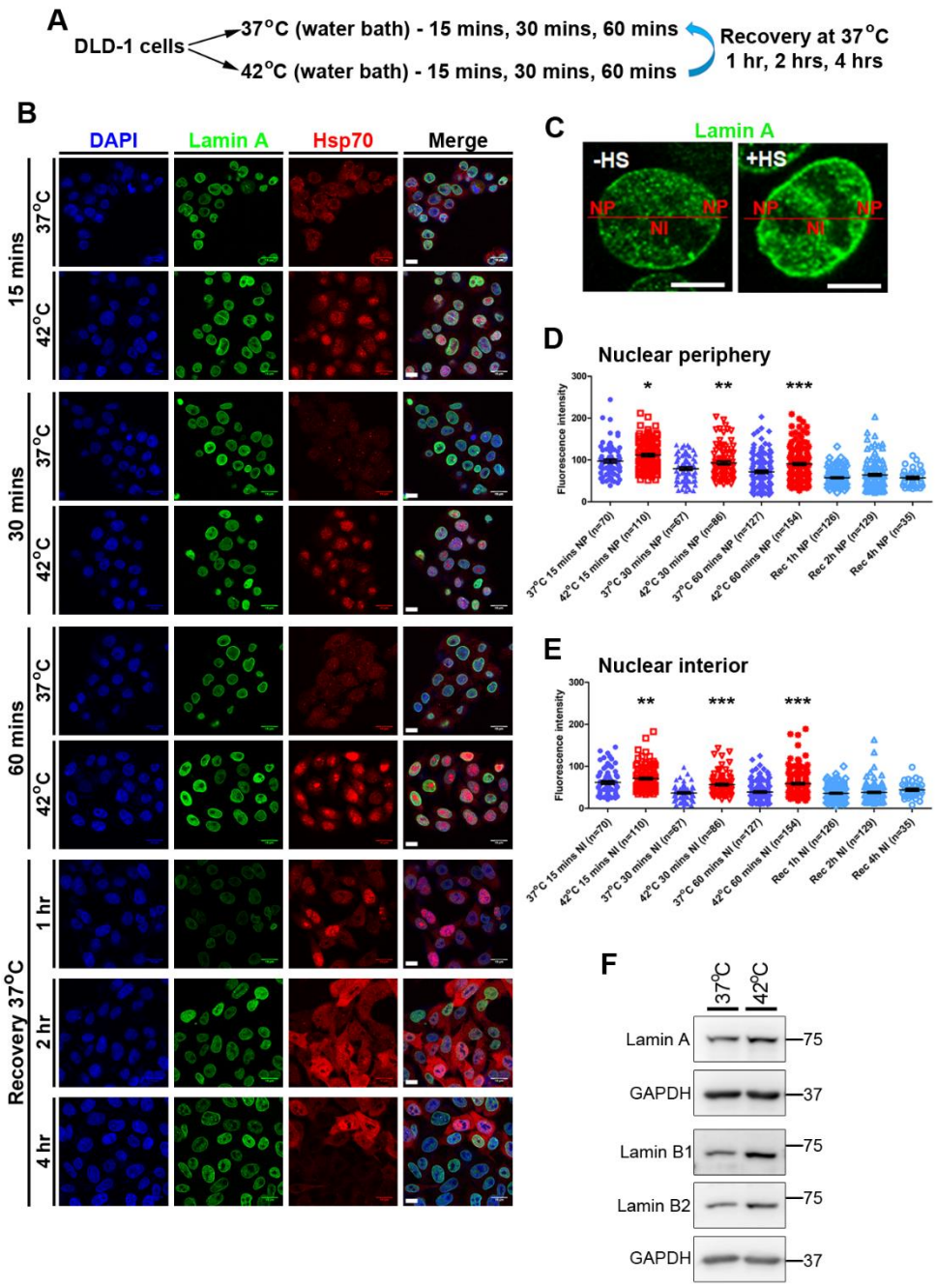

Figure 5.2 Lamin A expression is upregulated in the nuclear interior and periphery during heat shock response in DLD-1 cells. A) Experimental scheme. B) Representative mid-optical section images *(N=2)* from confocal z-stacks showing immunostaining of Lamin A and Hsp70 in DLD-1 cells exposed to heat shock at 42ºC for 15, 30, 60 mins (same time points at 37ºC were used as controls) and cells under recovery for 1, 2 and 4 hrs at 37ºC post 60 mins heat shock (Same experiment as Fig 5.1C). C) Schematic depicting approach for line scan analysis of a single representative nucleus. D) Dot scatter plot representing normalized fluorescence intensities (from line scan analysis of each individual nucleus) for Lamin A at the nuclear periphery in DLD-1 cells exposed to heat shock, control cells at 37ºC and cells under recovery. *(Combined data from N=2 independent biological replicates. Black horizontal bar: Mean ±SEM. n: number of nuclei).* * p<0.05, ** p<0.001, *** p<0.001 (Mann-Whitney test). E) Dot scatter plot representing normalized fluorescence intensities (from line scan analysis of each individual nucleus) for Lamin A at the nuclear interior in DLD-1 cells exposed to heat shock, control cells at 37ºC and cells under recovery. *(Combined data from N=2 independent biological replicates. Black horizontal bar: Mean ±SEM. n: number of nuclei).* ** p<0.01, *** p<0.001 (Mann-Whitney test). F) Representative western blots showing the expression levels of Lamin A, B1 and B2 in DLD-1 cells after heat shock at 42ºC for 60 mins. GAPDH was used as loading control *(N=2)*. **Scale bar ~10 µm.**

upon heat shock in C2C12 myoblast cells (Willsie and Clegg, 2002), suggesting a possible role of lamins during heat shock response. To study the role and regulation of nuclear lamins during heat shock, DLD-1 cells were subjected to heat shock at 42ºC for increasing time durations - 15, 30 and 60 mins (controls were for similar durations at 37ºC), followed by recovery at 37ºC for 1 hr, 2 hrs and 4 hrs (post 60 mins heat shock) and immunostaining was performed for Lamin A and Hsp70 (Fig 5.2A-B). Interestingly, Lamin A showed a significant increase both at the nuclear periphery and in the nucleoplasm upon heat shock by 15 mins. The increase in lamin A levels was sustained until ~60 mins of heat shock (Fig 5.2C-E, F). Lamin A intensity decreased to basal levels upon recovery (Fig 5.2D-E).

We next examined expression and localization of B-type lamins – Lamin B1 and B2, upon heat shock. DLD-1 cells subjected to 42ºC for 15 and 60 mins, and to 37ºC for recovery (1 hr and 2 hrs) were immunostained for Lamin B1 and B2 (Fig 5.3A-B). Quantification of fluorescence intensities showed that Lamin B1 and B2 were nearly absent in the nucleoplasm, in contrast to Lamin A. Lamin B1 levels at the nuclear periphery increased significantly at ~15 mins of heat shock and further by ~2.4 fold after 60 mins at 42ºC (Fig 5.3C, 5.2F). Lamin B1 fluorescence intensity fluctuated around basal levels during the recovery (Fig 5.3C). Lamin B2 on the other hand, showed minor changes in expression upon heat shock (Fig 5.3D, 5.2F). Additionally, examination of the transcript levels of lamins using qRT-PCR showed that Lamin B1 (~2.5 fold) and Lamin A (~1.5 fold) were significantly upregulated by ~10 mins at 42ºC, while Lamin B2 transcripts remained relatively unchanged until ~60 mins of heat shock (Fig 5.3E). Of note, no significant changes were observed in the nuclear area and circularity upon heat shock (Fig 5.3F-G). In summary, these results reiterate Lamin B1 as a heat shock responsive protein and

Figure 5.3

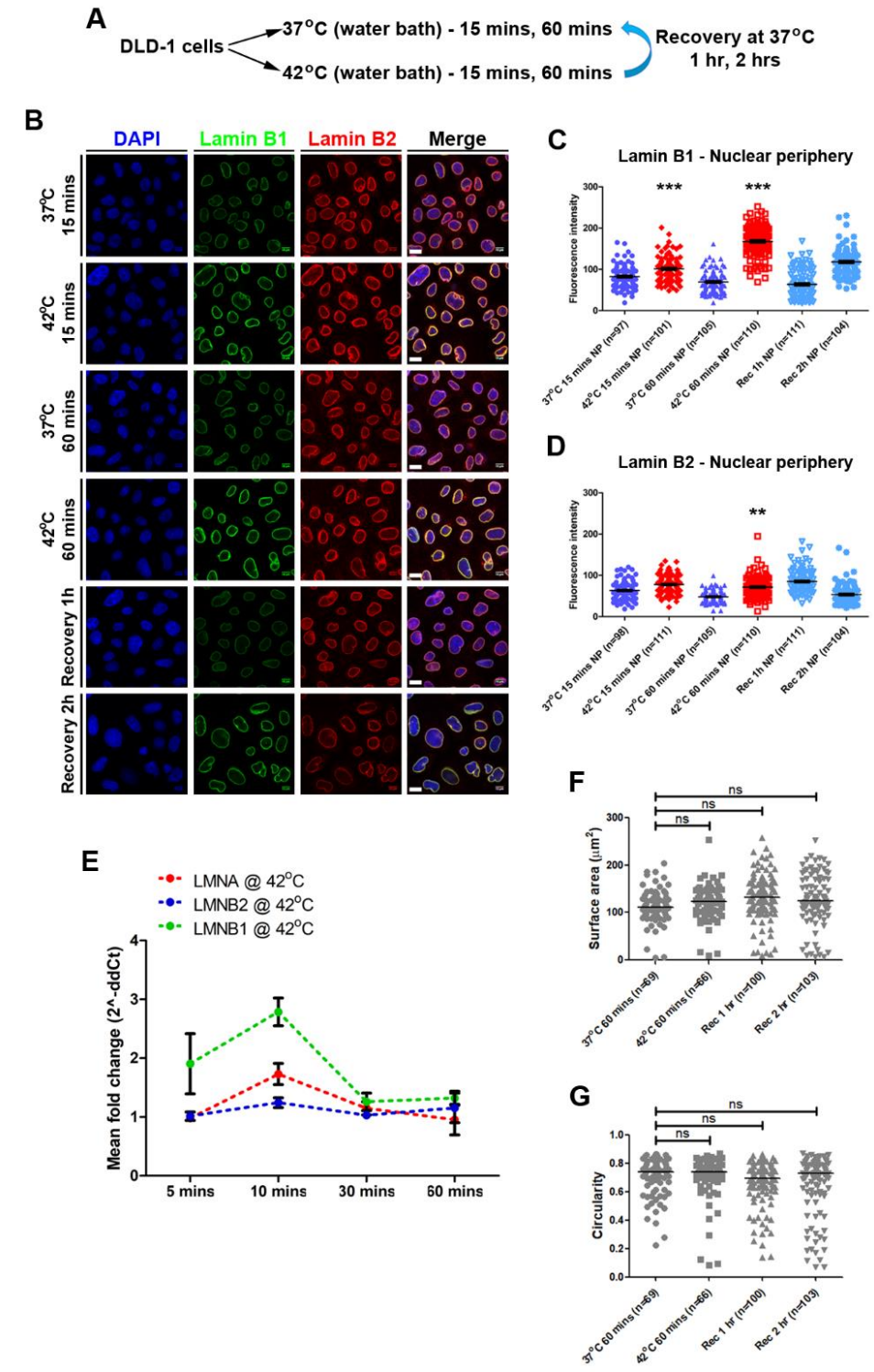

Figure 5.3 Lamin B1 expression is upregulated during heat shock response in DLD-1 cells. A) Experimental scheme. B) Representative mid-optical section images *(N=2)* from confocal z-stacks showing immunostaining of Lamin B1 and B**2** in DLD-1 cells exposed to heat shock at 42ºC for 15, 60 mins (same time points at 37ºC were used as controls) and cells under recovery for 1 and 2 hrs at 37ºC post 60 mins heat shock. C) Dot scatter plot representing normalized fluorescence intensities (from line scan analysis of each individual nucleus) for Lamin B1 at the nuclear periphery in DLD-1 cells exposed to heat shock, control cells at 37ºC and cells under recovery. *(Combined data from N=2 independent biological replicates. Black horizontal bar: Mean ±SEM. n: number of nuclei).* *** p<0.001 (Mann-Whitney test). **Scale bar ~10 µm.**

Figure 5.3 ***continued.*** D) Dot scatter plot representing normalized fluorescence intensities (from line scan analysis of each individual nucleus) for Lamin B2 at the nuclear interior in DLD-1 cells exposed to heat shock, control cells at 37ºC and cells under recovery. *(Combined data from N=2 independent biological replicates. Black horizontal bar: Mean ±SEM. n: number of nuclei)*. **p<0.01 (Mann-Whitney test). E) Measurement of *LMNA, LMNB1* and *LMNB2* expression using qRT-PCR in DLD-1 cells upon heat shock at 42ºC for 5, 10, 30 and 60 mins. Expression was normalized to internal control – GAPDH and then to respective 37ºC control. *(Combined data from N=2 independent biological replicates, Error bar: SEM)*. F-G) Dot scatter plot representing nuclear surface area (F) and nuclear circularity (G) in DLD-1 cells upon heat at 42ºC for 60 mins, control cells at 37ºC and cells under recovery. *(Combined data from N=2 independent biological replicates. Black horizontal bar: Median (M). n: number of nuclei, Mann-Whitney test)*. **Scale bar ~10 µm.**

additionally, demonstrate the heat shock mediated upregulation of Lamin A at the nuclear periphery as well as in the nucleoplasm, suggesting the involvement of lamins in heat shock response pathway.

5.2.3 Lamin A/C depletion abrogates nuclear translocation of Hsp70 upon heat shock

Heat shock mediated nuclear translocation of Hsp70 is an important step in the heat shock response pathway and is required for chaperoning activity, protection of DNA (nucleoplasmic and ribosomal) and maintenance of cell viability during heat shock (Kose and Imamoto, 2014; Kose et al., 2012; Yanoma et al., 2017). We asked if lamins are involved in the heat shock induced nuclear translocation of Hsp70. Independent siRNA-mediated knockdowns of Lamin A/C, B1 and B2 were performed in DLD-1 cells (non-targeting siRNA against LacZ was used as control). The siLacZ, siLamin A/C, B1 and B2 cells were subjected to heat shock at 42ºC for 60 mins (and at 37ºC as controls), followed by immunostaining for Hsp70 (Fig 5.4A-D). Quantification of nuclei with Hsp70 nuclear translocation revealed only ~10% of siLamin A/C nuclei with nuclear localization of Hsp70 upon heat shock, as compared to ~50-80% of siLacZ, siLamin B1 and B2 nuclei with nuclear/nucleolar Hsp70 (Fig 5.4E). Taken together, this suggests a potential role of Lamin A/C in regulating nuclear import of Hsp70 upon heat shock.

Figure 5.4

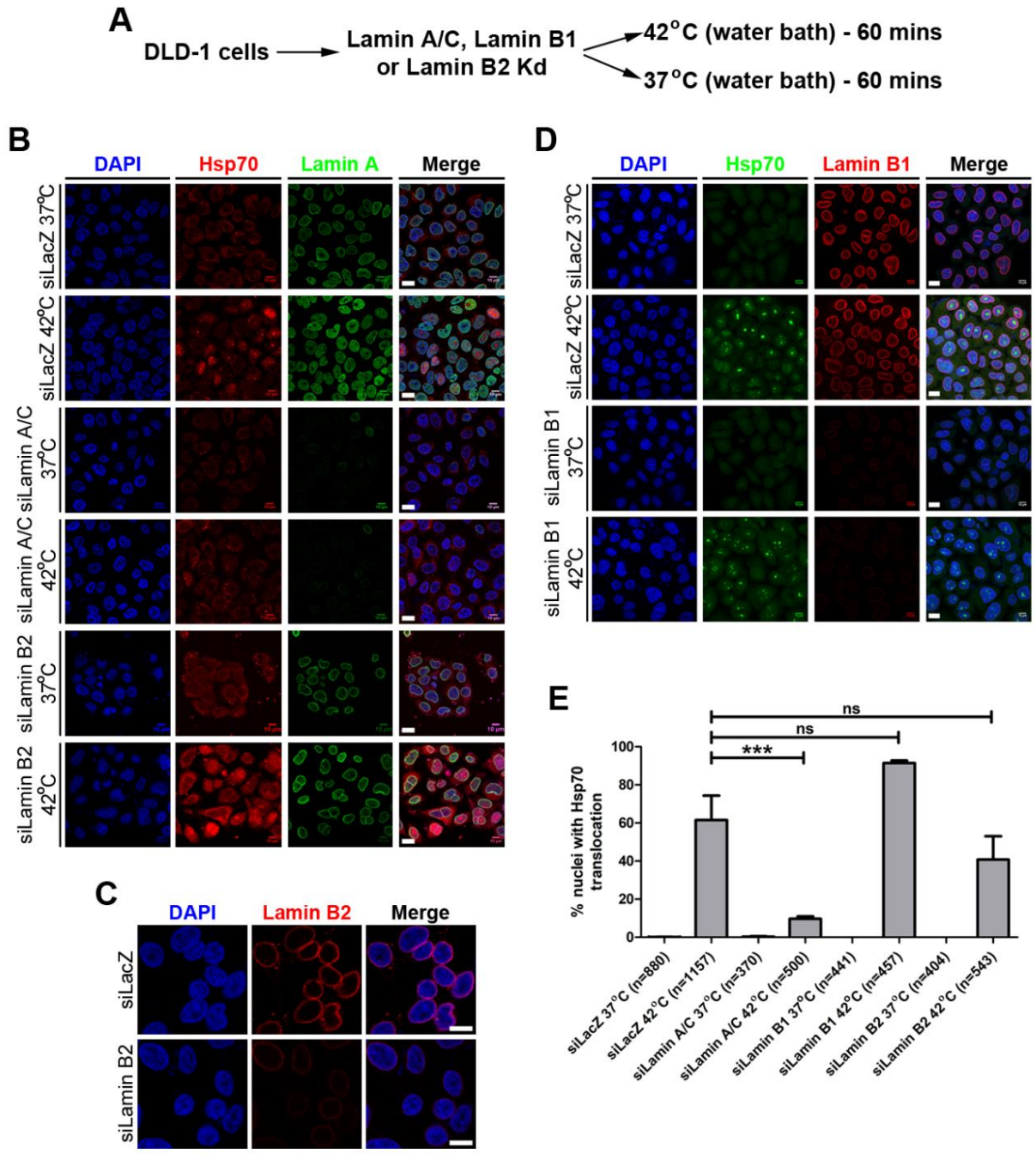

Figure 5.4 Lamin A/C depletion abrogates nuclear translocation of Hsp70 upon heat shock. A) Experimental scheme. B) Representative mid-optical section images *(N=3)* from confocal z-stacks showing immunostaining of Hsp70 and Lamin A in DLD-1 cells treated with either siLacZ, siLamin A/C or siLamin B2 and exposed to heat shock at 42ºC for 60 mins (same time point at 37ºC was used as control). C) Immunostaining to confirm Lamin B2 knockdown for Fig 5.4D. D) Representative mid-optical section images *(N=3)* from confocal z-stacks showing immunostaining of Hsp70 and Lamin B1 in DLD-1 cells treated with either siLacZ or siLamin B1 and exposed to heat shock at 42ºC for 60 mins (same time point at 37ºC was used as control). E) Quantification of % nuclei showing Hsp70 nuclear or nucleolar translocation after heat shock in siLacZ, siLamin A/C, siLamin B1 and siLamin B2 cells. Controls at 37ºC show no nuclear translocation of Hsp70. *(Combined data from N=3 independent biological replicates. Error bar: SEM. n: number of nuclei)*. *** p<0.0001 (Mann-Whitney test). **Scale bar ~10 µm.**

5.2.4 Lamin depletion specifically attenuates heat shock mediated upregulation of *HSPA1A*

To further dissect the role of nuclear lamins in modulating transcriptional responses upon heat shock induction, we examined expression levels of *HSPA1A* (part of the Hsp70 gene locus) upon depletion of nuclear lamins. DLD-1 cells with independent siRNA-mediated knockdowns of Lamin A/C, B1 and B2 (siLacZ was used as control) were subjected to heat shock for 60 mins, followed by qRT-PCR for *HSPA1A* (Fig 5.5A-B). In control cells (siLacZ treated), *HSPA1A* was upregulated to ~30 fold upon heat shock (Fig 5.5C). However, depletion of either Lamin A/C, B1 or B2 resulted in ~3-fold attenuation of the *HSPA1A* gene expression at 42ºC (Fig 5.5C).

Figure 5.5

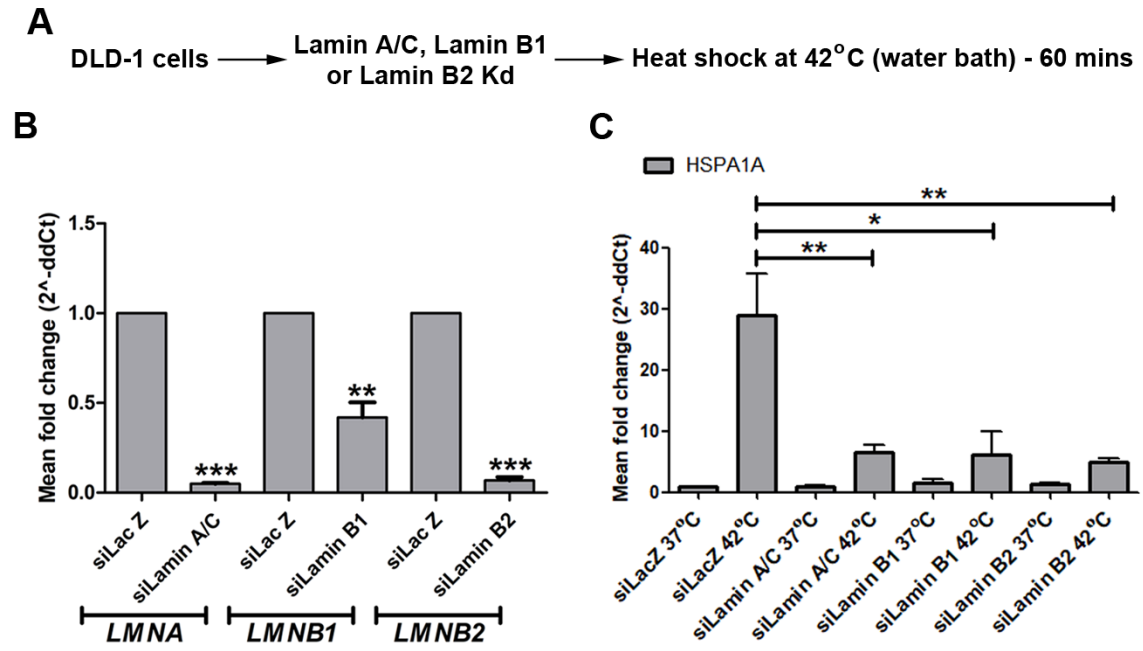

Figure 5.5 Lamin depletion specifically attenuates heat shock mediated upregulation of *HSPA1A*. A) Experimental scheme. B) Measurement of *LMNA*, *LMNB1* and *LMNB2* expression using qRT-PCR in DLD-1 cells treated with either siLacZ, siLamin A/C, siLamin B1 or siLamin B2. Expression was normalized to internal control – GAPDH and then to respective siLacZ control. *(Combined data from N=3 independent biological replicates, Error bar: SEM)*. ** p<0.001, *** p<0.0001 (Student's t-test). C) Measurement of *HSPA1A* expression using qRT-PCR in DLD-1 cells treated with either siLacZ, siLamin A/C, siLamin B1 or siLamin B2 upon heat shock at 42ºC for 60 mins (same time point at 37ºC was used as control). Expression was normalized to internal control – GAPDH and then to siLacZ 37ºC. *(Combined data from N=3 independent biological replicates. Error bar: SEM)*. * p<0.05, ** p<0.01 (Student's t-test).

5.2.5 Overexpression of siRNA resistant GFP-Lamin A rescues the *HSPA1A* expression and Hsp70 nuclear translocation following heat shock

To validate the impact of Lamin A/C depletion on heat shock mediated *HSPA1A* expression and Hsp70 translocation, we depleted Lamin A/C from DLD-1 cells using siRNA and further overexpressed a siResistant GFP-Lamin A (GFP-Lamin A*, Fig 5.6A). siLacZ treated cells overexpressing either EGFPN-1 (Empty vector) or GFP-Lamin A* and siLamin A/C treated cells overexpressing either EGFPN-1 (Empty vector) or GFP-Lamin A* showed nearly comparable extent of overexpression and were subjected to heat shock at 42ºC for 60 mins (Fig 5.6B). While the siLamin A/C+EGFPN-1 cells showed an attenuation of *HSPA1A* expression following heat shock (compared to siLacZ+EGFP-N1), the siLamin A/C+GFP-LA cells were able to significantly rescue the lowered expression of *HSPA1A* upon heat shock (compared to siLamin A/C+EGFP-N1) (Fig 5.6C). We next examined the extent of Hsp70 nuclear translocation in these cells (Fig 5.6D). While Lamin A overexpression on its own did not affect the extent of Hsp70 translocation in siLacZ treated cells, siLamin A/C+EGFP-N1 cells showed the expected abrogation of Hsp70 nuclear translocation (Fig 5.6E). Interestingly, overexpression of siResistant Lamin A in the background of Lamin A/C depletion significantly increased the % of nuclei showing Hsp70 translocation (Fig 5.6E). Taken together, these observations support the role of Lamin A in regulating *HSPA1A* expression and Hsp70 nuclear translocation in response to heat shock.

Figure 5.6

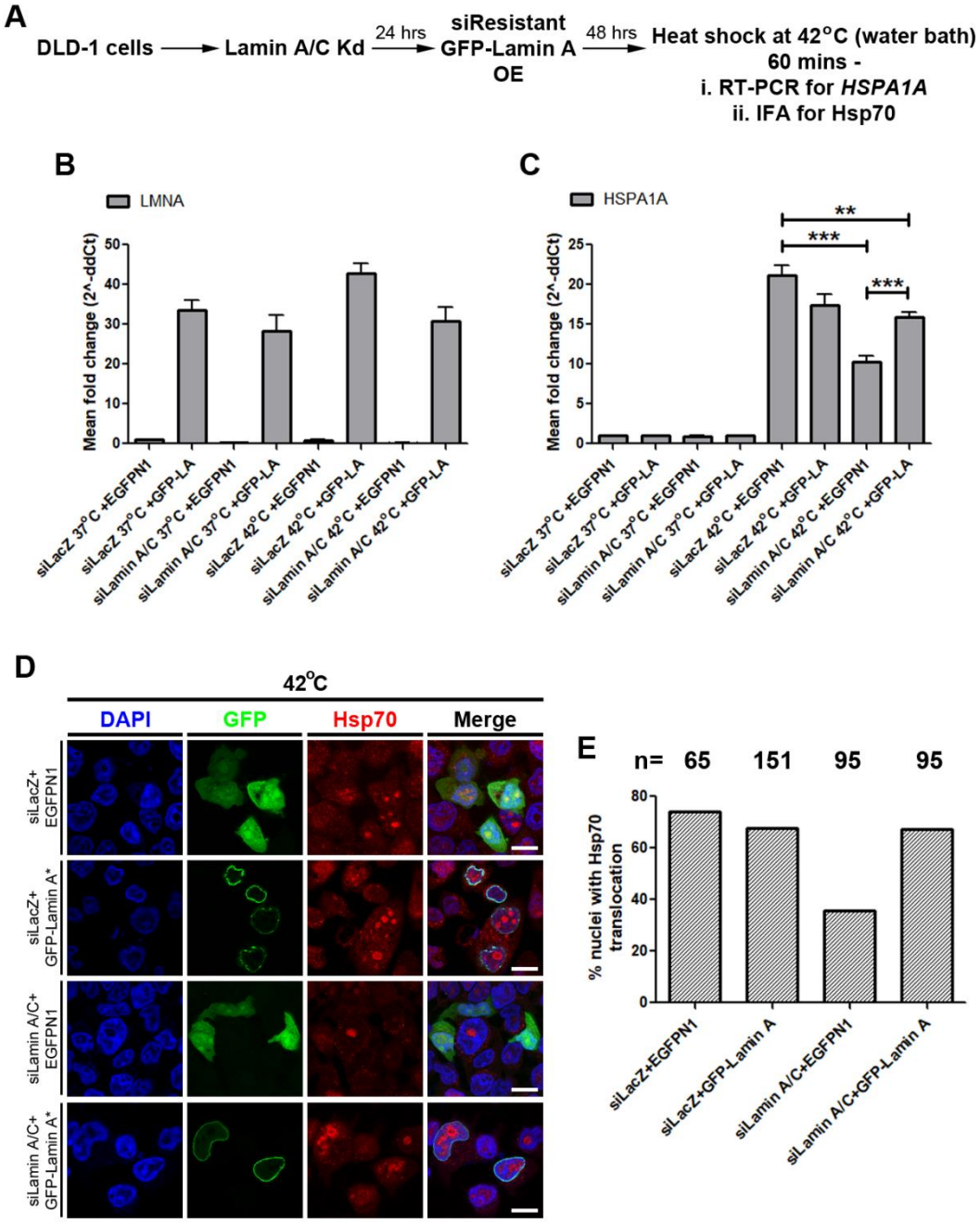

Figure 5.6 Overexpression of siRNA resistant GFP-Lamin A rescues the *HSPA1A* expression and Hsp70 nuclear translocation following heat shock. A) Experimental scheme. B) Measurement of *LMNA* expression using qRT-PCR in DLD-1 cells treated with either siLacZ or siLamin A/C and overexpressing EGFP-N1 or GFP-Lamin A*. Expression was normalized to internal control – GAPDH and then to siLacZ+EGFP-N1/37ºC control. *(Combined data from N=2 independent biological replicates, Error bar: SEM)*. C) Measurement of *HSPA1A* expression using qRT-PCR in DLD-1 cells treated with either siLacZ or siLamin A/C and overexpressing EGFP-N1 or GFP-Lamin A*. Expression was normalized to internal control – GAPDH and then to siLacZ+EGFP-N1/37ºC control. *(Combined data from N=2 independent biological replicates, Error bar: SEM)*. ** p<0.01, *** p<0.0001 (Student's t-test). D) Representative mid-optical section images *(N=1)* from confocal z-stacks showing immunostaining of Hsp70 in DLD-1 cells treated with either siLacZ or siLamin A/C, overexpressing EGFP-N1 or GFP-Lamin A* and exposed to heat shock at 42ºC for 60 mins. E) Quantification of % nuclei showing Hsp70 nuclear or nucleolar translocation after heat shock in siLacZ or siLamin A/C cells overexpressing EGFPN-1 or GFP-Lamin A*. **Scale bar ~10 µm.**

5.2.6 Lamin depletion does not affect the metal ion stress induced expression of *HSPA1A*

Induction of metal ion stress in cells using Cadmium Sulphate ($CdSO_4$) upregulates *HSPA1A* expression (Polla et al., 1995). $CdSO_4$ treatment serves as an independent stimulus for *HSPA1A* expression in the absence of heat shock (Hu et al., 2010). DLD-1 cells were initially treated with increasing concentrations of $CdSO_4$ solution (0, 5, 25 and 100 µM) for 2 hrs and analyzed for *HSPA1A* expression and Hsp70 nuclear translocation (Fig 5.7A). Both Hsp70 nuclear translocation and *HSPA1A* gene expression showed dose-dependent increase upon $CdSO_4$ treatment (Fig 5.7B-D). Using this concentration gradient, 100 µM $CdSO_4$ for 2 hrs was selected for further treatments. To study if the effect of Lamin A/C, B1 and B2 depletion on *HSPA1A* expression was heat shock pathway specific, we treated cells having siRNA-mediated knockdown of either of the lamins with 100 µM cadmium sulphate, followed by estimation of *HSPA1A* transcript levels using qRT-PCR (Fig 5.8A-D). We observed that lamin depletion did not affect $CdSO_4$ mediated upregulation of *HSPA1A* gene (Fig 5.8E). This contrasts with the requirement of lamins in heat shock-mediated increase of *HSPA1A* gene expression (Fig 5.5C), further suggesting that Lamins are specifically required for modulating the heat shock response.

5.2.7 Lamin A/C is required for heat shock mediated dynamics of the Hsp70 gene locus

The Hsp70 BAC transgene array contacts nuclear speckles upon heat shock - an event essential for its transcriptional upregulation (Khanna et al., 2014). Interestingly, movement towards nuclear speckles is required only for the heat shock mediated upregulation of Hsp70 transgene but not for metal ion stress induced expression (Hu et al., 2010). Since lamin depletion attenuated heat shock mediated upregulation of *HSPA1A* but not its metal ion stress induced expression (Fig 5.5C and 5.8E), we examined if lamin depletion impacts *HSPA1A* expression by affecting the heat shock

Figure 5.7

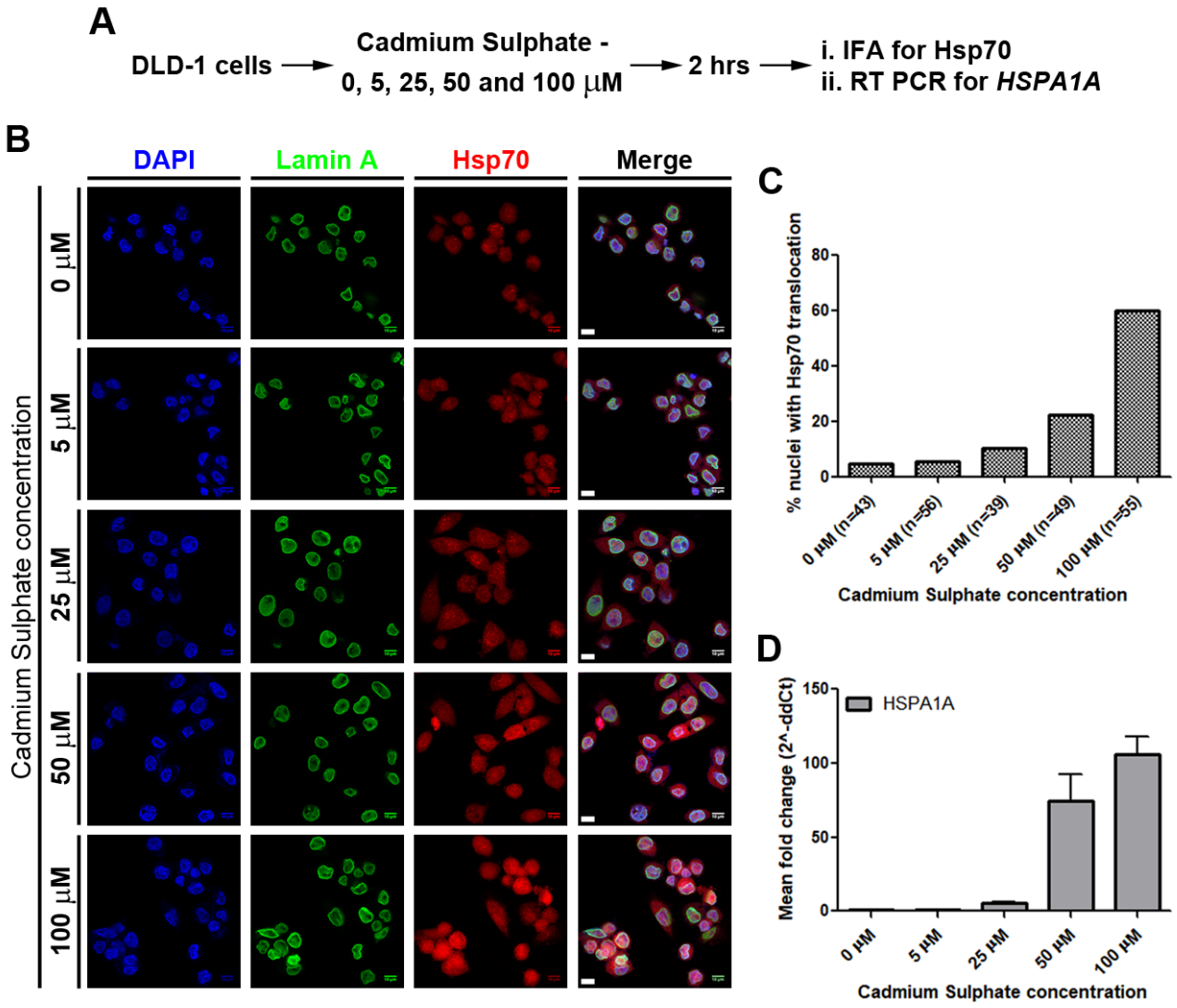

Figure 5.7 Cadmium sulphate induces expression of *HSPA1A*. A) Experimental scheme. B) Representative mid-optical section images from confocal z-stacks showing immunostaining of Lamin A and Hsp70 in DLD-1 cells treated with increasing concentration of cadmium sulphate (0 µM – 100 µM) for 2 hrs. Maximum volume of nuclease free water was used as control (0 µM). C) Quantification of % nuclei showing Hsp70 nuclear or nucleolar translocation after treatment with increasing concentration of cadmium sulphate (0 µM – 100 µM) for 2 hrs. NFW control (0 µM) showed no nuclear translocation of Hsp70. *(n: number of nuclei, Data from single experiment)*. D) Measurement of *HSPA1A* expression using qRT-PCR in DLD-1 cells after treatment with increasing concentration of cadmium sulphate (0 µM – 100 µM) for 2 hrs. Expression was normalized to internal control – GAPDH and then to 0 µM (NFW control). *(Data from single experiment, Error bar: SEM)*.

Figure 5.8

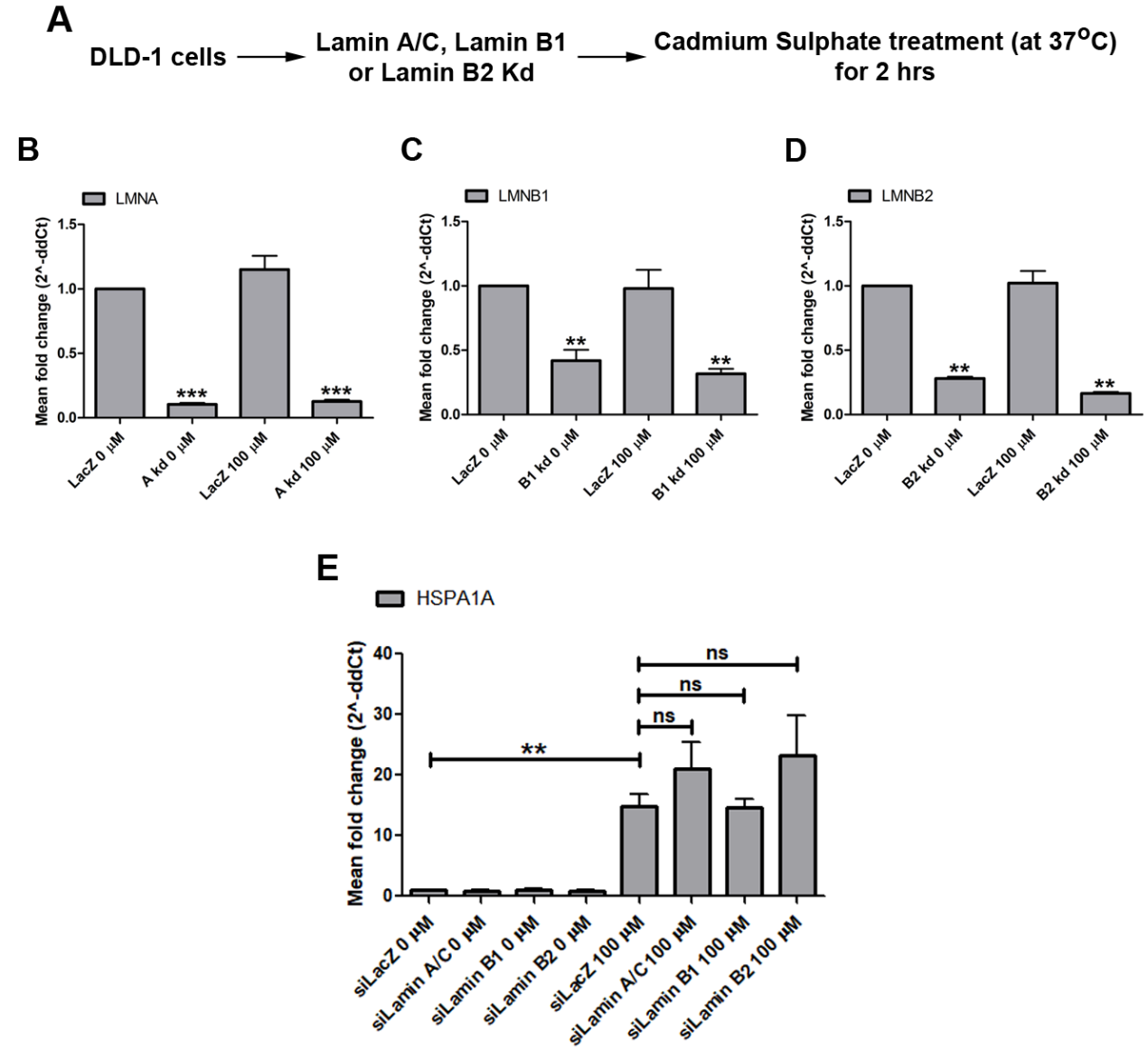

Figure 5.8 Lamin depletion does not affect the metal ion stress induced expression of *HSPA1A*. A) Experimental scheme. B-D) Measurement of *LMNA* (B), *LMNB1* (C) and *LMNB2* (D) expression using qRT-PCR in DLD-1 cells treated with either siLacZ, siLamin A/C, siLamin B1 or siLamin B2 and 100 µM cadmium sulphate for 2 hrs. Expression was normalized to internal control – GAPDH and then to siLacZ/0 µM. *(Combined data from N=3 independent biological replicates. Error bar: SEM).* ** p<0.001 *** p<0.0001 (Student's t-test). C) Measurement of *HSPA1A* expression using qRT-PCR in DLD-1 cells treated with either siLacZ, siLamin A/C, siLamin B1 or siLamin B2 upon 100 µM cadmium sulphate treatment at 37ºC for 120 mins (same volume of nuclease free water was added in control cells). Expression was normalized to internal control – GAPDH and then to siLacZ/0 µM. *(Combined data from N=3 independent biological replicates. Error bar: SEM).* ** p<0.001 (Student's t-test).

mediated movement of the Hsp70 locus. DLD-1 cells with independent siRNA-mediated knockdowns of Lamin A/C, B1 and B2 (non-targeting siRNA against LacZ was used as control) were subjected to either 42ºC or 37ºC for 60 mins, followed by immuno-3D FISH using one of the lamins as a marker of the nuclear lamina (Lamin B1 in Lamin A/C and B2 knockdown cells, Lamin A in Lamin B1 knockdown cells) and a BAC (Bacterial Artificial Chromosome) DNA probe for the *HSPA1A* gene locus (Fig 5.9A-E).

Quantification of the shortest distance of *HSPA1A* gene loci from the lamin staining in siLacZ, siLamin B1 and siLamin B2 treated cells showed a significant movement of the loci away from the nuclear periphery upon heat shock, potentially towards the nuclear speckles (Fig 5.9E – arrows, 5.9F). Interestingly, Lamin A/C knockdown abrogated the heat shock mediated movement of the gene loci towards the nuclear interior (Fig 5.9E – arrows, 5.9F). Taken together, these results indicate that Lamin A/C is involved in transcriptional upregulation of *HSPA1A* via facilitating the movement of Hsp70 gene locus towards the nuclear speckles, while the B-type lamins are not involved in this process.

5.2.8 Lamin A/C modulates Hsp70 gene locus movement potentially via Nuclear Myosin I

Nuclear myosin I (NM1) is an isoform of the *MYO1C* gene, localizes in the nucleus and is implicated in regulating long range movements of chromatin as well as chromosome territory movements (Chuang et al., 2006; Hofmann et al., 2006; Kulashreshtha et al., 2016; Pestic-Dragovich et al., 2000). NM1 directly interacts with emerin (Holaska and Wilson, 2007). However, the functional significance of this interaction is not well studied. It is speculated that the Lamin A-Emerin-NM1 complex in conjunction with nuclear actin regulates chromatin dynamics

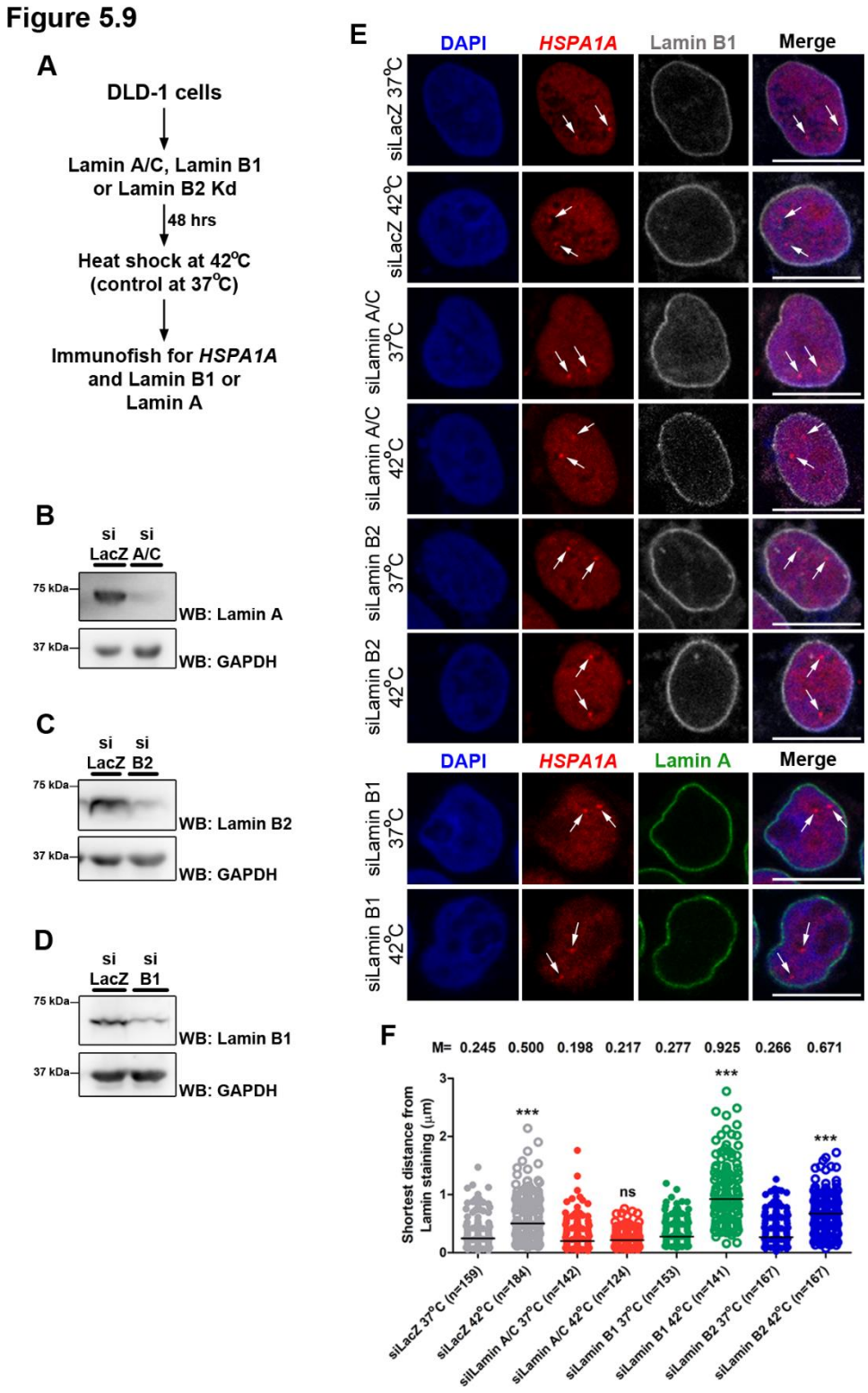

Figure 5.9 Lamin A/C is required for the heat shock mediated dynamics of the Hsp70 gene locus. A) Experimental scheme. B-D) Representative western blots confirming siRNA mediated knockdown of Lamin A (B), Lamin B2 (C) and Lamin B1 (D). GAPDH was used as loading control. E) Representative mid-optical section images *(N=2)* from confocal z-stacks showing immunostaining of Lamin B1 or Lamin A, and 3D-FISH for Hsp70 gene locus (using RP11-92G8 BAC DNA) in DLD-1 cells treated with either siLacZ, siLamin A/C, siLamin B1 or siLamin B2 upon heat shock at 42ºC for 60 mins (same time point at 37ºC was used as control). White arrows: Specific hybridization of BAC DNA probe showing 2 copies. F) Dot scatter plot representing the shortest distance of the Hsp70 loci from Lamin staining in DLD-1 cells treated with either siLacZ, siLamin A/C, siLamin B1 or siLamin B2 upon heat shock at 42ºC for 60 mins (same time point at 37ºC was used as control). *(Combined data from N=2 independent biological replicates. Black horizontal bar: Median (M). n: number of loci).* *** p<0.0001 (Mann-Whitney test). **Scale bar ~10 µm.**

(Mehta et al., 2008). Considering that NM1 is a nuclear motor protein, interacts with actin, and further actin is involved in Hsp70 gene locus movement, we examined NM1 localization upon Lamin A/C depletion (Khanna et al., 2014). We performed an immunostaining for NM1 in DLD-1 cells depleted of Lamin A/C (siLacZ cells were used as control) and subjected to heat shock at 42ºC for 60 mins (Fig 5.10A). Immunostaining detects NM1 both at the plasma membrane and as foci inside the nucleus (Fig 5.10A). We observed that heat shock increases the number of NM1 foci inside the nucleus in control cells (Fig 5.10B). However, in cells depleted of Lamin A/C, this increase in NM1 intranuclear foci upon heat shock was not seen (Fig 5.10B). Thus, presence of Lamin A/C may be required for the correct partitioning of NM1 between the cytoplasm and the nucleus, particularly under stress conditions.

We further investigated the role of NM1 during heat shock by examining the induction of *HSPA1A* upon NM1 inhibition using an inhibitor (BDM) (Chon et al., 2001; Steinberg and McIntosh, 1998). We initially determined that treating cells with 1 mM BDM for 90 mins depletes most of the intranuclear NM1 foci (Fig 5.10C). Cells independently treated with siRNAs against LacZ or Lamin A/C and under 1 mM BDM treatment were subjected to heat shock at 42ºC for 60 mins, followed by estimation of transcript levels of *HSPA1A* using qRT-PCR (Fig 5.10D). BDM treatment in siLacZ cells at 42ºC showed an attenuation of *HSPA1A* expression to the same extent as the depletion of Lamin A/C (Fig 5.10E). Additionally, BDM treatment in siLamin A/C cells at 42ºC further decreased the transcript levels of *HSPA1A* (Fig 5.10E). These results suggest that Lamin A/C may regulate Hsp70 locus movement during heat shock by modulating the number and potentially the activity of intranuclear NM1 foci.

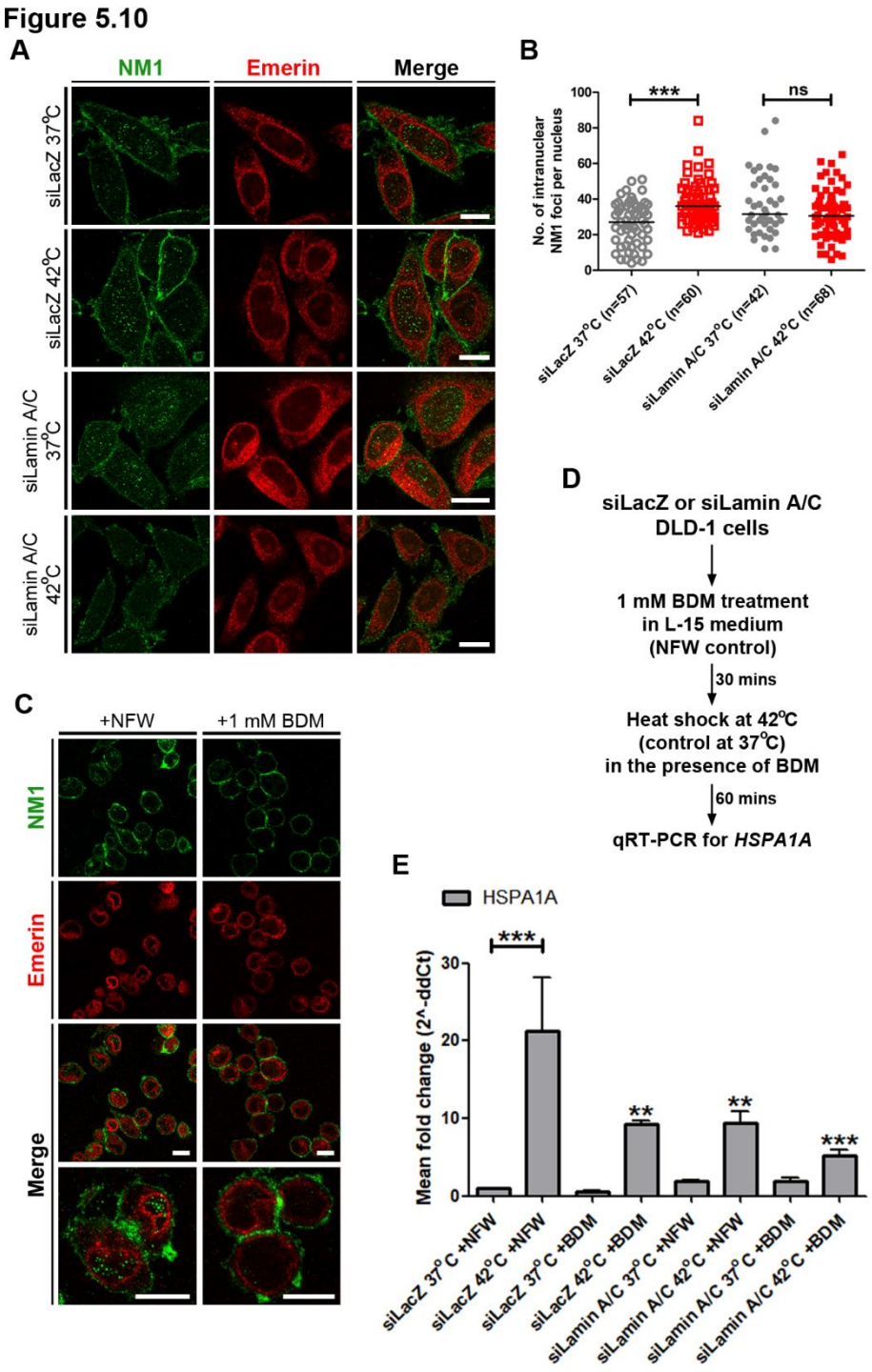

Figure 5.10 Lamin A/C modulates Hsp70 gene locus movement potentially via Nuclear Myosin I. A) Representative mid-optical section images from confocal z-stacks showing immunostaining of NM1 and emerin in DLD-1 cells treated with siLacZ or siLamin A/C and exposed to heat shock at 42ºC for 60 mins (same time point at 37ºC served as control). Immunostaining shows both cytoplasmic and intranuclear fractions of NM1. B) Quantification of intranuclear NM1 foci in DLD-1 cells treated with siLacZ or siLamin A/C and exposed to heat shock at 42ºC for 60 mins. *(Data from single experiment, n: number of nuclei, Black horizontal bar: Median)*. *** p<0.0001 (Mann-Whitney test). C) Immunostaining for NM1 and Emerin in DLD-1 treated with 1 mM BDM (or equal volume of nuclease free water) to confirm depletion of intranuclear NM1 foci and inhibition of NM1. D) Experimental scheme for coupling NM1 inhibition using BDM with heat shock. E) Measurement of *HSPA1A* expression using qRT-PCR in DLD-1 cells treated with either siLacZ or siLamin A/C, followed by NM1 inhibition using BDM treatment and heat shock at 42ºC (equal volume of nuclease free water was added in control cells). Expression was normalized to internal control – GAPDH and then to siLacZ 37ºC+NFW. *(Combined data from N=2 independent biological replicates. Error bar: SEM)*. ** p<0.001, *** p<0.0001 (Student's t-test). **Scale bar ~10 µm.**

Figure 5.11

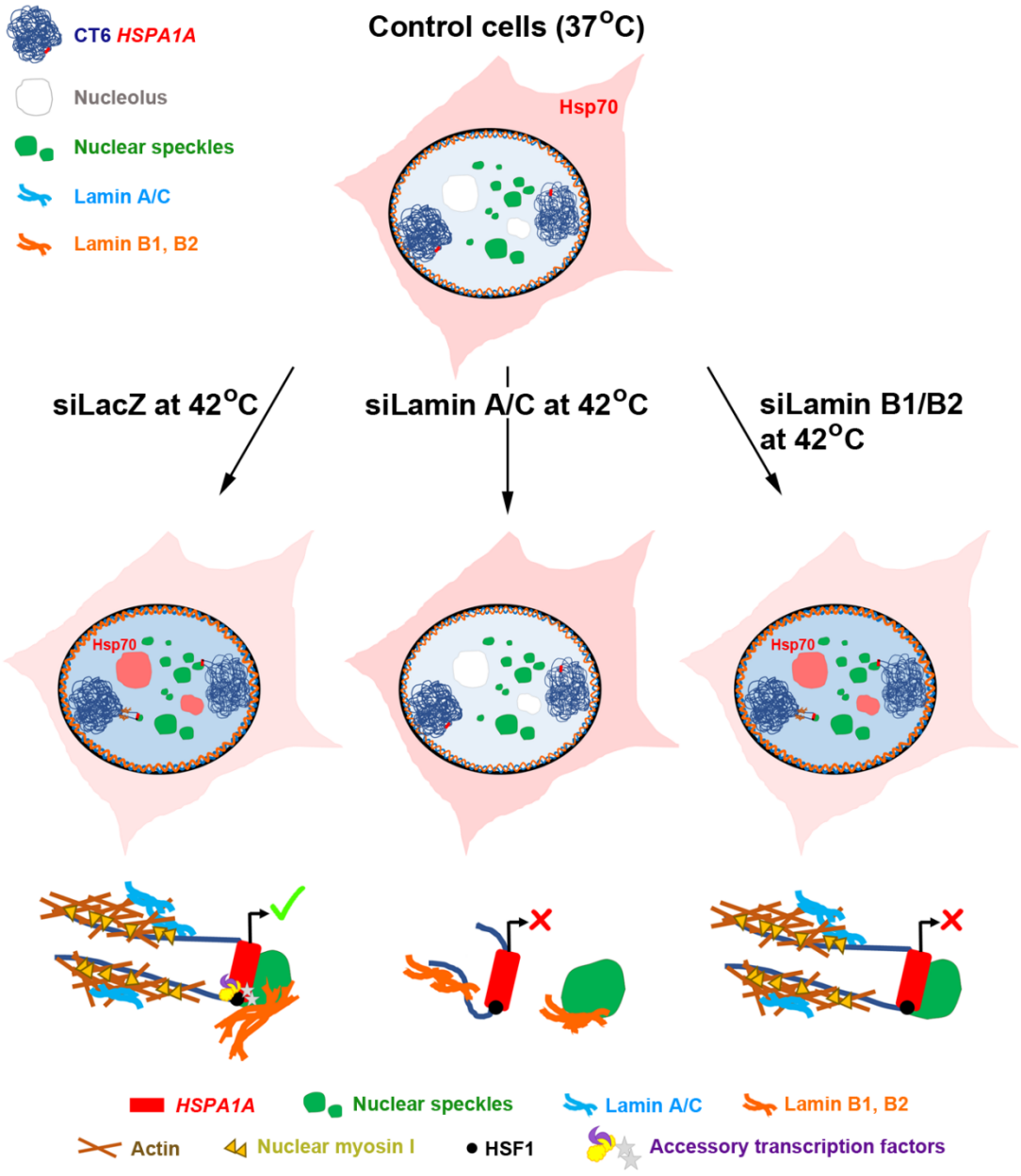

Figure 5.11 Speculative model depicting Lamin regulation of Hsp70 gene locus. Upon heat shock at 42ºC, the Hsp70 heat shock gene locus shows an actin dependent directional movement towards the nuclear speckles which further assists in accentuating the expression of this gene locus (refs). Additionally, Hsp70 protein translocates into the nucleus following hyperthermia to act as a molecular chaperone for nuclear proteins and protect genomic and ribosomal DNA integrity (refs). Depletion of Lamin A/C not only impairs the nuclear import of Hsp70 but also attenuates the heat shock mediated induction of *HSPA1A* – a gene which is part of the Hsp70 locus, by abrogating the movement of the gene locus towards nuclear speckles. We speculate that absence of Lamin A/C impairs the activity of the nuclear motor – NM1 and also impacts actin polymerization, which is known to be required for Hsp70 locus movement (ref). B-type lamins are not required for the initial contact of Hsp70 locus with nuclear speckles, but they affect *HSPA1A* expression by potentially assisting the recruitment of accessory transcription factors that leads to further upregulation following the speckle interaction.

5.3 Discussion

The heat shock response is a physiologically important regulatory network of molecular chaperones, activated in response to an aggregation of misfolded proteins upon heat shock (Richter et al., 2010). An efficient regulation of this network is maintained to ensure swift activation of the heat shock response (Velichko et al., 2013). Of the molecular chaperones activated during cellular stress, the Hsp70 sub-family displays an interesting transcriptional regulation wherein the Hsp70 gene locus moves directionally towards the nuclear speckles for transcriptional activation following heat shock (Khanna et al., 2014). Here we showed that Lamin A/C is an important regulator of the movement of Hsp70 gene locus. Additionally, lamins potentially modulate two different stages of *HSPA1A* (one of the genes in the Hsp70 locus) expression, namely i) initial movement towards nuclear speckles and ii) transcriptional upregulation after contact with nuclear speckles.

Nuclear lamins maintain structural properties of the nucleus and play important roles in DNA replication, transcription, positioning of chromosome territories and regulation of gene expression among others (Butin-Israeli et al., 2015; Dechat et al., 2008; Ghosh et al., 2015; Gibbs-Seymour et al., 2015; Ranade et al., 2017; Shumaker et al., 2008; Singh et al., 2013). Lamins regulate RNA Pol II transcription by potentially acting as scaffolds or docking sites for the polymerase and also for various transcription factors (Heessen and Fornerod, 2007; Spann et al., 2002). Lamins, along with other nuclear envelope proteins, directly interact with chromatin via Lamina Associated Domains (LADs) and these stretches of chromatin are typically enriched in the repressive histone mark H3K9me2, and lack RNA Pol II and histone modifications that represent active transcription (Guelen et al., 2008; Meuleman et al., 2013). Tethering of genomic loci to the nuclear lamina using

the LacI-lacO system induces transcriptional repression, however, genes do retain their transcriptional competence even when targeted to LADs (Finlan et al., 2008; Kumaran and Spector, 2008; Reddy et al., 2008; Zullo et al., 2012). As lamins modulate the response of the nucleus to various external mechanical stresses (Dahl et al., 2008; Hale et al., 2008; Lammerding et al., 2005; Osmanagic-Myers et al., 2015), studying their regulatory role is important to understand the impact of hyperthermia on nuclear structure and function. Lamin B is upregulated upon heat shock in U-1 melanoma and HeLa cells, while being downregulated in response to heat shock in CHO cells (Dynlacht et al., 1999; Falloon and Dynlacht, 2002; Zhu et al., 1999). Additionally, downregulation of Emerin and Lamin B1 is observed during heat shock recovery in HeLa S3 cells (Haddad and Paulin-Levasseur, 2008). These results point towards the diversity in lamin response, and potentially regulation, during heat shock depending on the cell type, temperature and time regimens.

5.3.1 Lamin expression during heat shock

Experiments in diploid DLD-1 cells indicate that both Lamin A and B1 are upregulated during heat shock at 42ºC (Fig 5.2D-E and 5.3C-D). Interestingly, the behavior of Lamin A and B1 varied in terms of i) Lamin B1 showed ~2.4 fold upregulation by 60 mins of heat shock, compared to ~1.5 fold increase in Lamin A, ii) the increased expression of Lamin A was more predominant in the nucleoplasm as compared to the nuclear periphery. Both Lamin A and B1 transcripts also showed an upregulation by 10 mins of heat shock suggesting that the transcripts may accumulate in the initial stage of heat shock, while the enhanced protein expression is more apparent during the later stage. However, additional characterization of cells upon heat shock in terms of (i) assessing the effect on Lamin expression using biochemical fractionation and immunostaining

using different antibodies, (ii) understanding the monomeric vs polymeric state of Lamins and (iii) elucidating the differential protein interactors of Lamins, is required to completely understand impact of heat shock signaling on nuclear lamins.

5.3.2 Modulation of Hsp70 nuclear import by Lamin A/C

To further understand the role of lamins in the heat shock response pathway, we performed independent lamin knockdowns and studied two important events in the pathway viz. nuclear translocation of Hsp70 and expression of a member of the Hsp70 gene family – *HSPA1A*. We observed that Lamin A/C, and not Lamin B1 or B2, modulate the nuclear translocation of Hsp70 following heat shock (Fig 5.4D, 5.6D-E). The nuclear import of Hsp70 is brought about by the import carrier Hikeshi (Imamoto and Kose, 2012). The effect of Lamin A/C depletion on nuclear translocation of Hsp70 may stem from a direct impact on Hikeshi activity or via an indirect effect on the nuclear pore complexes. Lamin A/C mutations that induce laminopathies and progeria have been shown to affect nuclear import via mislocalizing various nucleoporins (Nups) (Busch et al., 2009; Ferri et al., 2017; Xie et al., 2016), while EDFCs derived from Lamin A/C and B1 knockout mESCs show uneven distribution of nuclear pore complexes (Guo et al., 2014). Thus, understanding the contribution of Lamin A/C to the heat shock mediated nuclear import of Hsp70 will involve dissecting the above two possibilities in detail. Additionally, it is also important to study the regulation of Hsp70 nuclear import by Lamin A/C in non-heat shock conditions like induction by metal ion stress. This will further strengthen the regulatory crosstalk between heat shock and nuclear lamins.

5.3.3 Differential regulation of *HSPA1A* transcription by nuclear lamins

Extensive experiments have shown the requirement of a directional movement of the Hsp70 gene locus (of which *HSPA1A* is a part) towards nuclear speckles for transcriptional activation during heat shock (Jolly et al., 1999; Khanna et al., 2014). Furthermore, the *HSPA1A* promoter is the crucial genomic element required for this movement, as artificial introduction of this promoter upstream of any other gene (e.g. MT2A) results in heat shock induced movement towards nuclear speckles and transcriptional upregulation (Hu et al., 2010). Interestingly, while the endogenous Hsp70 gene contacts nuclear speckles both upon heat shock and metal stress (induced by cadmium sulphate treatment), the artificially integrated Hsp70 BAC transgene arrays only contact SC35 during heat shock (Jolly et al., 1999; Khanna et al., 2014). We observed that Lamins are all required for heat shock induced upregulation of *HSPA1A* but not for the cadmium sulphate mediated expression of this gene (Fig 5.5C and 5.8E). Studies have already shown that both metal stress response and heat shock induction result in *HSPA1A* gene transcription via the HSF1 pathway (Williams and Morimoto, 1990). This indicates that Lamins regulate heat shock response downstream of HSF1, HSF1 binding at the promoter of *HSPA1A* induces recruitment of the transcription machinery to the promoter, and further induces actin-dependent movement of the gene locus towards the nuclear speckles which is required for enhanced transcription (Khanna et al., 2014). Using a BAC DNA probe against the endogenous Hsp70 gene locus, we examined the movement of Hsp70 locus upon heat shock in the presence and absence of lamins and observed that only Lamin A/C depletion abrogated *HSPA1A* movement towards the nuclear interior (Fig 5.9E-F). This suggests the role of Lamin A/C specifically in regulating movement of the gene locus away from the nuclear periphery – a repressive milieu, towards nuclear interior where the SC35 speckles are predominantly observed, and thus facilitate its transcription. Lamin A/C and its

direct interactor – Emerin, both bind to and regulate actin polymerization (Holaska et al., 2004; Ondrej et al., 2008; Simon et al., 2010). Furthermore, Emerin directly interacts with the nuclear motor NM1 (Nuclear Myosin I) which assists in long range chromatin and chromosome territory movements and is required for chromatin remodeling during transcription by RNA Pol I, II and III (Almuzzaini et al., 2015; Chuang et al., 2006; Hofmann et al., 2006; Holaska and Wilson, 2007; Mehta et al., 2008; Percipalle et al., 2006; Pestic-Dragovich et al., 2000). Lamin A/C is also required for the correct inner nuclear membrane localization of Emerin (Vaughan et al., 2001). We observed that Lamin A/C was required for the heat shock induced increase in the number of intranuclear NM1 foci (Fig 5.10B) and found that inhibition of NM1 using BDM leads to attenuation of *HSPA1A* expression equivalent to that caused by Lamin A/C knockdown alone (Fig 5.10E). We therefore speculate that the absence of Lamin A/C could affect nuclear-cytoplasmic partitioning and activity of NM1, potentially via Emerin, and therefore abrogate the movement of Hsp70 locus upon heat shock (Fig 5.11). Additionally, Lamin A/C depletion itself could also affect the polymerization of actin that is required for the directional movement of *HSPA1A* (Khanna et al., 2004).

It is important to note that the absence of B-type lamins attenuates the heat shock mediated upregulation of *HSPA1A* (Fig 5.5C) but not the movement of the gene locus towards the nuclear interior (Fig 5.9F). Lamin B1 and B2 could therefore be important players in the recruitment of other accessory transcription factors required for the upregulation of Hsp70 locus expression after it has contacted the nuclear speckles (Fig 5.11). Our results highlight a novel regulatory role of nuclear lamins in the physiologically significant pathway of heat shock response at different stages like i) potential strengthening of the nucleus during heat shock, ii) assisting the movement of heat

shock gene locus via regulation of nuclear motor NM1 and iii) recruitment of transcription factors to the locus for transcriptional upregulation.

Chapter 6: Understanding the regulation of signal induced genome reorganization – current observations and future directions

Genome organization in the interphase nucleus is maintained in a flexible manner. Typically, while the genome is non-randomly organized and conserved through evolution, cell-type and tissue specific genome organization is allowed in a dynamic and reversible manner. However, the molecular basis of how the genome remains plastic and executes specific functions in a timely manner is an area of active investigation. Additionally, the re-organization of nuclear proteins, nuclear bodies and chromatin in response to extranuclear signals will provide fundamental insights into organizing principles that operate to maintain nuclear architecture. In this thesis, we have examined the role of nuclear envelope molecules as sensors, responders and effectors of extranuclear signaling into the nucleus.

6.1 Insights into signaling mechanisms underlying genome reorganization

6.1.1 Spatial organization of chromosome territories

Using soft polyacrylamide matrices to alter the force equilibrium of cells, we identified a novel signaling cascade wherein the inner nuclear membrane protein - emerin, is phosphorylated at its Tyr99 residue in cells on softer matrices, which further signals the selective repositioning of chromosome territories in a Lamin dependent manner. We observed that the positions of gene poor chromosome 18 territories – closer to the nuclear envelope, showed greater sensitivity to altered extracellular matrix stiffness than positions of gene rich chromosome 19 territories towards the nuclear interior, at similar time scales. This suggests that chromatin closer to the nuclear periphery may respond earlier to changes relayed via the nuclear envelope. However, it is important to note that in addition to their divergent gene densities and nuclear locations, Chr. 18 and 19 show contrasting transcriptional profiles when exposed to lowered matrix stiffness wherein chromosome 19 shows greater gene expression changes than chromosome 18. Thus, the inability of

chromosome 19 territories to regain their conserved nuclear locations upon increase in substrate stiffness within similar time-scales as CT18, may be because the transcriptional deregulation of CT19 has not yet recovered by then. An interesting parallel to study, is the response of CT1 positions to changes in substrate stiffness. Chr. 1 is (i) the maximally deregulated chromosome in cells on softer 2 kPa matrices, (ii) mislocalized by ~16% R.D (1.74 ± 0.1 μm) on 2 kPa matrices and (iii) partially able to regain its conserved location closer to the nuclear periphery upon increase in substrate stiffness. This further suggests the close interplay between gene density, transcriptional profiles, 3D topology of the chromosome territory and nuclear envelope proximity in modulating chromosome territory positions in response to altered nuclear mechanotransduction. Some of the interesting questions that remain to be answered are:

1) Impact of lowered extracellular substrate stiffness on the spatial positions of Chr. 2 – which has similar size and gene density as chromosome 1 (Chr. 1 – size: ~250 Mbp and gene density: ~20.31, Chr. 2 – size: ~242 Mbp and gene density: ~15.96) but shows only half the transcriptional deregulation as Chr. 1.

2) Impact of lowered extracellular substrate stiffness on the spatial positions of Chr. 4 – which has twice the size and nearly identical gene density as chromosome 18 (Chr. 18 – size: ~80 Mbp and gene density: ~12.35, Chr. 4 – size: ~190 Mbp and gene density: ~12.85) and also shows similar transcriptional deregulation as Chr. 18.

Our results highlight nuclear lamins as important effectors of chromosome territory repositioning in cells on softer matrices. These experiments reveal differential effects of A and B-type lamins on chromosome territory positions. B-type lamins function as tethers for heterochromatin and gene poor, peripheral chromosome territories to maintain them at their conserved nuclear locations at

the nuclear periphery. On the other hand, Lamin A influences positions of (i) gene rich chromosome territories potentially via its nucleoplasmic fraction and (ii) gene poor chromosomes only in the absence of strong tethering by B-type Lamins at the nuclear periphery. We speculate that stoichiometries of A and B-type lamins across different cell and tissue types and their protein-protein interactions potentially regulate which genomic sub-regions respond to extranuclear signals and also the extent of their response - both in terms of their transcriptional alterations and changes in spatial positions. We show the relay of mechanosensitive signals from Emerin to Lamin A via phosphorylation at Tyr99. Analysis of the distance between the phosphorylated and endogenous emerin bands shows a separation of ~2.6-3.8 kDa, greater than that induced by a single phosphorylation (at Tyr99). We surmise that emerin undergoes additional post translational modifications (PTMs) including phosphorylation, during the course of ~90 mins, that may be differentially regulated a) between matrices of different stiffness and b) depending on the presence or absence of the initial Tyr99 phosphorylation. It is therefore important to investigate – 1) the temporal expression patterns of lamins and LINC complex proteins, 2) post-translational modifications of emerin and 3) temporal response of chromosome territory positions and corresponding gene expression changes to altered extracellular matrix stiffness.

Figure 6.1

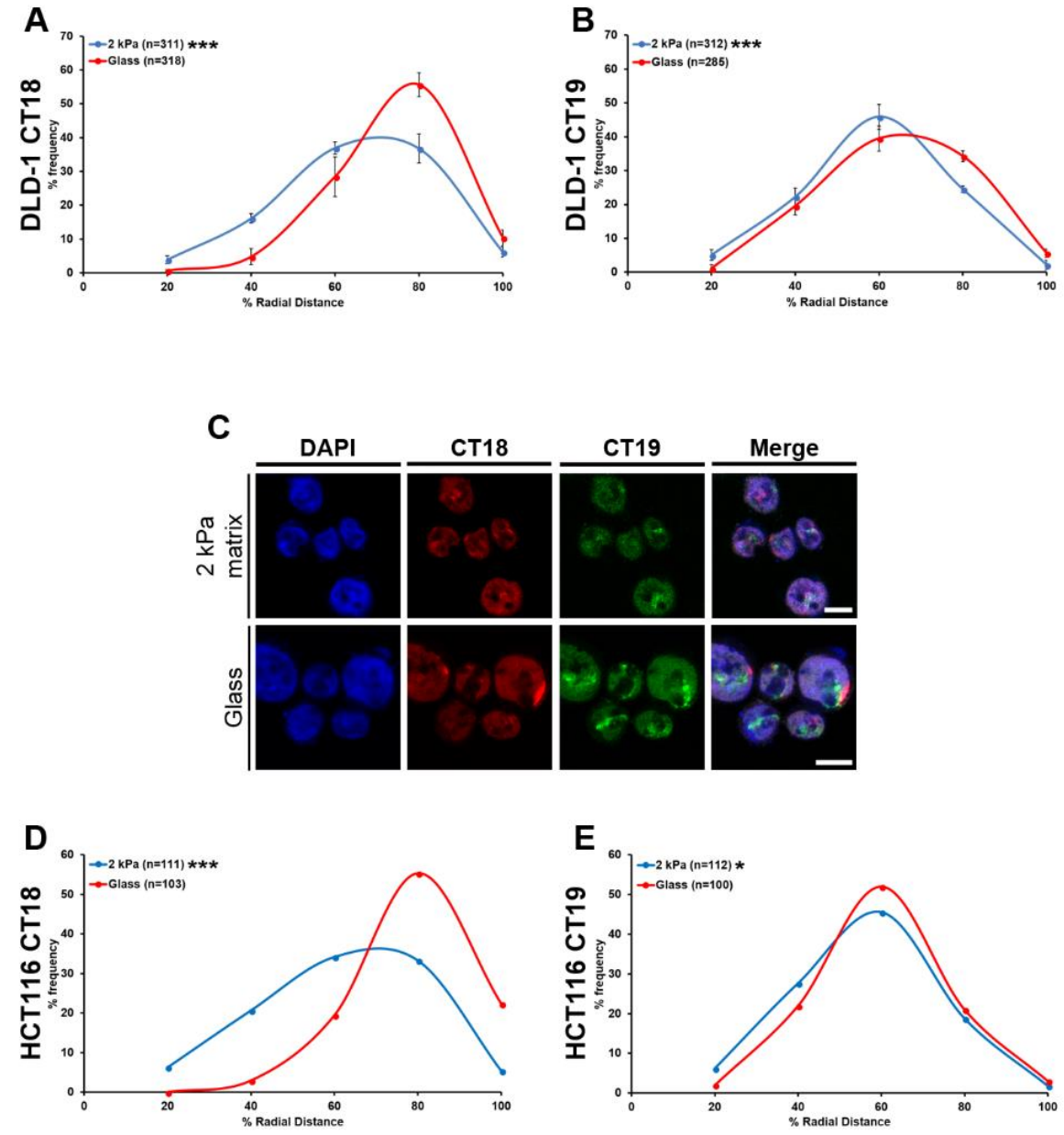

Figure 6.1 Chromosome 18 and 19 territories are mislocalized towards the nuclear interior in HCT116 cells on 2 kPa matrices. A-B) Radial distance distribution profiles of CT18 and 19 in DLD-1 cells on 2 kPa matrices (from Fig 3.8D-E). C) Representative mid-optical sections from confocal z-stacks of 3D-FISH hybridizations for CT18 and 19 in HCT116 cells on 2 kPa matrix and glass for 90 mins. D) Radial distance distribution profiles for CT18 on 2 kPa matrix (R.D ~53.64%) and glass (R.D ~70.64%). E) Radial distance distribution profiles for CT19 on 2 kPa matrix (R.D ~47.92%) and glass (R.D ~51.06%). *(D-E, Data from single biological replicate, n: number of CTs, X-axis: 0% - Nuclear center and 100% - Nuclear periphery)*. **Scale bar ~10 µm.**

Figure 6.2

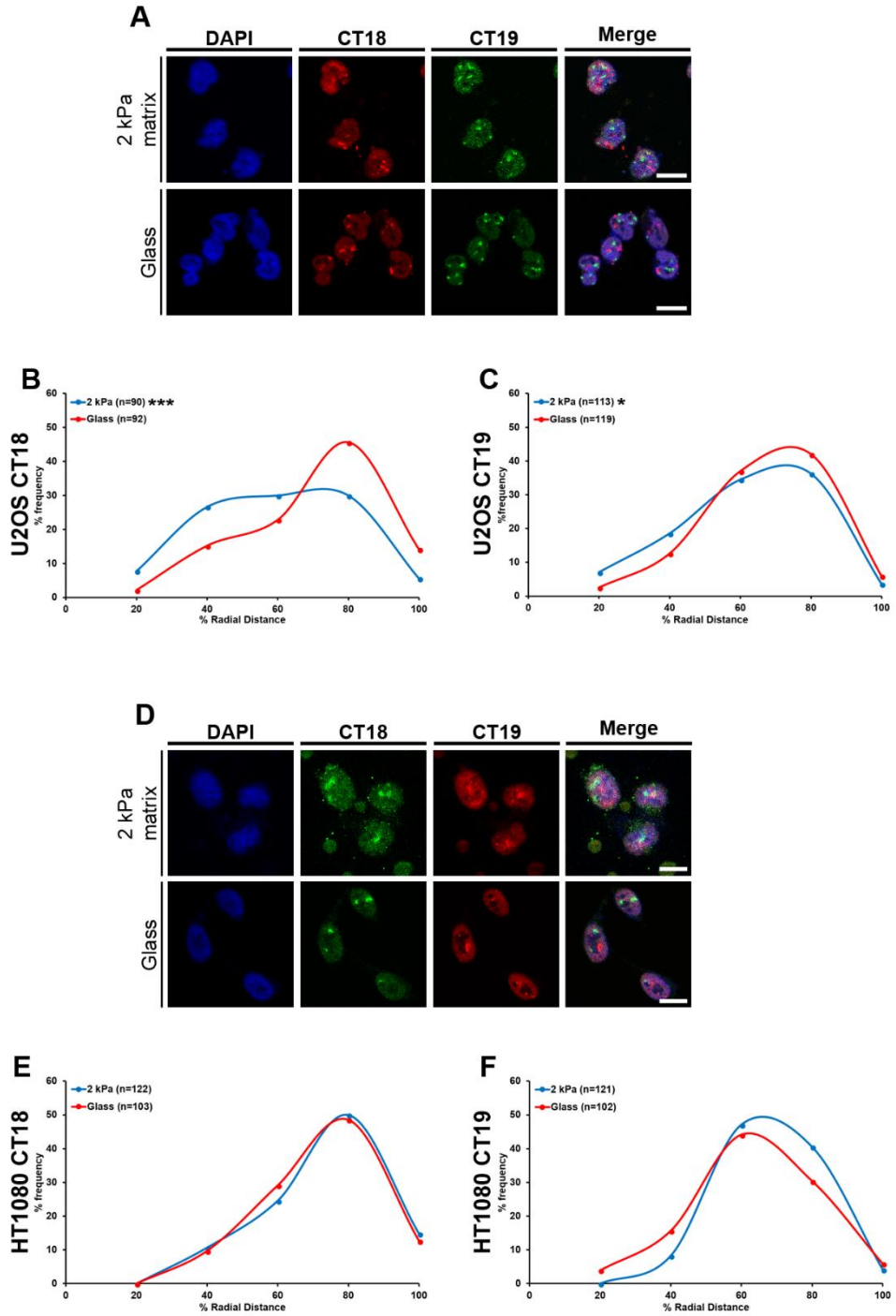

Figure 6.2 Chromosome 18 and 19 territories are mislocalized towards the nuclear interior in U2OS cells on 2 kPa matrices. A) Representative mid-optical sections from confocal z-stacks of 3D-FISH hybridizations for CT18 and 19 in U2OS cells on 2 kPa matrix and glass for 90 mins. B) Radial distance distribution profiles for CT18 on 2 kPa matrix (R.D ~51.47%) and glass (R.D ~64.25%). C) Radial distance distribution profiles for CT19 on 2 kPa matrix (R.D ~53.89%) and glass (R.D ~59.18%). *(B-C, Data from single biological replicate, n: number of CTs, X-axis: 0% - Nuclear center and 100% - Nuclear periphery).* **Chromosome 18 and 19 territories positions are unaffected in HT1080 cells on 2 kPa matrices.** D) Representative mid-optical sections from confocal z-stacks of 3D-FISH hybridizations for CT18 and 19 in HT1080 cells on 2 kPa matrix and glass for 90 mins. E) Radial distance distribution profiles for CT18 on 2 kPa matrix (R.D ~65.39%) and glass (R.D ~62.89%). F) Radial distance distribution profiles for CT19 on 2 kPa matrix (R.D ~58.35%) and glass (R.D ~55.12). *(E-F, Data from single biological replicate, n: number of CTs, X-axis: 0% - Nuclear center and 100% - Nuclear periphery).* **Scale bar ~10 µm.**

Figure 6.3

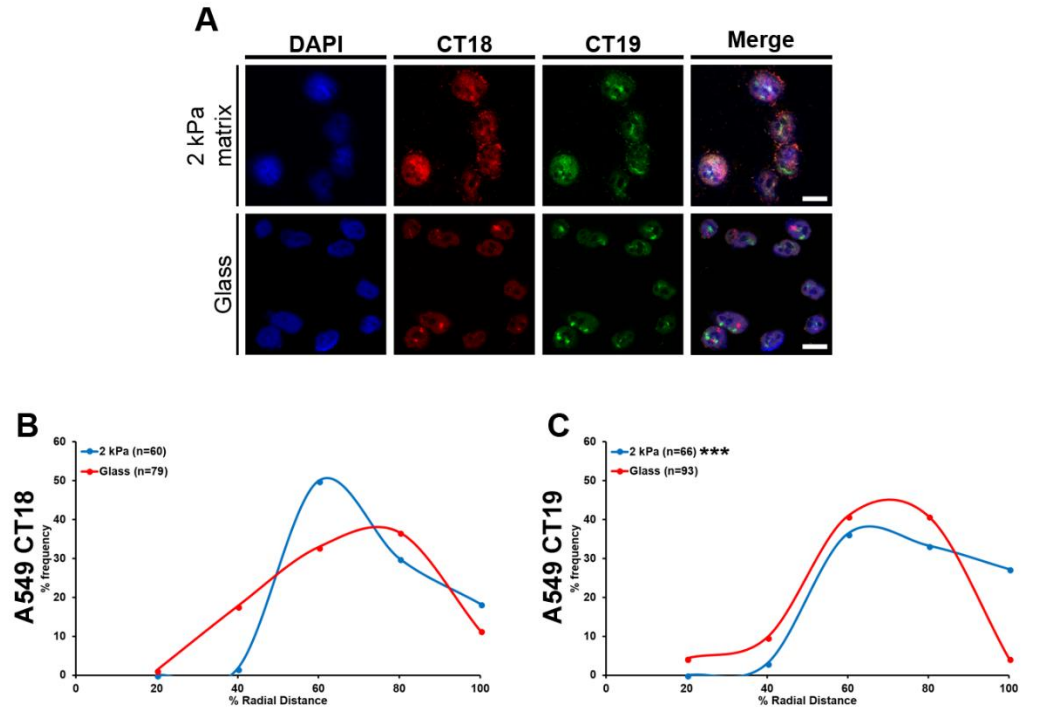

D

Cell line	No. of Chr. 18 copies	No. of Chr. 19 copies	% Radial Distance of CT18	% Radial Distance of CT19	Δ % R.D (CT18-CT19)	% Radial Distance of CT18	% Radial Distance of CT19	Δ % R.D (CT18-CT19)
	Matrix ➡			2 kPa			Glass	
DLD-1 (n=45-46)	2	2	56.56	49.40	7.16	66.38	54.73	11.65
HCT116 (n=44)	2	2	53.64	47.92	5.72	70.64	51.06	19.58
HT1080 (n=45-46)	2	2	65.39	58.35	7.04	62.89	55.12	7.77
U2OS (n=47)	2	3-4	51.47	53.89	- 2.42	64.25	59.18	5.07
A549 (n=66)	2-3	3-4	58.00	68.78	- 10.78	59.66	57.30	2.36

Figure 6.3 Chromosome 19 territories are mislocalized towards the nuclear periphery in A549 cells on 2 kPa matrices. A) Representative mid-optical sections from confocal z-stacks of 3D-FISH hybridizations for CT18 and 19 in A549 cells on 2 kPa matrix and glass for 90 mins. B) Radial distance distribution profiles for CT18 on 2 kPa matrix (R.D ~58.0%) and glass (R.D ~59.66%). C) Radial distance distribution profiles for CT19 on 2 kPa matrix (R.D ~68.78%) and glass (R.D ~57.30%). *(B-C, Data from single biological replicate, n: number of CTs, X-axis: 0% - Nuclear center and 100% - Nuclear periphery)*. D) Table summarizing the median % R.D values for CT18 and 19 in different cell lines exposed to lowered extracellular substrate stiffness. **Scale bar ~10 µm.**

We observed cell type specific responses to lowered extracellular matrix stiffness, in the repositioning of CT18 and 19. Like DLD-1, HCT116 (colorectal carcinoma) and U2OS (osteosarcoma) cells reposition CT18 and 19 towards the nuclear interior when exposed to softer (2 kPa) matrices for 90 mins (Fig 6.1A-E, 6.2A-C, 6.3D). On the other hand, the positions of CT18 and 19 are unaffected in HT1080 (fibrosarcoma) cells on 2 kPa matrices (90 mins) (Fig 6.2D-F, 6.3D). In the aneuploid lung carcinoma cell line – A549, with hardly any spatial separation between the gene rich CT19 and gene poor CT18, chromosome 19 territories are mislocalized towards the nuclear periphery in response to lowered matrix stiffness (2 kPa/90 mins) (Fig 6.3A-D). These results reiterate the importance of innate cell type specific differences, and potentially even tissue type specific differences, in regulating genome reorganization when cells experience altered environmental cues. Furthermore, studying the contribution of (i) transcriptional profiles (ii) stoichiometries of nuclear envelope factors such as lamins, emerin, LINC complex proteins, Lap2α/β, MAN1 among others, and (iii) stiffness of the tissue of origin, will provide insights into mechanisms of genome reorganization.

6.1.2 Transcriptional profiles

Gene expression changes in response to extranuclear signals, both biochemical and mechanical, are well studied (Chowdhury et al., 2010; Engler et al., 2006; Kocgozlu et al., 2010; Ma et al., 2008; Park et al., 2011; Rabineau et al., 2015; Stern et al., 2009). However, the crosstalk between transcriptional alterations and chromatin reorganization in response to external signals is not completely understood. We detect changes in gene expression profiles of cells on softer polyacrylamide matrices. However, in our study, we are unable to uncouple chromosome repositioning from its transcriptional deregulation. Furthermore, the regulation of topological

changes in chromosome territories and its contribution to transcriptional deregulation is also unclear. In addition to being a modulator of chromosome territory positions, Lamin A also contributes to transcriptional changes in cells on softer matrices. Myc, a direct interactor of Lamin A, potentially regulates the expression of a subset of downregulated genes on the softer matrices via miR-26a and miR-26b (Chang et al., 2008; Myant et al., 2015). The binding motifs for Transcription factor activating protein (AP1) - composed of c-Fos and c-Jun, are enriched in promoters of genes upregulated on 2 kPa matrices. Interestingly, Lamin A/C directly interacts with c-Fos and sequesters it at the nuclear periphery thereby negatively regulating AP1 activity (Ivorra et al., 2006). Lamin A is enriched in the nucleoplasm in cells on softer matrices (Buxboim et al., 2014; Swift et al., 2013). The nucleoplasmic accumulation of Lamin A on 2 kPa matrices potentially releases c-Fos from the nuclear periphery and subsequently activates a subset of AP1 responsive genes. Additionally, nucleoplasmic Lamin A-Lap2α complexes sequester hypo-phosphorylated Rb (Retinoblastoma) protein and delays its activation, which further maintain its interactor E2F1 in a repressed state (Johnson et al., 2004; Pekovic et al., 2007). This may be a possible reason for the downregulation of genes on 55 kPa matrices that contain consensus motifs for E2F1 binding. Taken together, this reiterates the ability of nuclear lamins to exert regulatory control both at the level of gene expression as well as organization of chromosome territories. Furthermore, our study also underscores the important role of lamins in nuclear mechanotransduction. Some of the important aspects that remain to be studied include:

1) Analyses of lamin occupancy on the genes deregulated in response to altered substrate stiffness.

2) Examining transcriptional profiles of cells in conditions where conserved chromosome positions have been recovered like – matrix switching assay, overexpression of Lamin B2-GFP or GFP-Emerin Y99F.

3) Spatial organization of highly deregulated gene clusters on softer matrices.

4) Dissecting the contribution of transcriptional changes to genome organization by treating cells with transcriptional activators or inhibitors and examining radial positioning of chromosome territories.

6.1.3 Positional regulation of gene expression

Spatial organization of a gene locus in the interphase nucleus is an important determinant of its expression and is stringently regulated, especially in dynamic physiologically relevant processes (Khanna et al., 2014; Meaburn et al., 2009; Meaburn et al., 2016; Volpi et al., 2000; Williams et al., 2002). An example in this context is the differentiation of myogenic progenitors into myotubes. The genes required for differentiation – *Myf5* and *MyoD*, are tethered at the nuclear periphery and repressed in the progenitor cells. Upon differentiation, these gene loci are disengaged from the nuclear lamina, move towards the nuclear interior and are transcriptionally activated. Additionally, *Pax7* – required for proliferation of the progenitors, is present towards the nuclear interior pre-differentiation and is tethered at the nuclear periphery in differentiated myotubes (Demmerle et al., 2013). This suggests the importance of spatial regulation of gene positions during different cellular processes. Interestingly, emerin binds *Myf5* and *MyoD* and is required for their correct positioning and expression during differentiation (Demmerle et al., 2013). Furthermore, tethering a reporter gene (herpes simplex virus thymidine kinase promoter and hygromycin resistance gene, Tk-hyg) to the nuclear lamina using a GFP-LacI-ΔEMD and lacO system induces transcriptional repression (Reddy et al., 2008). These transcriptional changes could be mediated in a sequence-specific manner – using Lamina Associating Sequences (LASs) to induce tethering with the nuclear lamina and recruitment of repressors like cKrox and HDAC3 (Zullo et al., 2012).

Additionally, tethering of chromosomes to the inner nuclear membrane using the LacI-lacO system can lead to repression of some genes near the nuclear periphery due to the activity of Class I/II HDACs located near the periphery (Finlan et al., 2008). Interestingly, genetic loci targeted to the nuclear periphery are capable of being transcriptionally active (Kumaran and Spector, 2008). Thus, nuclear proteins can act as modulators of gene loci positions and consequently, their expression (de Las Heras et al., 2017; Demmerle et al., 2013; Lund et al., 2013). The transcriptional and positional control of Hsp70 gene locus by nuclear lamins that we have demonstrated, is yet another example of the impact of lamins on signal induced gene expression changes and chromatin reorganization. These observations for the first time highlight the importance of (i) the functional divergence between Lamin A and B-type in their regulation of the dynamics and expression of Hsp70 gene locus (ii) protein-protein interactions of lamins (Lamin A-Emerin-NM1 in the heat shock response pathway and Lamin A-Emerin in the reorganization of chromosome territory) for chromatin reorganization and function in response to extranuclear signals. A detailed analysis of the transcription factors and epigenetic modulators of Hsp70 gene locus, along with an understanding of their relationship with nuclear lamins is essential to further dissect the molecular regulation of heat shock pathway by nuclear lamins.

6.2 Implications of a softer milieu on nuclear structure-function relationships

Lamin A expression levels positively correlate with an increase in tissue stiffness from as low as ~0.2 kPa (brain) to >40 kPa (bone) (Castéra et al., 2005; Engler et al., 2004; Lai-Fook and Hyatt, 2000; Swift and Discher, 2014; Swift et al., 2013; Wassenaar et al., 2016). We propose a speculative model wherein gene poor chromosome territories and heterochromatin organization

Figure 6.4

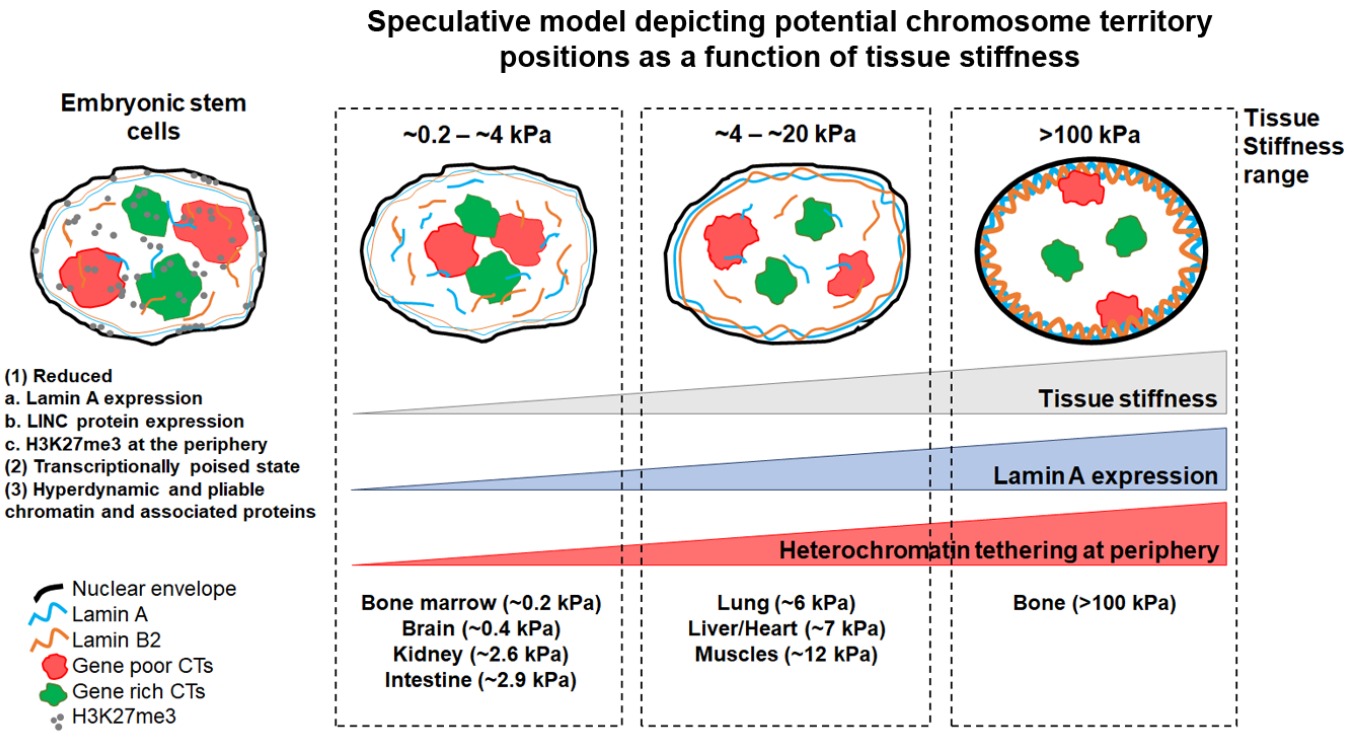

Speculative model depicting potential chromosome territory positions as a function of tissue stiffness. Embryonic stem cells (ES cells) have a "floppier" chromatin architecture in the interphase nucleus. Tissue specific genome organization is established during lineage specific differentiation. We speculate that cells in softer tissues have a relaxed organization of chromosome territories, that are reorganized and adopt more rigid configurations as a function of increased lamin levels and stiffness of the extracellular matrix.

are relatively more relaxed in cells within softer tissues, consistent with lowered Lamin A/C levels (Fig 6.4, Swift et al., 2013). In marked contrast, euchromatin or gene rich chromosome territories with (i) reduced LAD association (Guelen et al., 2008) (ii) proximity to the nuclear interior (Cremer et al., 2003) (iii) relatively greater number of housekeeping genes (Eisenberg and Levanon, 2013), may be less responsive to changes in extracellular matrix stiffness. DLD-1 cells on softer matrices seem to mimic the nuclear organization of human and murine embryonic stem cells in terms of comparatively lowered Lamin A/C and LINC levels and nucleoplasmic enrichment of H3K27me3 (Constantinescu et al., 2006; Higuchi et al., 2014; Khatau et al., 2012a).

Interestingly, the “softer” nucleus of stem cells correlates with (i) increased “floppiness” and plasticity of chromatin (Bošković et al., 2014; Melcer and Meshorer, 2010; Melcer et al., 2012; Talwar et al., 2013) (ii) comparatively lower levels of Lamin A/C (Constantinescu et al., 2006; Eckersley-Maslin et al., 2013) (iii) enhanced localization of H3K27me3 at the nuclear interior, reduction in H3K4me3 and a transcriptionally poised state (Bártová et al., 2008b; Harikumar and Meshorer, 2015). The decrease and redistribution of the nuclear envelope factors i.e. lamin/LINC proteins into the nucleoplasm is likely to contribute to transcriptional attenuation (Cesarini et al., 2015; Lund et al., 2013). This reiterates the fundamental role of nuclear envelope proteins in the regulation and maintenance of chromatin organization in differentiated cells and is consistent with elevated levels of A and B-type Lamins during organogenesis that further establish non-random chromatin organization in differentiated cells (Kim et al., 2011). It remains to be determined if differential levels of phospho-emerin/emerin are modulators of chromosome positioning in a tissue stiffness dependent manner.

Taken together, this study reveals a regulatory role of nuclear envelope proteins at the level of signal transduction into the nucleus, which further impinges on the spatio-functional dynamics of chromosome territories and gene loci in the interphase nucleus. The functional significance of chromosome positioning in terms of potentially altered chromatin contacts and its impact on the transcriptome remains to be examined in a cell-type and tissue specific context. It is therefore beyond doubt, that elucidating the mechanisms that regulate signal transduction into the nucleus will have far reaching consequences in understanding mechanobiology of tissue stiffness and the impact of environmental cues on diseases such as cardiomyopathies, muscular dystrophies and cancers.

References

Adam, S. A., Butin-Israeli, V., Cleland, M. M., Shimi, T. and Goldman, R. D. (2013). Disruption of lamin B1 and lamin B2 processing and localization by farnesyltransferase inhibitors. *Nucleus* **4**, 142–150.

Abiko, H., Fujiwara, S., Ohashi, K., Hiatari, R., Mashiko, T., Sakamoto, N., Sato, M. and Mizuno, K. (2015). Rho guanine nucleotide exchange factors involved in cyclic-stretch-induced reorientation of vascular endothelial cells. *J. Cell Sci.* **128**, 1683–1695.

Afgan, E., Baker, D., van den Beek, M., Blankenberg, D., Bouvier, D., Čech, M., Chilton, J., Clements, D., Coraor, N., Eberhard, C., et al. (2016). The Galaxy platform for accessible, reproducible and collaborative biomedical analyses: 2016 update. *Nucleic Acids Res.* **44**, W3–W10.

Alabert, C., Barth, T. K., Reverón-Gómez, N., Sidoli, S., Schmidt, A., Jensen, O. N., Imhof, A. and Groth, A. (2015). Two distinct modes for propagation of histone PTMs across the cell cycle. Genes Dev. **29**, 585–590.

Alam, S., Lovett, D. B., Dickinson, R. B., Roux, K. J. and Lele, T. P. (2014). Nuclear forces and cell mechanosensing. *Prog. Mol. Biol. Transl. Sci.* **126**, 205–215.

Alam, S. G., Zhang, Q., Prasad, N., Li, Y., Chamala, S., Kuchibhotla, R., Kc, B., Aggarwal, V., Shrestha, S., Jones, A. L., et al. (2016). The mammalian LINC complex regulates genome transcriptional responses to substrate rigidity. *Sci. Rep.* **6**, 38063.

Almuzzaini, B., Sarshad, A. A., Farrants, A.-K. Ö. and Percipalle, P. (2015). Nuclear myosin 1 contributes to a chromatin landscape compatible with RNA polymerase II transcription activation. *BMC Biol.* **13**, 35.

Amendola, M. and van Steensel, B. (2015). Nuclear lamins are not required for lamina-associated domain organization in mouse embryonic stem cells. *EMBO Rep.* **16**, 610–617.

Aronson, J. F. (1971). Demonstration of a colcemid-sensitive attractive force acting between the nucleus and a center. *J. Cell Biol.* **51**, 579–583.

Arslan-Yildiz, A., El Assal, R., Chen, P., Guven, S., Inci, F. and Demirci, U. (2016). Towards artificial tissue models: past, present, and future of 3D bioprinting. *Biofabrication* **8**, 014103.

Assoian, R. K. and Klein, E. A. (2008). Growth control by intracellular tension and extracellular stiffness. *Trends Cell Biol.* **18**, 347–352.

Aureille, J., Belaadi, N. and Guilluy, C. (2017). Mechanotransduction via the nuclear envelope: a distant reflection of the cell surface. *Curr. Opin. Cell Biol.* **44**, 59–67.

Badique, F., Stamov, D. R., Davidson, P. M., Veuillet, M., Reiter, G., Freund, J.-N., Franz, C. M. and Anselme, K. (2013). Directing nuclear deformation on micropillared surfaces by substrate geometry and cytoskeleton organization. *Biomaterials* **34**, 2991–3001.

Baharvand, H., Azarnia, M., Parivar, K. and Ashtiani, S. K. (2005). The effect of extracellular matrix on embryonic stem cell-derived cardiomyocytes. *J. Mol. Cell. Cardiol.* **38**, 495–503.

Baker, E. L., Bonnecaze, R. T. and Zaman, M. H. (2009). Extracellular matrix stiffness and architecture govern intracellular rheology in cancer. *Biophys. J.* **97**, 1013–1021.

Baler, R., Dahl, G. and Voellmy, R. (1993). Activation of human heat shock genes is accompanied by oligomerization, modification, and rapid translocation of heat shock transcription factor HSF1. *Mol. Cell. Biol.* **13**, 2486–2496.

Bank, E. M. and Gruenbaum, Y. (2011). The nuclear lamina and heterochromatin: a complex relationship. *Biochem. Soc. Trans.* **39**, 1705–1709.

Bar, D. Z., Davidovich, M., Lamm, A. T., Zer, H., Wilson, K. L. and Gruenbaum, Y. (2014). BAF-1 mobility is regulated by environmental stresses. *Mol. Biol. Cell* **25**, 1127–1136.

Barton, L. J., Soshnev, A. A. and Geyer, P. K. (2015). Networking in the nucleus: a spotlight on LEM-domain proteins. *Curr. Opin. Cell Biol.* **34**, 1–8.

Bártová, E., Krejcí, J., Harnicarová, A. and Kozubek, S. (2008a). Differentiation of human embryonic stem cells induces condensation of chromosome territories and formation of heterochromatin protein 1 foci. *Differentiation.* **76**, 24–32.

Bártová, E., Galiová, G., Krejcí, J., Harnicarová, A., Strasák, L. and Kozubek, S. (2008b). Epigenome and chromatin structure in human embryonic stem cells undergoing differentiation. *Dev. Dyn.* **237**, 3690–3702.

Beck, J. N., Singh, A., Rothenberg, A. R., Elisseeff, J. H. and Ewald, A. J. (2013). The independent roles of mechanical, structural and adhesion characteristics of 3D hydrogels on the regulation of cancer invasion and dissemination. *Biomaterials* **34**, 9486–9495.

Bengtsson, L. (2007). What MAN1 does to the Smads. TGFbeta/BMP signaling and the nuclear envelope. *FEBS J.* **274**, 1374–1382.

Berk, J. M. and Wilson, K. L. (2016). Simple Separation of Functionally Distinct Populations of Lamin-Binding Proteins. *Meth. Enzymol.* **569**, 101–114.

Berk, J. M., Tifft, K. E. and Wilson, K. L. (2013). The nuclear envelope LEM-domain protein emerin. *Nucleus* **4**, 298–314.

Bolzer, A., Kreth, G., Solovei, I., Koehler, D., Saracoglu, K., Fauth, C., Müller, S., Eils, R., Cremer, C., Speicher, M. R., et al. (2005). Three-dimensional maps of all chromosomes in human male fibroblast nuclei and prometaphase rosettes. *PLoS Biol.* **3**, e157.

Bonne, G. and Quijano-Roy, S. (2013). Emery-Dreifuss muscular dystrophy, laminopathies, and other nuclear envelopathies. *Handb. Clin. Neurol.* **113**, 1367–1376.

Booth-Gauthier, E. A., Du, V., Ghibaudo, M., Rape, A. D., Dahl, K. N. and Ladoux, B. (2013). Hutchinson-Gilford progeria syndrome alters nuclear shape and reduces cell motility in three dimensional model substrates. *Integr Biol (Camb)* **5**, 569–577.

Bošković, A., Eid, A., Pontabry, J., Ishiuchi, T., Spiegelhalter, C., Raghu Ram, E. V. S., Meshorer, E. and Torres-Padilla, M.-E. (2014). Higher chromatin mobility supports totipotency and precedes pluripotency in vivo. *Genes Dev.* **28**, 1042–1047.

Boudreau, N. and Bissell, M. J. (1998). Extracellular matrix signaling: integration of form and function in normal and malignant cells. *Curr. Opin. Cell Biol.* **10**, 640–646.

Boyle, S., Gilchrist, S., Bridger, J. M., Mahy, N. L., Ellis, J. A. and Bickmore, W. A. (2001). The spatial organization of human chromosomes within the nuclei of normal and emerin-mutant cells. *Hum. Mol. Genet.* **10**, 211–219.

Brachner, A. and Foisner, R. (2011). Evolvement of LEM proteins as chromatin tethers at the nuclear periphery. *Biochem. Soc. Trans.* **39**, 1735–1741.

Brachner, A., Reipert, S., Foisner, R. and Gotzmann, J. (2005). LEM2 is a novel MAN1-related inner nuclear membrane protein associated with A-type lamins. *J. Cell Sci.* **118**, 5797–5810.

Brandt, A., Papagiannouli, F., Wagner, N., Wilsch-Bräuninger, M., Braun, M., Furlong, E. E., Loserth, S., Wenzl, C., Pilot, F., Vogt, N., et al. (2006). Developmental control of nuclear size and shape by Kugelkern and Kurzkern. *Curr. Biol.* **16**, 543–552.

Bray, M.-A. P., Adams, W. J., Geisse, N. A., Feinberg, A. W., Sheehy, S. P. and Parker, K. K. (2010). Nuclear morphology and deformation in engineered cardiac myocytes and tissues. *Biomaterials* **31**, 5143–5150.

Bridger, J. M., Boyle, S., Kill, I. R. and Bickmore, W. A. (2000). Re-modelling of nuclear architecture in quiescent and senescent human fibroblasts. *Curr. Biol.* **10**, 149–152.

Burke, B., Mounkes, L. C. and Stewart, C. L. (2001). The nuclear envelope in muscular dystrophy and cardiovascular diseases. *Traffic* **2**, 675–683.

Busch, A., Kiel, T., Heupel, W.-M., Wehnert, M. and Hübner, S. (2009). Nuclear protein import is reduced in cells expressing nuclear envelopathy-causing lamin A mutants. *Exp. Cell Res.* **315**, 2373–2385.

Butin-Israeli, V., Adam, S. A., Jain, N., Otte, G. L., Neems, D., Wiesmüller, L., Berger, S. L. and Goldman, R. D. (2015). Role of lamin b1 in chromatin instability. *Mol. Cell. Biol.* **35**, 884–898.

Buxboim, A., Swift, J., Irianto, J., Spinler, K. R., Dingal, P. C. D. P., Athirasala, A., Kao, Y.-R. C., Cho, S., Harada, T., Shin, J.-W., et al. (2014). Matrix elasticity regulates lamin-A,C phosphorylation and turnover with feedback to actomyosin. *Curr. Biol.* **24**, 1909–1917.

Caille, N., Thoumine, O., Tardy, Y. and Meister, J.-J. (2002). Contribution of the nucleus to the mechanical properties of endothelial cells. *J. Biomech.* **35**, 177–187.

Capanni, C., Mattioli, E., Columbaro, M., Lucarelli, E., Parnaik, V. K., Novelli, G., Wehnert, M., Cenni, V., Maraldi, N. M., Squarzoni, S., et al. (2005). Altered pre-lamin A processing is a common mechanism leading to lipodystrophy. *Hum. Mol. Genet.* **14**, 1489–1502.

Capell, B. C. and Collins, F. S. (2006). Human laminopathies: nuclei gone genetically awry. Nat. Rev. Genet. **7**, 940–952.

Castéra, L., Vergniol, J., Foucher, J., Le Bail, B., Chanteloup, E., Haaser, M., Darriet, M., Couzigou, P. and De Lédinghen, V. (2005). Prospective comparison of transient elastography, Fibrotest, APRI, and liver biopsy for the assessment of fibrosis in chronic hepatitis C. *Gastroenterology* **128**, 343–350.

Celedon, A., Hale, C. M. and Wirtz, D. (2011). Magnetic manipulation of nanorods in the nucleus of living cells. *Biophys. J.* **101**, 1880–1886.

Cesarini, E., Mozzetta, C., Marullo, F., Gregoretti, F., Gargiulo, A., Columbaro, M., Cortesi, A., Antonelli, L., Di Pelino, S., Squarzoni, S., et al. (2015). Lamin A/C sustains PcG protein architecture, maintaining transcriptional repression at target genes. *J. Cell Biol.* **211**, 533–551.

Chalut, K. J., Höpfler, M., Lautenschläger, F., Boyde, L., Chan, C. J., Ekpenyong, A., Martinez-Arias, A. and Guck, J. (2012). Chromatin decondensation and nuclear softening accompany Nanog downregulation in embryonic stem cells. *Biophys. J.* **103**, 2060–2070.

Chambliss, A. B., Khatau, S. B., Erdenberger, N., Robinson, D. K., Hodzic, D., Longmore, G. D. and Wirtz, D. (2013). The LINC-anchored actin cap connects the extracellular milieu to the nucleus for ultrafast mechanotransduction. *Sci. Rep.* **3**, 1087.

Champy, C. and Carleton, H., M. (1921). Memoirs: Observations on the shape of the nucleus and its determinants. *J. Cell Sci.* **s2-65**, 589-625.

Chang, T.-C., Yu, D., Lee, Y.-S., Wentzel, E. A., Arking, D. E., West, K. M., Dang, C. V., Thomas-Tikhonenko, A. and Mendell, J. T. (2008). Widespread microRNA repression by Myc contributes to tumorigenesis. *Nat. Genet.* **40**, 43–50.

Chen, C. S., Mrksich, M., Huang, S., Whitesides, G. M. and Ingber, D. E. (1997). Geometric control of cell life and death. *Science* **276**, 1425–1428.

Chen, Z.-J., Wang, W.-P., Chen, Y.-C., Wang, J.-Y., Lin, W.-H., Tai, L.-A., Liou, G.-G., Yang, C.-S. and Chi, Y.-H. (2014). Dysregulated interactions between lamin A and SUN1 induce abnormalities in the nuclear envelope and endoplasmic reticulum in progeric laminopathies. *J. Cell Sci.* **127**, 1792–1804.

Chen, H., Comment, N., Chen, J., Ronquist, S., Hero, A., Ried, T. and Rajapakse, I. (2015). Chromosome conformation of human fibroblasts grown in 3-dimensional spheroids. *Nucleus* **6**, 55–65.

Chen, H., Seaman, L., Liu, S., Ried, T. and Rajapakse, I. (2017). Chromosome conformation and gene expression patterns differ profoundly in human fibroblasts grown in spheroids versus monolayers. *Nucleus* **8**, 383–391.

Chi, Y.-H., Chen, Z.-J. and Jeang, K.-T. (2009). The nuclear envelopathies and human diseases. *J. Biomed. Sci.* **16**, 96.

Chikashige, Y., Haraguchi, T. and Hiraoka, Y. (2007). Another way to move chromosomes. *Chromosoma* **116**, 497–505.

Chin, L., Xia, Y., Discher, D. E. and Janmey, P. A. (2016). Mechanotransduction in cancer. Curr. Opin. Chem. Eng. **11**, 77–84.

Chon, K., Hwang, H. S., Lee, J. H. and Song, K. (2001). The myosin ATPase inhibitor 2,3-butanedione-2-monoxime disorganizes microtubules as well as F-actin in Saccharomyces cerevisiae. *Cell Biol. Toxicol.* **17**, 383–393.

Chowdhury, F., Li, Y., Poh, Y.-C., Yokohama-Tamaki, T., Wang, N. and Tanaka, T. S. (2010). Soft substrates promote homogeneous self-renewal of embryonic stem cells via downregulating cell-matrix tractions. *PLoS ONE* **5**, e15655.

Chuang, C.-H., Carpenter, A. E., Fuchsova, B., Johnson, T., de Lanerolle, P. and Belmont, A. S. (2006). Long-range directional movement of an interphase chromosome site. *Curr. Biol.* **16**, 825–831.

Clements, L., Manilal, S., Love, D. R. and Morris, G. E. (2000). Direct interaction between emerin and lamin A. *Biochem. Biophys. Res. Commun.* **267**, 709–714.

Cohen, T. V., Kosti, O. and Stewart, C. L. (2007). The nuclear envelope protein MAN1 regulates TGFbeta signaling and vasculogenesis in the embryonic yolk sac. *Development* **134**, 1385–1395.

Constantinescu, D., Gray, H. L., Sammak, P. J., Schatten, G. P. and Csoka, A. B. (2006). Lamin A/C expression is a marker of mouse and human embryonic stem cell differentiation. *Stem Cells* **24**, 177–185.

Cook, D. R., Solski, P. A., Bultman, S. J., Kauselmann, G., Schoor, M., Kuehn, R., Friedman, L. S., Cowley, D. O., Van Dyke, T., Yeh, J. J., et al. (2011). The ect2 rho Guanine nucleotide exchange factor is essential for early mouse development and normal cell cytokinesis and migration. *Genes Cancer* **2**, 932–942.

Corrigan, D. P., Kuszczak, D., Rusinol, A. E., Thewke, D. P., Hrycyna, C. A., Michaelis, S. and Sinensky, M. S. (2005). Prelamin A endoproteolytic processing in vitro by recombinant Zmpste24. Biochem. J. **387**, 129–138.

Crabbe, L., Cesare, A. J., Kasuboski, J. M., Fitzpatrick, J. A. J. and Karlseder, J. (2012). Human telomeres are tethered to the nuclear envelope during postmitotic nuclear assembly. *Cell Rep.* **2**, 1521–1529.

Cremer, M., von Hase, J., Volm, T., Brero, A., Kreth, G., Walter, J., Fischer, C., Solovei, I., Cremer, C. and Cremer, T. (2001). Non-random radial higher-order chromatin arrangements in nuclei of diploid human cells. *Chromosome Res.* **9**, 541–567.

Cremer, M., Küpper, K., Wagler, B., Wizelman, L., von Hase, J., Weiland, Y., Kreja, L., Diebold, J., Speicher, M. R. and Cremer, T. (2003). Inheritance of gene density-related

higher order chromatin arrangements in normal and tumor cell nuclei. *J. Cell Biol.* **162**, 809–820.

Crisp, M. and Burke, B. (2008). The nuclear envelope as an integrator of nuclear and cytoplasmic architecture. *FEBS Lett.* **582**, 2023–2032.

Crisp, M., Liu, Q., Roux, K., Rattner, J. B., Shanahan, C., Burke, B., Stahl, P. D. and Hodzic, D. (2006). Coupling of the nucleus and cytoplasm: role of the LINC complex. *J. Cell Biol.* **172**, 41–53.

Croft, J. A., Bridger, J. M., Boyle, S., Perry, P., Teague, P. and Bickmore, W. A. (1999). Differences in the localization and morphology of chromosomes in the human nucleus. *J. Cell Biol.* **145**, 1119–1131.

Dahl, K. N., Kahn, S. M., Wilson, K. L. and Discher, D. E. (2004). The nuclear envelope lamina network has elasticity and a compressibility limit suggestive of a molecular shock absorber. *J. Cell Sci.* **117**, 4779–4786.

Dahl, K. N., Scaffidi, P., Islam, M. F., Yodh, A. G., Wilson, K. L. and Misteli, T. (2006). Distinct structural and mechanical properties of the nuclear lamina in Hutchinson-Gilford progeria syndrome. *Proc Natl Acad Sci USA* **103**, 10271–10276.

Dahl, K. N., Ribeiro, A. J. S. and Lammerding, J. (2008). Nuclear shape, mechanics, and mechanotransduction. *Circ. Res.* **102**, 1307–1318.

Daugaard, M., Rohde, M. and Jäättelä, M. (2007). The heat shock protein 70 family: Highly homologous proteins with overlapping and distinct functions. *FEBS Lett.* **581**, 3702–3710.

Davidson, P. M., Denais, C., Bakshi, M. C. and Lammerding, J. (2014). Nuclear deformability constitutes a rate-limiting step during cell migration in 3-D environments. Cell. Mol. Bioeng. **7**, 293–306.

De, S. and Babu, M. M. (2010). Genomic neighbourhood and the regulation of gene expression. *Curr. Opin. Cell Biol.* **22**, 326–333.

de Las Heras, J. I., Zuleger, N., Batrakou, D. G., Czapiewski, R., Kerr, A. R. W. and Schirmer, E. C. (2017). Tissue-specific NETs alter genome organization and regulation even in a heterologous system. *Nucleus* **8**, 81–97.

Dechat, T., Korbei, B., Vaughan, O. A., Vlcek, S., Hutchison, C. J. and Foisner, R. (2000). Lamina-associated polypeptide 2alpha binds intranuclear A-type lamins. *J. Cell Sci.* **113 Pt 19**, 3473–3484.

Dechat, T., Pfleghaar, K., Sengupta, K., Shimi, T., Shumaker, D. K., Solimando, L. and Goldman, R. D. (2008). Nuclear lamins: major factors in the structural organization and function of the nucleus and chromatin. *Genes Dev.* **22**, 832–853.

Dechat, T., Adam, S. A., Taimen, P., Shimi, T. and Goldman, R. D. (2010). Nuclear lamins. *Cold Spring Harb. Perspect. Biol.* **2**, a000547.

Deguchi, S., Maeda, K., Ohashi, T. and Sato, M. (2005). Flow-induced hardening of endothelial nucleus as an intracellular stress-bearing organelle. *J. Biomech.* **38**, 1751–1759.

Delpire, E., Duchêne, C., Goessens, G. and Gilles, R. (1985). Effects of osmotic shocks on the ultrastructure of different tissues and cell types. *Exp. Cell Res.* **160**, 106–116.

Demirovic, D., de Toda, I. M., Nizard, C. and Rattan, S. I. S. (2014). Differential translocation of heat shock factor-1 after mild and severe stress to human skin fibroblasts undergoing aging in vitro. *J. Cell Commun. Signal.* **8**, 333–339.

Demmerle, J., Koch, A. J. and Holaska, J. M. (2013). Emerin and histone deacetylase 3 (HDAC3) cooperatively regulate expression and nuclear positions of MyoD, Myf5, and Pax7 genes during myogenesis. *Chromosome Res.* **21**, 765–779.

Ding, X., Xu, R., Yu, J., Xu, T., Zhuang, Y. and Han, M. (2007). SUN1 is required for telomere attachment to nuclear envelope and gametogenesis in mice. *Dev. Cell* **12**, 863–872.

Downing, T. L., Soto, J., Morez, C., Houssin, T., Fritz, A., Yuan, F., Chu, J., Patel, S., Schaffer, D. V. and Li, S. (2013). Biophysical regulation of epigenetic state and cell reprogramming. *Nat. Mater.* **12**, 1154–1162.

Dreuillet, C., Tillit, J., Kress, M. and Ernoult-Lange, M. (2002). In vivo and in vitro interaction between human transcription factor MOK2 and nuclear lamin A/C. *Nucleic Acids Res.* **30**, 4634–4642.

DuFort, C. C., Paszek, M. J. and Weaver, V. M. (2011). Balancing forces: architectural control of mechanotransduction. *Nat. Rev. Mol. Cell Biol.* **12**, 308–319.

Dupin, I. and Etienne-Manneville, S. (2011). Nuclear positioning: mechanisms and functions. *Int. J. Biochem. Cell Biol.* **43**, 1698–1707.

Dupin, I., Camand, E. and Etienne-Manneville, S. (2009). Classical cadherins control nucleus and centrosome position and cell polarity. *J. Cell Biol.* **185**, 779–786.

Dupin, I., Sakamoto, Y. and Etienne-Manneville, S. (2011). Cytoplasmic intermediate filaments mediate actin-driven positioning of the nucleus. *J. Cell Sci.* **124**, 865–872.

Dynlacht, J. R., Story, M. D., Zhu, W. G. and Danner, J. (1999). Lamin B is a prompt heat shock protein. *J. Cell. Physiol.* **178**, 28–34.

D'Angelo, M. A. (2018). Nuclear pore complexes as hubs for gene regulation. *Nucleus* **9**, 142–148.

Eckersley-Maslin, M. A., Bergmann, J. H., Lazar, Z. and Spector, D. L. (2013). Lamin A/C is expressed in pluripotent mouse embryonic stem cells. *Nucleus* **4**, 53–60.

Ehrbar, M., Sala, A., Lienemann, P., Ranga, A., Mosiewicz, K., Bittermann, A., Rizzi, S. C., Weber, F. E. and Lutolf, M. P. (2011). Elucidating the role of matrix stiffness in 3D cell migration and remodeling. *Biophys. J.* **100**, 284–293.

Eisenberg, E. and Levanon, E. Y. (2013). Human housekeeping genes, revisited. *Trends Genet.* **29**, 569–574.

Engler, A. J., Griffin, M. A., Sen, S., Bönnemann, C. G., Sweeney, H. L. and Discher, D. E. (2004). Myotubes differentiate optimally on substrates with tissue-like stiffness: pathological implications for soft or stiff microenvironments. *J. Cell Biol.* **166**, 877–887.

Engler, A. J., Sen, S., Sweeney, H. L. and Discher, D. E. (2006). Matrix elasticity directs stem cell lineage specification. *Cell* **126**, 677–689.

Enyedi, B. and Niethammer, P. (2016). A case for the nuclear membrane as a mechanotransducer. *Cell. Mol. Bioeng.* **9**, 247–251.

Evans, N. D., Minelli, C., Gentleman, E., LaPointe, V., Patankar, S. N., Kallivretaki, M., Chen, X., Roberts, C. J. and Stevens, M. M. (2009). Substrate stiffness affects early differentiation events in embryonic stem cells. *Eur. Cell. Mater.* **18**, 1–13; discussion 13.

Evans, N. D., Gentleman, E., Chen, X., Roberts, C. J., Polak, J. M. and Stevens, M. M. (2010). Extracellular matrix-mediated osteogenic differentiation of murine embryonic stem cells. *Biomaterials* **31**, 3244–3252.

Fabrikant, G., Gupta, S., Shivashankar, G. V. and Kozlov, M. M. (2013). Model of T-cell nuclear deformation by the cortical actin layer. *Biophys. J.* **105**, 1316–1323.

Fairley, E. A. L., Riddell, A., Ellis, J. A. and Kendrick-Jones, J. (2002). The cell cycle dependent mislocalisation of emerin may contribute to the Emery-Dreifuss muscular dystrophy phenotype. *J. Cell Sci.* **115**, 341–354.

Falloon, E. A. and Dynlacht, J. R. (2002). Reversible changes in the nuclear lamina induced by hyperthermia. *J. Cell. Biochem.* **86**, 451–460.

Ferreira, H. C., Towbin, B. D., Jegou, T. and Gasser, S. M. (2013). The shelterin protein POT-1 anchors Caenorhabditis elegans telomeres through SUN-1 at the nuclear periphery. *J. Cell Biol.* **203**, 727–735.

Ferri, G., Storti, B. and Bizzarri, R. (2017). Nucleocytoplasmic transport in cells with progerin-induced defective nuclear lamina. *Biophys. Chem.* **229**, 77–83.

Finan, J. D., Leddy, H. A. and Guilak, F. (2011). Osmotic stress alters chromatin condensation and nucleocytoplasmic transport. *Biochem. Biophys. Res. Commun.* **408**, 230–235.

Finlan, L. E., Sproul, D., Thomson, I., Boyle, S., Kerr, E., Perry, P., Ylstra, B., Chubb, J. R. and Bickmore, W. A. (2008). Recruitment to the nuclear periphery can alter expression of genes in human cells. *PLoS Genet.* **4**, e1000039.

Fischer, R. S., Myers, K. A., Gardel, M. L. and Waterman, C. M. (2012). Stiffness-controlled three-dimensional extracellular matrices for high-resolution imaging of cell behavior. *Nat. Protoc.* **7**, 2056–2066.

Folkman, J. and Moscona, A. (1978). Role of cell shape in growth control. *Nature* **273**, 345–349.

Foster, H. A., Abeydeera, L. R., Griffin, D. K. and Bridger, J. M. (2005). Non-random chromosome positioning in mammalian sperm nuclei, with migration of the sex chromosomes during late spermatogenesis. *J. Cell Sci.* **118**, 1811–1820.

Foster, H. A., Griffin, D. K. and Bridger, J. M. (2012). Interphase chromosome positioning in in vitro porcine cells and ex vivo porcine tissues. *BMC Cell Biol.* **13**, 30.

Frantz, C., Stewart, K. M. and Weaver, V. M. (2010). The extracellular matrix at a glance. *J. Cell Sci.* **123**, 4195–4200.

Fraser, P. and Bickmore, W. (2007). Nuclear organization of the genome and the potential for gene regulation. *Nature* **447**, 413–417.

Furukawa, K., Sugiyama, S., Osouda, S., Goto, H., Inagaki, M., Horigome, T., Omata, S., McConnell, M., Fisher, P. A. and Nishida, Y. (2003). Barrier-to-autointegration factor plays crucial roles in cell cycle progression and nuclear organization in Drosophila. *J. Cell Sci.* **116**, 3811–3823.

Futcher, B. (1996). Cyclins and the wiring of the yeast cell cycle. *Yeast* **12**, 1635–1646.**Gadea, G. and Blangy, A.** (2014). Dock-family exchange factors in cell migration and disease. *Eur. J. Cell Biol.* **93**, 466–477.

Gauvin, T. J., Young, L. E. and Higgs, H. N. (2015). The formin FMNL3 assembles plasma membrane protrusions that participate in cell-cell adhesion. *Mol. Biol. Cell* **26**, 467–477.

Georges, P. C. and Janmey, P. A. (2005). Cell type-specific response to growth on soft materials. *J. Appl. Physiol.* **98**, 1547–1553.

Georges, P. C., Miller, W. J., Meaney, D. F., Sawyer, E. S. and Janmey, P. A. (2006). Matrices with compliance comparable to that of brain tissue select neuronal over glial growth in mixed cortical cultures. *Biophys. J.* **90**, 3012–3018.

Gerace, L. and Burke, B. (1988). Functional organization of the nuclear envelope. *Annu. Rev. Cell Biol.* **4**, 335–374.

Gerashchenko, M. V., Chernoivanenko, I. S., Moldaver, M. V. and Minin, A. A. (2009). Dynein is a motor for nuclear rotation while vimentin IFs is a "brake". *Cell Biol. Int.* **33**, 1057–1064.

Gesson, K., Rescheneder, P., Skoruppa, M. P., von Haeseler, A., Dechat, T. and Foisner, R. (2016). A-type lamins bind both hetero- and euchromatin, the latter being regulated by lamina-associated polypeptide 2 alpha. *Genome Res.* **26**, 462–473.

Ghosh, S., Liu, B., Wang, Y., Hao, Q. and Zhou, Z. (2015). Lamin A Is an Endogenous SIRT6 Activator and Promotes SIRT6-Mediated DNA Repair. *Cell Rep.* **13**, 1396–1406.

Giancotti, F. G. and Ruoslahti, E. (1999). Integrin signaling. *Science* **285**, 1028–1032.

Gibbs-Seymour, I., Markiewicz, E., Bekker-Jensen, S., Mailand, N. and Hutchison, C. J. (2015). Lamin A/C-dependent interaction with 53BP1 promotes cellular responses to DNA

damage. *Aging Cell* **14**, 162–169.

Göndör, A. and Ohlsson, R. (2009). Chromosome crosstalk in three dimensions. *Nature* **461**, 212–217.

Gospodarowicz, D., Greenburg, G. and Birdwell, C. R. (1978). Determination of cellular shape by the extracellular matrix and its correlation with the control of cellular growth. *Cancer Res.* **38**, 4155–4171.

Gruenbaum, Y. and Medalia, O. (2015). Lamins: the structure and protein complexes. *Curr. Opin. Cell Biol.* **32**, 7–12.

Gu, Y. (2018). The nuclear pore complex: a strategic platform for regulating cell signaling. *New Phytol.* **219**, 25–30.

Guelen, L., Pagie, L., Brasset, E., Meuleman, W., Faza, M. B., Talhout, W., Eussen, B. H., de Klein, A., Wessels, L., de Laat, W., et al. (2008). Domain organization of human chromosomes revealed by mapping of nuclear lamina interactions. *Nature* **453**, 948–951.

Guilluy, C., Osborne, L. D., Van Landeghem, L., Sharek, L., Superfine, R., Garcia-Mata, R. and Burridge, K. (2014). Isolated nuclei adapt to force and reveal a mechanotransduction pathway in the nucleus. *Nat. Cell Biol.* **16**, 376–381.

Guo, Y., Kim, Y., Shimi, T., Goldman, R. D. and Zheng, Y. (2014). Concentration-dependent lamin assembly and its roles in the localization of other nuclear proteins. *Mol. Biol. Cell* **25**, 1287–1297.

Haddad, N. and Paulin-Levasseur, M. (2008). Effects of heat shock on the distribution and expression levels of nuclear proteins in HeLa S3 cells. *J. Cell. Biochem.* **105**, 1485–1500.

Hale, C. M., Shrestha, A. L., Khatau, S. B., Stewart-Hutchinson, P. J., Hernandez, L., Stewart, C. L., Hodzic, D. and Wirtz, D. (2008). Dysfunctional connections between the nucleus and the actin and microtubule networks in laminopathic models. *Biophys. J.* **95**, 5462–5475.

Hanley, P. J., Xu, Y., Kronlage, M., Grobe, K., Schön, P., Song, J., Sorokin, L., Schwab, A. and Bähler, M. (2010). Motorized RhoGAP myosin IXb (Myo9b) controls cell shape and motility. *Proc Natl Acad Sci USA* **107**, 12145–12150.

Haraguchi, T., Holaska, J. M., Yamane, M., Koujin, T., Hashiguchi, N., Mori, C., Wilson, K. L. and Hiraoka, Y. (2004). Emerin binding to Btf, a death-promoting transcriptional repressor, is disrupted by a missense mutation that causes Emery-Dreifuss muscular dystrophy. *Eur. J. Biochem.* **271**, 1035–1045.

Harikumar, A. and Meshorer, E. (2015). Chromatin remodeling and bivalent histone modifications in embryonic stem cells. *EMBO Rep.* **16**, 1609–1619.

Harris, H. (1967). The reactivation of the red cell nucleus. *J. Cell Sci.* **2**, 23–32.

Hattori, N., Niwa, T., Kimura, K., Helin, K. and Ushijima, T. (2013). Visualization of

multivalent histone modification in a single cell reveals highly concerted epigenetic changes on differentiation of embryonic stem cells. *Nucleic Acids Res.* **41**, 7231–7239.

Heessen, S. and Fornerod, M. (2007). The inner nuclear envelope as a transcription factor resting place. *EMBO Rep.* **8**, 914–919.

Hengsberger, S., Kulik, A. and Zysset, P. (2002). Nanoindentation discriminates the elastic properties of individual human bone lamellae under dry and physiological conditions. *Bone* **30**, 178–184.

Hernandez, L., Roux, K. J., Wong, E. S. M., Mounkes, L. C., Mutalif, R., Navasankari, R., Rai, B., Cool, S., Jeong, J.-W., Wang, H., et al. (2010). Functional coupling between the extracellular matrix and nuclear lamina by Wnt signaling in progeria. *Dev. Cell* **19**, 413–425.

Hezwani, M. and Fahrenkrog, B. (2017). The functional versatility of the nuclear pore complex proteins. *Semin. Cell Dev. Biol.* **68**, 2–9.

Higuchi, S., Watanabe, T. M., Kawauchi, K., Ichimura, T. and Fujita, H. (2014). Culturing of mouse and human cells on soft substrates promote the expression of stem cell markers. *J. Biosci. Bioeng.* **117**, 749–755.

Ho, C. Y., Jaalouk, D. E., Vartiainen, M. K. and Lammerding, J. (2013). Lamin A/C and emerin regulate MKL1-SRF activity by modulating actin dynamics. *Nature* **497**, 507–511.

Hofmann, W. A., Johnson, T., Klapczynski, M., Fan, J.-L. and de Lanerolle, P. (2006). From transcription to transport: emerging roles for nuclear myosin I. *Biochem. Cell Biol.* **84**, 418–426.

Holaska, J. M. and Wilson, K. L. (2007). An emerin "proteome": purification of distinct emerin-containing complexes from HeLa cells suggests molecular basis for diverse roles including gene regulation, mRNA splicing, signaling, mechanosensing, and nuclear architecture. *Biochemistry* **46**, 8897–8908.

Holaska, J. M., Lee, K. K., Kowalski, A. K. and Wilson, K. L. (2003). Transcriptional repressor germ cell-less (GCL) and barrier to autointegration factor (BAF) compete for binding to emerin in vitro. *J. Biol. Chem.* **278**, 6969–6975.

Holaska, J. M., Kowalski, A. K. and Wilson, K. L. (2004). Emerin caps the pointed end of actin filaments: evidence for an actin cortical network at the nuclear inner membrane. *PLoS Biol.* **2**, E231.

Holaska, J. M., Rais-Bahrami, S. and Wilson, K. L. (2006). Lmo7 is an emerin-binding protein that regulates the transcription of emerin and many other muscle-relevant genes. *Hum. Mol. Genet.* **15**, 3459–3472.

Horn, H. F., Kim, D. I., Wright, G. D., Wong, E. S. M., Stewart, C. L., Burke, B. and Roux, K. J. (2013). A mammalian KASH domain protein coupling meiotic chromosomes to the cytoskeleton. *J. Cell Biol.* **202**, 1023–1039.

Hu, Y., Plutz, M. and Belmont, A. S. (2010). Hsp70 gene association with nuclear speckles is Hsp70 promoter specific. *J. Cell Biol.* **191**, 711–719.

Huang, D. W., Sherman, B. T. and Lempicki, R. A. (2009a). Systematic and integrative analysis of large gene lists using DAVID bioinformatics resources. *Nat. Protoc.* **4**, 44–57.

Huang, D. W., Sherman, B. T. and Lempicki, R. A. (2009b). Bioinformatics enrichment tools: paths toward the comprehensive functional analysis of large gene lists. *Nucleic Acids Res.* **37**, 1–13.

Imai, S., Nishibayashi, S., Takao, K., Tomifuji, M., Fujino, T., Hasegawa, M. and Takano, T. (1997). Dissociation of Oct-1 from the nuclear peripheral structure induces the cellular aging-associated collagenase gene expression. *Mol. Biol. Cell* **8**, 2407–2419.

Imamoto, N. and Kose, S. (2012). Heat-shock stress activates a novel nuclear import pathway mediated by Hikeshi. *Nucleus* **3**, 422–428.

Ingber, D. E. (2006). Cellular mechanotransduction: putting all the pieces together again. *FASEB J.* **20**, 811–827.

Ingber, D. E., Madri, J. A. and Jamieson, J. D. (1981). Role of basal lamina in neoplastic disorganization of tissue architecture. *Proc Natl Acad Sci USA* **78**, 3901–3905.

Irianto, J., Swift, J., Martins, R. P., McPhail, G. D., Knight, M. M., Discher, D. E. and Lee, D. A. (2013). Osmotic challenge drives rapid and reversible chromatin condensation in chondrocytes. *Biophys. J.* **104**, 759–769.

Ishimura, A., Ng, J. K., Taira, M., Young, S. G. and Osada, S.-I. (2006). Man1, an inner nuclear membrane protein, regulates vascular remodeling by modulating transforming growth factor beta signaling. *Development* **133**, 3919–3928.

Ivorra, C., Kubicek, M., González, J. M., Sanz-González, S. M., Alvarez-Barrientos, A., O'Connor, J.-E., Burke, B. and Andrés, V. (2006). A mechanism of AP-1 suppression through interaction of c-Fos with lamin A/C. *Genes Dev.* **20**, 307–320.

Jaalouk, D. E. and Lammerding, J. (2009). Mechanotransduction gone awry. *Nat. Rev. Mol. Cell Biol.* **10**, 63–73.

Jaenisch, R. and Bird, A. (2003). Epigenetic regulation of gene expression: how the genome integrates intrinsic and environmental signals. *Nat. Genet.* **33 Suppl**, 245–254.

Jain, N., Iyer, K. V., Kumar, A. and Shivashankar, G. V. (2013). Cell geometric constraints induce modular gene-expression patterns via redistribution of HDAC3 regulated by actomyosin contractility. *Proc Natl Acad Sci USA* **110**, 11349–11354.

Joddar, B. and Ito, Y. (2013). Artificial niche substrates for embryonic and induced pluripotent stem cell cultures. *J. Biotechnol.* **168**, 218–228.

Johnson, B. R., Nitta, R. T., Frock, R. L., Mounkes, L., Barbie, D. A., Stewart, C. L., Harlow, E. and Kennedy, B. K. (2004). A-type lamins regulate retinoblastoma protein function by

promoting subnuclear localization and preventing proteasomal degradation. *Proc Natl Acad Sci USA* **101**, 9677–9682.

Jolly, C., Morimoto, R., Robert-Nicoud, M. and Vourc'h, C. (1997). HSF1 transcription factor concentrates in nuclear foci during heat shock: relationship with transcription sites. *J. Cell Sci.* **110 (Pt 23)**, 2935–2941.

Jolly, C., Vourc'h, C., Robert-Nicoud, M. and Morimoto, R. I. (1999). Intron-independent association of splicing factors with active genes. *J. Cell Biol.* **145**, 1133–1143.

Jung, H.-J., Nobumori, C., Goulbourne, C. N., Tu, Y., Lee, J. M., Tatar, A., Wu, D., Yoshinaga, Y., de Jong, P. J., Coffinier, C., et al. (2013). Farnesylation of lamin B1 is important for retention of nuclear chromatin during neuronal migration. *Proc Natl Acad Sci USA* **110**, E1923-32.

Kalhor, R., Tjong, H., Jayathilaka, N., Alber, F. and Chen, L. (2011). Genome architectures revealed by tethered chromosome conformation capture and population-based modeling. *Nat. Biotechnol.* **30**, 90–98.

Kaminski, A., Fedorchak, G. R. and Lammerding, J. (2014). The cellular mastermind(?)-mechanotransduction and the nucleus. *Prog. Mol. Biol. Transl. Sci.* **126**, 157–203.

Kanehisa, M. and Goto, S. (2000). KEGG: kyoto encyclopedia of genes and genomes. Nucleic Acids Res. **28**, 27–30.

Kanehisa, M., Sato, Y., Kawashima, M., Furumichi, M. and Tanabe, M. (2016). KEGG as a reference resource for gene and protein annotation. Nucleic Acids Res. **44**, D457-62.

Kanta, J. (2015). Collagen matrix as a tool in studying fibroblastic cell behavior. *Cell Adh. Migr.* **9**, 308–316.

Kantidze, O. L., Velichko, A. K. and Razin, S. V. (2015). Heat Stress-Induced Transcriptional Repression. *Biochemistry Mosc* **80**, 990–993.

Karolchik, D., Hinrichs, A. S., Furey, T. S., Roskin, K. M., Sugnet, C. W., Haussler, D. and Kent, W. J. (2004). The UCSC Table Browser data retrieval tool. *Nucleic Acids Res.* **32**, D493-6.

Khanna, N., Hu, Y. and Belmont, A. S. (2014). HSP70 transgene directed motion to nuclear speckles facilitates heat shock activation. *Curr. Biol.* **24**, 1138–1144.

Khatau, S. B., Hale, C. M., Stewart-Hutchinson, P. J., Patel, M. S., Stewart, C. L., Searson, P. C., Hodzic, D. and Wirtz, D. (2009). A perinuclear actin cap regulates nuclear shape. *Proc Natl Acad Sci USA* **106**, 19017–19022.

Khatau, S. B., Kusuma, S., Hanjaya-Putra, D., Mali, P., Cheng, L., Lee, J. S. H., Gerecht, S. and Wirtz, D. (2012a). The differential formation of the LINC-mediated perinuclear actin cap in pluripotent and somatic cells. *PLoS ONE* **7**, e36689.

Khatau, S. B., Bloom, R. J., Bajpai, S., Razafsky, D., Zang, S., Giri, A., Wu, P.-H., Marchand,

J., Celedon, A., Hale, C. M., et al. (2012b). The distinct roles of the nucleus and nucleus-cytoskeleton connections in three-dimensional cell migration. *Sci. Rep.* **2**, 488.

Kim, J. B. (2005). Three-dimensional tissue culture models in cancer biology. *Semin. Cancer Biol.* **15**, 365–377.

Kim, Y., Sharov, A. A., McDole, K., Cheng, M., Hao, H., Fan, C.-M., Gaiano, N., Ko, M. S. H. and Zheng, Y. (2011). Mouse B-type lamins are required for proper organogenesis but not by embryonic stem cells. *Science* **334**, 1706–1710.

Kind, J. and van Steensel, B. (2014). Stochastic genome-nuclear lamina interactions: modulating roles of Lamin A and BAF. *Nucleus* **5**, 124–130.

Kind, J., Pagie, L., Ortabozkoyun, H., Boyle, S., de Vries, S. S., Janssen, H., Amendola, M., Nolen, L. D., Bickmore, W. A. and van Steensel, B. (2013). Single-cell dynamics of genome-nuclear lamina interactions. *Cell* **153**, 178–192.

Kocgozlu, L., Lavalle, P., Koenig, G., Senger, B., Haikel, Y., Schaaf, P., Voegel, J.-C., Tenenbaum, H. and Vautier, D. (2010). Selective and uncoupled role of substrate elasticity in the regulation of replication and transcription in epithelial cells. *J. Cell Sci.* **123**, 29–39.

Kochin, V., Shimi, T., Torvaldson, E., Adam, S. A., Goldman, A., Pack, C.-G., Melo-Cardenas, J., Imanishi, S. Y., Goldman, R. D. and Eriksson, J. E. (2014). Interphase phosphorylation of lamin A. *J. Cell Sci.* **127**, 2683–2696.

Korfali, N., Wilkie, G. S., Swanson, S. K., Srsen, V., de Las Heras, J., Batrakou, D. G., Malik, P., Zuleger, N., Kerr, A. R. W., Florens, L., et al. (2012). The nuclear envelope proteome differs notably between tissues. *Nucleus* **3**, 552–564.

Kose, S. and Imamoto, N. (2014). Nucleocytoplasmic transport under stress conditions and its role in HSP70 chaperone systems. *Biochim. Biophys. Acta* **1840**, 2953–2960.

Kose, S., Furuta, M. and Imamoto, N. (2012). Hikeshi, a nuclear import carrier for Hsp70s, protects cells from heat shock-induced nuclear damage. *Cell* **149**, 578–589.

Krachmarov, C. P. and Traub, P. (1993). Heat-induced morphological and biochemical changes in the nuclear lamina from Ehrlich ascites tumor cells in vivo. *J. Cell. Biochem.* **52**, 308–319.

Kulashreshtha, M., Mehta, I. S., Kumar, P. and Rao, B. J. (2016). Chromosome territory relocation during DNA repair requires nuclear myosin 1 recruitment to chromatin mediated by ϒ-H2AX signaling. *Nucleic Acids Res.* **44**, 8272–8291.

Kumaran, R. I. and Spector, D. L. (2008). A genetic locus targeted to the nuclear periphery in living cells maintains its transcriptional competence. *J. Cell Biol.* **180**, 51–65.

Kuroda, M., Tanabe, H., Yoshida, K., Oikawa, K., Saito, A., Kiyuna, T., Mizusawa, H. and Mukai, K. (2004). Alteration of chromosome positioning during adipocyte differentiation. *J. Cell Sci.* **117**, 5897–5903.

Labbé, J.-C., McCarthy, E. K. and Goldstein, B. (2004). The forces that position a mitotic

spindle asymmetrically are tethered until after the time of spindle assembly. *J. Cell Biol.* **167**, 245–256.

Lai-Fook, S. J. and Hyatt, R. E. (2000). Effects of age on elastic moduli of human lungs. *J. Appl. Physiol.* **89**, 163–168.

Lammerding, J., Hsiao, J., Schulze, P. C., Kozlov, S., Stewart, C. L. and Lee, R. T. (2005). Abnormal nuclear shape and impaired mechanotransduction in emerin-deficient cells. *J. Cell Biol.* **170**, 781–791.

Langmead, B. and Salzberg, S. L. (2012). Fast gapped-read alignment with Bowtie 2. *Nat. Methods* **9**, 357–359.

Lanzuolo, C., Lo Sardo, F., Diamantini, A. and Orlando, V. (2011). PcG complexes set the stage for epigenetic inheritance of gene silencing in early S phase before replication. *PLoS Genet.* **7**, e1002370.

Le, H. Q., Ghatak, S., Yeung, C.-Y. C., Tellkamp, F., Günschmann, C., Dieterich, C., Yeroslaviz, A., Habermann, B., Pombo, A., Niessen, C. M., et al. (2016). Mechanical regulation of transcription controls Polycomb-mediated gene silencing during lineage commitment. *Nat. Cell Biol.* **18**, 864–875.

Lee, K. K., Haraguchi, T., Lee, R. S., Koujin, T., Hiraoka, Y. and Wilson, K. L. (2001). Distinct functional domains in emerin bind lamin A and DNA-bridging protein BAF. *J. Cell Sci.* **114**, 4567–4573.

Lehner, C. F., Stick, R., Eppenberger, H. M. and Nigg, E. A. (1987). Differential expression of nuclear lamin proteins during chicken development. *J. Cell Biol.* **105**, 577–587.

Leipzig, N. D. and Shoichet, M. S. (2009). The effect of substrate stiffness on adult neural stem cell behavior. *Biomaterials* **30**, 6867–6878.

Li, Y., Chu, J. S., Kurpinski, K., Li, X., Bautista, D. M., Yang, L., Sung, K.-L. P. and Li, S. (2011). Biophysical regulation of histone acetylation in mesenchymal stem cells. *Biophys. J.* **100**, 1902–1909.

Li, Q., Kumar, A., Makhija, E. and Shivashankar, G. V. (2014). The regulation of dynamic mechanical coupling between actin cytoskeleton and nucleus by matrix geometry. *Biomaterials* **35**, 961–969.

Liang, Y., Chiu, P. H., Yip, K. Y. and Chan, S. Y. (2011). Subcellular localization of SUN2 is regulated by lamin A and Rab5. *PLoS ONE* **6**, e20507.

Libotte, T., Zaim, H., Abraham, S., Padmakumar, V. C., Schneider, M., Lu, W., Munck, M., Hutchison, C., Wehnert, M., Fahrenkrog, B., et al. (2005). Lamin A/C-dependent localization of Nesprin-2, a giant scaffolder at the nuclear envelope. *Mol. Biol. Cell* **16**, 3411–3424.

Lieberman-Aiden, E., van Berkum, N. L., Williams, L., Imakaev, M., Ragoczy, T., Telling,

A., Amit, I., Lajoie, B. R., Sabo, P. J., Dorschner, M. O., et al. (2009). Comprehensive mapping of long-range interactions reveals folding principles of the human genome. *Science* **326**, 289–293.

Lin, H.-H., Lin, H.-K., Lin, I.-H., Chiou, Y.-W., Chen, H.-W., Liu, C.-Y., Harn, H. I.-C., Chiu, W.-T., Wang, Y.-K., Shen, M.-R., et al. (2015). Mechanical phenotype of cancer cells: cell softening and loss of stiffness sensing. *Oncotarget* **6**, 20946–20958.

Lin, F., Morrison, J. M., Wu, W. and Worman, H. J. (2005). MAN1, an integral protein of the inner nuclear membrane, binds Smad2 and Smad3 and antagonizes transforming growth factor-beta signaling. *Hum. Mol. Genet.* **14**, 437–445.

Liu, J., Rolef Ben-Shahar, T., Riemer, D., Treinin, M., Spann, P., Weber, K., Fire, A. and Gruenbaum, Y. (2000). Essential roles for Caenorhabditis elegans lamin gene in nuclear organization, cell cycle progression, and spatial organization of nuclear pore complexes. *Mol. Biol. Cell* **11**, 3937–3947.

Lombardi, M. L. and Lammerding, J. (2011). Keeping the LINC: the importance of nucleocytoskeletal coupling in intracellular force transmission and cellular function. *Biochem. Soc. Trans.* **39**, 1729–1734.

Lombardi, M. L., Jaalouk, D. E., Shanahan, C. M., Burke, B., Roux, K. J. and Lammerding, J. (2011). The interaction between nesprins and sun proteins at the nuclear envelope is critical for force transmission between the nucleus and cytoskeleton. *J. Biol. Chem.* **286**, 26743–26753.

Lu, P., Weaver, V. M. and Werb, Z. (2012). The extracellular matrix: a dynamic niche in cancer progression. *J. Cell Biol.* **196**, 395–406.

Lund, E., Oldenburg, A. R., Delbarre, E., Freberg, C. T., Duband-Goulet, I., Eskeland, R., Buendia, B. and Collas, P. (2013). Lamin A/C-promoter interactions specify chromatin state-dependent transcription outcomes. *Genome Res.* **23**, 1580–1589.

Lund, E. G., Duband-Goulet, I., Oldenburg, A., Buendia, B. and Collas, P. (2015). Distinct features of lamin A-interacting chromatin domains mapped by ChIP-sequencing from sonicated or micrococcal nuclease-digested chromatin. *Nucleus* **6**, 30–39.

Luxton, G. W. G., Gomes, E. R., Folker, E. S., Vintinner, E. and Gundersen, G. G. (2010). Linear arrays of nuclear envelope proteins harness retrograde actin flow for nuclear movement. *Science* **329**, 956–959.

Ma, W., Tavakoli, T., Derby, E., Serebryakova, Y., Rao, M. S. and Mattson, M. P. (2008). Cell-extracellular matrix interactions regulate neural differentiation of human embryonic stem cells. *BMC Dev. Biol.* **8**, 90.

Ma, Y., Kanakousaki, K. and Buttitta, L. (2015). How the cell cycle impacts chromatin architecture and influences cell fate. *Front. Genet.* **6**, 19.

Makhija, E., Jokhun, D. S. and Shivashankar, G. V. (2016). Nuclear deformability and telomere dynamics are regulated by cell geometric constraints. *Proc Natl Acad Sci USA* **113**, E32-40.

Makowska, K. A., Hughes, R. E., White, K. J., Wells, C. M. and Peckham, M. (2015). Specific myosins control actin organization, cell morphology, and migration in prostate cancer cells. *Cell Rep.* **13**, 2118–2125.

Malhas, A., Lee, C. F., Sanders, R., Saunders, N. J. and Vaux, D. J. (2007). Defects in lamin B1 expression or processing affect interphase chromosome position and gene expression. *J. Cell Biol.* **176**, 593–603.

Mammoto, A., Connor, K. M., Mammoto, T., Yung, C. W., Huh, D., Aderman, C. M., Mostoslavsky, G., Smith, L. E. H. and Ingber, D. E. (2009). A mechanosensitive transcriptional mechanism that controls angiogenesis. *Nature* **457**, 1103–1108.

Maninová, M., Klímová, Z., Parsons, J. T., Weber, M. J., Iwanicki, M. P. and Vomastek, T. (2013). The reorientation of cell nucleus promotes the establishment of front-rear polarity in migrating fibroblasts. *J. Mol. Biol.* **425**, 2039–2055.

Maniotis, A. J., Chen, C. S. and Ingber, D. E. (1997). Demonstration of mechanical connections between integrins, cytoskeletal filaments, and nucleoplasm that stabilize nuclear structure. *Proc Natl Acad Sci USA* **94**, 849–854.

Markiewicz, E., Tilgner, K., Barker, N., van de Wetering, M., Clevers, H., Dorobek, M., Hausmanowa-Petrusewicz, I., Ramaekers, F. C. S., Broers, J. L. V., Blankesteijn, W. M., et al. (2006). The inner nuclear membrane protein emerin regulates beta-catenin activity by restricting its accumulation in the nucleus. *EMBO J.* **25**, 3275–3285.

Martin, R. M. and Cardoso, M. C. (2010). Chromatin condensation modulates access and binding of nuclear proteins. *FASEB J.* **24**, 1066–1072.

Marullo, F., Cesarini, E., Antonelli, L., Gregoretti, F., Oliva, G. and Lanzuolo, C. (2016). Nucleoplasmic Lamin A/C and Polycomb group of proteins: An evolutionarily conserved interplay. *Nucleus* **7**, 103–111.

Mattout, A. and Meshorer, E. (2010). Chromatin plasticity and genome organization in pluripotent embryonic stem cells. *Curr. Opin. Cell Biol.* **22**, 334–341.

McBeath, R., Pirone, D. M., Nelson, C. M., Bhadriraju, K. and Chen, C. S. (2004). Cell shape, cytoskeletal tension, and RhoA regulate stem cell lineage commitment. *Dev. Cell* **6**, 483–495.

McCord, R. P., Nazario-Toole, A., Zhang, H., Chines, P. S., Zhan, Y., Erdos, M. R., Collins, F. S., Dekker, J. and Cao, K. (2013). Correlated alterations in genome organization, histone methylation, and DNA-lamin A/C interactions in Hutchinson-Gilford progeria syndrome. *Genome Res.* **23**, 260–269.

McGregor, A. L., Hsia, C.-R. and Lammerding, J. (2016). Squish and squeeze-the nucleus as a physical barrier during migration in confined environments. *Curr. Opin. Cell Biol.* **40**, 32–40.

McKee, C. T., Raghunathan, V. K., Nealey, P. F., Russell, P. and Murphy, C. J. (2011). Topographic modulation of the orientation and shape of cell nuclei and their influence on the measured elastic modulus of epithelial cells. *Biophys. J.* **101**, 2139–2146.

McNamara, L. E., Burchmore, R., Riehle, M. O., Herzyk, P., Biggs, M. J. P., Wilkinson, C. D. W., Curtis, A. S. G. and Dalby, M. J. (2012). The role of microtopography in cellular mechanotransduction. *Biomaterials* **33**, 2835–2847.

Meaburn, K. J., Cabuy, E., Bonne, G., Levy, N., Morris, G. E., Novelli, G., Kill, I. R. and Bridger, J. M. (2007). Primary laminopathy fibroblasts display altered genome organization and apoptosis. *Aging Cell* **6**, 139–153.

Meaburn, K. J., Newbold, R. F. and Bridger, J. M. (2008). Positioning of human chromosomes in murine cell hybrids according to synteny. *Chromosoma* **117**, 579–591.

Meaburn, K. J., Gudla, P. R., Khan, S., Lockett, S. J. and Misteli, T. (2009). Disease-specific gene repositioning in breast cancer. *J. Cell Biol.* **187**, 801–812.

Meaburn, K. J., Agunloye, O., Devine, M., Leshner, M., Roloff, G. W., True, L. D. and Misteli, T. (2016). Tissue-of-origin-specific gene repositioning in breast and prostate cancer. *Histochem. Cell Biol.* **145**, 433–446.

Mehta, I. S., Elcock, L. S., Amira, M., Kill, I. R. and Bridger, J. M. (2008). Nuclear motors and nuclear structures containing A-type lamins and emerin: is there a functional link? *Biochem. Soc. Trans.* **36**, 1384–1388.

Mehta, I. S., Amira, M., Harvey, A. J. and Bridger, J. M. (2010). Rapid chromosome territory relocation by nuclear motor activity in response to serum removal in primary human fibroblasts. *Genome Biol.* **11**, R5.

Mehta, I. S., Kulashreshtha, M., Chakraborty, S., Kolthur-Seetharam, U. and Rao, B. J. (2013). Chromosome territories reposition during DNA damage-repair response. *Genome Biol.* **14**, R135.

Melcer, S. and Meshorer, E. (2010). Chromatin plasticity in pluripotent cells. *Essays Biochem.* **48**, 245–262.

Melcer, S., Hezroni, H., Rand, E., Nissim-Rafinia, M., Skoultchi, A., Stewart, C. L., Bustin, M. and Meshorer, E. (2012). Histone modifications and lamin A regulate chromatin protein dynamics in early embryonic stem cell differentiation. *Nat. Commun.* **3**, 910.

Mellad, J. A., Warren, D. T. and Shanahan, C. M. (2011). Nesprins LINC the nucleus and cytoskeleton. *Curr. Opin. Cell Biol.* **23**, 47–54.

Memon, S. B., Lian, L., Gadahi, J. A. and Genlin, W. (2016). Proteomic response of mouse pituitary gland under heat stress revealed active regulation of stress responsive proteins. *J. Therm. Biol.* **61**, 82–90.

Meshorer, E., Yellajoshula, D., George, E., Scambler, P. J., Brown, D. T. and Misteli, T.

(2006). Hyperdynamic plasticity of chromatin proteins in pluripotent embryonic stem cells. *Dev. Cell* **10**, 105–116.

Meuleman, W., Peric-Hupkes, D., Kind, J., Beaudry, J.-B., Pagie, L., Kellis, M., Reinders, M., Wessels, L. and van Steensel, B. (2013). Constitutive nuclear lamina-genome interactions are highly conserved and associated with A/T-rich sequence. *Genome Res.* **23**, 270–280.

Mewborn, S. K., Puckelwartz, M. J., Abuisneineh, F., Fahrenbach, J. P., Zhang, Y., MacLeod, H., Dellefave, L., Pytel, P., Selig, S., Labno, C. M., et al. (2010). Altered chromosomal positioning, compaction, and gene expression with a lamin A/C gene mutation. *PLoS ONE* **5**, e14342.

Miller, R. T. and Janmey, P. A. (2015). Relationship of and cross-talk between physical and biologic properties of the glomerulus. *Curr. Opin. Nephrol. Hypertens.* **24**, 393–400.

Mislow, J. M. K., Holaska, J. M., Kim, M. S., Lee, K. K., Segura-Totten, M., Wilson, K. L. and McNally, E. M. (2002). Nesprin-1alpha self-associates and binds directly to emerin and lamin A in vitro. *FEBS Lett.* **525**, 135–140.

Mitchell, M. J., Denais, C., Chan, M. F., Wang, Z., Lammerding, J. and King, M. R. (2015). Lamin A/C deficiency reduces circulating tumor cell resistance to fluid shear stress. *Am J Physiol, Cell Physiol* **309**, C736-46.

Mootha, V. K., Lindgren, C. M., Eriksson, K.-F., Subramanian, A., Sihag, S., Lehar, J., Puigserver, P., Carlsson, E., Ridderstråle, M., Laurila, E., et al. (2003). PGC-1alpha-responsive genes involved in oxidative phosphorylation are coordinately downregulated in human diabetes. *Nat. Genet.* **34**, 267–273.

Morimoto, R. I. (1998). Regulation of the heat shock transcriptional response: cross talk between a family of heat shock factors, molecular chaperones, and negative regulators. *Genes Dev.* **12**, 3788–3796.

Morimoto, A., Shibuya, H., Zhu, X., Kim, J., Ishiguro, K., Han, M. and Watanabe, Y. (2012). A conserved KASH domain protein associates with telomeres, SUN1, and dynactin during mammalian meiosis. *J. Cell Biol.* **198**, 165–172.

Myant, K., Qiao, X., Halonen, T., Come, C., Laine, A., Janghorban, M., Partanen, J. I., Cassidy, J., Ogg, E.-L., Cammareri, P., et al. (2015). Serine 62-Phosphorylated MYC Associates with Nuclear Lamins and Its Regulation by CIP2A Is Essential for Regenerative Proliferation. *Cell Rep.* **12**, 1019–1031.

Naetar, N. and Foisner, R. (2009). Lamin complexes in the nuclear interior control progenitor cell proliferation and tissue homeostasis. *Cell Cycle* **8**, 1488–1493.

Nagano, A. and Arahata, K. (2000). Nuclear envelope proteins and associated diseases. *Curr. Opin. Neurol.* **13**, 533–539.

Nagayama, K., Yahiro, Y. and Matsumoto, T. (2011). Stress fibers stabilize the position of intranuclear DNA through mechanical connection with the nucleus in vascular smooth muscle cells. *FEBS Lett.* **585**, 3992–3997.

Nagele, R. G., Freeman, T., McMorrow, L., Thomson, Z., Kitson-Wind, K. and Lee, H. y (1999). Chromosomes exhibit preferential positioning in nuclei of quiescent human cells. *J. Cell Sci.* **112 (Pt 4)**, 525–535.

Neumann, F. R. and Nurse, P. (2007). Nuclear size control in fission yeast. *J. Cell Biol.* **179**, 593–600.

Nguyen-Ngoc, K.-V., Cheung, K. J., Brenot, A., Shamir, E. R., Gray, R. S., Hines, W. C., Yaswen, P., Werb, Z. and Ewald, A. J. (2012). ECM microenvironment regulates collective migration and local dissemination in normal and malignant mammary epithelium. *Proc Natl Acad Sci USA* **109**, E2595-604.

Nicolini, C., Belmont, A. S. and Martelli, A. (1986). Critical nuclear DNA size and distribution associated with S phase initiation. Peripheral location of initiation and termination sites. *Cell Biophys.* **8**, 103–117.

Oldenburg, A. R. and Collas, P. (2016). Mapping Nuclear Lamin-Genome Interactions by Chromatin Immunoprecipitation of Nuclear Lamins. *Methods Mol. Biol.* **1411**, 315–324.

Ondrej, V., Lukásová, E., Krejcí, J., Matula, P. and Kozubek, S. (2008). Lamin A/C and polymeric actin in genome organization. *Mol. Cells* **26**, 356–361.

Osmanagic-Myers, S., Dechat, T. and Foisner, R. (2015). Lamins at the crossroads of mechanosignaling. *Genes Dev.* **29**, 225–237.

Oswald, E. S., Chao, P. G., Bulinski, J. C., Ateshian, G. A. and Hung, C. T. (2006). Chondrocyte nuclear response to osmotic loading. *Conf. Proc. IEEE Eng. Med. Biol. Soc.* **1**, 3659–3661.

Pampaloni, F., Reynaud, E. G. and Stelzer, E. H. K. (2007). The third dimension bridges the gap between cell culture and live tissue. *Nat. Rev. Mol. Cell Biol.* **8**, 839–845.

Pan, Z., Yan, C., Peng, R., Zhao, Y., He, Y. and Ding, J. (2012). Control of cell nucleus shapes via micropillar patterns. *Biomaterials* **33**, 1730–1735.

Parada, L. A., McQueen, P. G., Munson, P. J. and Misteli, T. (2002). Conservation of relative chromosome positioning in normal and cancer cells. *Curr. Biol.* **12**, 1692–1697.

Parada, L. A., McQueen, P. G. and Misteli, T. (2004). Tissue-specific spatial organization of genomes. *Genome Biol.* **5**, R44.

Paradisi, M., McClintock, D., Boguslavsky, R. L., Pedicelli, C., Worman, H. J. and Djabali, K. (2005). Dermal fibroblasts in Hutchinson-Gilford progeria syndrome with the lamin A G608G mutation have dysmorphic nuclei and are hypersensitive to heat stress. *BMC Cell Biol.* **6**, 27.

Park, J. S., Chu, J. S., Tsou, A. D., Diop, R., Tang, Z., Wang, A. and Li, S. (2011). The effect of matrix stiffness on the differentiation of mesenchymal stem cells in response to TGF-β. *Biomaterials* **32**, 3921–3930.

Pauli, D., Arrigo, A. P. and Tissières, A. (1992). Heat shock response in Drosophila. *Experientia* **48**, 623–629.

Pekovic, V., Harborth, J., Broers, J. L. V., Ramaekers, F. C. S., van Engelen, B., Lammens, M., von Zglinicki, T., Foisner, R., Hutchison, C. and Markiewicz, E. (2007). Nucleoplasmic LAP2alpha-lamin A complexes are required to maintain a proliferative state in human fibroblasts. *J. Cell Biol.* **176**, 163–172.

Peñalver Bernabé, B., Shin, S., Rios, P. D., Broadbelt, L. J., Shea, L. D. and Seidlits, S. K. (2016). Dynamic transcription factor activity networks in response to independently altered mechanical and adhesive microenvironmental cues. *Integr Biol (Camb)* **8**, 844–860.

Percipalle, P., Fomproix, N., Cavellán, E., Voit, R., Reimer, G., Krüger, T., Thyberg, J., Scheer, U., Grummt, I. and Farrants, A.-K. O. (2006). The chromatin remodelling complex WSTF-SNF2h interacts with nuclear myosin 1 and has a role in RNA polymerase I transcription. *EMBO Rep.* **7**, 525–530.

Peric-Hupkes, D. and van Steensel, B. (2010). Role of the nuclear lamina in genome organization and gene expression. *Cold Spring Harb. Symp. Quant. Biol.* **75**, 517–524.

Peric-Hupkes, D., Meuleman, W., Pagie, L., Bruggeman, S. W. M., Solovei, I., Brugman, W., Gräf, S., Flicek, P., Kerkhoven, R. M., van Lohuizen, M., et al. (2010). Molecular maps of the reorganization of genome-nuclear lamina interactions during differentiation. *Mol. Cell* **38**, 603–613.

Pestic-Dragovich, L., Stojiljkovic, L., Philimonenko, A. A., Nowak, G., Ke, Y., Settlage, R. E., Shabanowitz, J., Hunt, D. F., Hozak, P. and de Lanerolle, P. (2000). A myosin I isoform in the nucleus. *Science* **290**, 337–341.

Pochukalina, G. N., Ilicheva, N. V., Podgornaya, O. I. and Voronin, A. P. (2016). Nucleolus-like body of mouse oocytes contains lamin A and B and TRF2 but not actin and topo II. *Mol. Cytogenet.* **9**, 50.

Politz, J. C. R., Scalzo, D. and Groudine, M. (2013). Something silent this way forms: the functional organization of the repressive nuclear compartment. *Annu. Rev. Cell Dev. Biol.* **29**, 241–270.

Polla, B. S., Stubbe, H., Kantengwa, S., Maridonneau-Parini, I. and Jacquier-Sarlin, M. R. (1995). Differential induction of stress proteins and functional effects of heat shock in human phagocytes. *Inflammation* **19**, 363–378.

Prokocimer, M., Davidovich, M., Nissim-Rafinia, M., Wiesel-Motiuk, N., Bar, D. Z., Barkan, R., Meshorer, E. and Gruenbaum, Y. (2009). Nuclear lamins: key regulators of nuclear structure and activities. *J. Cell. Mol. Med.* **13**, 1059–1085.

Polychronidou, M. and Grobhans, J. (2011). Determining nuclear shape: the role of farnesylated nuclear membrane proteins. *Nucleus* **2**, 17–23.

Rabineau, M., Flick, F., Mathieu, E., Tu, A., Senger, B., Voegel, J.-C., Lavalle, P., Schaaf, P., Freund, J.-N., Haikel, Y., et al. (2015). Cell guidance into quiescent state through chromatin remodeling induced by elastic modulus of substrate. *Biomaterials* **37**, 144–155.

Raices, M. and D'Angelo, M. A. (2017). Nuclear pore complexes and regulation of gene expression. *Curr. Opin. Cell Biol.* **46**, 26–32.

Ramírez, F., Ryan, D. P., Grüning, B., Bhardwaj, V., Kilpert, F., Richter, A. S., Heyne, S., Dündar, F. and Manke, T. (2016). deepTools2: a next generation web server for deep-sequencing data analysis. *Nucleic Acids Res.* **44**, W160-5.

Ranade, D., Koul, S., Thompson, J., Prasad, K. B. and Sengupta, K. (2017). Chromosomal aneuploidies induced upon Lamin B2 depletion are mislocalized in the interphase nucleus. *Chromosoma* **126**, 223–244.

Rao, M. V. and Zaidel-Bar, R. (2016). Formin-mediated actin polymerization at cell-cell junctions stabilizes E-cadherin and maintains monolayer integrity during wound repair. *Mol. Biol. Cell* **27**, 2844–2856.

Razafsky, D. and Hodzic, D. (2009). Bringing KASH under the SUN: the many faces of nucleo-cytoskeletal connections. *J. Cell Biol.* **186**, 461–472.

Reddy, K. L., Zullo, J. M., Bertolino, E. and Singh, H. (2008). Transcriptional repression mediated by repositioning of genes to the nuclear lamina. *Nature* **452**, 243–247.

Reis-Sobreiro, M., Chen, J.-F., Novitskaya, T., You, S., Morley, S., Steadman, K., Gill, N. K., Eskaros, A., Rotinen, M., Chu, C.-Y., et al. (2018). Emerin deregulation links nuclear shape instability to metastatic potential. *Cancer Res.* **78**, 6086–6097.

Reuter, J. A., Ortiz-Urda, S., Kretz, M., Garcia, J., Scholl, F. A., Pasmooij, A. M. G., Cassarino, D., Chang, H. Y. and Khavari, P. A. (2009). Modeling inducible human tissue neoplasia identifies an extracellular matrix interaction network involved in cancer progression. *Cancer Cell* **15**, 477–488.

Richter, K., Haslbeck, M. and Buchner, J. (2010). The heat shock response: life on the verge of death. *Mol. Cell* **40**, 253–266.

Roix, J. J., McQueen, P. G., Munson, P. J., Parada, L. A. and Misteli, T. (2003). Spatial proximity of translocation-prone gene loci in human lymphomas. *Nat. Genet.* **34**, 287–291.

Röber, R. A., Weber, K. and Osborn, M. (1989). Differential timing of nuclear lamin A/C expression in the various organs of the mouse embryo and the young animal: a developmental study. *Development* **105**, 365–378.

Roca-Cusachs, P., Alcaraz, J., Sunyer, R., Samitier, J., Farré, R. and Navajas, D. (2008). Micropatterning of single endothelial cell shape reveals a tight coupling between nuclear volume in G1 and proliferation. *Biophys. J.* **94**, 4984–4995.

Roskelley, C. D., Desprez, P. Y. and Bissell, M. J. (1994). Extracellular matrix-dependent tissue-specific gene expression in mammary epithelial cells requires both physical and biochemical signal transduction. *Proc Natl Acad Sci USA* **91**, 12378–12382.

Rowat, A. C., Lammerding, J. and Ipsen, J. H. (2006). Mechanical properties of the cell nucleus and the effect of emerin deficiency. *Biophys. J.* **91**, 4649–4664.

Rowat, A. C., Jaalouk, D. E., Zwerger, M., Ung, W. L., Eydelnant, I. A., Olins, D. E., Olins, A. L., Herrmann, H., Weitz, D. A. and Lammerding, J. (2013). Nuclear envelope composition determines the ability of neutrophil-type cells to passage through micron-scale constrictions. *J. Biol. Chem.* **288**, 8610–8618.

Rozwadowska, N., Kolanowski, T., Wiland, E., Siatkowski, M., Pawlak, P., Malcher, A., Mietkiewski, T., Olszewska, M. and Kurpisz, M. (2013). Characterisation of nuclear architectural alterations during in vitro differentiation of human stem cells of myogenic origin. *PLoS ONE* **8**, e73231.

Sabò, A., Kress, T. R., Pelizzola, M., de Pretis, S., Gorski, M. M., Tesi, A., Morelli, M. J., Bora, P., Doni, M., Verrecchia, A., et al. (2014). Selective transcriptional regulation by Myc in cellular growth control and lymphomagenesis. *Nature* **511**, 488–492.

Sakaki, M., Koike, H., Takahashi, N., Sasagawa, N., Tomioka, S., Arahata, K. and Ishiura, S. (2001). Interaction between emerin and nuclear lamins. *J. Biochem.* **129**, 321–327.

Sandí, M.-J., Marshall, C. B., Balan, M., Coyaud, É., Zhou, M., Monson, D. M., Ishiyama, N., Chandrakumar, A. A., La Rose, J., Couzens, A. L., et al. (2017). MARK3-mediated phosphorylation of ARHGEF2 couples microtubules to the actin cytoskeleton to establish cell polarity. *Sci. Signal.* **10**,.

Sarge, K. D., Murphy, S. P. and Morimoto, R. I. (1993). Activation of heat shock gene transcription by heat shock factor 1 involves oligomerization, acquisition of DNA-binding activity, and nuclear localization and can occur in the absence of stress. *Mol. Cell. Biol.* **13**, 1392–1407.

Sato, S., Burgess, S. B. and McIlwain, D. L. (1994). Transcription and motoneuron size. *J. Neurochem.* **63**, 1609–1615.

Scherthan, H., Sfeir, A. and de Lange, T. (2011). Rap1-independent telomere attachment and bouquet formation in mammalian meiosis. *Chromosoma* **120**, 151–157.

Schmidt, E. E. and Schibler, U. (1995). Cell size regulation, a mechanism that controls cellular RNA accumulation: consequences on regulation of the ubiquitous transcription factors Oct1 and NF-Y and the liver-enriched transcription factor DBP. *J. Cell Biol.* **128**, 467–483.

Schneider, C. A., Rasband, W. S. and Eliceiri, K. W. (2012). NIH Image to ImageJ: 25 years of image analysis. *Nat. Methods* **9**, 671–675.

Schoenfelder, S., Sexton, T., Chakalova, L., Cope, N. F., Horton, A., Andrews, S., Kurukuti, S., Mitchell, J. A., Umlauf, D., Dimitrova, D. S., et al. (2010). Preferential associations between co-regulated genes reveal a transcriptional interactome in erythroid cells. *Nat. Genet.* **42**, 53–61.

Sen Gupta, A. and Sengupta, K. (2017). Lamin B2 modulates nucleolar morphology, dynamics, and function. *Mol. Cell. Biol.* **37**, e00274-17.

Sengupta, K., Upender, M. B., Barenboim-Stapleton, L., Nguyen, Q. T., Wincovitch, S. M., Garfield, S. H., Difilippantonio, M. J. and Ried, T. (2007). Artificially introduced aneuploid chromosomes assume a conserved position in colon cancer cells. *PLoS ONE* **2**, e199.

Sengupta, K., Camps, J., Mathews, P., Barenboim-Stapleton, L., Nguyen, Q. T., Difilippantonio, M. J. and Ried, T. (2008). Position of human chromosomes is conserved in mouse nuclei indicating a species-independent mechanism for maintaining genome organization. *Chromosoma* **117**, 499–509.

Shimi, T., Pfleghaar, K., Kojima, S., Pack, C.-G., Solovei, I., Goldman, A. E., Adam, S. A., Shumaker, D. K., Kinjo, M., Cremer, T., et al. (2008). The A- and B-type nuclear lamin networks: microdomains involved in chromatin organization and transcription. *Genes Dev.* **22**, 3409–3421.

Shimi, T., Butin-Israeli, V. and Goldman, R. D. (2012). The functions of the nuclear envelope in mediating the molecular crosstalk between the nucleus and the cytoplasm. *Curr. Opin. Cell Biol.* **24**, 71–78.

Shimi, T., Kittisopikul, M., Tran, J., Goldman, A. E., Adam, S. A., Zheng, Y., Jaqaman, K. and Goldman, R. D. (2015). Structural organization of nuclear lamins A, C, B1, and B2 revealed by superresolution microscopy. *Mol. Biol. Cell* **26**, 4075–4086.

Shin, K.-J., Kim, Y. L., Lee, S., Kim, D.-K., Ahn, C., Chung, J., Seong, J. Y. and Hwang, J.-I. (2009). Lysophosphatidic acid signaling through LPA receptor subtype 1 induces colony scattering of gastrointestinal cancer cells. *J. Cancer Res. Clin. Oncol.* **135**, 45–52.

Shumaker, D. K., Solimando, L., Sengupta, K., Shimi, T., Adam, S. A., Grunwald, A., Strelkov, S. V., Aebi, U., Cardoso, M. C. and Goldman, R. D. (2008). The highly conserved nuclear lamin Ig-fold binds to PCNA: its role in DNA replication. *J. Cell Biol.* **181**, 269–280.

Slater, D. N., Rice, S., Stewart, R., Melling, S. E., Hewer, E. M. and Smith, J. H. F. (2005). Proposed Sheffield quantitative criteria in cervical cytology to assist the grading of squamous cell dyskaryosis, as the British Society for Clinical Cytology definitions require amendment. *Cytopathology* **16**, 179–192.

Simon, D. N., Zastrow, M. S. and Wilson, K. L. (2010). Direct actin binding to A- and B-type

lamin tails and actin filament bundling by the lamin A tail. *Nucleus* **1**, 264–272.

Singh, M., Hunt, C. R., Pandita, R. K., Kumar, R., Yang, C.-R., Horikoshi, N., Bachoo, R., Serag, S., Story, M. D., Shay, J. W., et al. (2013). Lamin A/C depletion enhances DNA damage-induced stalled replication fork arrest. *Mol. Cell. Biol.* **33**, 1210–1222.

Smith, D. E. and Fisher, P. A. (1984). Identification, developmental regulation, and response to heat shock of two antigenically related forms of a major nuclear envelope protein in Drosophila embryos: application of an improved method for affinity purification of antibodies using polypeptides immobilized on nitrocellulose blots. *J. Cell Biol.* **99**, 20–28.

Smith, D. E., Gruenbaum, Y., Berrios, M. and Fisher, P. A. (1987). Biosynthesis and interconversion of Drosophila nuclear lamin isoforms during normal growth and in response to heat shock. *J. Cell Biol.* **105**, 771–790.

Smith, E. R., Meng, Y., Moore, R., Tse, J. D., Xu, A. G. and Xu, X.-X. (2017). Nuclear envelope structural proteins facilitate nuclear shape changes accompanying embryonic differentiation and fidelity of gene expression. *BMC Cell Biol.* **18**, 8.

Snyers, L. and Schöfer, C. (2008). Lamina-associated polypeptide 2alpha forms complexes with heat shock proteins Hsp70 and Hsc70 in vivo. *Biochem. Biophys. Res. Commun.* **368**, 767–771.

Somech, R., Shaklai, S., Amariglio, N., Rechavi, G. and Simon, A. J. (2005). Nuclear envelopathies--raising the nuclear veil. *Pediatr. Res.* **57**, 8R–15R.

Spann, T. P., Goldman, A. E., Wang, C., Huang, S. and Goldman, R. D. (2002). Alteration of nuclear lamin organization inhibits RNA polymerase II-dependent transcription. *J. Cell Biol.* **156**, 603–608.

Sproul, D., Gilbert, N. and Bickmore, W. A. (2005). The role of chromatin structure in regulating the expression of clustered genes. *Nat. Rev. Genet.* **6**, 775–781.

Stark, C., Breitkreutz, B.-J., Reguly, T., Boucher, L., Breitkreutz, A. and Tyers, M. (2006). BioGRID: a general repository for interaction datasets. *Nucleic Acids Res.* **34**, D535-9.

Starr, D. A., Hermann, G. J., Malone, C. J., Fixsen, W., Priess, J. R., Horvitz, H. R. and Han, M. (2001). unc-83 encodes a novel component of the nuclear envelope and is essential for proper nuclear migration. *Development* **128**, 5039–5050.

Steinberg, G. and McIntosh, J. R. (1998). Effects of the myosin inhibitor 2,3-butanedione monoxime on the physiology of fission yeast. *Eur. J. Cell Biol.* **77**, 284–293.

Stephens, A. D., Banigan, E. J., Adam, S. A., Goldman, R. D. and Marko, J. F. (2017). Chromatin and lamin A determine two different mechanical response regimes of the cell nucleus. *Mol. Biol. Cell* **28**, 1984–1996.

Stephens, A. D., Banigan, E. J. and Marko, J. F. (2018a). Separate roles for chromatin and lamins in nuclear mechanics. *Nucleus* **9**, 119–124.

Stephens, A. D., Liu, P. Z., Banigan, E. J., Almassalha, L. M., Backman, V., Adam, S. A., Goldman, R. D. and Marko, J. F. (2018b). Chromatin histone modifications and rigidity affect nuclear morphology independent of lamins. *Mol. Biol. Cell* **29**, 220–233.

Stern, M. M., Myers, R. L., Hammam, N., Stern, K. A., Eberli, D., Kritchevsky, S. B., Soker, S. and Van Dyke, M. (2009). The influence of extracellular matrix derived from skeletal muscle tissue on the proliferation and differentiation of myogenic progenitor cells ex vivo. *Biomaterials* **30**, 2393–2399.

Stetler, R. A., Gan, Y., Zhang, W., Liou, A. K., Gao, Y., Cao, G. and Chen, J. (2010). Heat shock proteins: cellular and molecular mechanisms in the central nervous system. *Prog. Neurobiol.* **92**, 184–211.

Stewart, C. L. and Burke, B. (2014). The missing LINC: a mammalian KASH-domain protein coupling meiotic chromosomes to the cytoskeleton. *Nucleus* **5**, 3–10.

Stick, R. and Hausen, P. (1985). Changes in the nuclear lamina composition during early development of Xenopus laevis. *Cell* **41**, 191–200.

Subramanian, A., Tamayo, P., Mootha, V. K., Mukherjee, S., Ebert, B. L., Gillette, M. A., Paulovich, A., Pomeroy, S. L., Golub, T. R., Lander, E. S., et al. (2005). Gene set enrichment analysis: a knowledge-based approach for interpreting genome-wide expression profiles. *Proc Natl Acad Sci USA* **102**, 15545–15550.

Sun, H. B., Shen, J. and Yokota, H. (2000). Size-dependent positioning of human chromosomes in interphase nuclei. *Biophys. J.* **79**, 184–190.

Swift, J. and Discher, D. E. (2014). The nuclear lamina is mechano-responsive to ECM elasticity in mature tissue. *J. Cell Sci.* **127**, 3005–3015.

Swift, J., Ivanovska, I. L., Buxboim, A., Harada, T., Dingal, P. C. D. P., Pinter, J., Pajerowski, J. D., Spinler, K. R., Shin, J.-W., Tewari, M., et al. (2013). Nuclear lamin-A scales with tissue stiffness and enhances matrix-directed differentiation. *Science* **341**, 1240104.

Szklarczyk, D., Franceschini, A., Wyder, S., Forslund, K., Heller, D., Huerta-Cepas, J., Simonovic, M., Roth, A., Santos, A., Tsafou, K. P., et al. (2015). STRING v10: protein-protein interaction networks, integrated over the tree of life. *Nucleic Acids Res.* **43**, D447-52.

Taimen, P., Pfleghaar, K., Shimi, T., Möller, D., Ben-Harush, K., Erdos, M. R., Adam, S. A., Herrmann, H., Medalia, O., Collins, F. S., et al. (2009). A progeria mutation reveals functions for lamin A in nuclear assembly, architecture, and chromosome organization. *Proc Natl Acad Sci USA* **106**, 20788–20793.

Talwar, S., Kumar, A., Rao, M., Menon, G. I. and Shivashankar, G. V. (2013). Correlated spatio-temporal fluctuations in chromatin compaction states characterize stem cells. *Biophys. J.* **104**, 553–564.

Tanabe, H., Müller, S., Neusser, M., von Hase, J., Calcagno, E., Cremer, M., Solovei, I.,

Cremer, C. and Cremer, T. (2002). Evolutionary conservation of chromosome territory arrangements in cell nuclei from higher primates. *Proc Natl Acad Sci USA* **99**, 4424–4429.

Tanguay, R. M. (1983). Genetic regulation during heat shock and function of heat-shock proteins: a review. *Can. J. Biochem. Cell Biol.* **61**, 387–394.

Taniura, H., Glass, C. and Gerace, L. (1995). A chromatin binding site in the tail domain of nuclear lamins that interacts with core histones. *J. Cell Biol.* **131**, 33–44.

Tapley, E. C. and Starr, D. A. (2013). Connecting the nucleus to the cytoskeleton by SUN-KASH bridges across the nuclear envelope. *Curr. Opin. Cell Biol.* **25**, 57–62.

Taranum, S., Vaylann, E., Meinke, P., Abraham, S., Yang, L., Neumann, S., Karakesisoglou, I., Wehnert, M. and Noegel, A. A. (2012). LINC complex alterations in DMD and EDMD/CMT fibroblasts. *Eur. J. Cell Biol.* **91**, 614–628.

Teixeira, A. I., Ilkhanizadeh, S., Wigenius, J. A., Duckworth, J. K., Inganäs, O. and Hermanson, O. (2009). The promotion of neuronal maturation on soft substrates. *Biomaterials* **30**, 4567–4572.

Thomson, I., Gilchrist, S., Bickmore, W. A. and Chubb, J. R. (2004). The radial positioning of chromatin is not inherited through mitosis but is established de novo in early G1. *Curr. Biol.* **14**, 166–172.

Tifft, K. E., Bradbury, K. A. and Wilson, K. L. (2009). Tyrosine phosphorylation of nuclear-membrane protein emerin by Src, Abl and other kinases. *J. Cell Sci.* **122**, 3780–3790.

Tkachenko, E., Gutierrez, E., Saikin, S. K., Fogelstrand, P., Kim, C., Groisman, A. and Ginsberg, M. H. (2013). The nucleus of endothelial cell as a sensor of blood flow direction. *Biol. Open* **2**, 1007–1012.

Trapnell, C., Pachter, L. and Salzberg, S. L. (2009). TopHat: discovering splice junctions with RNA-Seq. *Bioinformatics* **25**, 1105–1111.

Trapnell, C., Williams, B. A., Pertea, G., Mortazavi, A., Kwan, G., van Baren, M. J., Salzberg, S. L., Wold, B. J. and Pachter, L. (2010). Transcript assembly and quantification by RNA-Seq reveals unannotated transcripts and isoform switching during cell differentiation. *Nat. Biotechnol.* **28**, 511–515.

van Berkum, N. L., Lieberman-Aiden, E., Williams, L., Imakaev, M., Gnirke, A., Mirny, L. A., Dekker, J. and Lander, E. S. (2010). Hi-C: a method to study the three-dimensional architecture of genomes. *J. Vis. Exp.*

van de Corput, M. P. C., de Boer, E., Knoch, T. A., van Cappellen, W. A., Quintanilla, A., Ferrand, L. and Grosveld, F. G. (2012). Super-resolution imaging reveals three-dimensional folding dynamics of the β-globin locus upon gene activation. *J. Cell Sci.* **125**, 4630–4639.

Vanderwaal, R. P., Maggi, L. B., Weber, J. D., Hunt, C. R. and Roti Roti, J. L. (2009). Nucleophosmin redistribution following heat shock: a role in heat-induced radiosensitization.

Cancer Res. **69**, 6454–6462.

Vaughan, A., Alvarez-Reyes, M., Bridger, J. M., Broers, J. L., Ramaekers, F. C., Wehnert, M., Morris, G. E., Whitfield WGF and Hutchison, C. J. (2001). Both emerin and lamin C depend on lamin A for localization at the nuclear envelope. *J. Cell Sci.* **114**, 2577–2590.

Velichko, A. K., Markova, E. N., Petrova, N. V., Razin, S. V. and Kantidze, O. L. (2013). Mechanisms of heat shock response in mammals. *Cell. Mol. Life Sci.* **70**, 4229–4241.

Versaevel, M., Grevesse, T. and Gabriele, S. (2012). Spatial coordination between cell and nuclear shape within micropatterned endothelial cells. *Nat. Commun.* **3**, 671.

Viale-Bouroncle, S., Gosau, M., Küpper, K., Möhl, C., Brockhoff, G., Reichert, T. E., Schmalz, G., Ettl, T. and Morsczeck, C. (2012). Rigid matrix supports osteogenic differentiation of stem cells from human exfoliated deciduous teeth (SHED). *Differentiation.* **84**, 366–370.

Vishavkarma, R., Raghavan, S., Kuyyamudi, C., Majumder, A., Dhawan, J. and Pullarkat, P. A. (2014). Role of actin filaments in correlating nuclear shape and cell spreading. *PLoS ONE* **9**, e107895.

Villalobos, D. P., Bautista, R., Canovas, F., M. and Claros, M., G. (2004). Isolation of bacterial artificial chromosome DNA by means of improved alkaline lysis and double potassium acetate precipitation. *Plant Mol Biol Rep.* **22,** 1-7.

Volpi, E. V., Chevret, E., Jones, T., Vatcheva, R., Williamson, J., Beck, S., Campbell, R. D., Goldsworthy, M., Powis, S. H., Ragoussis, J., et al. (2000). Large-scale chromatin organization of the major histocompatibility complex and other regions of human chromosome 6 and its response to interferon in interphase nuclei. *J. Cell Sci.* **113 (Pt 9)**, 1565–1576.

Walters, B. D. and Stegemann, J. P. (2014). Strategies for directing the structure and function of three-dimensional collagen biomaterials across length scales. *Acta Biomater.* **10**, 1488–1501.

Wang, H. B., Dembo, M. and Wang, Y. L. (2000). Substrate flexibility regulates growth and apoptosis of normal but not transformed cells. *Am J Physiol, Cell Physiol* **279**, C1345-50.

Wang, J. H. C. and Thampatty, B. P. (2006). An introductory review of cell mechanobiology. *Biomech. Model. Mechanobiol.* **5**, 1–16.

Wang, Y., Nagarajan, M., Uhler, C. and Shivashankar, G. V. (2017). Orientation and repositioning of chromosomes correlate with cell geometry-dependent gene expression. *Mol Biol Cell.* **28(14)**, 1997-2009.

Wang, P.-Y., Yu, J., Lin, J.-H. and Tsai, W.-B. (2011). Modulation of alignment, elongation and contraction of cardiomyocytes through a combination of nanotopography and rigidity of substrates. *Acta Biomater.* **7**, 3285–3293.

Wang, Y., Maharana, S., Wang, M. D. and Shivashankar, G. V. (2014). Super-resolution microscopy reveals decondensed chromatin structure at transcription sites. *Sci. Rep.* **4**, 4477.

Wanzel, M., Herold, S. and Eilers, M. (2003). Transcriptional repression by Myc. *Trends Cell Biol.* **13**, 146–150.

Wassenaar, P. A., Eleswarpu, C. N., Schroeder, S. A., Mo, X., Raterman, B. D., White, R. D. and Kolipaka, A. (2016). Measuring age-dependent myocardial stiffness across the cardiac cycle using MR elastography: A reproducibility study. *Magn. Reson. Med.* **75**, 1586–1593.

Watt, F. M., Jordan, P. W. and O'Neill, C. H. (1988). Cell shape controls terminal differentiation of human epidermal keratinocytes. *Proc Natl Acad Sci USA* **85**, 5576–5580.

Wiegert, J. S. and Bading, H. (2011). Activity-dependent calcium signaling and ERK-MAP kinases in neurons: a link to structural plasticity of the nucleus and gene transcription regulation. *Cell Calcium* **49**, 296–305.

Williams, G. T. and Morimoto, R. I. (1990). Maximal stress-induced transcription from the human HSP70 promoter requires interactions with the basal promoter elements independent of rotational alignment. *Mol. Cell. Biol.* **10**, 3125–3136.

Williams, R. R. E., Broad, S., Sheer, D. and Ragoussis, J. (2002). Subchromosomal positioning of the epidermal differentiation complex (EDC) in keratinocyte and lymphoblast interphase nuclei. *Exp. Cell Res.* **272**, 163–175.

Willsie, J. K. and Clegg, J. S. (2002). Small heat shock protein p26 associates with nuclear lamins and HSP70 in nuclei and nuclear matrix fractions from stressed cells. *J. Cell. Biochem.* **84**, 601–614.

Wilschut, K. J., Haagsman, H. P. and Roelen, B. A. J. (2010). Extracellular matrix components direct porcine muscle stem cell behavior. *Exp. Cell Res.* **316**, 341–352.

Wilson, K. L. and Berk, J. M. (2010). The nuclear envelope at a glance. *J. Cell Sci.* **123**, 1973–1978.

Wilson, K. L. and Foisner, R. (2010). Lamin-binding Proteins. *Cold Spring Harb. Perspect. Biol.* **2**, a000554.

Winer, J. P., Janmey, P. A., McCormick, M. E. and Funaki, M. (2009). Bone marrow-derived human mesenchymal stem cells become quiescent on soft substrates but remain responsive to chemical or mechanical stimuli. *Tissue Eng. Part A* **15**, 147–154.

Worman, H. J., Ostlund, C. and Wang, Y. (2010). Diseases of the nuclear envelope. *Cold Spring Harb. Perspect. Biol.* **2**, a000760.

Wu, D., Flannery, A. R., Cai, H., Ko, E. and Cao, K. (2014). Nuclear localization signal deletion mutants of lamin A and progerin reveal insights into lamin A processing and emerin targeting. *Nucleus* **5**, 66–74.

Xia, J., Benner, M. J. and Hancock, R. E. W. (2014). NetworkAnalyst--integrative approaches for protein-protein interaction network analysis and visual exploration. *Nucleic Acids Res.* **42**, W167-74.

Xia, J., Gill, E. E. and Hancock, R. E. W. (2015). NetworkAnalyst for statistical, visual and network-based meta-analysis of gene expression data. *Nat. Protoc.* **10**, 823–844.

Xie, W., Chojnowski, A., Boudier, T., Lim, J. S. Y., Ahmed, S., Ser, Z., Stewart, C. and Burke, B. (2016). A-type Lamins Form Distinct Filamentous Networks with Differential Nuclear Pore Complex Associations. *Curr. Biol.* **26**, 2651–2658.

Yamada, K. M., Pankov, R. and Cukierman, E. (2003). Dimensions and dynamics in integrin function. *Braz. J. Med. Biol. Res.* **36**, 959–966.

Yang, L., Munck, M., Swaminathan, K., Kapinos, L. E., Noegel, A. A. and Neumann, S. (2013). Mutations in LMNA modulate the lamin A--Nesprin-2 interaction and cause LINC complex alterations. *PLoS ONE* **8**, e71850.

Yanoma, T., Ogata, K., Yokobori, T., Ide, M., Mochiki, E., Toyomasu, Y., Yanai, M., Kogure, N., Kimura, A., Suzuki, M., et al. (2017). Heat shock-induced HIKESHI protects cell viability via nuclear translocation of heat shock protein 70. *Oncol. Rep.* **38**, 1500–1506.

Ye, Q., Callebaut, I., Pezhman, A., Courvalin, J. C. and Worman, H. J. (1997). Domain-specific interactions of human HP1-type chromodomain proteins and inner nuclear membrane protein LBR. *J. Biol. Chem.* **272**, 14983–14989.

Yen, A. and Pardee, A. B. (1979). Role of nuclear size in cell growth initiation. *Science* **204**, 1315-1317.

Yeung, T., Georges, P. C., Flanagan, L. A., Marg, B., Ortiz, M., Funaki, M., Zahir, N., Ming, W., Weaver, V. and Janmey, P. A. (2005). Effects of substrate stiffness on cell morphology, cytoskeletal structure, and adhesion. *Cell Motil. Cytoskeleton* **60**, 24–34.

Yourek, G., Hussain, M. A. and Mao, J. J. (2007). Cytoskeletal changes of mesenchymal stem cells during differentiation. *ASAIO J.* **53**, 219–228.

Zastrow, M. S., Vlcek, S. and Wilson, K. L. (2004). Proteins that bind A-type lamins: integrating isolated clues. *J. Cell Sci.* **117**, 979–987.

Zhang, T., Cooper, S. and Brockdorff, N. (2015). The interplay of histone modifications - writers that read. *EMBO Rep.* **16**, 1467–1481.

Zheng, X., Kim, Y. and Zheng, Y. (2015). Identification of lamin B-regulated chromatin regions based on chromatin landscapes. *Mol. Biol. Cell* **26**, 2685–2697.

Zhu, W. G., Roberts, Z. V. and Dynlacht, J. R. (1999). Heat-induced modulation of lamin B content in two different cell lines. *J. Cell. Biochem.* **75**, 620–628.

Zink, D., Fischer, A. H. and Nickerson, J. A. (2004). Nuclear structure in cancer cells. *Nat. Rev. Cancer* **4**, 677–687.

Zink, D., Amaral, M. D., Englmann, A., Lang, S., Clarke, L. A., Rudolph, C., Alt, F., Luther, K., Braz, C., Sadoni, N., et al. (2004). Transcription-dependent spatial arrangements of CFTR and adjacent genes in human cell nuclei. *J. Cell Biol.* **166**, 815–825.

Zinner, R., Albiez, H., Walter, J., Peters, A. H. F. M., Cremer, T. and Cremer, M. (2006). Histone lysine methylation patterns in human cell types are arranged in distinct three-dimensional nuclear zones. *Histochem. Cell Biol.* **125**, 3–19.

Zuleger, N., Boyle, S., Kelly, D. A., de las Heras, J. I., Lazou, V., Korfali, N., Batrakou, D. G., Randles, K. N., Morris, G. E., Harrison, D. J., et al. (2013). Specific nuclear envelope transmembrane proteins can promote the location of chromosomes to and from the nuclear periphery. *Genome Biol.* **14**, R14.

Zullo, J. M., Demarco, I. A., Piqué-Regi, R., Gaffney, D. J., Epstein, C. B., Spooner, C. J., Luperchio, T. R., Bernstein, B. E., Pritchard, J. K., Reddy, K. L., et al. (2012). DNA sequence-dependent compartmentalization and silencing of chromatin at the nuclear lamina. *Cell* **149**, 1474–1487.

Zwerger, M., Roschitzki-Voser, H., Zbinden, R., Denais, C., Herrmann, H., Lammerding, J., Grütter, M. G. and Medalia, O. (2015). Altering lamina assembly reveals lamina-dependent and -independent functions for A-type lamins. *J. Cell Sci.* **128**, 3607–3620.

Appendix

Figure A1

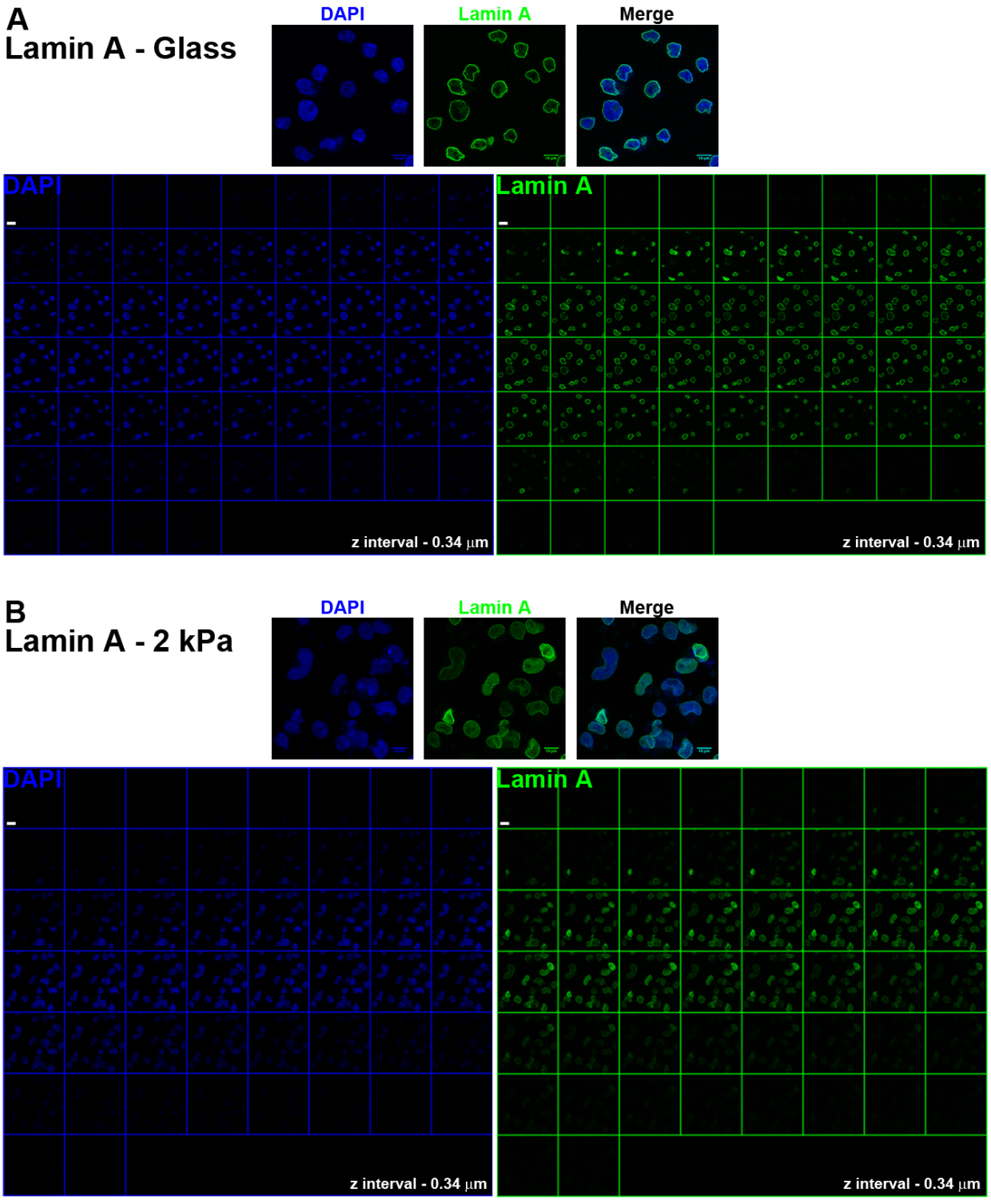
A
Lamin A - Glass
DAPI
Lamin A
Merge
DAPI
Lamin A
z interval - 0.34 µm
z interval - 0.34 µm
B
Lamin A - 2 kPa
DAPI
Lamin A
Merge
DAPI
Lamin A
z interval - 0.34 µm
z interval - 0.34 µm

Figure A2

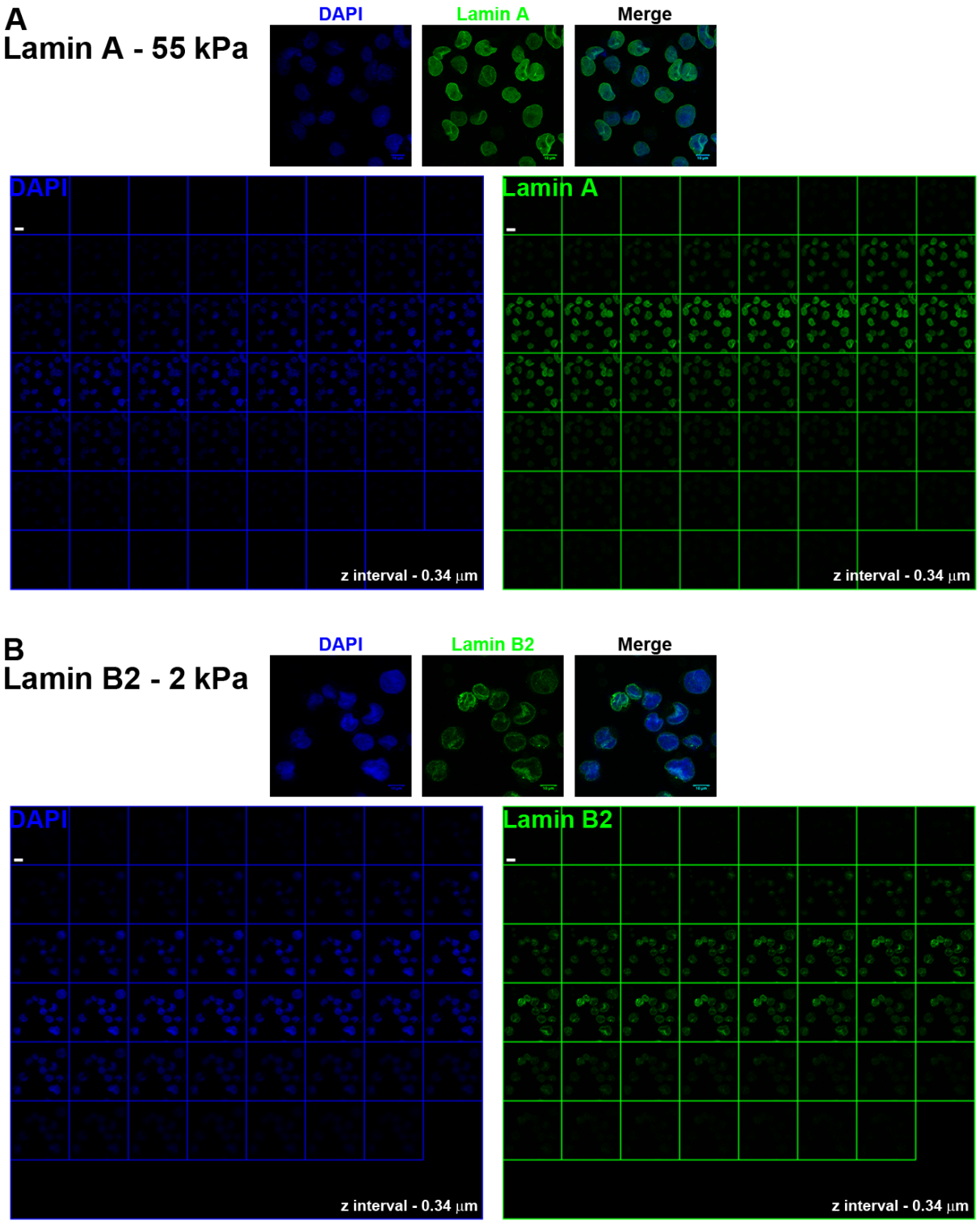
A
Lamin A - 55 kPa
DAPI
Lamin A
Merge
DAPI
Lamin A
z interval - 0.34 μm
z interval - 0.34 μm
B
Lamin B2 - 2 kPa
DAPI
Lamin B2
Merge
DAPI
Lamin B2
z interval - 0.34 μm
z interval - 0.34 μm

Figure A3

A
Lamin B1 - 2 kPa

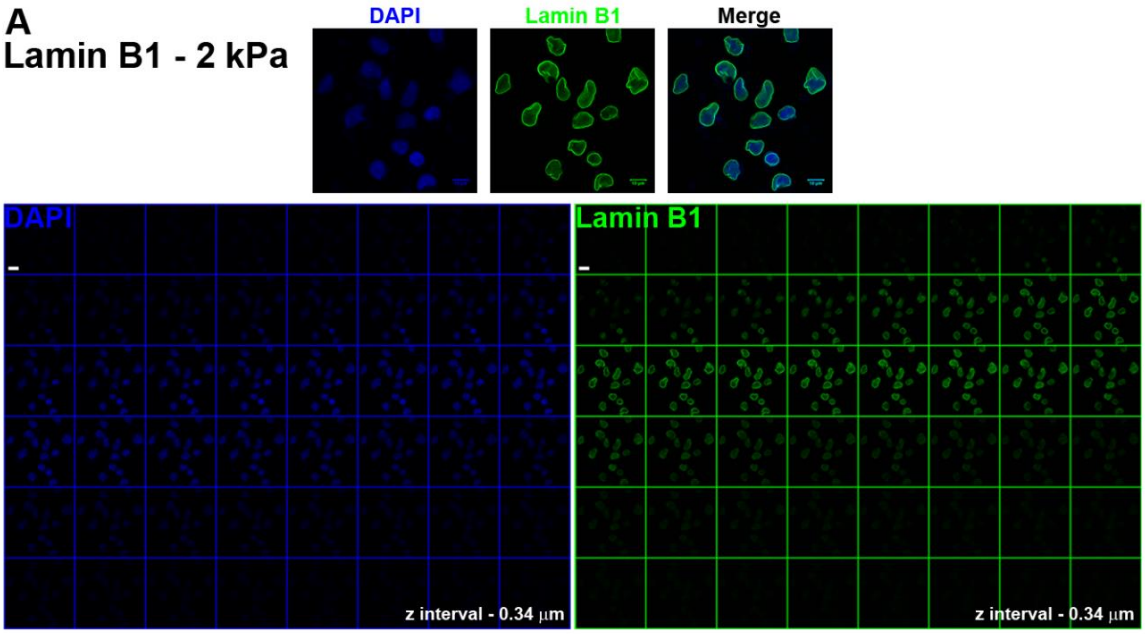

B
Lamin B1 and
Lamin B2 - Glass